UNIVERSITAT DE BARCELONA

Selective scintillation resins for radioactivity analysis: From extractant development to method application

Isaac Giménez Guerra

Isaac Giménez Guerra

Tesi doctoral

2025

Selective scintillation resins for radioactivity analysis:

From extractant development to method application

Isaac Giménez Guerra

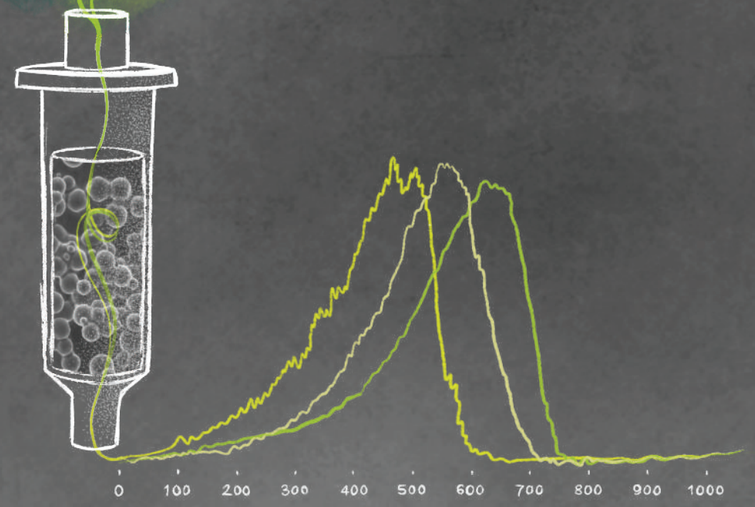

Universitat de Barcelona

Doctorat en Química Analítica i Medi Ambient

Selective scintillation resins for radioactivity analysis:

From extractant development to method application

Resines selectives escintil·ladores per a l'anàlisi de la radioactivitat:

Des del desenvolupament de l'extractant fins a l'aplicació del mètode

Isaac Giménez Guerra

Directors

Dr. Alex Tarancón Sanz, Professor agregat

Dr. Héctor Bagán Navarro, Professor agregat

Tutor

Dr. Alex Tarancón Sanz, Professor agregat

El Dr. Alex Tarancón Sanz, professor agregat del Departament d'Enginyeria Química i Química Analítica de la Universitat de Barcelona i el Dr. Héctor Bagán Navarro, professor agregat del Departament d'Enginyera Química i Química Analítica de la Universitat de Barcelona

FAN CONSTAR

que el present treball d'investigació ha estat realitzat per el Sr. Isaac Giménez Guerra al Departament d'Enginyeria Química i Química Analítica de la Universitat de Barcelona sota la seva direcció.

Dr. Alex Tarancón Sanz

Dr. Héctor Bagán Navarro

Barcelona, Març 2025

You're Gonna Carry That Weight
-Spike

Agraïments

Vull agrair primerament que aquesta etapa s'ha acabat. Espero que amb el temps, la meva visió respecte a aquesta etapa canviï, i pugui trobar-hi la part positiva.

Seguidament, m'agradaria agrair a tothom qui ha format part d'aquesta etapa. Començant pels meus directors Alex i Hèctor, per aquests anys, no només de tesis sinó també de TFG i TFM. Gràcies per mostrar-me el món de la radioquímica i compartir amb mi la vostra estima cap a la recerca. He après molt de vosaltres sent la part personal la més important. A tots els integrants de grup Questram-R. Especialment agrair a en Joan, per tots els anys compartits, no només de tesis, sinó també de vida. Per sempre estar disposat a escoltar i ajudar. A en Dídac per posar-me de peus a terra i fer-me adonar de coses que jo mateix no veia. A tu Arnau, per ser un desastre a la vida, però tenir un gran fons, per tots els riures i moments compartits, no oblidis mai les "guindilles", em trobaràs a faltar i ho saps. Sense vosaltres tres aquesta etapa hauria sigut encara més difícil, moltíssimes gràcies, us dec molt. En aquest grup, també voldria encabir al nostre Xavi, per ser la persona més supportive, noble i altruista que he conegut, gràcies per formar part d'aquesta etapa. Voldria també agrair a tothom que ha passat pel grup, recordant des de l'Aina i l'Edu, amb qui vaig començar la tesi, passant per la Sara, el Yorgos, i l'Aindara i tots els moments viscuts amb ells, i acabant per les últimes incorporacions, Irene, i Elena, que ho feu tot ben fàcil. També vull agrair a l'Araceli, Galeote, Aleix, Ivan i polete, no només per aquesta etapa viscuda junts sinó per tota la carrera i suport donat. Igualment vull agrair-te a tu Jordi "mercenario" Fons, per fer-me recapacitar en moltes "calentades" amb les teves paraules, i a tu Ines per tots els moments junts a les conferències. No puc oblidar-me de tu Jaime, on les birres i els riures no han faltat mai i has fet aquest període més amè.

Vull agrair també a la Giulia Sormani, l'Ali Hassanali i l'Alex Rodríguez, per donar-me l'oportunitat d'aprendre de vosaltres durant la meva estada a Trieste. Gracies per sempre estar oberts a tot. Ha sigut un honor poder treballar amb vosaltres, us admiro com a investigadors, però encara més pel tipus de persona que sou. Moltes gràcies per tot i per posar-ho sempre tot tan fàcil. Continuant amb l'estada, voldria agrair a totes les persones que vaig conèixer, entre ells en José, la Marta, la Debora i el Debarshi, que

van fer l'estança tan agradable i que van fer que la pogués gaudir al màxim. En especial agradecerte a ti Gonzalo, por incluirme des de el primer momento, ayudarme con todo y por todos los "puchos" hechos. Vorrei anche ringraziarti a te Antonio A.K.A. Antoñete. Sei la persona più gentile che abbia mai conosciuto. Sono felice di averti trovato e di aver condiviso con te tutto il tempo trascorso a Trieste. Spero di averti sempre come amico! Sei il mio caro amico, grazie mille per tutto. Along with Antonio, I would also like to thank Harshith for all the talks and time we spent together, always with a Negroni in hand. Without you, the experience would have been completely different. Thank you so much!

Voldria també agrair a tots els integrants de la UEC Horta i donar-vos les gràcies per haver-me acollit sempre, i per ajudar-me a tirar endavant una etapa personal de la qual no em creia capaç de sortir. Especialment, m'agradaria agrair a tu Kalvin o més ben dit "Coach" per fer-me passar tan bons moments, ajudar-me i compartir el fanatisme de l'escalada. Per molt que diguis, no ets "cuartogradista".... A la Thais, per la teva bondat, sinceritat i saber fer, per les bromes i els riures. Vull agrair també al Juan, per tots els moments al bulder i fora i a l'Òscar, perquè sempre gaudim quan escalem junts. Vull agrair també a la Gaia, per totes les cordades junts, divendres de "feina" escalant, diversió i fer-me sentir tan còmode. Per tot això i molt més on no arriben les paraules, moltes gràcies a tots.

A ti, Andrea, por todo lo vivido y por siempre entenderme. Por valorarme, quererme y apoyarme. Te mereces lo mejor.

A ti Oliver, por siempre estar. Hasta el momento, lo hemos compartido todo. Gracias por estar en los momentos buenos, en los no tan buenos i sobre todo en los malos y oscuros. Quizás la persona que más me conoce y con la que más cómodo me siento, muchas gracias por todo. Parte de lo conseguido es gracias a ti.

A ti Anna, porque nunca fallas, por el cariño incondicional y el apoyo desde el dia 1 en cualquier cosa que me proponga. A ti Alex, porque has estado des de siempre (literal), dispuesto a ayudar y escuchar en cualquier cosa. A los dos mil gracias.

A tu Maite, treballar amb tu has sigut sempre un plaer, haver d'anar al ICP es va convertir en un anem a veure la Maite, que sempre m'alegrava els dies. Per sempre escoltar-me i

aconsellar-me. Perquè sempre m'has ajudat i sempre has trobat les paraules per fer-me avançar. Et mereixes tot lo bo que et pugui passar i més. Ets un amor de persona.

Finalmente agradecer a mis padres y hermano, sin vosotros nada hubiera sido posible. Para mí no ha sido una etapa fácil, la cual he sufrido, pero sé que vosotros la habéis sufrido conmigo casi tanto o más que yo. Por ese amor incondicional que espero que nunca falte, y que parece que no valore, aunque sí que lo hago, muchas gracias por todo, os quiero mucho.

Me gustaría cerrar los agradecimientos agradeciéndote a ti Yayo, que te echo mucho de menos y ojalá estuvieras aquí para poder ver hasta donde hemos llegado. Si no hubiera sido por ti, a día de hoy, no sería quien soy.

Estic convençut que em deixo gent, però de totes formes **Moltes Gràcies** a tots!

ACRONYMS & ABBREVIATIONS

βCDs	Beta-cyclodextrin
APS	3-aminopropyl trimethoxy silane
ARS	Acute radiation syndrome
BisMSB	1,4-Bis(2-methyl styryl) benzene
CMPO	Octyl(phenyl)-N,N-diisobutyl-carbamoyl-methylphosphine oxide
CPM	Counts per minute
CPS	Counts per second
CSN	Consejo de Seguridad Nuclear
DCC	Dicyclohexyl carbodiimide
DCH18C6	Dicyclohexano-18-crown-6
DFT	Density functional theory
DIC	N, N'-diisopropyl carbodiimide
DIM	Di-isopropyl naphthalene
DMSO	Dimethyl sulfoxide
DtBuCH18C6	4',4"(5")-Di-tert-butyldicyclohexano-18-crown-6
DTM	Difficult-to-measure
DVB	Divinylbenzene
Dw	Distribution weight ratio
EC-LSC	Extraction chromatography and LSC
EDC	3-dimethylaminopropyl ethyl carbodiimide
EGDMA	Ethylene glycol dimethacrylate
$EGPO_4$	Bis[2-(methacryloyloxy)ethyl] phosphate
E_{max}	Maximum energy
HDEHP	Di(2-ethylhexyl) phosphoric acid
HPGe	High-purity germanium
ICP-MS	Inductively coupled plasma mass spectrometry
IER	Ion exchange resins
IIP	Ion-imprinted polymers
IP	Imprinted polymers
LRA	Laboratori de Radiologia Ambiental
LSC	Liquid scintillating counting
MAA	Methacrylic acid
MD	Molecular dynamics
MDPA	Methanediphosphonic acid
MIP	Molecular imprinted polymers
MMA	Methyl methacrylate
MS	Mass spectrometry
NMR	Nuclear magnetic resonance
PBC	Periodic Boundary Conditions
PET	Positron emission tomography
PLI	Pulse length index
PMT	Photomultiplier tube

POPOP	1,4-Bis(5-phenyl-2-oxazolyl) benzene
PPO	2,5-diphenyloxazole
PSCs	Proximity scintillation counts
PSm	Plastic scintillation microspheres
Psresin	Plastic scintillation resin
PVA	Polyvinyl alcohol
REA	Red de Estaciones Automáticas
REM	Red de Estaciones de Muestreo
ROS	Reactive oxygen species
Sc-Fe-IIP	Scintillating iron imprinted polymer
Sc-IIP	Scintillation ion-imprinted polymer
SEM	Scanning electron microscopy
SPE	Solid-phase extraction
SQP(E)	External standard quenching parameter
St	Styrene
SUC-LSC	Successive precipitation and LSC
TBP	Tributyl phosphate
THF	Tetrahydrofuran
TTA	Thenoyltrifluoroacetone-benzene
VPA	Vinyl phosphonic acid
WHAM	Weighted Histogram Analysis Method

Index

i. ABSTRACT I

ii. RESUMEN III

iii. RESUM V

iv. THESIS STRUCTURE VII

CHAPTER 1 - General introduction

1.1. Radioactivity 3

1.1.1. History of radioactivity 3

1.1.2. Types of radioactivity 6

1.1.3. Origin of radioactivity 10

1.1.4. Biological effects of radioactivity 15

1.1.5. Measurement of radioactivity 17

1.1.5.1. Gas ionization detectors 17

1.1.5.2. Scintillation detectors 20

1.1.5.3. Semiconductor detectors 21

1.1.5.4. Mass spectrometry (MS) 24

1.1.6. Chemical separation 25

1.1.7. General problems in detection of ionizing radiation 28

1.2. Analysis of alpha and beta-emitting radionuclides through scintillation 30

1.2.1. Scintillation mechanism 30

1.2.2. Detection efficiency and quenching 32

1.2.3. Photomultiplier 34

1.2.4. Background 35

1.2.5. Background mitigation 38

1.2.6. Liquid scintillation counting (LSC) 39

1.2.6.1. LS cocktail composition 39

1.2.6.2. Applications and limitations 40

1.2.7. Plastic scintillation microspheres (PSm) 42

1.2.8. LSC vs PSm 45

1.3. Plastic scintillation resins (PSresin) 47

1.3.1. PSresin characteristics 47

1.3.2. PSresin preparation 49

1.3.3. Current PSresin 50

1.3.4. Other PSresin 54

1.4. Imprinted polymers (IP) 56
1.4.1. Imprinted polymer components and characteristics 57
1.4.2. Types of IP 59
1.4.3. IIP elaboration 59
1.4.4. Polymerization methods 61
1.4.5. Scintillating IIP 63
1.5. Computational chemistry techniques for the development of new resins 65
1.5.1. Density functional theory (DFT) 66
1.5.2. Molecular dynamics (MD) 68
1.5.2.1. Enhance sampling techniques 70
1.6. References 76
CHAPTER 2 - Objectives
2.1. Objectives 85
CHAPTER 3 - Development of new scintillating materials for alpha-emitting and DTM radionuclides and computational tools for their implementation
3.1. Introduction 89
3.1.1. Alpha emitting radionuclides 89
3.1.2. DTM radionuclides 91
3.1.3. Computational strategy for extractant development 93
3.2. Results 95
Article #1 99
Article #2 113
Article #3 127
Article #4 145
3.3. Discussion 171
3.3.1. Development of a new PSresin for alpha-emitting radionuclides 171
3.3.2. Development of a scintillating iron imprinted polymer for ^{55}Fe 183
3.3.3. Computational strategies for resins development 190
3.4. References 200
CHAPTER 4 - Development of greener and faster alternatives for radiostrontium and plutonium isotope measurement
4.1. Introduction 205
4.1.1. Radiostrontium 205
4.1.2. Plutonium 208
4.2. Results 211
Article #5 215

Article #6 225
Article #7 237
4.3. Discussion 251
4.3.1. Determination of ^{90}Sr in presence of ^{210}Pb 251
4.3.2. Simultaneous measure of ^{89}Sr and ^{90}Sr 255
4.3.3. Plutonium determination 258
4.3.4. Radiostrontium and plutonium sequential determination 264
4.4. References 270
CHAPTER 5 - Conclusions
5.1. Conclusions 275

i. ABSTRACT

The present PhD thesis focuses on developing innovative strategies for the fast, accurate, reliable, and environmentally friendly determination of radionuclides. This has included developing new scintillating materials and analytical methodologies that address the limitations of current conventional methods.

For this purpose, two different selective scintillating materials were developed. The first one was a PSresin intended for the determination of the gross alpha parameter (α-PSresin), and included the synthesis and optimization of the used extractant, its immobilization, and the scaling-up for commercial purposes. The second material was a scintillating ion imprinted polymer for ^{55}Fe, being the first selective and scintillating imprinted material for radioanalytical purposes. Additionally, the potential of computational tools for the design of new extractants was evaluated, demonstrating their effectiveness in reducing development costs and time.

From the analytical point of view, specific working methodologies have been developed providing satisfactory results and becoming a green and fast alternative for radionuclide determination compared to conventional methods. In particular, a new analytical method has been developed for the gross alpha parameter using the α-PSresin developed in this PhD thesis. Furthermore, novel analytical methods were established for the determination of plutonium isotopes and radiostrontium using the existing AL-PSresin and CE-PSresin, respectively. In addition, sequential methodologies allowing the tandem determination of these radionuclides were also successfully developed using both PSresins in combination.

The application of the developed methodologies for radionuclide analysis in this study have demonstrated to reduce the analysis time, cost and use of toxic reagents compared to the conventional methods, all while keeping equal or lower limits of detections. These methods represent an accurate and reliable alternative for environmental monitoring and decommissioning purposes, with the added benefit of being environmentally conscious.

Key words: Radioactivity, Plastic Scintillation, Radiochemical Separations, Scintillation Polymers

ii. RESUMEN

La presente tesis doctoral se centra en el desarrollo de nuevas estrategias para la determinación rápida, precisa, y respetuosa con el medio ambiente de isotopos radioactivos. Esto ha incluido el desarrollo de nuevos materiales centelladores y metodologías analíticas destinadas a abordar las limitaciones de los métodos convencionales actuales.

Con este propósito, se desarrollaron dos nuevos materiales centelladores selectivos. El primero es una PSresin diseñada para la determinación de emisores alfa y la medición del parámetro alfa total (α-PSresin), y que incluye la síntesis y optimización del extractante utilizado, su inmovilización y la escalabilidad para fines comerciales. El segundo material es el primer polímero impreso centellador desarrollado para ^{55}Fe con fines radioanalíticos, dada la ausencia de extractantes selectivos para hierro. Adicionalmente, se evaluó el potencial de técnicas computacionales para el diseño de nuevos extractantes, demostrando su efectividad en la reducción de coste y tiempo de desarrollo.

Desde el punto de vista analítico, se han desarrollado diferentes metodologías analiticas las cuales han proporcionado resultados satisfactorios, convirtiéndose en una alternativa verde y rápida para la determinación de radionúclidos. En particular, se ha desarrollado un nuevo método analítico para el parámetro alfa total utilizando la α-PSresin desarrollada en esta tesis doctoral. Asimismo, se desarrollaron nuevos métodos analíticos para la determinación de isótopos de plutonio y radioestroncio Además, se desarrollaron exitosamente metodologías secuenciales que permiten la determinación en tándem de estos radionúclidos utilizando ambas resinas.

Los métodos desarrollados en esta tesis han permitido reducir el tiempo de análisis, costes y el uso de reactivos tóxicos en comparación con los métodos convencionales, manteniendo límites de detección iguales o incluso inferiores. Estos métodos representan una alternativa verde y rápida para las tareas analíticas en vigilancia ambiental y los procesos de desmantelamiento.

Key words: Radioactividad, centelleo plástico, separaciones radioquímicas, polímeros centelladores

iii. RESUM

Aquesta tesi doctoral es centra en el desenvolupament de noves estratègies per a la determinació ràpida, precisa i verda de radionúclids. Això inclou el desenvolupament de nous materials selectius i escintil·ladors i metodologies analítiques destinades a millorar les limitacions dels mètodes convencionals actuals.

Amb aquest objectiu, es van desenvolupar dos nous materials escintil·ladors selectius. El primer una PSresin dissenyada per a la determinació d'emissors alfa i la mesura del paràmetre alfa total, que inclou la síntesi i l'optimització de l'extractant utilitzat, la seva immobilització i l'escalabilitat per a fins comercials. El segon material va ser el primer polímer imprès escintil·lador desenvolupat per a ^{55}Fe, donada l'absència d'extractants selectius per a ferro. Addicionalment, es va avaluar el potencial d'eines computacionals per al disseny de nous extractants, demostrant-ne l'efectivitat en la reducció de costos i de temps associats al desenvolupament d'aquests.

Des del punt de vista analític, s'han desenvolupat diferents metodologies analítiques les quals han proporcionat resultats satisfactoris, convertint-se en una alternativa verda i ràpida per a la determinació de radionúclids. En particular, s'ha desenvolupat un nou mètode analític per al paràmetre alfa total utilitzant l'α-PSresin desenvolupada en aquesta tesi doctoral. Així mateix, es van desenvolupar nous mètodes analítics per a la determinació d'isòtops de plutoni i d'estronci utilitzant les resines existents, AL-PSresin i CE-PSresin, respectivament. A més, es van desenvolupar amb èxit metodologies seqüencials que permeten la determinació en tàndem d'aquests radionúclids utilitzant ambdues PSresin en sèrie.

Els mètodes desenvolupats en aquesta tesi han permès una reducció en el temps d'anàlisi, costos i ús de reactius tòxics en comparació dels mètodes convencionals, mantenint límits de detecció iguals o fins i tot inferiors. Aquests mètodes representen una alternativa verda i ràpida per a les tasques analítiques en vigilància ambiental i els processos de desmantellament.

Key words: Radioactivitat, Escintil·lació Plàstica, Separacions Radioquímiques, polímers escintil·ladors

iv. THESIS STRUCTURE

This thesis contains the research included in seven scientific publications and it is organized into 5 chapters.

The first chapter introduces the general aspects of radioactivity, including its fundamental principles and the different types of radioactive decay. It also covers the main techniques and detectors used for measuring radioactivity, focusing on scintillation counters, liquid scintillation counting (LSC), and the use of plastic scintillation microspheres (PSm). The chapter explores the most common strategies for developing polymeric scintillating materials, and includes the theoretical basis of molecular dynamics in the last section of the chapter, offering an understanding of the computational methods that can be employed in the development of these materials.

The second chapter presents the main objective of this thesis together with the specific goals for its achievement.

In the third and fourth chapters, all the research of the thesis is presented. The third chapter is focused on the development of new scintillation materials based on two different strategies. A new PSresin for alpha-emitting radionuclides determination which has been lately optimized for gross alpha determination and a novel scintillating iron imprinted polymer for ^{55}Fe determination. Additionally, a computational strategy is presented to reduce the time required for the development of these materials. The fourth chapter presents the research regarding the development of green and fast alternatives to conventional methods for radiostrontium and plutonium determination using PSresin. Both chapters include a short specific introduction and a final discussion where the presented work is further discussed and compared. The scientific publications of these chapters are listed below:

- Chapter 3

Article #1: **I. Giménez**, H. Bagán, A. Tarancón, J.F. García, PSresin for the analysis of alpha-emitting radionuclides: Comparison of diphosphonic acid-based extractants, Applied Radiation and Isotopes 178 (2021) 109969. https://doi.org/10.1016/J.APRADISO.2021.109969

Article #2: I. Giménez, H. Bagán, A. Tarancón, Fast analysis of gross alpha with a new plastic scintillation resin, Anal Chim Acta 1248 (2023) 340905. https://doi.org/10.1016/j.aca.2023.340905

Article #3: I. Giménez, H. Bagán, Scintillating Iron Imprinted Polymers (Sc-Fe-IIP): Novel material for ^{55}Fe selective recognition, Microchemical Journal 208 (2024) 112268 https://doi.org/10.1016/j.microc.2024.112268

Article #4: I. Giménez.; G. Sormani, A. Rodríguez, A. Hassanali, H. Bagán, A. Tarancón, Design of radionuclide separations based on MD simulations, Anal Chim Acta 1356 (2025) 344047. https://doi.org/10.1016/j.aca.2025.344047 (This article results from the PhD stay at the Abdus Salam International Centre for Theoretical Physics (ICTP, Trieste, Italy).

- Chapter 4

Article #5: I. Giménez, J. Rotger, E. Apellániz, H. Bagán, J. Tent, A. Rigol, A. Tarancón, A new method based on selective fluorescent polymers (PSresin) for the analysis of ^{90}Sr in presence of ^{210}Pb in environmental samples, Applied Radiation and Isotopes 199 (2023). https://doi.org/10.1016/j.apradiso.2023.110879.

Article #6: A. Torres, **I. Giménez**, H. Bagán, A. Tarancón, Analysis of isotopes of plutonium in water samples with a PSresin based on aliquat·336, Applied Radiation and Isotopes 187 (2022) 110333. https://doi.org/10.1016/j.apradiso.2022.110333.

Article #7: I. Giménez, H. Bagán, A. Tarancón, Simultaneous radionuclide determination using PSresin: 2in2 and 2in1 tandem configuration, Anal Chim Acta 1337 (2025) 343573. https://doi.org/10.1016/j.aca.2024.343573

Finally, the conclusions derived from this thesis are presented.

CHAPTER 1 - General introduction

1.1. Radioactivity

Radioactivity is a phenomenon where an unstable atomic nucleus undergoes spontaneous decay into a more stable configuration by emitting particles and/or electromagnetic radiation. The energy released during this process is sufficient to ionize atoms, thereby classifying it as ionizing radiation [1].

1.1.1. History of radioactivity

X-rays were first discovered by Wilhelm Conrad Röntgen in 1895. Röntgen experimented with a cathode ray tube and observed that a screen coated with a fluorescent material emitted light when the tube was operating and focused toward the screen. Röntgen noticed that the fluorescence occurred even when opaque materials shielded the screen. This unexpected fluorescence led Röntgen to hypothesize the existence of an unknown form of radiation that can pass through the materials. To further investigate this, he conducted more experiments and found that these rays were capable of penetrating various materials, including human tissues, while leaving shadows on a photographic plate. Owing to the mysterious and unknown nature of these rays, Röntgen referred to them as "X-rays," with the "X" signifying their unknown or variable nature. It was then when, Röntgen captured the first-ever radiography, using his wife's hand, Anna Bertha Ludwig, holding a lead ring (Fig1.1)[2].

Fig1.1 The first X-ray by Wilhelm Röntgen on Anna Bertha Ludwig in 1895
(Attribution-NonCommercial 4.0 International (CC BY-NC 4.0). Source: Wellcome Collection. https://wellcomecollection.org/works/wjc8ejn2)

This development led to the discovery of X-rays and marked the beginning of radiography. Röntgen's significant contributions to science were recognized when he was awarded the first Nobel Prize in Physics in 1901, commemorating his pioneering work in the field.

This recent discovery encouraged the work of Henri Becquerel, who, by chance, discovered radioactivity just one year later, in 1896. Following in his father's footsteps, Henri Becquerel began studying fluorescence processes in 1883. He was particularly interested in uranium salts and studied the fluorescence of double uranium and potassium salts. After the discovery of X-rays, he hypothesized that the fluorescence he observed could be X-rays generated when the salts were excited by sunlight.

To investigate this effect, Becquerel shielded the fluorescent uranium salt with a photographic film and exposed the entire setup to sunlight, expecting the photographic film to blacken. This expectation was met. Nonetheless, unsatisfied with this result, Becquerel continued his experiments to reproduce and confirm the findings. However, due to a lack of sunny days, he had to wait several days to conduct further experiments. During this waiting period, he kept the setup ready in the dark.

Surprisingly, after four days of waiting, he discovered pronounced blackening marks on the photographic film, which were even more intense than in the previous experiment. This contradicted his initial hypothesis that sunlight was the main factor, leading him to conclude that the phenomenon originated directly from the uranium salt. Further studies with different uranium salts, not just the fluorescent ones, confirmed that this was a specific characteristic of uranium [3].

Some years later, Marie Curie, together with her husband Pierre Curie and inspired by the uranium rays discovered by Henri Becquerel, discovered two more radioactive elements, polonium and radium, and their possible applications. They studied the effects of radioactivity on different tissues and their possible medical applications. Additionally, they both developed and refined chemical methods to isolate radium and polonium from other elements in solution, based on selective precipitation and solvent extraction strategies. The techniques and principles developed by Marie Curie laid the groundwork for the field of radiochemistry, enabling the isolation and study of

radioactive isotopes. However, Marie Curie's passion was the reason for his death, as she developed an aplastic pernicious anemia due to her overexposure to radioactive materials. Nevertheless, her contributions to the scientific community were awarded not only once but twice. The first time was in 1903 with the physics Nobel Prize shared with Henri Becquerel and her husband, Pierre Curie, and the second time was with the chemistry Nobel Prize in 1911 [4].

In the following years, the number of radionuclides discovered continued to grow, with the discovery of actinium (1899), radon and thorium (1900), etc. In the early 1900s, even though several radionuclides were discovered, the nature of the radiation emitted by them was still unclear. Henri Becquerel, Marie, and Pierre Curie along with Rutherford observed that there were at least two distinct types of radiation. One type exhibited low penetrating power, being easily stopped by a sheet of paper, whereas the other type was much more penetrating, requiring an aluminum sheet to be stopped. Moreover, they observed that both were charged particles and when the particles were subjected to electric and magnetic fields, the particles deviated in opposite directions, meaning that one was positively charged, named alpha particle (α), and the other particle was negatively charged, named beta particle (β).

In the late 1900s, Ernest Rutherford in collaboration with Paul Villard, made a significant discovery that expanded our understanding of radioactivity. They identified a third type of ionizing radiation, distinct from the previously observed alpha (α) and beta (β) particles. This newly discovered radiation was similar to X-rays but had a shorter wavelength. Notably, it did not show deflection in the presence of electric or magnetic fields, a characteristic that sets it apart from alpha and beta particles. This third type of radiation was classified as electromagnetic radiation and termed gamma radiation (γ). Its properties were experimentally confirmed in 1914 by Rutherford himself and his collaborator Andrade [5].

The discovery of radioactivity became day by day, more notorious. To investigate radioactivity, researchers needed to be able to detect and quantify it. In 1908, Rutherford and Geiger, knowing that alpha particles were able to pass through very thin solids, developed the first method of detecting particles, using a gold foil and a screen. The particles hit the screen, producing barely detectable flashes of light. The flashes of

light were then counted in a dark room one by one, spending several hours counting. To reduce the counting time required, Geiger built a device that automatically counted the individual particles. This early device, named Geiger counter, was only capable of detecting alpha particles. A later version developed by Geiger and his student Walther Müller in the late 1920s was sensitive to all types of ionizing radiation and was named Geiger-Müller detector. In 1940, the first proportional counters and photomultiplier tubes were developed, along with the discovery of scintillating materials, which would enable the future development of scintillating detectors. Finally, in 1963, the first semiconductor detector was developed. All detectors developed have been improved along with technological advancement year after year, and the use of one or another detector depends on different aspects, one of which is the type of radioactivity that is aimed at being measured.

1.1.2. Types of radioactivity

Radioactivity can be classified in function of the type of particle emitted into alpha particle, beta particle, or gamma radiation [1,3,6].

Alpha particles consist of two protons and two neutrons, with a mass of four units and a positive charge of two (identical to the nucleus of helium ^{4}He). Alpha particles are emitted from the nuclei of some radionuclides during a radioactive decay, called alpha decay (Eq.1.1).

$$ {}^{A}_{Z}X \rightarrow {}^{A-4}_{Z-2}Y + {}^{4}_{2}He^{2+} \qquad \text{(Eq.1.1)} $$

The energy of an alpha particle is discrete and characteristic of its emitter. Due to their large mass and charge, alpha particles are highly ionizing and capable of strongly interacting with matter. They can only travel a few centimeters in air and less than a tenth of a millimeter in biological tissue. For this reason, alpha particles are particularly dangerous if inhaled or ingested, as they can cause serious cell damage, but they are not as harmful for external exposure.

Beta particles refer to high-energy electrons (β^-) or their antiparticles, positrons (β^+), emitted from an unstable nucleus during radioactive decay, called beta decay. The

emission of an electron entails the emission of an antineutrino and the emission of a positron entails the emission of a neutrino (Eq.1.2 and 1.3).

$$\beta^-: {}^{A}_{Z}X \rightarrow {}^{A}_{Z+1}X + e^- + \bar{\nu} \quad \text{(Eq.1.2)}$$

$$\beta^+: {}^{A}_{Z}X \rightarrow {}^{A}_{Z-1}X + e^+ + \nu \quad \text{(Eq.1.3)}$$

Negative beta decay occurs in neutron-rich nuclei, whereas positive beta decay occurs in proton-rich nuclei. In beta decay, the energy released during the decay process is shared between the beta particle (electron or positron) and the antineutrino or neutrino. Therefore, the energy of these particles ranges from 0, when all the energy is carried away by the antineutrino or neutrino, to maximum energy (E_{max}), when all the energy is carried by the beta particle. This maximum energy is characteristic of the emitting radionuclide. Due to the light mass of beta particles, they are much less ionizing compared to alpha particles when interacting with matter. However, beta particles can travel tens of centimeters in air and penetrate a few millimeters into skin or tissue. Beta particles can cause burns and, if ingested, can damage internal cells and organs.

Proton-rich nuclei can also decay following electron capture. Electron capture is a type of radioactive decay where the nucleus of an atom absorbs an electron of internal shells, K or L, combining it with a proton generating a neutron, emitting only a neutrino (Eq.1.4).

$${}^{A}_{Z}X + e^- \rightarrow {}^{A}_{Z-1}X + \nu \quad \text{(Eq.1.4)}$$

Owing to the electron capture process, a vacancy is created in the inner shell. This vacancy leads to the transition of electrons from higher energy levels to the inner shell, releasing energy in the form of characteristic X-rays or Auger electrons. Electron capture compete with positron emission primarily due to energy considerations, as electron

capture requires less energy. The availability of inner-shell electrons and the specific nuclear and atomic properties also play roles in determining the preferred decay mode.

Gamma radiation consists of electromagnetic radiation, which is monoenergetic and characteristic of each nucleus. Gamma radiation occurs when a nucleus is left in an excited state, after an alpha or beta decay, and emits gamma rays to release the excess energy reaching the ground state through one or several gamma emissions (Eq.1.5).

$$ {}^{A}_{Z}X^{*} \rightarrow {}^{A}_{Z}X + \gamma \qquad \text{(Eq.1.5)} $$

Gamma rays have a very high penetration power, requiring thick lead or concrete blocks to stop them, and a low ionizing power. For that reason, gamma radiation is particularly dangerous in the case of external irradiation.

In all cases, the danger posed by radioactive substances depends on their activity, which refers to the number of atoms disintegrated per unit of time and is expressed in Becquerels (Bq, disintegration·s^{-1}). The activity of a radioactive material depends on the number of nuclei (N) and the decay constant (λ), which is characteristic of each radionuclide. The decay constant represents the probability in which a radionuclide will decay within a fixed time period (Eq. 1.6).

$$ A(t) = -\frac{dN}{dt} = \lambda \mathrm{N(t)} \qquad \text{(Eq.1.6)} $$

Where A(t) is the activity at time t, λ is the decay constant ($time^{-1}$), and N(t) is the number of nuclei in the radioactive sample at time t.

The decay constant is related to the interval of time required to reduce the number of atomic nuclei to half of the initial nuclei value, called half-life time ($T_{1/2}$) (Eq1.7).

$$t_{1/2} = \frac{\ln 2}{\lambda} \quad \text{(Eq 1.7)}$$

Activity decreases over time as the number of radioactive nuclei on a radioactive substance source decrease. Thus, the activity at time t is governed by the radioactive decay law (Eq 1.8).

$$A(t) = A(0)e^{-\lambda t} \quad \text{(Eq 1.8)}$$

Where A(t) is the activity at time t, A(0) is the activity at time 0, λ is the decay constant (time^{-1}), and t is the time passed.

Certain radionuclides do not directly decay into a stable isotope and may undergo a series of decays until a stable isotope is reached. In such decay chains, a special condition known as secular equilibrium [7] can occur when two criteria are met: (1) the half-life of the parent radionuclide is significantly longer than that of the daughter radionuclide, and (2) the system is observed for a time long enough —typically several daughter half-lives—for equilibrium to be established. In secular equilibrium, the decay rate of the parent radionuclide (and thus the production rate of the daughter) remains approximately constant, and the activity of the daughter radionuclide becomes equal to that of the parent (Fig. 1.2). If the second condition is not met, and the observation period is shorter or the half-lives are not sufficiently different, a condition called transient equilibrium may occur instead.

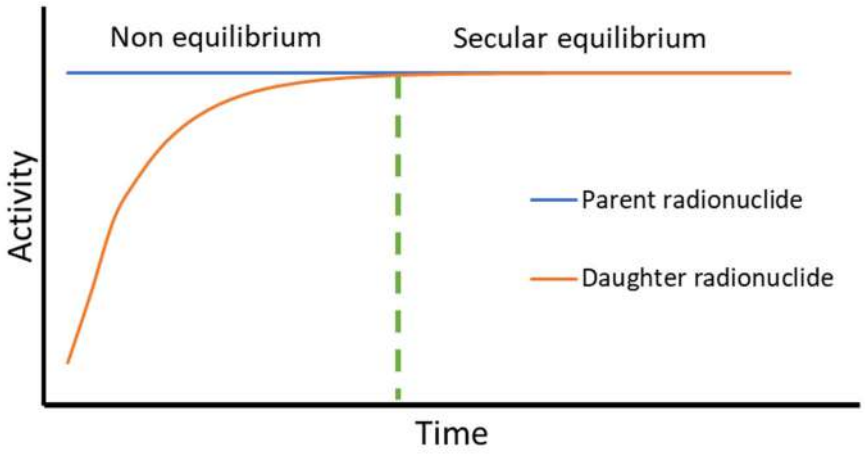

Fig1.2 Secular equilibrium scheme

1.1.3. Origin of radionuclides

Radionuclides can be categorized into two main categories based on their origin: natural and artificial. Natural radionuclides are commonly found in the Earth's rocks and soil, as well as in water bodies such as oceans, and therefore, being also present in building materials and indoor environments. In contrast, artificial radionuclides are generated through human activities, particularly due to nuclear reactions. Major sources of artificial radionuclides include nuclear power production, nuclear weapon explosions (both attacks and tests), and the operation of particle accelerators [1,5,8].

Natural Origin

This category can be further divided into two main subcategories, primordial and cosmogenic radionuclides.

Primordial radionuclides

Primordial radionuclides have existed on Earth since its formation. These radionuclides have half-lives that exceed 4.5 billion years, corresponding to the age of the Earth. Their long half-lives have enabled them to persist, contributing to the natural background radiation in the environment. Primordial radionuclides were formed through nuclear processes in stars and supernovas during the formation of the solar system. They can either decay directly into stable nuclei (non-series radionuclides) or decay through a series of intermediate radionuclides, with shorter half-lives, before reaching a stable isotope (decay-series radionuclides).

^{40}K, which primarily decays by beta emission to ^{40}Ca, and ^{87}Rb, which decays by beta emission to ^{87}Sr are found among the non-series radionuclides. ^{40}K has a natural isotopic abundance of 0.0117 %. Potassium is the seventh most abundant element in the Earth's crust and the sixth most abundant element in oceanic solutions, contributing significantly to the natural radiation background. ^{87}Rb has a natural isotopic abundance of 27.9 % and is commonly found in minerals such as feldspar and mica, contributing to the natural radiation background, due to its beta decay. Additionally, it is used in the rubidium-strontium dating method to determine the age of rocks and minerals.

Among the decay-series radionuclides, the uranium, thorium, and actinium series are found. There is a fourth series, which is called the neptunium series, but because of the short half-life of ^{237}Np ($2.144 \cdot 10^6$ years) this decay series is extinct, but there is still the presence of one of its decay products, ^{209}Bi. Regarding the existing series, the actinium series does not play a significant role in radioactivity background levels, due to a low natural abundance of ^{235}U (less than 5 % on an activity basis). Therefore, the decay products of the uranium and thorium decay series, are the main contributors to the natural environmental radioactivity levels. Fig 1.3 shows the radionuclides involved in the uranium series and their decay modes.

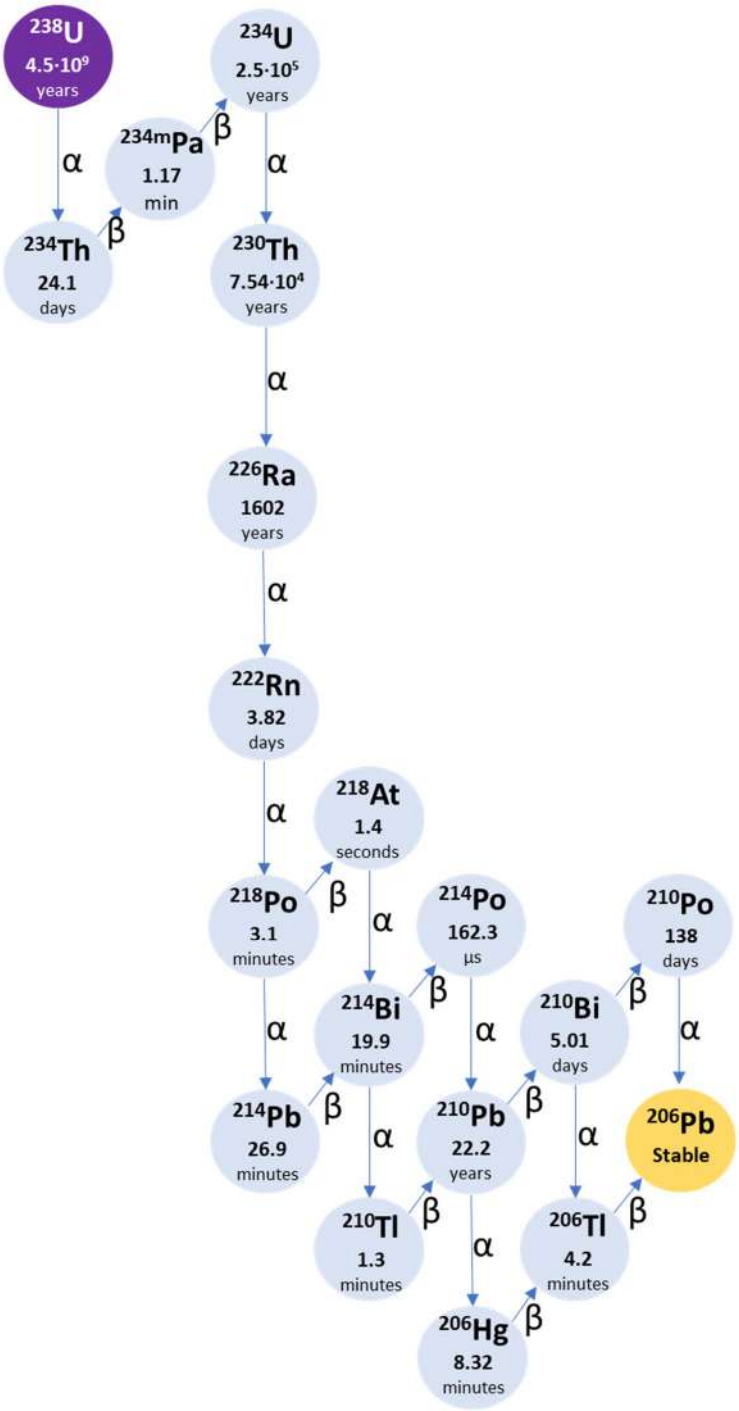

Fig 1.3 Radionuclides involved in the uranium series with their decay modes, decay energy type, and half-life times

Cosmogenic radionuclides

Cosmic rays are high-energy radiation consisting of protons, neutrons, and alpha particles. These rays originate from sources outside our solar system, including distant stars and galaxies, as well as from the sun. When cosmic rays interact with the Earth's atmosphere and surface, they can induce nuclear reactions that can produce a cascade of secondary particles and cosmogenic radionuclides. The lifetimes of these radionuclides can range from seconds to millions of years. Examples of cosmogenic radionuclides include tritium (^{3}H), beryllium-7 (^{7}Be), and carbon-14 (^{14}C).

Natural phenomena, such as accumulation and leaching, as well as certain human activities, can enhance the natural concentration of these radionuclides, thereby increasing the potential hazard associated with these naturally occurring radioactive elements.

Artificial Origin

Contrary to natural origin radionuclides, radionuclides of artificial origin or anthropogenic radionuclides, are all those radionuclides that are generated as a result of nuclear reactions because of human activities. Some are produced in particle accelerators, mainly for medical purposes, such as ^{131}I which is used for thyroid disease, or ^{99m}Tc, which is generated as a decay product of ^{99}Mo, and it is mainly used for disease diagnosis, due to its low energy and short half-life. ^{99m}Tc emits gamma rays, which are ideal for diagnostic imaging because they provide clear images while causing minimal radiation damage, additionally, the short half-life of 6 hours limits the radiation dose to patients, reducing long-term exposure risks. In nuclear medicine, it is often complexed with ligands to target specific tissues or organs, such as in the form of ^{99m}Tc-methylene diphosphonate for bone scans or ^{99m}Tc-sestamibi for cardiac imaging.

One significant source of anthropogenic radionuclides generation, and the cause of its dispersion in the environment, is the production of energy through nuclear fission of ^{235}U. This fission process involves the collision of a neutron, which destabilizes the nucleus, causing it to split into two smaller nuclei, known as fission products. These products which are typically smaller nuclei than the original ones, are often highly

radioactive, and play a significant role in the operation of nuclear reactors and the management of nuclear waste. Fission products can be classified into two groups: light fission products (mass numbers around 90-100) such as ^{90}Sr and heavy fission products (mass numbers around 130-140) such as ^{137}Cs. This nucleus splitting not only releases a substantial amount of energy, but also additional neutrons, and a large quantity of ionizing radiation.

During nuclear fission processes, also activation products are generated. Those radionuclides are generated when stable nuclei in reactor materials (such as fuel, cladding, coolant, and structural materials) capture neutrons released during the fission and become radioactive. Examples of these radionuclides include ^{51}Cr, ^{54}Mn, ^{55}Fe, ^{59}Fe, and ^{60}Co. Activation products are also produced by the capture of neutrons leading to new isotopes, such as is the case of ^{241}Am, which is produced in nuclear power plants during activation of ^{239}Pu and ^{240}Pu by neutrons, which is followed by beta decay of ^{241}Pu.

Another significant source of anthropogenic radionuclides in the past has been nuclear weapon testing. In a nuclear explosion, more than 200 nuclides from 35 different elements are produced. In addition, the neutrons released during the explosion, similar to those produced in cosmic-ray interactions, can also generate atmospheric radionuclides.

Each country disposes of different networks and programs to detect the presence of radionuclides in the environment and monitor the evolution of radioactive elements and its radiation levels, determine the cause of potential increases in radioactive levels in the environment, and establish corrective measures. In the particular case of Spain, the surveillance programs PVRA and REVIRA, have been established for this aim. The PVRA focuses on nuclear power plants and nuclear waste management and the REVIRA program, which includes the “Red de Estaciones Automáticas” (REA) and the “Red de Estaciones de Muestreo” (REM), is focused on monitoring the environmental radioactivity in air, water, soil, and dairy products. Both programs seek compliance with the legislation levels to ensure human and environmental safety. These legislation safety levels are based on ionizing radiation's biological effects.

1.1.4. Biological effects of radioactivity

Ionizing radiation can interact with biological tissues, leading to a cascade of events that result in molecular and cellular damage. This damage, either directly or indirectly, can affect biomolecules. Direct damage specially occurs when ionizing radiation collides with DNA, breaking one or both strands of the DNA and leading to chromosomal aberrations. Indirect damage occurs through the generation of reactive oxygen species (ROS) due to interactions of ionizing radiation with water molecules within the cell. These ROS include hydroxyl radicals, superoxide's, and hydrogen peroxides. Reactive oxygen species can induce various forms of damage, such as modifications of sugars, DNA strand breaks, amino acid oxidation, and lipid peroxidation.

Exposure to ionizing radiation can be classified as external or internal. External exposure involves contact with airborne radioactive materials, such as dust, liquids, or aerosols, that may deposit on the skin, clothing, or other surfaces. It can also occur from irradiation by external sources, such as during medical treatments where ionizing radiation is required, for example, X-rays used in radiography. External exposure ceases when the radiation source is shielded or when the individual moves away from it. Internal exposure, on the other hand, results from the intake of radioactive materials. This can occur through ingestion of contaminated food, contact with a wound, inhalation, or other routes. Internal exposure ends when the radionuclide is eliminated from the body, either naturally or through medical intervention.

The radiation exposure is measured by the radiation dose. Three types of doses are used:

- Absorbed dose: This is the amount of radiation energy deposited in a unit mass of tissue and it is expressed in grays (Gy).
- Equivalent dose: This is calculated for individual organs and it is based on the absorbed dose to an organ adjusted to account for the effectiveness of the type of radiation. This dose is expressed in sieverts (Sv).

- Effective dose: This dose is calculated for the whole body and is the addition of the equivalent dose to all organs, each adjusted to account for the sensitivity of the organ to radiation and it is also expressed in Sv.

Among these doses, the absorbed dose is a measurable physical quantity, whereas the equivalent dose and effective dose are used specifically for radiological protection purposes. The biological effect can be divided into two categories: deterministic effects and stochastic effects [9–11].

Deterministic effect

Deterministic effects follow a dose-response curve, where biological effects manifest only after surpassing a certain threshold dose, and their severity increases with the radiation dose. High doses of ionizing radiation can cause a range of effects, including cataracts, skin burns, sterility, hair loss, and even death.

When multiple biological tissues and/or organs are affected, acute radiation syndrome (ARS) may develop. ARS typically occurs when the whole-body equivalent dose exceeds approximately 0.7 Sv, with the first manifesting symptom often being hematopoietic syndrome (or bone marrow syndrome), which impairs blood cell production. At doses between 4–8 Sv, approximately 50% of exposed individuals may die within 30 days without medical treatment; this threshold is known as the lethal dose 50/30 ($LD_{50}/_{30}$). The actual lethality of radiation exposure, however, strongly depends on factors such as dose rate, individual health status, and the availability and quality of medical care. At doses above 10 Sv, gastrointestinal syndrome typically occurs, causing severe damage to the digestive tract and leading to death within days to weeks. At doses greater than 30–50 Sv, neurovascular and multi-organ failure ensue rapidly, usually resulting in death within 24–72 hours [12,13].

Stochastic effect

Stochastic effects are those that occur probabilistically; the likelihood of an effect occurring increases with the dose, but the severity of the effect is independent of the dose as it follows a probabilistic distribution. These effects typically exhibit a latent

period, meaning that adverse effects may manifest several years after exposure. Stochastic effects can be classified into three categories [12–14]:

- The genetic effect, which leads to mutations in highly specific cells, specifically sperm or egg cells. Mutations occurring in these reproductive cells are transmitted to the offspring of the exposed individual.
- The somatic effect, which directly affects the exposed individual, develops some kind of cancer, which can be lethal.
- The in-utero effect, which affects the fetus by producing different kinds of malfunctions on it. The most common are intrauterine death, growth retardation, developmental abnormalities, and childhood cancers. The malfunction depends on the fetal stage in which the exposure occurred.

These different effects depend on the type of radiation, its energy, and exposure duration. To assess these risks, it is needed to detect, identify and quantify radioactivity levels accurately which is selectively achieve through different detection techniques.

1.1.5. Measurement of radioactivity

Measurement of radionuclide activity is essential across various fields, including environmental science, healthcare industry, and nuclear safety. It can be accomplished radiometrically, by measuring the radiation emitted by the radionuclides or by mass spectrometry (MS) by measuring the number of radioactive atoms [15]. Detectors used in radiometric measurements include gas ionization detectors, scintillation detectors, and semiconductor detectors, whereas, in mass spectrometry, the most used equipment are ICP-MS and ICP-MS/MS.

1.1.5.1. Gas ionization detectors

Gas ionization detectors are among the oldest methods for radioactivity measurement, although they are still used. A gas ionization detector consists of a chamber with two electrodes filled with an ionizable gas, such as Ar or Ne. An electric field is applied across the chamber by establishing a potential between the two electrodes. When an alpha or beta particle or a gamma ray hits the gas filling the

chamber, it loses its energy through the ionization of the gas. The cations generated in the process are captured by the cathode of the chamber and the electrons are collected in the anode. For each ionization, an electric pulse is generated and measured. There are three different types of gas ionizing detectors: the ionizing chamber, the proportional counter, and the Geiger-Müller counter [16].

Ionizing chambers

In ionization chambers, the electric pulse generated is proportional to the energy lost by the particle or ray as it interacts with the filling gas. During ionization, ion pairs are produced. The electric field causes these ions to move toward the electrodes, with an applied voltage of approximately 100-200 volts. In an ionization chamber, the anode is typically a central wire or plate, while the cathode forms the walls of the chamber. An insulator is usually present to separate the anode and cathode, preventing current leakage.

In most ionization chambers, the sample is positioned close to the detector, allowing radiation to directly enter the chamber. Ionization chambers are characterized by their capacity of measuring high radiation levels, being very stable over time with low dependence on gas gain effect and its simple design. However, these counters are not sensitive to low level radiation, they are slow responding to changes in radiation intensity and they are not capable to distinguish between particle types. Therefore, ionization chambers are commonly used for the calibration of gamma sources and for measuring exposure rates from gamma rays and X-rays, not being suitable for alpha and beta emitters determination.

Proportional counters

In proportional counters, the electric pulse generated is proportional to the energy lost by the particle or ray. However, the pulse height response in a proportional counter is several orders of magnitude higher than in an ionization chamber. While ionization chambers record only the ions and electrons from the primary ionization events, proportional counters amplify the number of ions and electrons by a factor of 100 to 10000, depending on the voltage applied, which ranges from 100 to 1000 volts. This

amplification is due to a phenomenon called gas multiplication. This phenomenon occurs when free electrons in a strong electric field gain sufficient energy to cause secondary ionization of the filling gas. This results in a cascade of electrons known as the Townsend avalanche.

Proportional counters typically consist of a cylindrical container filled with a gas mixture, which includes a noble gas and a quench gas, such as Ar or CH_4 respectively. The anode is a thin central wire, while the cathode forms the walls of the cylindrical chamber. The quench gas prevents continuous discharges, ensuring stable operation.

These counters are characterized by its high sensitivity as can detect low levels of radiation and small energy deposits. Additionally, it allows radiation type differentiation due to the proportionality between the pulse height and the energy radiation, allowing the detection of alpha, beta and gamma emitters. However, proportional counters are limited to the gas life time as it degrades over time and its performance depends on temperature and pressure due to its complex electronics. Moreover, the sample preparation for these counters, consists of the evaporation of the sample on a thin planchet which is then placed inside the chamber into a sample holder aligned with the detector's windows opening. This sample deposition must achieve a thin layer to avoid self-absorption phenomena. This directly affects the calibration, as standards must be prepared similarly to ensure that the detector response is consistent and accurate for the specific sample type. This sample preparation can be challenging being long and tedious being not appropriate in some situations where a fast response is required.

Geiger-Müller counter

The electric field applied in a Geiger-Müller counter is the highest among the three types discussed, with a voltage of around 1000 volts. Unlike ionization chambers and proportional counters, a Geiger-Müller counter cannot distinguish between different radiation energies because the filling gas is ionized to its maximum extent. This is due to the very high voltage, which produces pulses of consistent size regardless of the energy of the incoming radiation, giving no energy information or type of radiation being then

only used for radiation presence detection as they can mainly detect gamma rays and high energy beta emissions.

Geiger-Müller counters consist of a cylindrical or tube-shaped container filled with a low-pressure inert gas and a quench gas. The anode is typically a central wire or rod, while the cathode forms the outer metal wall of the tube. Similar to ionization chambers, the radiation source is directly positioned close to the detector.

1.1.5.2. Scintillation detectors

A scintillation counter comprises two main components, the scintillator which responds to incident radiation and converts its kinetic energy into photons, and a photodetector, typically a photomultiplier tube (PMT), which is responsible for detecting the photons emitted by the scintillator and converting them into an electrical signal. The PMT amplifies the weak light signals to produce a measurable electronic pulse. Scintillation counters are valued for their high sensitivity and fast response time, making them suitable for a range of applications from low-level radiation detection to high energy particle measurements.

Charged particles (alpha and beta particles) excite the scintillator along its path, whereas, for uncharged particles, gamma rays, the scintillation can be produced after different processes such as the photoelectric effect, the Compton scattering, or pair production. There are two main type of scintillators: inorganic and organic scintillators.

Inorganic scintillators

Inorganic scintillators are typically crystals grown in high-temperature furnaces. These crystalline materials have two distinct energy bands: the valence band and the conduction band. When ionizing radiation interacts with the scintillator, the absorbed energy may excite electrons from the valence band to the conduction band, creating a hole in the valence band. The excited electrons and holes can move through the crystal lattice and may become trapped at defect sites or activator sites (intentional impurities added to the material). During the recombination of the electrons with the holes, energy is released in the form of photons. This process is facilitated by the presence of activator compounds such as thallium or silver.

Examples of inorganic scintillator crystals include thallium-doped sodium iodide (NaI(Tl)), cesium iodide (CsI), zinc sulfide (ZnS), sodium iodide (NaI), and lithium iodide (LiI). The emitted photons are typically in the UV-visible range, peaking between 400 to 600 nm, depending on the type of crystal used. Due to the hygroscopic nature of some inorganic scintillators, they are usually housed in airtight containers to protect them from moisture, which is a significant drawback [17]. The sample is directly placed near the scintillator crystal.

Inorganic scintillators have high efficiency in the detection of gamma rays and high selectivity allowing for gamma spectrometry which allows for the identification of different gamma emitters present in a sample without requiring a previous target element isolation but no alpha or beta emitters determination. These scintillators have a wide range of applications, from medical imaging and positron emission tomography (PET) to industrial radiography and environmental monitoring [17].

Organic scintillators:

Organic scintillators are mixtures of organic solvents and fluorescent solutes. The scintillators produce photons with a wavelength between 370-750 nm, typically peaking at 425 nm, via a series of processes that are initialized when charged particles interact with the material via excitation. Organic scintillators, are characterized by having high detection efficiencies and are mainly used for the detection of alpha and beta particles. However, due to an inherent lack of selectivity of scintillators, the measurement requires a previous chemical separation, to isolate the target radionuclide. Organic scintillators can be classified as liquid scintillators or plastic scintillators. The mechanism and properties of organic scintillators will be explained in section 1.2.

1.1.5.3. Semiconductor detectors

In these detectors the ionizing radiation interacts with the semiconductor, producing an electron-hole pair by exciting an electron from the valence band to the conduction band. An electric field applied across the semiconductor material causes the electrons to move toward the positive electrode and the holes toward the negative electrode. This movement generates an electric signal that can be detected/measured. The number of electron-hole pairs generated in a semiconductor detector is

proportional to the energy deposited by the incoming radiation (such as alpha particles or gamma rays) enabling spectrometry determinations.

In semiconductor detectors, two semiconducting parts can be differentiated depending on the type of doping substance included in it (n or p). N-type semiconductors contain extra mobile electrons and are obtained by the addition of donor impurities, such as phosphorous or arsenic atoms with a valance state of +5 in the framework. P-type semiconductors contain extra holes and are obtained by the addition of acceptor atoms such as boron or indium atoms +3 valence state in the framework [18].

Semiconductor detectors are based on silicon and germanium crystals and are typically used in alpha and gamma spectrometry.

The mobility of electrons and holes depends on the semiconductor material. In germanium, the mobility is significantly higher than in silicon. Consequently, the depleted zone is deeper in germanium than in silicon. The deeper depletion zone allows for the absorption of more penetrating radiation, making germanium detectors ideal for gamma spectrometry, but with a high background signal and requiring a larger amount of sample. Conversely, silicon detectors are more suitable for detecting alpha particles, which lose energy over a short range, giving a lower background signal and less sample needed. Therefore, germanium detectors are made as large as possible, whereas silicon detectors are typically only a few millimeters thick.

Silicon semiconductors

Silicon semiconductor detectors are used for alpha spectrometry due to their high energy resolution and efficiency in detecting charged particles. There are various types of silicon detectors used in alpha spectrometry, including surface barrier detectors, passivated ion-implanted planar silicon detectors, and silicon drift detectors.

The advantages of using silicon detectors for alpha spectrometry include their high energy resolution, which typically ranges from 10 to 30 keV full-width at half-maximum. This high resolution allows for the precise identification of alpha-emitting isotopes. The detectors thin entrance windows minimize energy losses and enhance efficiency. Their

compact size and reliability, coupled with low electronic noise, contribute to accurate and stable measurements.

Alpha samples must be uniformly deposited on the planchet as a thin layer, to ensure accurate measurements and avoid self-absorption. Sample preparation is usually challenging and time-consuming as requires large pretreatments to eliminate chemical interferences. Unlike gamma spectrometry, which can measure gamma rays directly even in complex matrices, alpha spectrometry deals with particles that have very short ranges and are easily absorbed or scattered by other materials, therefore small amount of sample is used, consequently requiring long counting times to achieve the established limit of detection, increasing the time required for the analysis, sometimes not suitable, especially in emergencies [19,20].

Germanium semiconductors

Germanium semiconductor detectors are used in gamma spectrometry allowing for precise measurement of the energy and identification of the gamma-emitting radionuclides [21,22].

High-purity germanium (HPGe) detectors, which are the most used type for gamma spectrometry are found among of germanium semiconductors detectors. These detectors are made from ultra-pure germanium crystals, often cooled to liquid nitrogen temperatures (77 K) to reduce electronic noise and prevent thermal excitation of charge carriers. This cooling allows the achievement of a high energy resolution (around 1.85 KeV at the 1.33 MeV energy of the gamma line ^{60}Co) [23]. HPGe detectors can distinguish gamma energies down to a few tenths of a percent, which is better than other detectors such as sodium iodide scintillation detectors.

Their resolution makes them suitable for a wide range of applications, including environmental monitoring, nuclear safeguards, etc., and enable precise identification of radionuclides, even in samples with overlapping or closely spaced energy peaks.

Sample preparation for gamma spectrometry is considered fast and easy. Samples are placed in suitable containers, to minimize gamma attenuation due to their low detection efficiency. There is no need of a previous chemical separation of the target radionuclide, given its monoenergetic radiation and high resolution of the detector.

1.1.5.4. Mass spectrometry (MS)

MS is an analytical technique based on the measurement of the mass-to-charge ratio of ions reaching the detector. It is extensively used in different fields to determine trace and ultra-trace elements by measuring the number of atoms of the particular isotope present in the sample.

The activity of a radioactive source depends on the number of atoms present and the decay constant rate. Consequently, only high half-life radionuclides will have enough atoms to be detected by mass spectrometry.

Inductively coupled plasma mass spectrometry (ICP-MS) is the most common MS technique. In ICP-MS sample is loaded into an ion source operating at atmospheric pressure. The sample can be either an aqueous sample, which is introduced in the form of an aerosol mist, or a solid sample, which is introduced by laser ablation. The sample is decomposed into atomic components in an argon plasma which has a temperature of around 7000 K. The high temperature ensures a high ionization degree, with around 1 % of multiply charged ions. The generated positively charged ions are extracted and passed through a mass filter, separating ions by their mass-to-charge ratio.

A significant drawback is the presence of isobaric and polyatomic interferences. Isobaric interferences are those radionuclides with the same mass as the aimed one. For example (^{238}Pu for ^{238}U or ^{79}Br for ^{79}Se). Polyatomic interferences are two or more atoms bonded that act as a single unit and that are products of a chemical reaction. Some examples are $^{238}U^{1}H$ and $^{204}Pb^{35}Cl$ which interfere with ^{239}Pu. Additionally, ICP-MS suffers from low abundance sensitivity and tailing, leading to challenges in detecting radionuclides due to interference from adjacent peaks, increased background noise, and reduced resolution [15,24]. The limitations can be partially mitigated with triple quadrupole MS equipment (ICP-MS/MS) which includes three quadrupoles in series. The first quadrupole acts as a mass filter to select the ions of interest from the ionized sample. The second quadrupole acts as a collision/reaction cell where selected ions react with gas molecules loaded onto the quadrupole. This eliminates isobaric and polyatomic interferences. The third quadrupole acts as a second mass filter, enhancing resolution and reducing tailing.

Mass spectrometry can be used for the determination of long-lived radionuclides such as environmental ^{238}U or ^{232}Th in aqueous solution and soil samples, reaching low detection limits (0.01-0.6 ng · L^{-1}). However, this is not always suitable for fission and activation products produced in emergency or decommissioning scenarios such as ^{55}Fe due to their low half-lives or for ^{79}Se due to high difficulties due to spectral interferences, for which scintillation techniques are more suitable. Additionally, ICP-MS and ICP-MS/MS requires of a prior chemical separation to isolate the target radionuclides from the sample matrix to enhance measurement accuracy, sensitivity, and specificity. Moreover, these techniques are expensive, and extremely high radioactive radionuclides can affect the instrumentation, limiting its possible uses.

1.1.6. Chemical separation

Radiochemical separations are important steps in the analysis of radionuclides, especially for alpha and beta emitting radionuclides regardless the detectors used. The main goal is the isolation of the target radionuclide from complex matrices, reduce the number of radioactive interferences, and concentrate the target radionuclide for accurate detection and quantification. Some of the primary radiochemical separation strategies used are:

- Ion exchange chromatography

Ion exchange chromatography consists of the use of ion exchange resins (IER), where the separation of ions is based on their charge and affinity. IER are insoluble polymers (often polystyrene, methacrylic acid, and/or divinyl benzene derivatives) with charged groups (either cationic or anionic) distributed regularly along the polymer backbone, mainly on the surface. Regarding the ionizable functional groups, the most used ones are -COOH, $-SO_3H$, $-NH_2$, secondary and tertiary amines. IERs are mainly used in cartridge or column configuration. The IER is packed in a cartridge, in which the aqueous sample solution containing the target radionuclide is loaded, allowing the interaction of all charged particles with the resin. Subsequently, few rinses are performed to wash out different interferent elements and for finally eluting the target radionuclide.

Ion exchange chromatography involves relatively simple equipment and a straightforward procedure, and has been widely used in various separation processes.

While it can be sensitive to matrix effects, especially in complex samples where multiple ions compete for binding sites, its effectiveness depends significantly on the type of ion exchanger used and the design of the separation protocol. Ion exchange resins can exhibit excellent selectivity under optimized conditions, and have been successfully employed in the separation of closely related species such as lanthanides, alkali metals, and halogens. Furthermore, ion exchangers offer the advantage of high capacity for charged species, making them suitable for both trace and bulk separations. Despite these strengths, practical applications may involve multiple steps, including column conditioning and sequential elution, which can be time-consuming. Often, ion exchange chromatography is used in combination with other chemical separation techniques to enhance selectivity and efficiency [25,26]. Some examples are the Dowex1 for plutonium analysis in water samples [27] or the Dower1x8 for uranium [28].

- Solvent extraction

Solvent extraction, also known as liquid-liquid extraction, relies on the partitioning of radionuclides between two immiscible liquid phases, typically an aqueous phase and an organic solvent. This method is highly effective for isolating radionuclides from complex matrices and is commonly employed in nuclear fuel reprocessing, waste treatment, and radiochemical analysis. The process involves transferring the radionuclide of interest from one phase (usually an aqueous solution) into another phase (typically an organic solvent) that has a high affinity for the radionuclide, often through the formation of a complex with a specific extractant mixed in the organic phase. This strategy is characterized by its high selectivity, thanks to the extractant used, enabling efficient isolation of the target radionuclide. Additionally, a wide variety of extractants can be tailored to the specific chemical properties of the radionuclide of interest, allowing for customized separations based on different affinities, complexation strengths, and solvent properties. The main drawbacks are the generation of hazardous wastes (organic and radioactive) and the lack of phase separation or emulsion formation in high organic matter content samples, which disables the separation. In some cases, the incomplete stripping or inadequate phase separation can lead to cross-contamination of radionuclides between phases, complicating the purity and accuracy of the separated radionuclide. In addition, some of the organic solvents used might be

highly flammable and can form explosives mixtures with air, which render this chemical separation less safe than others. Some examples of extractants used are tributyl phosphate (TBP) for uranium [29] and plutonium [30] extraction and the di(2-ethylhexyl) phosphoric acid (HDEHP) used for actinides and lanthanides separation[31,32].

- Successive precipitations

Successive precipitations rely on the formation of insoluble solid compounds that selectively incorporate the radionuclides of interest, separating them from the solution. These techniques are commonly employed due to their simplicity, cost-effectiveness, and ability to handle large sample volumes. The precipitation is achieved by the addition of precipitating agents (such as oxalates, carbonates, etc.), changes in pH, or temperature effects. However, for achieving a proper isolation of the target radionuclide, usually several numbers of precipitations are required as the precipitating agent used might precipitate more elements together with the target one, which makes it a very tedious and time-consuming strategy. Fig 1.4 shows as an example the radiostrontium determination through precipitation separation.

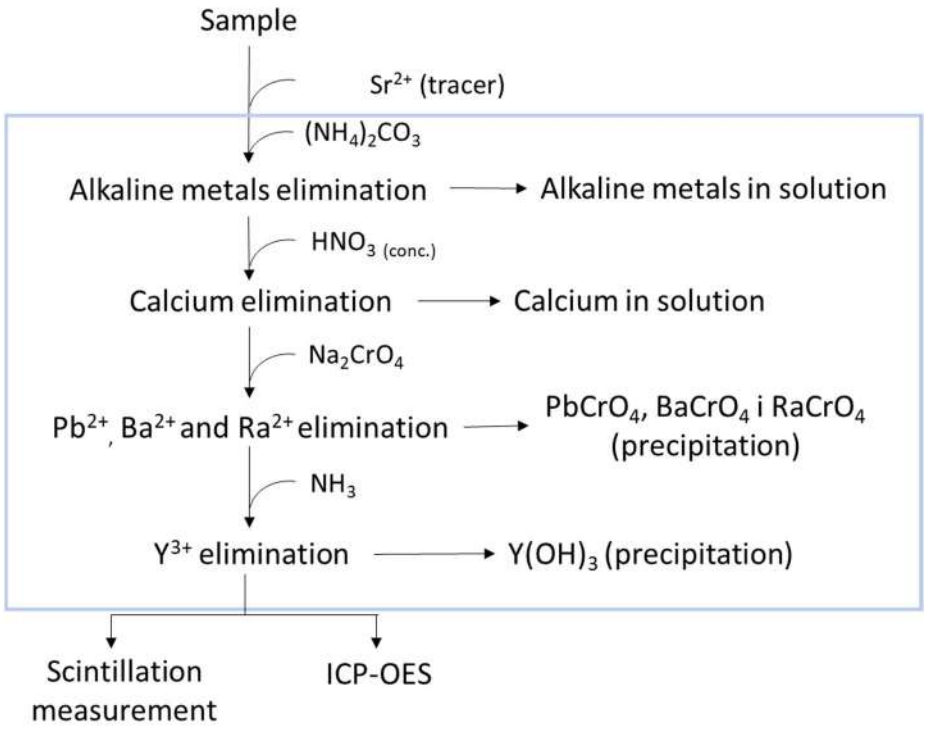

Fig 1.4 Successive precipitations method for radiostrontium determination

- Extraction chromatography

Lastly, extraction chromatography is a liquid-solid extraction, where a selective extractant is impregnated on a stationary phase. Extraction chromatography involves the partitioning of radionuclides between a mobile phase (typically an aqueous solution) and a stationary phase (extraction resin). This resin is usually packed in a cartridge and the sample is passed through it, being the radionuclides selectively retained and lately eluted based on their interaction with the extractant and the rinses solution used. This strategy is one of the most used nowadays, as it is considered very fast, selective, and simple. Moreover, it can be used in tandem allowing the proper isolation of more than one radionuclide at the same time. The main drawback of this technique is the generation of mixed wastes when scintillating detectors take part in the final measure. There are several extraction resins commercially available, developed by Triskem International and Eichrom Technologies, such as the UTEVA resin [33] used for uranium analysis, TEVA resin that can be used either for technetium or plutonium determination [34], DGA resin for americium determination [35], etc.

1.1.7. General problems in detection of ionizing radiation

Ionizing radiation measurement plays a crucial role in various fields, including environmental monitoring, emergency response, decommissioning of nuclear facilities, and nuclear medicine. Accurate assessment of radionuclide levels is essential to ensure environmental and human safety, driving the ongoing development and application of analytical methods. For gamma-emitting radionuclides, quantification is well-established in routine analytical laboratories due to the direct applicability of gamma spectrometry. Gamma emitter determination does not require prior chemical separation or sample preconcentration, allowing for the simultaneous identification and quantification of multiple gamma emitters in complex samples thanks to the high penetration power of gamma radiation which minimizes matrix effects.

In contrast, the determination of alpha and beta emitters always necessitates a prior chemical separation, which involves the use of hazardous reagents that pose environmental and health risks. Additionally, these chemical separations frequently fail to achieve sufficient decontamination factors, leading to suboptimal isolation and

quantification of the target radionuclides, a part of being long and tedious procedures. The determination of alpha- and beta-emitting radionuclides often relies on alpha spectrometry in case of alpha emitters and scintillation for alpha and beta emitters. In the specific case of alpha emitters, the determination through alpha spectrometry is widely used, however, as previously mentioned, the planchet preparation can be very challenging and given the detection efficiencies of this technique the counting time required is quite long, not always aligning with the required response time demanded by authorities. As alternative, the use of scintillation detectors allows for faster results due to their higher detection efficiency and reduced counting times and it is not limited only to alpha emitters. However, some alpha and beta determination is still challenging. For example, the quantification of the so-called difficult-to-measure (DTM) radionuclides, such as ^{55}Fe or ^{63}Ni, face significant challenges due to their low energies and the complexity of isolating these radionuclides from interferences in complex matrices. Additionally, current methods can be time-consuming, as exemplified by the gross alpha determination, which requires approximately 48 hours from sample reception to obtain results, and the obtained results often lack reliability [36].

Consequently, there is a growing need to develop novel analytical methodologies, particularly for alpha- and beta-emitting radionuclides, which overcome the limitations of conventional techniques. This includes enhancing the detection of DTM radionuclides and adopting greener, faster, and more effective approaches that reduce the environmental impact and improve their determination. The advancement of these methods is essential for accurate radionuclide quantification, especially in scenarios where traditional approaches fall short. Being scintillation techniques an excellent tool to improve and solve the current problems faced in alpha and beta emitters determination.

1.2. Analysis of alpha and beta-emitting radionuclides through scintillation

Liquid and plastic scintillation are two types of scintillation methods used for measuring alpha and beta particles, which are the focus of this work. Both techniques utilize organic scintillators that become excited by the emitted ionizing radiation and subsequently emit light (photons) as a result of this excitation [1,5,15].

1.2.1. Scintillation mechanism

The measurement process involves putting in contact the sample containing the radioactive target, with a scintillation material within a vial. This scintillation material comprises one or two aromatic components that act as solvents, and two distinct fluorescent solutes – a primary and a secondary one (See Fig.1.5). This composition facilitates the efficient capture of the particle energy and its conversion into detectable photons, establishing scintillation techniques as a robust method for radiometric analysis [37].

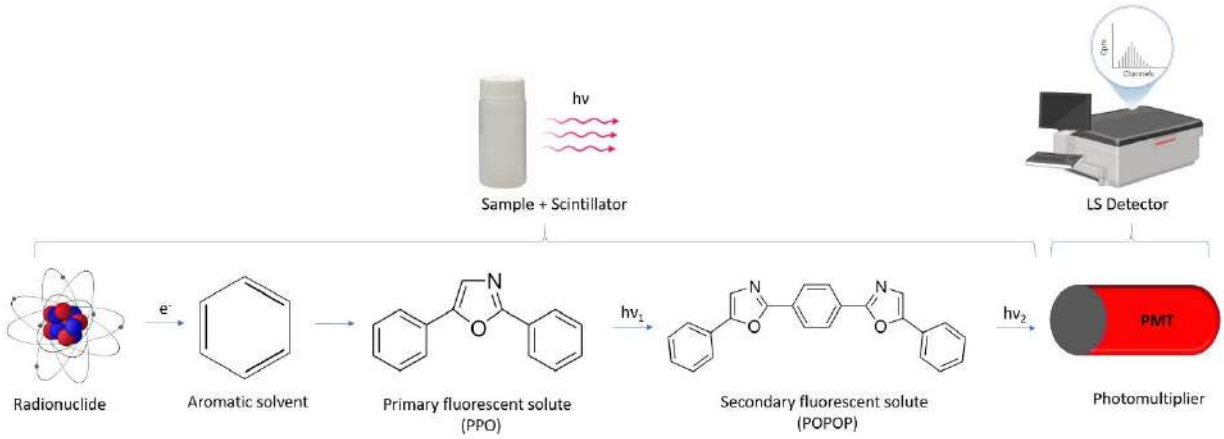

Fig. 1.5 Scintillation mechanism

Plastic and liquid scintillators are based on aromatic compounds, typically benzene derivatives. When a particle is emitted and reaches the scintillator, it transfers part of its energy to the aromatic solvent, exciting the π orbital system. Upon returning to the ground state, two scenarios can occur: non-radiative energy transfer to another aromatic solvent or fluorescent solute molecules, or radiative energy transfer to the primary fluorescent solute (typically 1-3 % by weight in plastic and liquid scintillators), exciting it. The de-excitation of the primary fluorescent solute emits photons that excite

the secondary fluorescent solute (typically 0.01-0.2 % by weight in liquid and plastic scintillators). The secondary fluorescent solute acts as a wavelength shifter, reducing the reabsorption of the emitted light by the aromatic solvent or the primary fluorescent solute, which results in a shortening of the attenuation length by shifting the light to longer wavelengths and make it optimum for the PMT [37].

This process is repeated several times until the radioactive particle is fully attenuated leading to several excited solvent molecules and the production of several photons in a few nanoseconds. Those photons are detected by a photomultiplier generating an electric pulse whose area is proportional to the number of photons detected and proportional to the energy of the radioactive particle.

Hence, the excitation of organic molecules is the key point that enables the detection of radionuclides. This phenomenon can be elucidated through the transition in electronic states within the π orbital system of delocalized electrons, inducing either fluorescence or phosphorescence processes (See Fig.1.6).

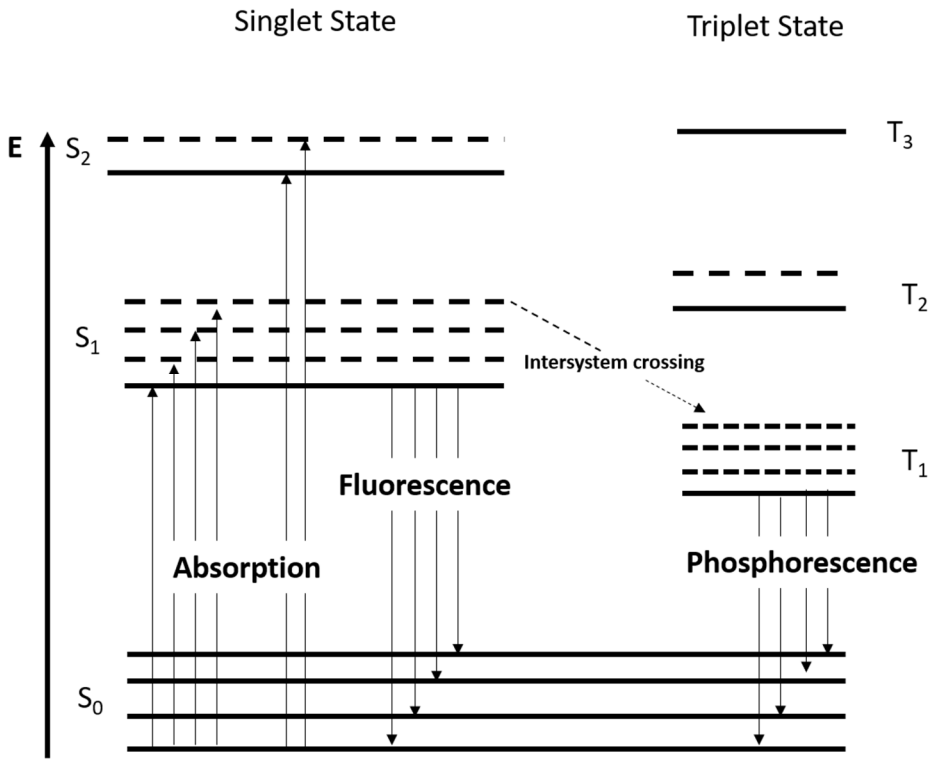

Fig1.6 π orbital system example scheme with its processes

When a charged particle passes through the solvent, the electrons are excited to a higher energy state. Each excited molecule can produce a photon during the de-excitation process. In the case of excitation by a beta particle, this de-excitation is typically induced by internal conversion, resulting in a rapid transition from an excited singlet state (where electron spins are paired) to the ground state.

When the interaction is with an alpha particle, electrons may be promoted to higher energy levels because of their higher power. This interaction can also lead to the population of triplet states (where electron spins are parallel) due to spin-flip events, which conserve angular momentum during the collision process. However, de-excitation from the triplet state to the ground state is forbidden by selection rules associated with electronic transitions. This prohibition arises from a mismatch in total angular momentum between the excited triplet state and the ground singlet state, thereby violating angular momentum conservation.

The de-excitation of an excited triplet state occurs through triplet-triplet annihilation. This process takes place when two triplet states encounter each other, resulting in an energy transfer from one triplet to the other, ultimately forming a singlet exciton. The singlet exciton can then follow a radiative decay pathway, emitting a photon, while the remaining triplet state is deactivated [38,39]. The photons produced by the de-excitation of a triplet state are known as delayed fluorescence.

This phenomenon allows for the discrimination between beta and alpha particles based on their distinct photon pulse durations. When analyzing the photons generated by the scintillation process based on decay time, two distinct regions can be observed. The primary component of light emission exhibits fast-exponential decay within the nanosecond range, which is caused by beta and gamma radiation. In contrast, the secondary component has a slower pulse decay due to triplet transitions, and is caused predominantly by alpha radiation.

1.2.2. Detection efficiency and quenching

The emitted photons generated in the scintillating process are detected by the photomultiplier, triggering a current pulse that is recorded as a count. The accumulative count over a given time interval is termed the count rate. The ratio between the count

rate (in counts per minute, CPM, or counts per second (CPS)) and the disintegrations, activity, (in disintegrations per minute, dpm, or disintegrations per second (Bq)) yields the detection efficiency (see Eq.1.7).

$$Detection\ efficiency = \frac{Sample\ count\ rate\ (cpm) - blank\ count\ rate(cpm)}{Activity\ (dpm)} * 100 \quad \text{(Eq.1.7)}$$

The detection efficiency serves as a metric that indicates the likelihood of detecting decays of a radionuclide under specific conditions. These conditions include factors such as the type of particle or ray emitted, scintillator material, sample composition, and detector characteristics.

When ionizing radiation interacts with the scintillator several molecules become excited, and the scintillation process results in the production of a photon package proportional to the energy of the ionizing radiation source. Each photon package can be classified according to its intensity into different channels generating a spectrum. The spectrum obtained is also characteristic of the conditions of measurement (radionuclide, sample, scintillator, and detector).

Some phenomena, known as quenching, might interfere in the different steps of the scintillation process decreasing or even eliminating the production of photons. This may lead to a shift in the spectrum and a decrease in detection efficiency. Depending on which part of the scintillation mechanism the quenching affects, five different types of quenching can occur:

- Particle quenching: This is the reduction of the energy of the emitted particle when it passes through the sample solution before reaching the scintillator.
- Ionization quenching: This phenomenon involves the ionization of solvent molecules instead of their excitation. This quenching phenomenon produces a non-linear arrangement of energy.
- Chemical quenching: This phenomenon is caused by the presence of chemical substances that hinder the energy transfer between the

aromatic solvent and the fluorescent solutes. It arises from the excitation of non-fluorescent molecules through secondary electron capture processes or dipole-dipole interactions.

- Color quenching: This phenomenon is caused by the presence of colored substances in the sample that absorbs the photons emitted by the fluorescent solute before they can be detected by the photomultiplier.
- Optical quenching: Loss of photons occurring due to inefficient light transmission on their path to the detector, often attributed to changes in the refractive index of the materials on the photon path.

Quenching effects can be quantified using a quenching parameter, which can be quantified through the spectra. The quenching parameter is usually determined by the detector utilizing an external gamma source capable to generate a substantial number of Compton electrons in the measurement vial. The one used in this study is the SQP(E) parameter and It corresponds to the channel where 99.5 % of the spectrum counts are confined [40].

1.2.3. Photomultiplier

Photomultipliers convert the emitted photons into an electric signal that can be further analyzed. Fig 1.7 illustrates the basic structure of a photomultiplier. A photomultiplier consists of two main components, the photocathode and the dynodes [5]:

- The photocathode is a photoelectric cell that ejects electrons from a metal plate when it is exposed to light. It is typically made from alkali metals and exhibits semiconductor properties.
- The dynodes are metal plates coated with bialkali substances and function as electrodes. They serve as electron multipliers through secondary emission, where each dynode is connected to the previous one with an increasingly positive voltage.

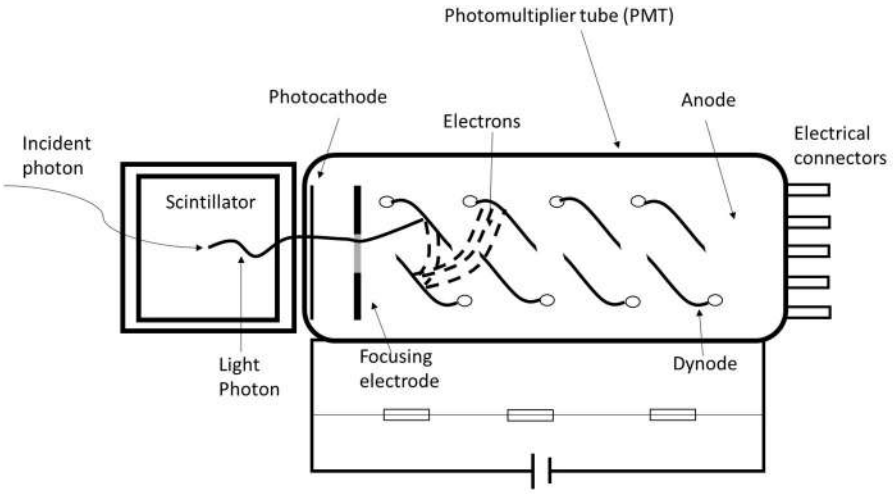

Fig1.7 Photomultiplier scheme

The scintillation light is absorbed in the photocathode by the photoelectric effect and photoelectrons are released. The released photoelectrons are accelerated towards the dynode chain. Upon the impact with the first dynode of a photoelectron, the release of additional electrons is produced. These electrons are accelerated towards the next dynode and the process is repeated as many times as dynodes the photomultiplier contains. The electric signal collected in the anode, contains the information of the number of photoelectrons generated on the photocathode which is related to the light released by the scintillator. To not affect the electron trajectory, the photomultipliers work under vacuum conditions. Depending on the detector design, 1 to 3 photomultipliers can be utilized, enabling coincidence counting and improving the detection sensitivity by reducing background signals.

1.2.4. Background

The background is an important aspect in the measurement of radioactivity in particular in the case of low-level activity samples. This registered signal is not provided by the sample, and it is quantified by the measurement of blank samples. There are different contributing sources to the background signal, some of them due to the components of the detector and others due to natural radioactivity (mainly cosmic rays and radionuclides in materials)[41].

Electronic noise

Several potential sources can affect the performance of a PMT, and hence the background level. The most common are the afterpulse noise and the dark noise.

- Afterpulse noise: Afterpulses are secondary pulses that occur following the initial pulse induced by a single photoelectron. These pulses are primarily caused by the ionization of residual gas molecules within the PMT. The accelerated electrons that travel between the first and second dynodes, can ionize these residual gas molecules, creating positive ions. These ions can slowly drift toward the photocathode, where they eventually strike and release additional electrons. These newly released electrons are then multiplied within the PMT, producing delayed pulses that appear as afterpulses, contributing to noise in the signal.
- Dark noise: Photomultipliers can produce a signal even in the absence of light due to the small electric current that flows through photosensitive devices from thermal emissions of electrons from the photocathode, leakage current between dynodes, or high-energy radiation interacting with the PMT components. This leakage current is also temperature-dependent and increase with rising temperatures due to enhanced carrier mobility and generation.

Additionally, as electronic noise, it is found the cross-talk, mainly in scintillator detectors with more than one photomultiplier. The cross-talk refers to unintended interaction or interference due to adjacent detector elements. Different types of contributions from cross-talk can be found:

- Optical cross-talk: it occurs when light produced in one photomultiplier can spread to an adjacent multiplier. This can occur due to imperfect reflective coatings or gaps between detectors.
- Electrical cross-talk: it is an electrical signal from a scintillation event in one photomultiplier can induce a signal in the electronics of a neighboring photomultiplier. This cross-talk can be produced due to inductive coupling in the electronics.

- Radiative cross-talk: it is produced due to secondary gamma rays generated by the primary interaction in one photomultiplier, which is detected in the adjacent one.

Cosmic radiation

Cosmic rays can reach the detector and interact with its components, producing signals that may be mistaken for signals originating from the sample. Moreover, cosmic rays can interact with the organic scintillator used, generating new signals that contribute to the background signal.

Radionuclides in materials

Some materials used in scintillator detectors can contain impurities of radionuclides. For example, ^{14}C, ^{40}K or ^{3}H can be present in the scintillator's cocktails used for liquid scintillating counting or the presence of ^{210}Pb in the shielding used in the detectors that could be also detected by the PMT of the detector increasing that way the background signal.

Luminescence

Luminescence refers to the emission of photons by the scintillating material that are not directly produced by the radioactive source to be analyzed. Typically, luminescence signals appear in low-energy channels on the spectrum, usually ranging between 0 to 200. There are different types of luminescence:

- Photoluminescence: occurs when the scintillating material is excited by ambient light during sample manipulation. To mitigate photoluminescence, it is recommended to store the sample vial in darkness for 1-2 hours before measurement.
- Chemiluminescence: This luminescence is the emission of light as result of a chemical reaction. The energy released from the chemical reaction directly excite molecules to higher energy states, which then emit light as they return to their ground state. Chemiluminescence can be managed by deoxygenating the sample, maintaining proper temperature control

to slow down the reaction rate, adding specific inhibitors, or avoiding reactive species (highly acidic or oxidants).

1.2.5. Background mitigation

Scintillator detectors include different components to reduce the influence of the previous mentioned factors on the background signal.

Electronic noise mitigation

The use of optical barriers and/or reflective barriers between photomultipliers, a careful design of the electronics, and advanced signal processing, are techniques that can be employed to reduce the cross-talk effects [42]. Scintillator detectors are equipped with a refrigeration system to reduce the influence of dark noise. Additionally, electronic noise is the major contributor to the background signal in those scintillation detectors where only one PMT is used. This effect can be mitigated by using more than one PMT working in coincidence mode.

Cosmic rays' suppression

To mitigate this effect, scintillator detectors are equipped with shielding to reduce background radiation and enhance measurement sensitivity. This shielding aims to block or at least minimize the impact of cosmic particles on the detector. There are two main types of shielding: passive and active.

Passive shielding involves using high-density materials with a high atomic number, like lead, copper, or steel, to cover the scintillator detector and prevent cosmic radiation from reaching it.

Active shielding employs a scintillator and a photomultiplier system to detect signals produced by cosmic radiation. A secondary scintillation material is implemented surrounding or being very close to the main scintillator. This system can reject these signals if they are detected in time coincidence by the photomultiplier measuring the sample.

Both types of shielding can be used alone or in tandem to provide comprehensive protection against cosmic radiation.

1.2.6. Liquid scintillation counting (LSC)

LSC is one of the main techniques for the measurement of radionuclides and the most commonly used scintillation technique. Its main application is the determination of beta emitters such as ^{3}H, ^{14}C, ^{90}Sr, ^{210}Pb, ^{32}P, etc. in a wide range of sample matrixes (environmental, biomedical, or decommissioning field). Alpha emitters can also be measured by LSC.

In this technique, the scintillating material is an organic liquid (LSC cocktail), which is mixed with the sample, and forms an emulsion, ensuring a close contact between the scintillating material and the sample, resulting in high detection efficiencies. LSC cocktails consist of at least three main components: the solvent, the fluorescent solutes, and the surfactants [37,43,44].

1.2.6.1. LS cocktail composition

Solvent

The solvent constitutes the 60-99% of the scintillation cocktail volume. Aromatic compounds are commonly used as solvents, and ideal properties include a high flash point, low vapor pressure, low toxicity, biodegradability, and resistance to chemical and color quenching. Some of the most common solvents used are the alkyl phenol ethoxylates, however, secondary solvent compound can be also present such as di-isopropyl naphthalene (DIN) isomeric mixtures to fine-tune the properties of the cocktail depending on the intended use.

Fluorescent solutes

The fluorescent solutes are in charge of the conversion of the excited energy released by the solvent into photons of a suitable wavelength for its detection by the photomultiplier. Fluorescent solutes are characterized by having a large π system or linked benzene rings. LSC cocktails typically contain two different fluorescent solutes. The primary fluorescent solute, which has an emission wavelength <400 nm, is typically 2,5-diphenyloxazole (PPO) or p-terphenyl. The secondary fluorescent solute, which acts as a wavelength shifter with an emission wavelength >400 nm, being optimum for the PMT, is typically 1,4-Bis(5-phenyl-2-oxazolyl) benzene (POPOP) and

1,4-Bis(2-methyl styryl) benzene (Bis-MSB). Fig 1.8, shows the structures of primary and secondary fluorescent solutes.

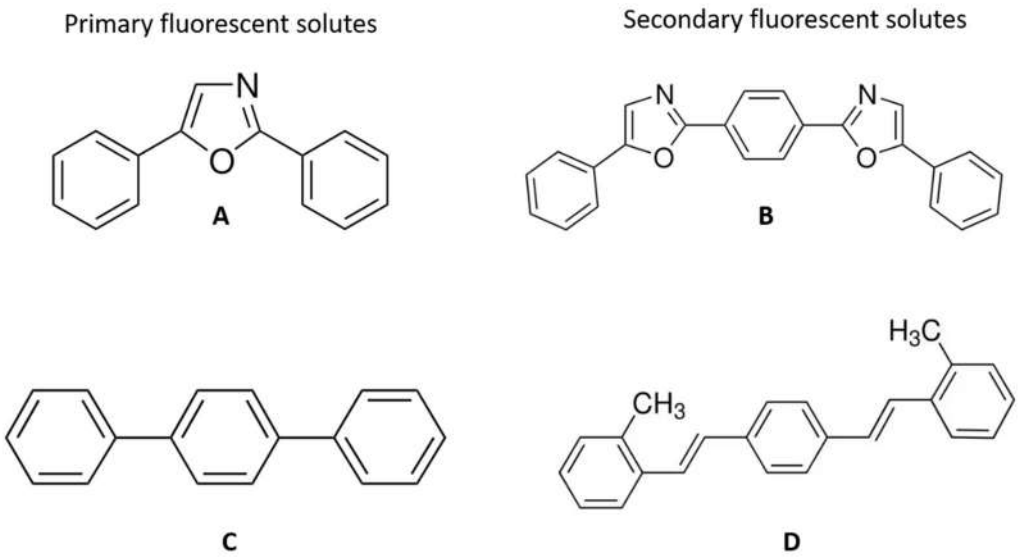

Fig 1.8 Primary and secondary fluorescent solutes. PPO (A), POPOP (B), P-terphenyl (C) and Bis-MSB (D)

Surfactant

Surfactants, such as alkylphenol polyglycol ethers, allow a good and homogeneous mixture of the aqueous sample and the organic compounds of the cocktail resulting in a very close contact between the radionuclides and the cocktail components. This allows the measurement of alpha and beta emitters with very high detection efficiencies as the distance between the radioactive particle and the cocktail is negligible.

1.2.6.2. Applications and limitations

LSC is the primary technique for beta and alpha-emitting radionuclides determination. However, it requires a previous chemical separation. Beta emitters have a continuous energy spectrum which complicates the simultaneous detection of beta emitters with similar energies. Alpha emitters, on the other hand, emit at specific energies but produce fewer photons per unit of energy compared to beta emitters. This is due to ionizing quenching phenomena, not allowing then the simultaneous determination of them. Consequently, alpha and beta emitters may appear in similar counting channels, complicating their quantification. Hence, the process begins with a

chemical separation to isolate the target radionuclide. Following separation, the resulting aqueous solution is mixed with an LSC cocktail and introduced in the detector. LSC offers the highest detection efficiency for beta and alpha emitters because the scintillator is in direct contact with the radioactive particles. This direct contact, along with the method's simplicity and speed, makes LSC particularly advantageous.

However, LSC is susceptible to matrix effects that can hinder accurate measurements. For example, in the quantification of ^{55}Fe, the presence of high concentrations of stable iron can cause color quenching. The proper selection of an LSC cocktail is essential for the partial mitigation of this problem for reliable measurements. Key considerations include the cocktail's capacity and stability; it must have sufficient capacity to accommodate the sample without phase separation. Additionally, samples containing alkaline materials or strong acids are particularly prone to color formation and chemiluminescence often due to reactions with free peroxides generated by ethoxylates in the cocktail. In this situation the use of cocktails with free radical scavengers can mitigate peroxide formation. For alpha-beta discrimination, cocktails containing secondary compounds, such as DIN, that enhance the delayed fluorescence of alpha particles improve the accuracy of differentiation.

Commercially available LSC cocktails often contain alkylphenol ethoxylates and di-isopropylnaphthalene as solvent compounds. However, these compounds are subject to the REACH regulation (EC 1907/2006) [45], which aims to protect human health and the environment from chemical risks. Both alkylphenol ethoxylates and di-isopropyl naphthalene are both persistent, bio-accumulative, and toxic. Moreover, alkylphenol ethoxylates are endocrine disruptors and can affect aquatic life, while di-isopropyl naphthalene is toxic to water fleas. Given the environmental concerns and regulatory changes affecting these compounds, as well as the challenges of managing the mixed wastes generated by LSC (radioactive aqueous solutions combined with toxic organic solvents), there is growing interest in alternative scintillation techniques for alpha and beta-emitting radionuclides, such as plastic scintillation microspheres.

1.2.7. Plastic scintillation microspheres (PSm)

Plastic scintillation microsphere are plastic scintillators in microsphere shape, where the aromatic solvent is a polymeric matrix such as polystyrene or poly(vinyltolune), accounting for up to the 95 % of the material composition in which the fluorescent solutes are trapped allowing for the scintillation mechanism. Extra compounds can be included to the PSm composition to modify the properties of the polymer, such as crosslinking molecules, to increase the rigidity and stability over extreme conditions of the resulting polymer, or molecule to enhance the alpha-beta discrimination such as DIN or biphenyl. The polymeric matrix used can act as primary fluorescent solutes. However, due to the high possibility of self-absorption at its own wavelength emission, is needed a primary fluorescent solute (typically PPO) for the obtention of an efficient PSm, and a secondary fluorescent solute (typically POPOP) acting as a wavelength shifter as in LSC.

The use of PSm resemblance the use of LSC cocktails, however, PSm are characterized by non-mixed waste generation, as the aqueous samples are heterogeneously mixed with the PSm, which after the measurement can be easily separated by simple filtration. In addition, PSm can be used for further application, such as in continuous monitoring equipment (by packing the PSm in cartridges), samples with high salt contents (no phase separation will be found, given the intrinsic heterogeneity of the resulting mixture), and thanks to the solid surface of them the immobilization of selective extractant could be performed, conferring selective capabilities to the PSm.

The size of the microspheres is an important factor in the measurement with PSm, as detection is significantly affected by two types of quenching that usually are not significant in LS: particle and optical quenching. Particle quenching occurs when the energy of radioactive particles is reduced by interactions with the sample as it travels through the sample medium before reaching the PSm. Optical quenching, on the other hand, involves a decrease in the number of photons that reach the photomultiplier tubes due to inefficient light transmission caused by successive changes in the refractive index encountered along the path (around 1.55 for PS and 1.33 for water). Both quenching parameters have opposite behavior regarding the diameter. When the diameter of the microspheres increases, the distance that the emitted particle must travel to reach the scintillator increases. That leads to an increase in the particle

quenching and a decrease in the detection efficiency. However, the path of the photons generated is simpler, and the number of changes in the refractive index before reaching the photomultiplier tube decreases. That leads to a decrease in the optical quenching and an increase in the detection efficiency. For that reason, the diameter of the PSm must be optimized to balance the effect of these two quenching phenomena. In the case of beta-emitting radionuclides, for PSm diameter ranging from 15 to 150 µm, beta-emitting radionuclides with low, medium and high energy such as ^{3}H, ^{14}C and $^{90}Sr/^{90}Y$, good detection efficiencies are obtained, peaking the maximum detection efficiency value around 15 µm (4.75 %, 74 % and 192 % respectively for ^{3}H, ^{14}C and $^{90}Sr/^{90}Y$). As the diameter of the PSm decreases, the surface area increases, leading to a reduction in the average path length that electrons must travel. This results in an increase in the detection efficiency. This effect is particularly significant for low-energy beta-emitting radionuclides, such as tritium, where shorter paths minimize energy loss and improve its detection efficiency. In contrast, high-energy beta emitters like ^{14}C and $^{90}Sr/^{90}Y$ have greater penetration power due to their higher energies, making them less affected by changes in the PSm diameter. In the case of alpha-emitting radionuclides, the same trend is observed. For example, for ^{241}Am, its detection efficiency is higher than 95 % at 60 µm, peaking a 100 % around 15 µm. Therefore, in terms of detection capabilities, PSm with a diameter of around 15 µm would be the best choice [40]. However, the use of 15 µm PSm is challenging for continuous monitoring as the solution would not be able to pass the cartridge containing the PSm, being then usually used 60 µm PSm. Furthermore, when using PSm smaller than 60 µm, the alpha spectra become broader and shift to lower energy channels because the alpha particle's energy is distributed across multiple PSm, even though the detection efficiency is the highest. In contrast, with 60 µm PSm the particle's entire energy is deposited in a single PSm, as its diameter is comparable to the alpha particle's travel path, which give thinner and less quenched spectra.

PSm’s can be prepared through several strategies, being two of the most common one: thermal radical polymerization and extraction-evaporation.

Thermal radical polymerization

Polymerization is a process, in which small molecules, called monomers, chemically bind one to another producing a large chain or a network molecule, which is called polymer.

Thermal radical polymerization is a process where monomers are polymerized using a thermal initiator for the generation of reactive species. Three different steps are identified, the initiation (where reactive species, radicals, are generated starting the polymerization process by heat exposure), the propagation (where the active monomer reacts with another monomer, adding it to the growing chain, while keeping a radical to allow the addition of a new monomers in a row), and the termination (the active centers are neutralized, and the polymerization is stopped. This can occur by the combination of two radicals or a reaction with impurities).

Briefly, the process consists of mixing the appropriate monomers, additives and fluorescent solutes with the thermal initiator. For PSm preparation a heterogeneous polymerization is performed. An aqueous solution is prepared containing a surfactant in which a homogeneous organic phase, containing the monomers, additives (if required), fluorescent solutes, and thermal initiator is added. The resulting mixture is stirred, at constant temperatures giving as result the PSm [46]. Different polymerization types will be further addressed later.

Evaporation-extraction

In this strategy a polymer, already prepared, is dissolved in a suitable organic solvent together with the primary and secondary fluorescent solutes and additives (disperse phase), added to a water solution containing a surfactant (continuous phase), and stirred during a period at a controlled temperature until the formation of the plastic scintillator. During the process, organic droplets are generated in the continuous aqueous phase which are stabilized by the surfactant and the continuous stirring. The organic solvent, containing the polymer and the fluorescent solutes, is slowly evaporated, while, the polymer solidifies on the droplet's surface. As the organic solvent evaporates, it is promptly replaced by more solvent from the droplet. Consequently, the

droplet size decreases as solvent its lost resulting in the permanent solidification of the polymer.

The form and size of the generated droplet determine the shape and size of the resulting PSm. The droplet size can be controlled by the speed and type of stirring, the ratio of continuous phase to dispersed phase, and the composition of both phases. For instance, an increase in the amount of surfactant in the continuous phase leads to a smaller PSm size.

A key characteristic of this strategy is the selection of the organic solvent. The solvent must have a minimal solubility in water and a low boiling point. This choice allows for the slow extraction of the organic solvent solely through stirring, eliminating the need for additional temperature control [47].

1.2.8. LSC vs PSm

Liquid scintillation counting and plastic scintillation microspheres are effective techniques for determining alpha and beta emitters, but they have distinct differences.

- Detection efficiency: LSC offers high detection efficiency because the active isotope is in very close proximity to the scintillating material. In contrast, PSm involves a heterogeneous solid-liquid mixture, with the scintillator and aqueous sample are separated by a greater distance. This can lead to slightly lower detection efficiencies in PSm due to particle quenching, especially for low-level beta emitters such as tritium.
- Phase separation: PSm are not affected by phase separation, which can be an issue with LSC. Consequently, PSm are advantageous for measuring alpha and beta emitters in samples with highly acidic or oxidizing conditions, or high salt concentrations.
- Mixed waste management: One significant advantage of PSm is the ease of separating the scintillating material from the active sample solution. After measurement, the scintillating material can be readily separated by

filtering the heterogeneous mixture, addressing the issue of mixed waste associated with LSC.

- Sample compatibility: LSC can handle both aqueous and organic sample solutions, allowing them to form a homogeneous phase. In contrast, non-aqueous samples can be challenging for PSm, in particular when no crosslinker is present, as some organic matrices might either extract the fluorescent solute or dissolve the PSm.
- Regulatory considerations: Concerning the REACH regulation (EC 1907/2006), PSm's have become a more environmentally friendly alternative to LSC cocktails. This regulation, which aims to protect human health and the environment from chemical risks, does not directly affect the compounds used in PSm preparation.
- Preparation and selectivity: Both LSC and PSm offer ease of preparation and optimum similar detection efficiencies. However, they both lack selectivity and require prior chemical separation to remove potential interferences.

The required chemical separations for analyzing alpha and beta-emitting radionuclides often make the procedures time-consuming, costly, and environmentally unfriendly, especially in the case of LSC. To address these challenges, Bagan et al. [48], developed the first plastic scintillation resins (PSresin) a few years ago, as a tool to perform separation and detection using the same material, showing promising results for the determination of radiostrontium, and more recently a newer one for technetium [49] for river and sea water samples. These PSresins are scintillating selective resins which unify the separation and measurement in a single step, reducing time, resources and wastes generations. These two mentioned PSresins are already commercially available by Triskem International. However, there remain significant interest in developing new analytical methodologies utilizing these existing materials, for new samples and radionuclides.

1.3. Plastic scintillation resins (PSresin)

PSresins are obtained by immobilizing a selective extractant on the solid surface of the PSm, combining the chemical separation and detection capacities into a single material. This integration reduces the overall cost of analysis, minimizes processing time, and significantly lowers the number of reagents required, eliminating the need for LSC cocktails and thus providing a more environmentally friendly alternative to conventional methods. PSresin selectivity depends on the selective extractant used in their preparation. This extractant can be a single compound or more than one that is immobilized on the PSm surface. PSresin can be prepared by impregnation or deposition of the extractant on the PSm surface or by linking the extractant to the polymeric support by covalent bonding [40].

1.3.1. PSresin characteristics

The usual way to work with PSresin consists of packing the PSresin into a column, usually a solid phase extraction cartridge. The PSresin cartridge is connected to a pump or vacuum chamber and it is conditioned with the working media. Afterwards, the sample is passed through it. Finally, a few rinses are performed with the same working media or other extra solutions, to remove possible interference. Once the separation is performed, the PSresin cartridge is directly placed on a 20 ml polyethylene vial suitable for scintillation, and directly measured. Fig 1.9 shows a scheme of the PSresin separation usage.

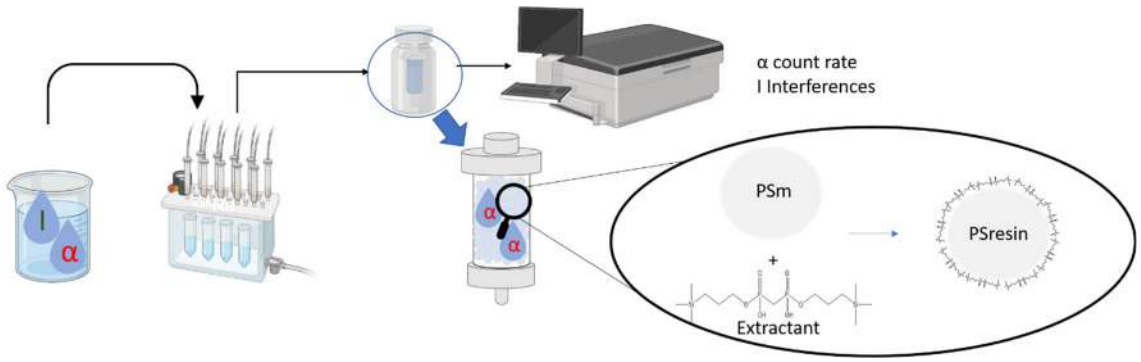

Fig 1.9 Separation and measurement scheme using PSresin

Once the separation has been performed, after the rinses step, it is important to ensure a complete solvent removal from the cartridge. The presence of solvent in the cartridge, attenuates the alpha and beta particles before reaching the scintillating microsphere, hence, leading to a decrease in the detection efficiency. The solvent removal is typically achieved by pumping the solution out, in the vacuum chamber.

To assess the yield retention with PSresin as well as with non-scintillating resin, the sample is spiked with a tracer, if possible, with the stable isotope. In case of no stable isotope, an analogous element must be found, which behaves in the same way as the target radionuclide. For example, europium is usually used for ^{241}Am. The tracer is then analyzed, before and after the sample passes through the column. Extraction chromatography resin sometimes might require previous coprecipitations, usually when analyzing large volumes of samples. In these situations, when working with PSresin the sample is spiked before the coprecipitation, and then it is measured before and after going through the PSresin cartridge. This is because the precipitation might not be quantitative, therefore, it is essential to know the coprecipitation yield and retention yield respectively. In those situations where the stable isotopes are present in the sample, if the initial amount is high enough, it could be directly used as a tracer, otherwise, the amount of tracer added has to be at least 20 times higher than the already present amount.

The use of PSresin, compared to conventional methods, has the advantage of unifying the chemical separation with the detection and not from suffering sample matrix effect as it is completely removed from the cartridge, leaving only the target radionuclide extracted, and ready to be measured. As a consequence, the detection efficiency is in general independent of the sample.

1.3.2. PSresin preparation

Immobilization

In the impregnation method, the selective extractant is dissolved in a volatile organic solvent, to which a known amount of PSms is added. The heterogeneous mixture is stirred for a few minutes and the organic solvent is slowly evaporated until the extractant coats the PSm surface. This evaporation can be forced or not with the use of a rotary evaporator. Sometimes the procedure is repeated several times to achieve a homogeneous coating on the polymeric support [40]. The PSm are coated with a thin layer of the selective extractant, attached to the support by weak forces. This strategy is widely used for resin preparation (scintillating or not).

The amount of extractant immobilized on the polymer support determines the maximum capacity of the resin for the target element and requires careful optimization. A thick layer of extractant on the PSm surface can increase the capacity, but it also raises the risk of particle quenching due to the greater distance between the radioactive particle and the scintillator. Moreover, it may lead to extractant weakly adhered to the polymer and problems with extractant leaching. A too-thin layer of extractant will lead to a poor capacity and usually a lack of homogeneity of the immobilized extractant on the PSm surface. Therefore, finding an optimal balance is essential to maximizing its characteristics.

In PSresin prepared by immobilization, the leaching of the extractant might occur, as it is attached to the surface of the PSm by weak forces. This can become an issue because large or low volumes of liquid, depending on the PSm-extractant-separation media interaction and affinity, could strip the extractant from the PSm surface, leading to a loss of the target radionuclide.

Covalent bounding

In this case, the selective extractant is linked to the surface of the polymer by a covalent bond. This implies the presence of reactive groups on the PSm, to perform the substitution reaction to link the extractant molecule. Typically, the reactive group is a chloride moiety as it is a good leaving group leading to efficient substitution reactions.

For this preparation, it is usually used PSm prepared by thermal radical polymerization with the incorporation of crosslinker compounds to confer extra stability and be more resistant to organic and aggressive media [46]. Chloride groups can be added during the polymerization of the monomer, where instead of only using styrene, 4-vinyl benzyl chloride is also added or by chlorination of the aromatic groups of the polymer. The reactive groups on the polymer surface are lately substituted by the extractant following the required reaction.

In PSresin prepared by covalent bound no leaching of the extractant should be observed, as the extractant is chemically bound to the polymer surface. However, the capacity of the final PSresin will depend on the number of reactive groups available for substitution. Steric hindrance caused by the size of the selective extractant can limit the number of reactive sites that are substituted. Additionally, unreacted groups can increase quenching. Thus, optimizing the substitution process is critical to enhancing resin capacity while minimizing quenching effects.

1.3.3. Current PSresin

Different PSresin based on the immobilization of selective extractants upon the surface of PSm have been developed, for radiostrontium (^{89}Sr and ^{90}Sr), ^{210}Pb, ^{99}Tc, etc.

Crown-ether PSresin

Crown ethers are cyclic arrangement of ethylene oxide (–CH_2CH_2O–) units, forming a flexible macrocyclic ligand. Each lone pairs of electrons of the oxygens, are strategically positioned to coordinate with a central cation via ion-dipole interactions. The geometrical compatibility between the cation and the cavity, coupled with the optimal alignment of the oxygen atoms' electron lone pairs, results in the formation of highly stable complexes. The selectivity of crown ethers depends therefore on the cavity size. Moreover, they can be mixed with extra compounds resulting in an extractant mixture that can fine tune the selectivity of them. In that sense, the dicyclohexano-18-crown-6 (DCH18C6) and di-tert-butylcyclohexano-18-crown-6 (DtBuCH18C6) have been widely studied for their binding affinity for strontium, in particular for the determination of radiostrontium, due to their high extraction ability and good selectivity at high nitric acid concentrations. These compounds have been used in the development of non-

scintillating resin developed by Horwitz et. al. and commercialized by Triskem International and Eichrom technologies, resulting in the Sr-resin, which uses as extractant a mixture of DtBuCH18C6, Fig 1.10, and 1-octanol, with a great extraction performance of radiostrontium [52]. Additionally, Triskem International developed few more resins based on this same crown ether used but in different solvents, modifying the behaviors and becoming more selective for one or another element. For example, TK-101 resin uses the DtBuCH18C6 together with a trade secret ionic liquid which makes the resin selective for ^{210}Pb at low-concentrated HCl media [53].

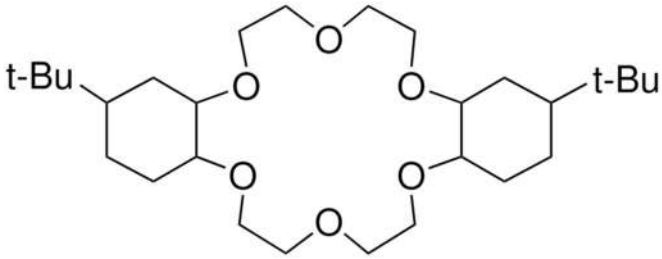

Fig. 1.10 4',4'(5')-di-t-butylcyclohexano-18-crown-6

Given the good performance of crown ether for radiostrontum isolation and determination over the last years, few PSresin have been developed for this purpose. The first resins used the SuperLig 620 commercial resin in their fabrication and two different approaches were studied. In the first one, the authors mixed the commercial SuperLig 620 resin with inorganic scintillating beads (cerium-activated lithium silicate glass scintillators), whereas in the second approach, the SuperLig 620 extractant was incorporated on commercial plastic scintillating beads by suspension polymerization, using 2-(1-naphthyl)-4-vinyl-5-phenyloxazole as a scintillator [50,51]. These two approaches were used for the development of microsensors for ^{90}Sr determination. Both resins had high strontium retentions 88 % and 92 % respectively, in low-concentration nitric acid (0.1 M). However, the detection efficiency was low 51 % and 63 %, respectively, due to the configuration of the resins.

Based on Sr-Resin, a PSresin was developed by immobilization of the same extractant (DtBuCH18C6 + 1-octanol) on the PSm surface. This PSresin had quantitative strontium retention in 6 or 8 M nitric acid concentration and an 83 % detection efficiency for ^{90}Sr, using 6 M $LiNO_3$ as the final rinse medium. This last medium is used to avoid

chemiluminescence produced by the plastic scintillator when high nitric acid concentrations are used [48].

This PSresin was applied to the determination of low-level activity samples for environmental monitoring such as drinking, river, and sea waters, with errors lower than 4%. Moreover, PSresin was applied in the determination of radiostrontium on more complex sample matrixes (milk, air filters, and vegetation), and activity levels were similar to the expected in case of emergencies, with errors lower than 7 % for spiked samples and reference materials. [40]. In those complex samples, a decrease of the retention yield to 70 %, was observed, especially in milk samples, due to high contents of calcium and stable strontium, which can bring the PSresin to saturation [54].

This PSresin has shown reliable performance and is a fast alternative to the conventional methods for radiostrontium measurement as the analysis takes less than 5-6 hours. Additionally, this PSresin also has an affinity for lead, leading to the possible determination of ^{210}Pb in 2 M nitric acid concentration with a retention yield of 90 % and a 44 % detection efficiency and quantification errors lower than 10 % [55].

This PSresin turns out to be a very versatile material with a very good performance for more than one radioisotope by modifying the working medium used. However, this can be a problem when measuring ^{90}Sr for environmental monitoring, which is an anthropogenic radionuclide, and the amount to be found can be null or low, whereas, ^{210}Pb, which is a natural origin radionuclide is always present in the environment, therefore, if a previous separation has not been performed, the measurement can lead to false positive results for ^{90}Sr, as the complete elution of lead while leaving retained strontium in the PSresin is not achieved. This is a situation for which there is still a need to develop an analytical method that allows a reliable measurement of ^{90}Sr, in environmental samples, in the presence of ^{210}Pb, as actual methods using PSresin do not allow a proper quantification of ^{90}Sr in presence of ^{210}Pb.

Aliquat·366 PSresin

Aliquat·336 (Fig 1.11) is a quaternary ammonium salt that has an affinity for tetra valent actinides and technetium. This extractant has been used by Triskem International and Eichrom for the development of the TEVA resin [34,56].

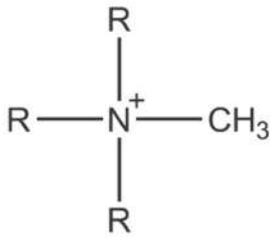

R=C_8H_{17} and $C_{10}H_{21}$

Fig1.11 Aliquat·336

This quaternary ammonium was also initially used for the development of a PSresin, by immobilizing Aliquat·336 and fluorescent solutes within the pores of an inert plastic support. This first approach was intended for ^{99}Tc, but it only had a 47 % detection efficiency as the fluorescent solutes were eluted. Lately, a few more scintillating resins based on aliquat·336 were developed by DeVol et al. by the immobilization of Aliquat·336 in PSm, as well as making a mixture of the commercial TEVA resin and commercial PSm. Among those trials, the immobilization of Aliquat·336 on commercial PSm, led to a 50 % detection efficiency while for the mixture of TEVA resin and PSm, a 7 % detection efficiency was obtained [57–59]. Finally, a PSresin was developed in our group in which Aliquiat·336 was immobilized on in-housed prepared PSm's. This PSresin had a quantitative retention of technetium as TcO_4^- with an 85 % detection efficiency in 0.1 M HCl, being lately commercialized by Triskem international under the name of TK-TcScint. This PSresin has been employed in the analysis of seawater and urine samples, with error values below 5 % for seawater and 8 % in the case of urine samples [49].

For Tc analysis, the retention yield is quantitative but the use of Re as a tracer is recommended, as it has a similar chemical behavior to Tc in the PSresin cartridge, and will allow the calculation of the retention yield. Additionally, in the case of uranium interference, rinses of a 0.1 M hydrofluoric acid and 0.1 M nitric acid mixture are

required, and in the case of ^{36}Cl interference an extra rinse with 0.5 M HCl must be performed [60,61].

1.3.4. Other PSresin

The main PSresin that have been developed, and had a good performance, were intended for beta-emitting radionuclides (^{90}Sr, ^{210}Pb, ^{99}Tc, etc..). However, few PSresin have been developed for the measurement of alpha-emitting radionuclides, aiming for the determination of the gross total alpha. One of the first scintillating resins developed used as extractant octyl(phenyl)-N,N-diisobutyl-carbamoyl-methylphosphine oxide (CMPO) dissolved in tributyl phosphate impregnated in a cross-linked polystyrene support with fluorescent molecules [62]. This PSresin demonstrated quantitative retention of target radionuclides in a 2 M HNO_3 medium, achieving detection efficiencies of approximately 97% with low quantification errors for high-level waste. However, the fluorescent molecules were prone to leaching, limiting the resin's application, and had short-term stability.

As an alternative Dipex, already used in non-scintillating resins, was evaluated as an extractant in two different approaches. The first approach consisted of a mixture of non-scintillating resin and commercial PSm, which led to unsatisfactory results and, hence, discarded. The second approach used Dipex as an extractant which was impregnated, together with fluorescent solutes, on the surface of polystyrene supports. This last approach had actinides quantitative retention in 0.1 M nitric acid, but detection efficiencies of 52 % and 66 % for natural uranium and ^{241}Am respectively [63]. This last approach led to quantification errors lower than 18 % for high-activity samples. Two more PSresins were developed for natural uranium determination. The first one used MnO_2 as an extractant, resulting in poor retention, 25 %, and low detection efficiency, 37 % [64]. The second one uses phosphonic acid covalently bound on a plastic scintillator surface, including a copolymerization of the plastic scintillator with ethylene glycol methacrylate phosphate and a polymerizable fluorescent molecule [65,66]. This second PSresin also led to poor retention capacity, 50 %, and a 40 % detection efficiency for uranium.

Currently, there are few PSresin developed for the analysis of beta emitting radionuclides which have a good performance. However, there are still more methodologies that can be developed using the already existing PSresins. For example, in the case of crown ether-PSresin, a new method for the analysis of ^{90}Sr in the presence of ^{210}Pb is required. Additionally, the Aliquat·336-PSresin is known to have an affinity for actinides, therefore, a new analytical method could be developed for the analysis of alpha-emitting radionuclide for which there is a lack of PSresin with good performance.

It is important to stand out, that even the great efforts made for the development of PSresin for the determination of alpha-emitting radionuclides, none of them, had a great performance capable of being an alternative to conventional methods, usually due to a lack of proper scintillating capabilities. Therefore, the development of new PSresin, or scintillating material, is required for alpha-emitting radionuclides and all those elements for which conventional methods fall short.

This development can be done based on the idea of PSresin, which has proven to be an excellent option, or by studying the addition of scintillating properties to other selective materials, such as imprinted polymers.

1.4. Imprinted polymers (IP)

Imprinted polymers (IP) are polymers used for the selective separation of a target element. These polymers were developed based on the concept of molecular recognition, where a specific cavity is produced to match the target element. The specific cavities are produced during the preparation of these types of polymers by the introduction of a template molecule for which the polymer will be selective, together with the rest of the compound. After polymerization, the template is removed, leaving behind the specific cavity in the polymer's structure. This cavity has a high affinity for molecules that are similar to the template, allowing the imprinted polymer to selectively bind those target molecules (see Fig.1.12).

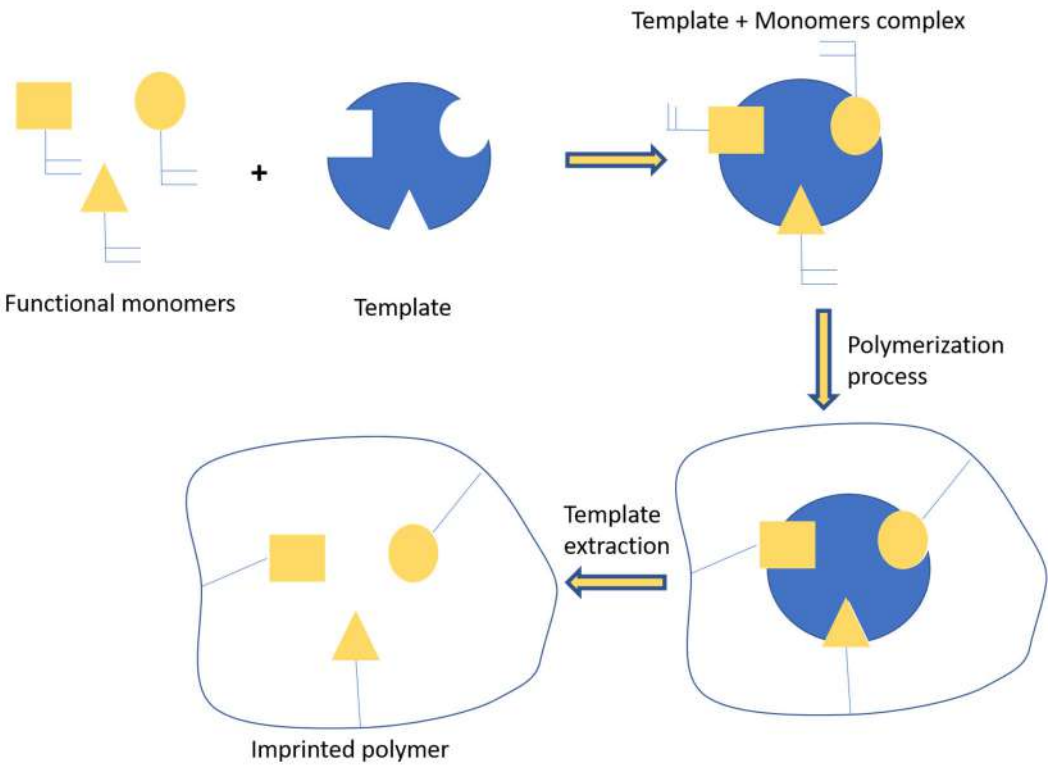

Fig1.12 Imprinted polymer concept scheme

Selective recognition of imprinted polymers arises due to a physical phenomenon, the cavity shape, left by the extracted template, not depending on selective extractants. The rigidity of the polymer enhances the specificity of the resulting cavity, preventing interferences with similar shapes or atomic or molecular weights from entering and

interacting with it. A flexible polymer matrix may alter its cavity structure over time or under stress, reducing the ability of the target molecule to rebind effectively, leading to lower sensitivity and efficiency. Additionally, the recognition capacity can be enhanced by complex formation with chelating agents in the cavity increasing the recognition selectivity and bounding strength by hydrogen bonding, dipole-dipole, and ionic interactions.

The key advantages of imprinted polymers lie in their chemical stability, robustness, reusability and no need of selective extractants. An IP can have several uses. As crosslinked polymers, they can withstand high temperatures, extreme pH conditions, and organic solvents. Additionally, imprinted polymers are highly customizable materials, allowing for tailored responses to the analysis of the target element.

There are few developed imprinted polymers used in the chemical separation of radionuclides, such as the one developed by Froidevaux et al. for ^{90}Y with an imprinting cavity made of [Y(6-(4-Vinylphenylcarbamoyl) pyridine-2-carboxylate)3] in a crosslinked-polystyrene backbone with a capacity up to 8 mg · g^{-1} IP and yttrium separation yields of 80 % [67]. Alternatively, Sadeghi and Mofrad developed an imprinted polymer for uranium as uranyl, using piroxicam and 4-vinylpyridine for the imprinting cavity in a polystyrene backbone, with a maximum uranyl capacity of 35 mg · g^{-1} IP and a chemical separation yield of 98 % [68].

1.4.1. Imprinted polymer components and characteristics

Different reagents are used for the development of IP, with the template molecule playing a pivotal role [69,70]:

- Template molecule: It is the molecule that serves as the target molecule or ion for which the imprinted polymer is designed.
- Monomer: It is a polymerizable molecule containing one vinyl group. The monomer is in charge of the polymer backbone. Usually, monomers are used together with crosslinker molecules.
- Crosslinker: It is a monomer but with two or more vinyl groups within their structure. This makes possible the reaction of these molecules from more than one site facilitating the creation of a three-dimensional

network on the polymer. This confers stability and rigidity to the polymer matrix, something very needed in imprinted polymers to assure the selectivity of the cavity.

- Chelating agent: It is a molecule in charge of increasing the selectivity recognition through the presence of functional groups. Chelating agents can be polymerized on the polymer backbone, if it presents at least one vinyl group or just be trapped in the polymeric network, if no vinyl groups are present.
- Additives: It refers to all those extra compounds used to modify the properties of the final IP, depending on the final intended application.
- Porogen: It is usually an organic solvent used for the increase of the porosity of the resulting IP.
- Initiator: Its role is to generate primary free radicals which then initiate the polymerization chain reaction among the polymerizable compounds.

After preparing the imprinted polymer, the template must be extracted with certain considerations in mind:

- Nature of the template-polymer interaction: If it is a non-covalent interaction a cleaning solution, aqueous or organic, which can disrupt the interaction is enough; in the case of covalent interactions, a chemical reaction is needed to break the bond, which can be very challenging.
- Polymer stability: the solution used for the template removal must leave the polymer stable and intact under the chosen temperature and pH conditions. Processes that might cause swelling, degradation, or other changes in the polymer must be avoided.
- Environmental considerations: Highly toxic or hazardous compounds should be avoided unless necessary.

Soxhlet extraction, ultrasonication, and acid-base washings are some of the common strategies for template removal.

1.4.2. Types of IP

There are two types of imprinted polymers: the molecular-imprinted polymers (MIP) and the ion-imprinted polymers (IIP) [69,71–75].

MIPs are focused on the recognition of organic molecules, proteins, and biomolecules, whereas IIPs are focused on ionic compounds. The interaction mechanism in MIPs is predominantly hydrogen bonds and Van der Waals forces and the binding site keeps the three-dimensional shape of the biomolecule, whereas in IIP the interaction mechanism is based on ionic and coordination interactions. In particular, for radioactivity analysis, IIPs are the most suitable ones as radioisotopes are usually found, in nature, as ionic species.

1.4.3. IIP elaboration

IIP can be elaborated following different strategies (see Fig 1.13): chemical immobilization, trapping, and surface imprinting [72,73,76].

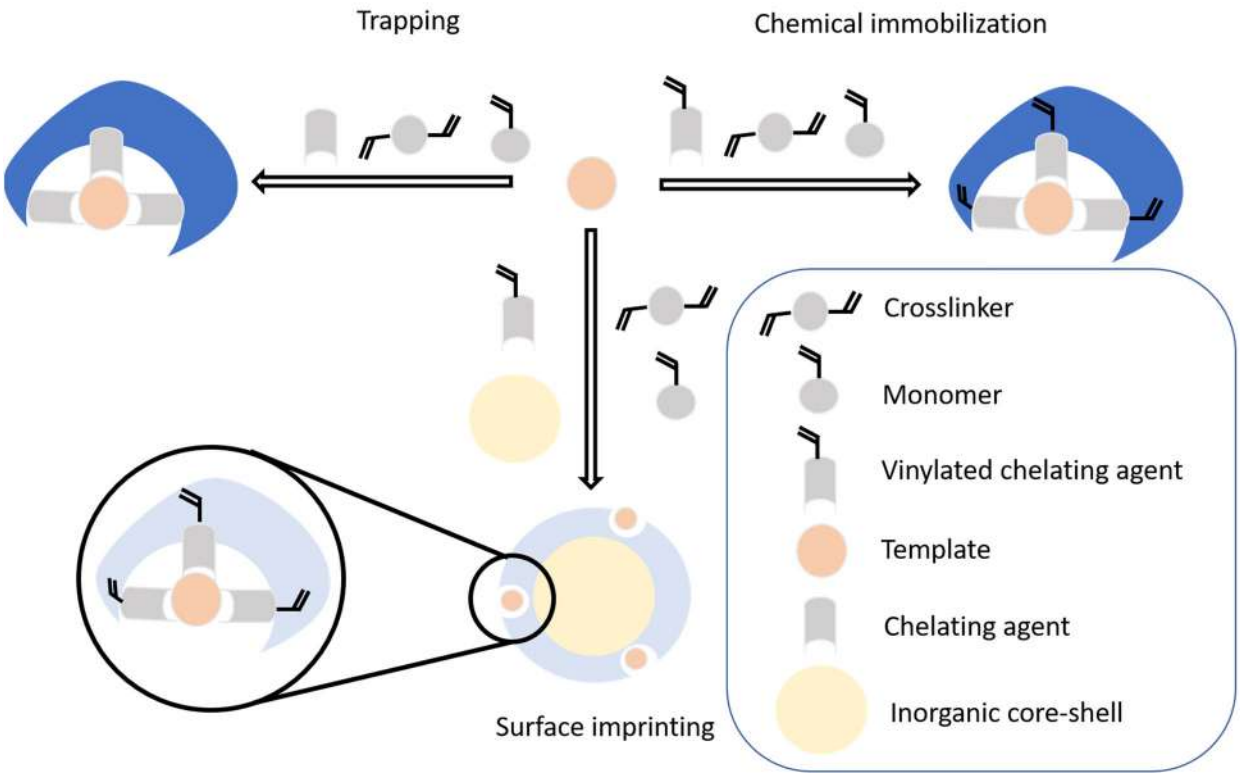

Fig1.13 Different IIP elaboration approaches.

Chemical immobilization

Chemical immobilization consists of chemically bounding the chelating agent in the polymer matrix. The chelating agent must contain at least one vinyl group, which allows its polymerization on the polymer backbone. This strategy can be implemented following two different procedures:

The first procedure consists of the previous preparation of a binary complex between the polymerizable chelating agent and the target metal ion, which is used as a template. The resulting binary compound is then polymerized with the rest of the elements to form the polymer (monomers and crosslinkers). The advantage of this procedure is the knowledge about the amount of complex added. Some drawbacks are the need for specific conditions for the dissolution of the binary complex previously prepared and the possibility that the binary compound polymerizes on its own.

The second procedure is a one-step synthesis, mixing all the compounds that take part in the final polymer (monomers, chelating agents, template, crosslinkers, etc.). This type of synthesis is also known as a one-pot reaction. The advantage of this procedure is its simplicity and this is why it is widely used. The counterpart of this procedure is the lack of knowledge about the amount of complex (template + chelating agent) that has been formed.

Trapping

The trapping strategy involves using a non-vinylated chelating agent, which will not be polymerized into the polymer matrix. This strategy is particularly useful when there are no vinylated chelating agents available for the target template or the complex formed is not stable. There is the possibility of adding vinyl groups to a promising chelating agent but this approach is not straightforward and often involves high-cost reactions with low recovery yields. As in chemical immobilization, the complex between the template and the chelating agent can be prepared in advance (binary compound) or in-situ by performing a one-pot reaction.

This strategy offers a wider list of possibilities for chelating agents with a strong affinity for the template. However, as it is not chemically bound to the polymer matrix, the chelating agent can be leached during the ion template removal or during the use of

the IIP when passing the sample, or it might not be homogenously distributed on the polymer, which will decrease the recognition capacity. Techniques like microanalysis, FTIR, or X-ray spectroscopy analysis can confirm the correct trapping of the compound on the polymer matrix.

Surface imprinting

The last approach for IIP elaboration is surface imprinting. This is a double-shell polymer in which the IIP is polymerized on the surface of an inert polymeric support. The core shells are usually inorganic compounds, such as silica gel particles, due to their higher stability to aggressive or organic media. For the top layer, vinylated chelating agents are used as they can be polymerized on the core-shell surface.

In Surface imprinting polymers all specific cavities are on the polymer surface, making all of them more accessible to the target element. Moreover, in the case of using inorganic core-shells, the number of monomers and crosslinkers used is lower, as only a layer is polymerized. However, in this strategy, the final target element capacity can be lower compared to the other two methods, as fewer specific cavities can be generated. In addition, the presence of cavities on the polymer surface makes them more susceptible to being modified or destroyed after a few uses. In addition, the core shell can modify the selectivity as it can interact with the template or even with other compounds.

1.4.4. Polymerization methods

The polymerization method may differ depending on the desired final shape and size of the polymer. This may also affect the properties of the resulting IIP. The polymerization methods are: bulk, heterogeneous, and homogeneous polymerization [69,72].

Bulk polymerization

Bulk polymerization is one of the most widely used methods for IIP preparation. It consists of mixing all the reagents that will take part in the IIP composition (monomers, crosslinkers, templates, etc.) in a vial or a bottle to be slowly polymerized. The

polymerization is performed by applying a temperature ramp without stirring. The resulting material is an irregular block that must be crushed and sieved to obtain fine particles.

This method is characterized for being easy and simple and easy to scale up. It allows the preparation of several IIPs at the same time; therefore, it is an interesting method for screening IIP conditions. However, this method does not use any kind of extra compounds apart from the monomer the crosslinker and the chelating agent, which can make difficult the preparation of a homogeneous phase due to solubility or miscibility problems. The crushing and sieving steps can be very time-consuming and, in the process, some of the specific cavities can be destroyed due to mechanical and thermal stress. The final obtained particles might not be homogeneous and some of the specific cavities can be too deep on the polymer matrix being not accessible for template extraction or posterior bounding.

Heterogeneous polymerization

Heterogeneous polymerization consists of using two immiscible phases, the dispersed and the continuous. There are two different types of heterogeneous polymerization, suspension and emulsion.

- Suspension polymerization: In suspension polymerization the continuous phase is typically water with a stabilizer (polyvinyl alcohol (PVA) as surfactant example) which induces the suspension of the dispersed phase. The dispersed phase is an organic solution that contains the monomer, the template, the crosslinker, the initiator, etc. Both phases are mixed and let polymerize while stirring resulting in an IIP in the form of microbeads.
- Emulsion polymerization: Emulsion polymerization is quite similar to suspension polymerization, with just small differences: the initiator must be dissolved in the continuous phase; therefore, it must be water soluble (e.g. potassium persulfate); and the surfactants are added to the dispersed phase.

Heterogeneous polymerization is a strategy that avoids the crushing and sieving steps. The use of solvents can facilitate the solubility of the template and additives in the dispersed phase, increasing the number of reagents that can be potentially used. The particle size can be controlled by the ratio between the continuous and dispersed phases, the stabilizer or surfactant concentration, and the concentration of the monomers and crosslinkers used in the dispersed phase. Nevertheless, this method requires continuous stirring, therefore, there is a need for more sophisticated equipment and the polymerization yield might be lower than in the case of bulk polymerization. In addition, the use of two non-miscible phases can lead to a partial loss of the template, because of its ionic nature, it could be solubilized in the continuous aqueous phase. This could be translated into the loss of selective recognition.

Homogeneous polymerization

In a homogeneous polymerization, all components are dissolved in a suitable solvent in which the polymerization is performed. The most important is precipitation polymerization.

Precipitation polymerization is the second most used polymerization method after the bulk polymerization given its simplicity. It consists of mixing all the reagents that will take part in the IIP composition in a vial or bottle with a large volume of organic solvent. The solution is then heavily stirred while applying a temperature ramp. As the polymer starts to form it precipitates in form of small beads. The size of the beads depends on the ratio between the IIP compounds and the solvent. Therefore, there is no need for further steps for crushing and sieving the polymer, similar to heterogeneous polymerization. However, depending on the solvent required homogeneity problems can be faced, in particular when using ionic templates, which can hinder an optimum imprinting process.

1.4.5. Scintillating IIP

Imprinted polymers have been already developed for the chemical separation of different elements, mainly for stable elements such as iron, lead, etc. with high selectivity and chemical separation yields. Given the good separation performance, the

development of a scintillation version of the IIP polymers, akin to the PSresin, would allow the development of scintillating materials, for those elements for which there are no selective extractants available or their synthesis is too expensive.

To confer scintillating capabilities to an IIP, it should have aromatic compounds in their structure, to be excited by the radioactive particle and pass this energy to the fluorescent solutes. Fluorescent solutes must be trapped inside the IIP, or vinyl groups can be added into them by synthetic modifications, but this may hamper the process. Additionally, when deciding the different compounds that will take part in the IIP composition, those compounds that are prone to cause quenching phenomena should be avoided, such as colored compounds. Finally, the shape and size of the aimed Sc-IIP is an important consideration, and based on the experience with PSresin, the microsphere shape with a size range between 10 to 100 μm should have the best scintillating performance.

To date, there does not exist a proper scintillating imprinted polymer for radionuclide determinations, but there is one developed by Lei et al. [77] where a scintillating molecular imprinted polymer for radiolabeled (S)-propranolol recognition was developed. The developed polymer incorporates an organic scintillator and an antenna (which acts as the organic solvent in the scintillating mechanism, and gets excited when the radiation arrives) in substitution with the aromatic organic solvents near the imprinted binding sites. Once the radioactive template was bound to the polymer, the radiation energy was effectively transferred, via the antenna component to the scintillator to the generation of the fluorescence signal. This material approach was developed for biological purposes but not for radioactivity measurement itself. The authors described that the developed imprinted polymer generated a typical dose-response curve with half of the maximum proximity scintillation counts (PSCs) at a 2 mg polymer concentration, with a 30 % template recognition and a 2 % of cross reactivity. This approach of Lei et al., even though the template recognition could be improved, demonstrates the possibility of incorporating scintillating capacities into an imprinted polymer.

1.5. Computational chemistry techniques for the development of new resins

The determination of beta and alpha-emitting radionuclides always depends on a previous chemical separation to isolate the target radionuclide. This chemical separation can be performed by different techniques, being extraction chromatography the most common one. As an alternative, PSresin has been developed over the last decades based on the same chemical separation principle including scintillating properties. The development of these types of materials, scintillating or not, always entails long trial periods of different extractants looking for the one that allows the specific separation of the target element with high selectivity. This task is challenging as depends on the availability of commercial extractants or the synthesis of them in the laboratory, requiring significant time, effort, and economic investment.

To mitigate the risk of investing excessive time, effort, and money into unsuccessful trials, computational techniques can be employed as a preliminary step. By using simulations, researchers can identify which compounds are likely to meet the desired criteria, in this case, a favorable radionuclide-extractant binding, allowing them to focus their efforts only on promising candidates. This approach streamlines the development process, making it more efficient and cost-effective, ultimately leading to the creation of more functional materials [78].

Computational methods play an important role in modern scientific research by enabling the simulation and analysis of molecular and atomic behavior. These methods utilize various theoretical frameworks based on:

- Fundamental description of atomic and molecular behaviors, typically, Ab initio quantum mechanics. This method employs rigorous mathematical principles to solve the Schrödinger equation, providing highly accurate predictions of molecular properties. However, Ab initio methods are computationally intensive and are typically reserved for small systems.
- Molecular mechanics, which rely on a combination of empirical data and mathematical models to understand the interactions between atoms and

molecules. This method offers computational efficiency and is suitable for simulating larger molecular systems.

- Semiempirical methods that strike a balance between accuracy and computational cost by combining Ab initio and empirical approaches. These methods use simplified models and parameters derived from experimental data, making them suitable for studying medium-sized molecular systems [79].

In essence, computational chemistry relies on mathematical descriptions to elucidate the behavior of atoms and molecules. Various computational techniques exist, each with its strengths and weaknesses. There is no one-size-fits-all method that guarantees perfection across all scenarios. However, by combining different methods, researchers can achieve a high level of performance with enhanced accuracy while saving significant time and resources.

The selection of a specific computational method depends on the nature of the research task and the available computational resources, considering factors such as the size and complexity of the molecular system and level of accuracy required.

In particular, for the assessment of organic molecules to be used as resin extractants for the extraction of metals from an aqueous solution, two strong methodologies can be used: The density functional theory (DFT) and molecular dynamics (MD).

1.5.1. Density functional theory (DFT)

Quantum mechanics computational methods include semiempirical and ab initio calculations to describe the behaviour of electrons in the studied system by solving the Schrödinger equation. The solving of the equation becomes incredibly challenging when more than one electron is involved, making it impossible to solve for almost all systems. To handle this, different approximations are used. The accuracy and reliability of the obtained solution in any quantum mechanical method will directly depend on the quality of these approximations (the approximation is searched to be as small as possible). Ab initio calculations do not require any kind of empirical parametrization while semiempirical calculations use empirical parametrizations.

DFT was developed by Walter Khon, Pierre Hohenberg, and Lu Jeu Sham. DFT does not focus on solving the many-electron wavefunction but instead uses the electron density of the system as a fundamental variable to solve. DFT rests on the idea that the properties of a system are determined by the electron density. This is derived from a function (or a function of functions) of its electron density which as a consequence the computational complexity scales with the number of electrons involved, N, allowing the application of quantum mechanics computational methods to larger molecules and supramolecular systems compared to other quantum methods.

To understand the affinity and capability of an extractant with a target element, DFT calculations can be used for the simulation of metal-host interactions. This simulation allows for the understanding of how metal atoms or ions interact with surrounding molecules and how these interactions affect their binding or encapsulation of them. DFT in the area of host-guest simulations is frequently used to calculate the binding energy between the target element and the organic molecule, to understand the stability of the resulting complex. In addition, DFT calculations are used to determine the geometry of the resulting complex, to understand the binding configuration and to predict structural changes in response to the binding, which determine the coordination geometry. These features allow studying the selectivity of the system which is essential for an optimum isolation of the target radionuclide.

DFT has been used to assess the binding affinity of different radionuclides with a target extractant. Piechowicz et al. studied the affinity of $^{90}Sr^{2+}$, $^{137}Cs^{+}$, and $^{233}UO_2^{2+}$ with bis-amidoxime polymers. In this study the authors were able to conclude that the bis-amidoxime ligand had a poor affinity for both strontium and caesium while a high affinity for uranyl, through the study of the Gibbs free energy. The DFT simulation results were successfully proved through experimental data proving the prediction capability of DFT calculations [80]. Liu et al studied the interaction of cerium, americium, and curium cations with crown ethers revealing a good agreement of the structure of cerium-crown ether matching with that from experimental data and showing comparable binding energies for americium and curium crown ether complexes with the cerium crown ether complex [81]. Even though DFT calculation can properly predict the affinity between a metal and an organic molecule, all the simulations are done in gas-phase, which means

that there is not the direct implication of solvent molecules and temperature. Jing et al. studied the selectivity of 18-crown-6 ether to Na^+, Li^+, K^+, Rb^+, and Cs^+ where the authors concluded that the metal ions selectivity followed the sequence, $Li^+ > Na^+ > K^+ > Rb^+ > Cs^+$. However, when the authors performed the same simulation but considering the solvent molecules and temperature, using MD simulations, the selectivity sequence change to $Li^+ << Na^+ < K^+ > Rb^+ > Cs^+$, resembling much more experimental data [82]. Thus, DFT is a strong simulation tool but there are cases where the presence of solvent and temperature can strongly modify the affinity making them more reliable with MD simulations.

1.5.2. Molecular dynamics (MD)

MD provides insights into how a system behaves over time, relying on fundamental physical models governing interatomic interactions. MD simulations are particularly adept at capturing dynamic phenomena such as conformational changes and ligand binding, offering a detailed view of atomic positions throughout the studied process, considering the temperature, the pressure and the solvation effect.

MD calculates the forces acting on each atom due to all the other atoms in the system. By applying Newton's laws of motion, the spatial positions of each atom can be predicted as a function of time. This computational process unfolds in discrete time steps, with forces on each atom computed iteratively to update their positions and velocities. The resulting trajectory essentially forms a three-dimensional "movie" depicting the atomic-level configuration at every time point of the simulated interval [83]. While MD simulations follow deterministic principles, the initial conditions, such as atomic positions and velocities, often involve random sampling based on a desired distribution (e.g., Maxwell-Boltzmann for velocities), which can introduce variability in the resulting trajectories.

MD simulations rely on a series of components to do the computational process. These include integration methods, periodic boundary conditions, neighbor searching, constraints, thermostats, and barostats, among others.

- Integration method: The integration method determines how the equations of motion are numerically solved. Two of the most commonly used are the

leap-frog integrator and the velocity-Verlet integrator, which were developed after modifications to the original Verlet algorithm.

- Periodic Boundary Conditions (PBC): These conditions allow a finite simulation box to effectively model an infinite system by replicating the box in all three dimensions. The use of PBC allows us to bridge the gap between a microscopic system and the macroscopic world.
- Neighbor Searching: This algorithm is used to rapidly identify nearby atoms within a predefined cutoff radius, enhancing computational efficiency. A common rule in periodic boundary conditions is the "minimum image convention," which ensures that each atom interacts only with the nearest image of another atom, except for long-range electrostatic interactions.
- Constraints: Constraints algorithms are used to keep specific bonds at constant lengths, preserving the structural integrity of the molecules. Two of them are the SHAKE and LINCS algorithms. The first one is characterized as being an iterative and highly accurate method suited for simple molecular systems, and the LINCS is a non-iterative method efficient for large systems.
- Thermostats and barostats: These tools regulate the system's temperature and pressure, respectively, to simulate experimental conditions accurately.

MD simulations rely on force fields to calculate forces between atoms. Force fields are a set of ideal values considering interaction parameters for bond stretching and bending, as well as less obvious factors such as torsion and through-space interactions. These interactions are parameterized based on ideal values tailored to each atom type in a given molecular environment. Atom types, representing specific elements within the molecule, play a pivotal role in force field parameterization. Ideal values are determined through experimental data, such as spectroscopic or crystallographic measurements, and from quantum mechanical calculations ensuring accuracy and reliability in force field predictions.

One of the main fields where MD is particularly employed is the area of drug discovery. A drug-ligand interaction is simulated to study its behavior in the desired working medium and temperature. At the qualitative level, simulations can provide useful information to identify the key interactions or predict the rearrangement of the

ligand. At the quantitative level, MD can be used to show the ligand binding affinity through free energy calculations. Free energy calculations are useful for describing the energy available for work under different constraints, associated with the transfer of molecules from one environment to another. The free energy of a system is perhaps the most important thermodynamic quantity, and is usually taken as the Helmholtz (systems where volume is constant) or Gibb's (systems where pressure is constant and work includes expansion or compression) free energy.

This idea could be applied as a virtual screening, where a set of ligands are simulated to bind a target checking the affinity and the viability of each one. For example, Chaumont and Wipff used molecular dynamics simulations to study the effect of ionic liquids in the extractions of strontium nitrate crown ethers complexes considering solvation effects, temperature, and dynamics stability with results in agreement with the classical extraction and ion exchange mechanism [84].

Free energy estimation can be obtained following different strategies, one usually used is enhanced sampling techniques, in particular: the umbrella sampling and metadynamics.

1.5.2.1. Enhance sampling techniques

Enhanced sampling techniques are computational methods designed to address the limitations encountered in traditional MD simulations. These limitations include slow convergence, difficulties in sampling rare events, and inadequate exploration of the system's phase space. Enhanced sampling techniques provide strategies to overcome these challenges and improve the effectiveness of molecular simulations [85].

Umbrella sampling is designed specifically for investigating processes characterized by high energy barriers. For instance, consider a molecule with two conformations, A and B. If the energy barrier between these conformations is too high, traditional MD simulations may have difficulties passing from transition A to B (See Fig. 1.14). In such cases, the system may remain trapped in conformation A indefinitely, unable to overcome the energy barrier or the transition process may proceed at an exceptionally slow pace [86,87].

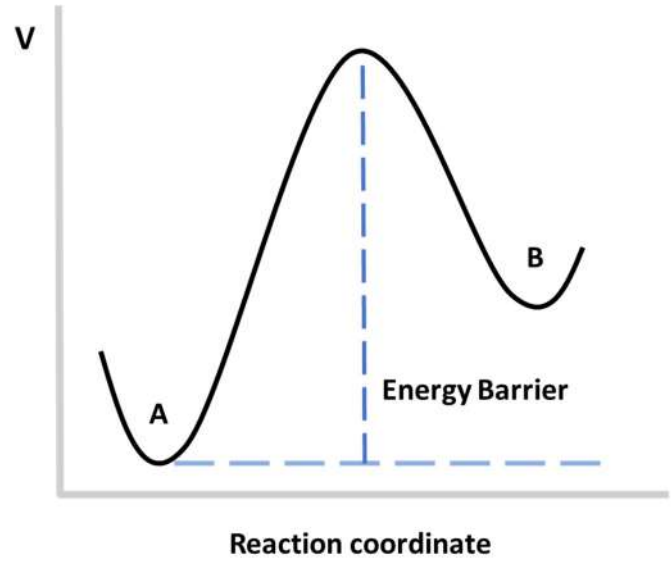

Fig 1.14 Example of a potential energy profile for a reaction process from A to B

This underscores the importance of achieving more efficient sampling by accelerating the dynamics to populate state B. To execute this effectively, a clear understanding of the coordinate that drives the reaction is needed. As an example, in a metal-ligand binding simulation, the reaction coordinate could be the distance between the center of mass of the ligand and the metal when both are in a bounded situation, which can be estimated previously by other tools, and the position where it is unlikely for them to interact. Once the reaction coordinate is chosen, it is divided into several windows forcing the simulation to sample each window along the whole trajectory.

Once the reaction coordinate is split into windows (n), an artificial potential is added to the unbiased potential, giving as a result a final biased potential. Usually, it is a harmonic potential function that depends on the reaction coordinate (Eq. 1.13).

$$V^b = V^u + \omega(\zeta) \rightarrow V^u + K_i(\zeta_i - \zeta_0)^2 \quad \text{(Eq.1.13)}$$

Where V^b refers to bias potential, V^u refers to unbiased potential, K_i refers to the force constant and used $\zeta_i \; and \; \zeta_0$ refers to the final (i) and initial(o) reaction coordinate variable.

This artificial potential applied is pivotal for confining the system within predefined windows during the molecular dynamics simulation. The force constant determines both the effectiveness of biasing the system and the number of windows into which the reaction coordinate needs to be split. Selecting a small force constant may render the bias potential insufficient to surpass energy barriers while opting for a large value could result in a narrow distribution of the biased potential. Consequently, to accurately compute free energy profiles, it becomes necessary to include numerous additional windows to ensure adequate overlap between neighboring regions. This approach can be computationally demanding. Hence, striking a balance between the force constant and the number of windows is essential. Typically, this balance is achieved through iterative trial-and-error processes, involving running short simulations until an optimal distribution overlap is attained.

When the simulation within the first window is completed (from 0 to i), the equilibrium value of the reaction coordinate is adjusted to transition to the next window (i to i+1), and a new simulation is initiated to calculate a new biased potential (Vi). This process is iteratively repeated across all the windows defined by the reaction coordinate until achieving the final point (n-1 to n). As a result, multiple molecular dynamics simulations are conducted at different points along the reaction coordinate range.

After collecting data from each window in the umbrella sampling simulations, one can compute the probability distribution along the reaction coordinate by calculating the frequency of the system visiting specific reaction coordinate values. With this biased probability distribution in hand, it is possible to calculate the unbiased free energy for each window along the reaction coordinate using Eq.1.14.

$$G_i^u(\zeta) = -\frac{1}{\beta} ln P_i^b(\zeta) - \omega_i(\zeta) + F \qquad \text{(Eq.1.14)}$$

Where $G_i^u(\zeta)$ represents the free energy for each window, β is the inverse of the Boltzmann constant and the temperature, $P_i^b(\zeta)$ refers to the biased probability distribution in each window, $\omega_i(\zeta)$ refers to the artificial applied harmonic potential in

each window and F is a constant which represents the free energy offset, which ensure that the profile is defined up to an arbitrary constant.

To reconstruct the global unbiased free energy profile through the entire reaction coordinate, the Weighted Histogram Analysis Method (WHAM) can be used. WHAM facilitates the combining of data collected from different windows, enabling the generation of a comprehensive, unbiased free energy profile along the reaction coordinate. For example, Sormani et al., used umbrella sampling techniques for the study of zirconium coordination with DFO and 4HSM ligands, leading to the understanding of the complex formation mechanism, the interaction of the solvent, and the affinity for each ligand [88].

Another enhanced sampling technique is metadynamics. Metadynamics operates by dynamically constructing a bias potential on-the-fly, based on a set of chosen collective variables. This bias potential guides the exploration of the potential energy landscape of the system, facilitating the sampling of rare events and accelerating convergence in molecular simulations. It was developed by Laio and Parrinello to improve the capacity of sampling and explore situations that classical molecular dynamics do not reach without meaning a high computational cost and time [89–91].

For metadynamics methods, it is extremely important to have an idea of the degrees of freedom that are relevant to the process because a collective variable or set of collective variables has to be selected before beginning the simulation, for example the coordination number between the extractant molecules and the target element or the distance between the center of masses of the extractant and the target element. Within the space of collective variables, Gaussian functions are regularly added to the potential of the system with an invariant deposition rate.

At the outset of the simulation, the system finds itself locked in a state of confinement, in a relative or absolute minimum of energy. Then, as time elapses, Gaussian functions are progressively incorporated into the potential, increasing its magnitude. Eventually, the accumulated biased potential surpasses an energy barrier separating distinct states, corresponding to a relative or absolute maximum, prompting the system to transition into a new relative or absolute minimum, which otherwise

would not be reached. It could be said then that in the metadynamics procedure, the basins of the potential energy surface are progressively filled, allowing the system to evolve from the initial state to the rest of the possible states (Figure 1.15).

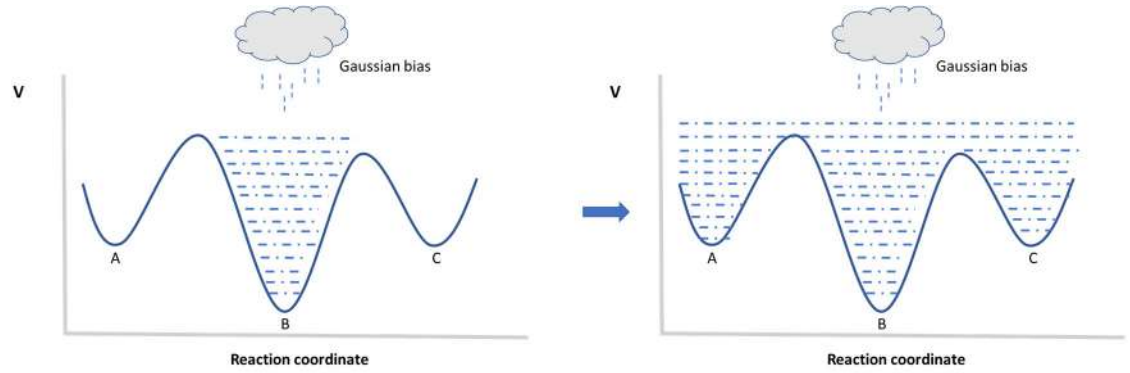

Fig1.15 Graphical representation of how Gaussian bias fills the basins of the potential energy surface

After the Gaussians accumulation, the plot of the number of Gaussian functions overtime during the simulation shows that, given enough time, the shape of the Gaussians starts to resemble the potential energy surface. Notably, it has been demonstrated that the bias potential converges to the negative of the unbiased potential, despite being offset by a constant. However, achieving satisfactory convergence necessitates multiple iterations, as the process does not smoothly converge to the free energy surface.

The bias Gaussian potential that is added remains fixed, lacking explicit control over the rate of bias potential accumulation. This rigidity may result in oversampling certain regions of the energy landscape, thereby impeding simulation convergence. To address this limitation, well-tempered metadynamics has been developed, offering a refined approach through the incorporation of a bias factor known as the well-tempering factor.

This parameter dynamically adjusts the height of Gaussian hills during the simulation, effectively curbing the accumulation of excessive bias potential and promoting a more balanced and uniform sampling across the landscape. By striking a delicate balance between exploration and convergence, the well-tempering factor facilitates smoother progression through the energy landscape.

Metadynamics allows the study of host-guest interactions by the study of the free energy, conformation, and evolution through time, as well as to identify the binding cavity. Nutho et al. used metadynamics simulations to study the dynamical behavior and binding affinities of complexes of eucalyptol with native beta-cyclodextrin(βCDs) and its derivatives. In the inclusion complex, eucalyptol is preferentially located within the hydrophobic cavity with the βCDs and derivative studied. Additionally, the structural and dynamical inclusion behavior of the complexes as well as the energetic details about host-guest interactions were simulated providing support information to experimental data[92]. Alternatively, Shadrack et al. studied the solvent effects on host-guest residence time and kinetics on Toussaintine-A unbinding from chitosan using well-tempered metadynamics and thermodynamic integration using two different solvents, DMSO and water [93].

Therefore, the use of molecular dynamics together with an enhanced sampling technique could be used to predict the interaction and affinity of a targeted radionuclide with a candidate extractant, considering certain experimental conditions as boundaries on the simulation, helping in the development of new resins, by streamlining the process and reducing the time and cost involved in the preparation of new extractants for the intended resins.

1.6. References

[1] L'Annunziata, Michael F. Radioactivity: introduction and history, from the quantum to quarks. Elsevier, 2016, ISBN-10 0444634894.

[2] M.C. Malley, Radioactivity: a history of a mysterious science, OUP USA, 2011. ISBN-10 019976641X.

[3] M.J. Ortega Aramburu, J. Jorba Bisbal, Las Radiaciones ionizantes: utilización y riesgos, 2nd ed., Edicions UPC, 1994. ISBN 9788483010884.

[4] José M. Sánchez Ron, Marie Curie, la radioactividad y los Premio Nobel, Anales de Química de La Real Sociedad Española de Química (2011) 107(1) 84–93. ISSN 1575-3417.

[5] M. García-León, Detecting Environmental Radioactivity Graduate Texts in Physics, Springer Nature, 2022. ISBN-10 3031009972.

[6] J. Lehto, X. Hou, Chemistry and analysis of radionuclides: laboratory techniques and methodology. John Wiley & Sons, 2011. ISBN 9783527326587.

[7] T.B. Greenslade, Simulated secular equilibrium, Phys Teach 40 (2002) 21–23. https://doi.org/10.1119/1.1457823.

[8] J. Masarik, Chapter 1 Origin and Distribution of Radionuclides in the Continental Environment, Radioactivity in the Environment 16 (2009) 1–25. https://doi.org/10.1016/S1569-4860(09)01601-5.

[9] S. Mohan, V. Chopra, Biological effects of radiation in Radiation Dosimetry Phosphors: Synthesis, Mechanisms, Properties and Analysis, Elsevier, (2022) 485–508. https://doi.org/10.1016/B978-0-323-85471-9.00006-3.

[10] IAEA Safety Standards for protecting people and the environment General Safety Guide No. GSG-7 Occupational Radiation Protection (2018). ISBN 978–92–0–102917–1.

[11] Diario Oficial de la Unión Europea, Directiva 2013/59/Euratom del Consejo, de 5 de diciembre de 2013, por la que se establecen normas de seguridad básicas para la protección contra los peligros derivados de la exposición a radiaciones ionizantes, y se derogan las Directivas 89/618/Euratom, 90/641/Euratom, 96/29/Euratom, 97/43/Euratom y 2003/122/Euratom.

[12] E.P. Cronkite, G. Brecher, Radioactivity: Effects of Whole Body Irradiation, Annu Rev Med 3 (1952) 193–214. https://doi.org/10.1146/annurev.me.03.020152.001205.

[13] P. Vaz, Radiological protection, safety and security issues in the industrial and medical applications of radiation sources, Radiation Physics and Chemistry 116 (2015) 48–55. https://doi.org/10.1016/j.radphyschem.2015.05.012.

[14] S. Choudhary, Deterministic and Stochastic Effects of Radiation, Cancer Ther Oncol Int J 12 (2018). https://doi.org/10.19080/ctoij.2018.12.555834.

[15] X. Hou, P. Roos, Critical comparison of radiometric and mass spectrometric methods for the determination of radionuclides in environmental, biological and nuclear waste samples, Anal Chim Acta 608 (2008) 105–139. https://doi.org/10.1016/j.aca.2007.12.012.

[16] G. Steinhauser, K. Buchtela, Gas ionization detectors, Elsevier Inc., 2020. https://doi.org/10.1016/B978-0-12-814397-1.00002-9.

[17] T. Yanagida, Inorganic scintillating materials and scintillation detectors, Proc Jpn Acad Ser B Phys Biol Sci 94 (2018) 75–97. https://doi.org/10.2183/pjab.94.007.

[18] G. Lutz, Semiconductor radiation detectors, Springer, 2007. ISBN-10. 3540648593.

[19] F. Shimura, Semiconductor silicon crystal technology, Elsevier, 2012. ISBN: 9780124312494.

[20] N. Vajda, R. Pöllänen, P. Martin, C.K. Kim, Alpha spectrometry, in: Handbook of Radioactivity Analysis: Volume 1: Radiation Physics and Detectors, Elsevier, 2020: pp. 493–573. https://doi.org/10.1016/B978-0-12-814397-1.00005-4.

[21] E.E. Haller, Germanium: From its discovery to SiGe devices, Mater Sci Semicond Process 9 (2006) 408–422. https://doi.org/10.1016/j.mssp.2006.08.063.

[22] I. Hossain, N. Sharip, K.K. Viswanathan, Efficiency and resolution of HPGe and NaI (Tl) detectors using gamma-ray spectroscopy, Scientific Research and Essays 7 (2012) 86–89. https://doi.org/10.5897/SRE11.1717.

[23] N. Hafızoğlu, Efficiency and energy resolution of gamma spectrometry system with HPGe detector depending on variable source-to-detector distances, Eur Phys J Plus 139 (2024) 134. https://doi.org/10.1140/epjp/s13360-024-04903-y.

[24] S.C. Wilschefski, M.R. Baxter, Inductively Coupled Plasma Mass Spectrometry: Introduction to Analytical Aspects, Clinical Biochemist Reviews 40 (2019) 115–133. https://doi.org/10.33176/AACB-19-00024.

[25] V. Sharma, Ion Exchange Resins and Their Applications, Journal of Drug Delivery and Therapeutics 4 (2014) 115–123. https://doi.org/10.22270/jddt.v4i4.925.

[26] A. Mushtaq, Inorganic ion-exchangers: Their role in chromatographic radionuclide generators for the decade 1993-2002, J Radioanal Nucl Chem 262 (2004) 797–810. https://doi.org/10.1007/s10967-004-0513-8.

[27] J. Akaishi, A method for determination of plutonium in blood by anion exchange, J Nucl Sci Technol 6 (1969) 12–19. https://doi.org/10.3327/jnst.6.12.

[28] D.L. Stoliker, N. Kaviani, D.B. Kent, J.A. Davis, Evaluating ion exchange resin efficiency and oxidative capacity for the separation of uranium (IV) and uranium (VI), Geochem Trans 14 (2013) 1. https://doi.org/10.1186/1467-4866-14-1.

[29] K.-W. Kim, E.-H. Lee, Y.-J. Shin, J.-H. Yoo, H.-S. Park, Removal of residual uranium in simulated radwaste solution by TBP extraction, Sep Sci Technol 30 (1995) 3351–3362. https://doi.org/10.1080/01496399508013150.

[30] V. Sagar, K.V. Chetty, D.D. Sood, Extraction of plutonium (III) by TBP in presence of uranium, Solvent Extraction and Ion Exchange 18 (2000) 307–317. https://doi.org/10.1080/07366290008934683.

[31] P.-W. Huang, C.-Z. Wang, Q.-Y. Wu, J.-H. Lan, G. Song, Z.-F. Chai, W.-Q. Shi, Theoretical studies on the synergistic extraction of Am^{3+} and Eu^{3+} with CMPO–HDEHP and CMPO–HEH [EHP] systems, Dalton Transactions 47 (2018) 5474–5482. https://doi.org/10.1039/C8DT00134K.

[32] P. Tkac, G.F. Vandegrift, G.J. Lumetta, A. V Gelis, Study of the interaction between HDEHP and CMPO and its effect on the extraction of selected lanthanides, Ind Eng Chem Res 51 (2012) 10433–10444. https://doi.org/10.1021/ie300326d.

[33] Triskem International, UTEVA resin, Triskem: Sharing Innovation 33 (2015) 3–6. www.triskem.com.

[34] TrisKem International, TEVA Product Sheet, 33 (2015) 1–4. www.triskem.com.

[35] Triskem International, DGA Resin (Normal and Branched), 33 (2015) 5–9. www.triskem.com.

[36] V. Jobbágy, E. Dupuis, H. Emteborg, M. Hult,: Performance evaluation of a European wide proficiency test on gross alpha/beta activity determination in drinking water, Applied Radiation and Isotopes 186 (2022) 110304. https://doi.org/10.1016/J.APRADISO.2022.110304.

[37] M.F. L'Annunziata, A. Tarancón, H. Bagán, J.F. García, Liquid scintillation analysis: principles and practice, in: Handbook of Radioactivity Analysis, Elsevier, 2020: pp. 575–801. https://doi.org/10.1016/B978-0-12-814397-1.00006-6.

[38] L. Zeng, L. Huang, J. Han, G. Han, Enhancing Triplet–Triplet Annihilation Upconversion: From Molecular Design to Present Applications, Acc Chem Res 55 (2022) 2604–2615. https://doi.org/10.1021/acs.accounts.2c00307.

[39] H. Sternlicht, G.C. Nieman, G.W. Robinson, Triplet—triplet annihilation and delayed fluorescence in molecular aggregates, J Chem Phys 38 (1963) 1326–1335. https://doi.org/10.1063/1.1733853.

[40] M. Hamel Editor, Plastic Scintillators, Chemistry and Applications, Springer Nature 140 (2021). ISBN 978-3-030-73487-9.

[41] Hamamatsu Photonics K.K., Photomultiplier tubes: Basics and Applications, 4th ed., 2007.

[42] O. Street, CROSS-TALK EXPLAINED Keigo Hirakawa Harvard University Department of Statistics and School of Engineering and Applied Sciences, Analysis 0 (2008) 677–680. https://doi.org/10.1109/ICIP.2008.4711845.

[43] D. Horrocks, Applications of liquid scintillation counting, Elsevier, 2012. ISBN: 9780323154130.

[44] C.T. Peng, Liquid Scintillation Counting Recent Applications and Development: Sample Preparation And Applications, Elsevier, 2012. ISBN: 9780124142961.

[45] E.S. Williams, J. Panko, D.J. Paustenbach, The European Union's REACH regulation: a review of its history and requirements, Crit Rev Toxicol 39 (2009) 553–575. https://doi.org/10.1080/10408440903036056.

[46] A. Coma, H. Bagán, A. Tarancón, Preparation and evaluation of crosslinked plastic scintillation microspheres (CPSm), Polym Test 137 (2024). https://doi.org/10.1016/j.polymertesting.2024.108514.

[47] L.M. Santiago, H. Bagán, A. Tarancón, J.F. Garcia, Synthesis of plastic scintillation microspheres: Evaluation of scintillators, Nucl Instrum Methods Phys Res A 698 (2013) 106–116. https://doi.org/10.1016/j.nima.2012.09.028.

[48] H. Bagán, A. Tarancón, G. Rauret, J.F. García, Radiostrontium separation and measurement in a single step using plastic scintillators plus selective extractants. Application to aqueous sample analysis, Anal Chim Acta 686 (2011) 50–56. https://doi.org/10.1016/j.aca.2010.11.048.

[49] J. Barrera, A. Tarancón, H. Bagán, J.F. García, A new plastic scintillation resin for single-step separation, concentration and measurement of technetium-99, Anal Chim Acta 936 (2016) 259–266. https://doi.org/10.1016/j.aca.2016.07.008.

[50] T.A. Devol, J.P. Clements, A. Farawila, M.J. O'Hara, O.B. Egorov, J.W. Grate, Characterization and application of SuperLig® 620 solid phase extraction resin for automated process monitoring of ^{90}Sr, J Radioanal Nucl Chem 282 (2009) 623–628. https://doi.org/10.1007/s10967-009-0219-z.

[51] A.F. Seliman, V.N. Bliznyuk, T.A. DeVol, Development of stable extractive scintillating materials for real-time quantification of radiostrontium in aqueous solutions, J Radioanal Nucl Chem 314 (2017) 743–751. https://doi.org/10.1007/s10967-017-5420-x.

[52] Triskem international, PRODUCT SHEET SR Resin, 33 (2015) 3–6. www.triskem.com.

[53] Triskem international, TK100/TK101 Resins, www.triskem.com.

[54] M. Sáez-Muñoz, H. Bagán, A. Tarancón, J.F. García, J. Ortiz, S. Martorell, Rapid method for radiostrontium determination in milk in emergency situations using PSresin, J Radioanal Nucl Chem 315 (2018) 543–555. https://doi.org/10.1007/s10967-017-5682-3.

[55] E. Lluch, J. Barrera, A. Tarancón, H. Bagán, J.F. García, Analysis of ^{210}Pb in water samples with plastic scintillation resins, Anal Chim Acta 940 (2016) 38–45. https://doi.org/10.1016/j.aca.2016.08.004.

[56] Eichrom Technologies Inc, TEVA® Resin. https://www.eichrom.com/eichrom/products/teva-resin/ (accessed April 17, 2024).

[57] L. Hughes, T.A. DeVol, On-line gross alpha radiation monitoring of natural waters with extractive scintillating resins, Nucl Instrum Methods Phys Res A 505 (2003) 435–438. https://doi.org/10.1016/S0168-9002(03)01115-X.

[58] O.B. Egorov, M.J. O'Hara, J.W. Grate, Equilibration-based preconcentrating minicolumn sensors for trace level monitoring of radionuclides and metal ions in water without consumable reagents, Anal Chem 78 (2006) 5480–5490. https://doi.org/10.1021/ac060355m.

[59] O.B. Egorov, S.K. Fiskum, M.J. O'Hara, J.W. Grate, Radionuclide sensors based on chemically selective scintillating microspheres: Renewable column sensor for analysis of 99Tc in water, Anal Chem 71 (1999) 5420–5429. https://doi.org/10.1021/ac990735q.

[60] A. Coma, A. Tarancón, H. Bagán, J.F. García, Automated separation of 99Tc using plastic scintillation resin PSresin and openview automated modular separation system (OPENVIEW-AMSS), J Radioanal Nucl Chem 321 (2019) 1057–1065. https://doi.org/10.1007/s10967-019-06659-7.

[61] A.Tarancón, , H.Bagán, J.F García,. Plastic scintillators and related analytical procedures for radionuclide analysis. J Radioanal Nucl Chem 314, (2017) 555–572 https://doi.org/10.1007/s10967-017-5494-5.

[62] J.E. Roane, T.A. DeVol, Simultaneous separation and detection of actinides in acidic solutions using an extractive scintillating resin, Anal Chem 74 (2002) 5629–5634. https://doi.org/10.1021/ac026050z.

[63] L. Hughes, T.A. DeVol, On-line gross alpha radiation monitoring of natural waters with extractive scintillating resins, in: Nucl Instrum Methods Phys Res A, 2003: pp. 435–438. https://doi.org/10.1016/S0168-9002(03)01115-X.

[64] B. Ayaz, T.A. DeVol, Application of MnO2 coated scintillating and extractive scintillating resins to screening for radioactivity in groundwater, Nucl Instrum Methods Phys Res A 505 (2003) 458–461. https://doi.org/10.1016/S0168-9002(03)01120-3.

[65] C.E. Duval, T.A. DeVol, S.M. Husson, Extractive scintillating polymer sensors for trace-level detection of uranium in contaminated ground water, Anal Chim Acta 947 (2016) 1–8. https://doi.org/10.1016/j.aca.2016.09.029.

[66] C.E. Duval, W.A. Hardy, S. Pellizzeri, T.A. DeVol, S.M. Husson, Phosphonic acid and alkyl phosphate-derivatized resins for the simultaneous concentration and detection of uranium in environmental waters, React Funct Polym 137 (2019) 133–139. https://doi.org/10.1016/j.reactfunctpolym.2019.01.015.

[67] P. Froidevaux, P.A. Pittet, D. Bühlmann, F. Bochud, M. Straub, Ion-imprinted resin for use in an automated solid phase extraction system for determining 90Sr in environmental and human samples, J Radioanal Nucl Chem 330 (2021) 797–804. https://doi.org/10.1007/s10967-021-07974-8.

[68] S. Sadeghi, A.A. Mofrad, Synthesis of a new ion imprinted polymer material for separation and preconcentration of traces of uranyl ions, React Funct Polym 67 (2007) 966–976. https://doi.org/10.1016/j.reactfunctpolym.2007.05.020.

[69] M. Budnicka, M. Sobiech, J. Kolmas, P. Luliński, Frontiers in ion imprinting of alkali- and alkaline-earth metal ions – Recent advancements and application to

environmental, food and biomedical analysis, TrAC - Trends in Analytical Chemistry 156 (2022) 116711. https://doi.org/10.1016/j.trac.2022.116711.

[70] V.V. Kusumkar, M. Galamboš, E. Viglašová, M. Daňo, J. Šmelková, Ion-imprinted polymers: Synthesis, characterization, and adsorption of radionuclides, Materials 14 (2021) 1–29. https://doi.org/10.3390/ma14051083.

[71] J.J. Belbruno, Molecularly Imprinted Polymers, Chem Rev 119 (2019) 94–119. https://doi.org/10.1021/acs.chemrev.8b00171.

[72] C. Branger, W. Meouche, A. Margaillan, Recent advances on ion-imprinted polymers, React Funct Polym 73 (2013) 859–875. https://doi.org/10.1016/j.reactfunctpolym.2013.03.021.

[73] G. Vasapollo, R. Del Sole, L. Mergola, M.R. Lazzoi, A. Scardino, S. Scorrano, G. Mele, Molecularly imprinted polymers: Present and future prospective, Int J Mol Sci 12 (2011) 5908–5945. https://doi.org/10.3390/ijms12095908.

[74] M. Sobiech, P. Luliński, Molecularly imprinted solid phase extraction – recent strategies, future prospects and forthcoming challenges in complex sample pretreatment process, TrAC - Trends in Analytical Chemistry 174 (2024). https://doi.org/10.1016/j.trac.2024.117695.

[75] X. Zhou, B. Wang, R. Wang, Insights into ion-imprinted materials for the recovery of metal ions: Preparation, evaluation and application, Sep Purif Technol 298 (2022) 121469. https://doi.org/10.1016/j.seppur.2022.121469.

[76] T.P. Rao, R. Kala, S. Daniel, Metal ion-imprinted polymers-Novel materials for selective recognition of inorganics, Anal Chim Acta 578 (2006) 105–116. https://doi.org/10.1016/j.aca.2006.06.065.

[77] L. Ye, I. Surugiu, K. Haupt, Scintillation proximity assay using molecularly imprinted microspheres, Anal Chem 74 (2002) 959–964. https://doi.org/10.1021/ac015629e.

[78] E. Rieffel, W. Polak, Quantum computing: a gentle introduction, MIT Press, 2011. ISBN 978-0-262-01506-6.

[79] R. Sheehan, P.J. Cragg, Computational Techniques (DFT , MM , TD - DFT , PCM), in: Supramol Chem, Wiley, 2012. https://doi.org/10.1002/9780470661345.smc023.

[80] M. Piechowicz, R. Chiarizia, L. Soderholm, Insight into selectivity: Uptake studies of radionuclides $^{90}Sr^{2+}$, $^{137}Cs^{+}$, and $^{233}UO_2^{2+}$ with bis-amidoxime polymers, Dalton Transactions 47 (2018) 5348–5358. https://doi.org/10.1039/c7dt04935h.

[81] Y. Liu, A.T. Ta, K.C. Park, S. Hu, N.B. Shustova, S.R. Phillpot, Binding of radionuclides and surrogate to 18-crown-6 ether by density functional theory, Microporous and Mesoporous Materials 364 (2024). https://doi.org/10.1016/j.micromeso.2023.112882.

[82] Z. Jing, G. Wang, Y. Zhou, D. Pang, F. Zhu, H. Liu, Selectivity of 18-crown-6 ether to alkali ions by density functional theory and molecular dynamics simulation, J Mol Liq 311 (2020). https://doi.org/10.1016/j.molliq.2020.113305.

[83] K. Zhou, B. Liu, Molecular dynamics simulation: fundamentals and applications, Academic Press, 2022. ISBN-10 0128164190.

[84] A. Chaumont, G. Wipff, Strontium nitrate extraction to ionic liquids by a crown ether: A molecular dynamics study of aqueous interfaces with C_4mim^+-vs C_8mim^+-based ionic liquids, Journal of Physical Chemistry B 114 (2010) 13773–13785. https://doi.org/10.1021/jp106441h.

[85] R.C. Bernardi, M.C.R. Melo, K. Schulten, Enhanced sampling techniques in molecular dynamics simulations of biological systems, Biochimica et Biophysica Acta (BBA)-General Subjects 1850 (2015) 872–877. https://doi.org/10.1016/j.bbagen.2014.10.019.

[86] W. You, Z. Tang, C.E.A. Chang, Potential Mean Force from Umbrella Sampling Simulations: What Can We Learn and What Is Missed?, J Chem Theory Comput 15 (2019) 2433–2443. https://doi.org/10.1021/acs.jctc.8b01142.

[87] J. Kästner, Umbrella sampling, Wiley Interdiscip Rev Comput Mol Sci 1 (2011) 932–942. https://doi.org/10.1002/wcms.66.

[88] G. Sormani, A. Korde, A. Rodriguez, M. Denecke, A. Hassanali, Zirconium Coordination Chemistry and Its Role in Optimizing Hydroxymate Chelation: Insights from Molecular Dynamics, ACS Omega 8 (2023) 36032–36042. https://doi.org/10.1021/acsomega.3c04083.

[89] M. Invernizzi, M. Parrinello, Rethinking Metadynamics: From Bias Potentials to Probability Distributions, Journal of Physical Chemistry Letters 11 (2020) 2731–2736. https://doi.org/10.1021/acs.jpclett.0c00497.

[90] D. Ray, M. Parrinello, Kinetics from Metadynamics: Principles, Applications, and Outlook, J Chem Theory Comput 19 (2023) 5649–5670. https://doi.org/10.1021/acs.jctc.3c00660.

[91] A. Laio, M. Parrinello, Escaping free-energy minima, Proceedings of the national academy of sciences 99.20 (2002): 12562-12566. https://doi.org/10.1073/pnas.202427399.

[92] B. Nutho, N. Nunthaboot, P. Wolschann, N. Kungwan, T. Rungrotmongkol, Metadynamics supports molecular dynamics simulation-based binding affinities of eucalyptol and beta-cyclodextrin inclusion complexes, RSC Adv 7 (2017) 50899–50911. https://doi.org/10.1039/c7ra09387j.

[93] D.M. Shadrack, L.W. Kiruri, H. Swai, S.S. Nyandoro, Solvent effects on host-guest residence time and kinetics: further insights from metadynamics simulation of Toussaintine-A unbiding from chitosan nanoparticle, J Mol Model 27 (2021). https://doi.org/10.1007/s00894-021-04735-y.

CHAPTER 2 - Objectives

2.1. Objectives

The main objective of this thesis is the development of new selective strategies for radionuclide determination by: developing greener and faster methods as an alternative to the conventional ones; developing new scintillating materials, and implementing computational techniques to accelerate the process of resin development.

This goal is delineated into several specific objectives:

1. Development of a new PSresin for the analysis of alpha-emitting radionuclides and the gross total alpha parameter, along with the methodology utilizing this material.

2. Development of novel methods utilizing PSresin for the detection and analysis of radionuclides such as radiostrontium and plutonium isotopes.

3. The exploration of utilizing PSresin in tandem to achieve the separation and measurement of mixtures radionuclides.

4. Development of a new scintillating ion imprinted polymer specifically designed for difficult-to-measure (DTM) radionuclides, with a particular focus on addressing challenges associated with ^{55}Fe detection.

5. Demonstration of the feasibility of implementing computational techniques for the development and optimization of scintillating resins, showing the potential for advanced modelling methods in material design and characterization.

CHAPTER 3 - Development of new scintillating materials for alpha-emitting and DTM radionuclides and computational tools for their implementation

3.1. Introduction

Conventional methods for radionuclide determination are often time-consuming, labour-intensive, and costly [1]. These methods typically involve extensive sample pre-treatments, including successive precipitations, evaporations, organic matter decomposition, selective separations, and valence adjustments. Additionally, a subset of radionuclides, known as difficult-to-measure radionuclides, presents further challenges, as conventional approaches lack the materials and methods necessary for their efficient isolation and precise analysis.

As discussed, selective scintillating materials, such as PSresin, offers potential to streamline the analytical process by unifying the selective separation and the measurement, thereby reducing the overall analysis time. Furthermore, if selective materials are specifically developed for this purpose, they could significantly improve the determination of DTM radionuclides.

To streamline the development of these materials, a strategy involving molecular dynamics simulations and enhanced sampling techniques was developed to predict the affinity between an extractant and a target element in various media. This approach was specifically studied with a crown ether system targeting Sr^{2+} and Pb^{2+} and has been experimentally validated.

3.1.1. Alpha emitting radionuclides

Among the various alpha-emitting radionuclides, actinides represent a substantial group. Actinides should be detected across multiple matrices, including natural waters, soils, and biological samples, as nuclear contamination of these samples may result from nuclear accidents, acts of terrorism, or the legal or illegal discharge of waste from nuclear facilities. Furthermore, actinides need to be monitor during decommissioning of nuclear facilities, to correctly classify wastes as conventional or radioactive based on their activity level.

Screening parameters are frequently employed to speed up the contamination assessments during decommissioning or environmental monitoring. One key parameter is gross alpha, which provides an accumulative measure of all alpha emitters in a sample.

If the gross alpha activity is below a specified threshold, radionuclide-specific analysis may not be necessary, reducing both time and cost. In environmental monitoring, the gross alpha parameter typically includes actinides, radium, and polonium, particularly for natural water sources. However, in decommissioning, nuclear accidents, or terrorist incidents, gross alpha measurements focus mainly on actinides, as the contributions of radium and polonium (naturally occurring radionuclides) are generally negligible.

Gross alpha activity can be measured by proportional counting or LSC. Both methods require extensive sample preparation. For proportional counting, the sample must be deposited on a planchet in a thinly uniform layer to prevent self-absorption, moreover, pre-concentration and radiochemical purification are necessary. In LSC, liquid samples can be directly mixed with the scintillation cocktail for measurement, but pre-concentration and evaporation steps are still required to achieve optimal detection limits. Thus, both techniques involve similar sample preparation challenges.

In addition, gross alpha determination poses significant challenges in reproducibility, with 60-70% of laboratories falling outside acceptable ranges in interlaboratory comparisons [2]. This variability is partly due to the lack of a common calibration strategy. Since gross alpha includes radionuclides with varying energies, selecting an appropriate calibration standard is complex.

To overcome these limitations, a novel PSresin was developed for gross alpha determination. Potential extractants considered for this PSresin development included dipentyl pentylphosphonate, N,N,N',N'-tetra-n-octyldiglycolamide, and bis(2-ethylhexyl) methanediphosphonic acid, each previously used in commercially available non-scintillating resins (Uteva, DGA, and Actinide resins, respectively) [3–5].

Dipentyl pentylphosphonate has a high affinity for uranium, thorium, neptunium, and plutonium, making it suitable for environmental monitoring applications where uranium is the primary contributor to gross alpha activity. However, this extractant does not effectively retain radium or polonium, so it was not selected. N, N, N', N'-tetra-n-octyldiglycolamide has a strong affinity for actinides, making it ideal for gross alpha determinations in decommissioning or emergency scenarios involving nuclear accidents, but it lacks effectiveness for broader environmental monitoring. In contrast, bis(2-

ethylhexyl) methanediphosphonic acid presents high affinity for all actinides and can retain radium and polonium depending on the media used for chemical separation. Given these properties, the PSresin developed in this project was based on bis(2-ethylhexyl) methanediphosphonic acid and its derivatives.

3.1.2. DTM radionuclides

Numerous radionuclides are generated in nuclear power plants as a by-product of reactor operations. Fig 3.1 illustrates the various radionuclides produced and their specific locations within reactor components. During the dismantling of nuclear facilities, authorities must ensure that all generated waste is free of radionuclides, necessitating extensive analysis. DTM radionuclides are found among the most challenging to be analysed.

According to ISO standard 24390:2023, a DTM radionuclide is defined as a "*radionuclide whose radioactivity is difficult to measure directly from the outside of the waste packages by non-destructive assay means*" [6]. DTM radionuclides are characterized by their low energy emissions, the wide range of matrices in which they occur, and interferences that hinder their precise isolation for measurement. Measuring DTM radionuclides is essential in several areas, particularly, as mentioned, in the decommissioning of nuclear facilities and nuclear waste management. However, conventional methods continue to face challenges in accurately determining DTMs in diverse matrices.

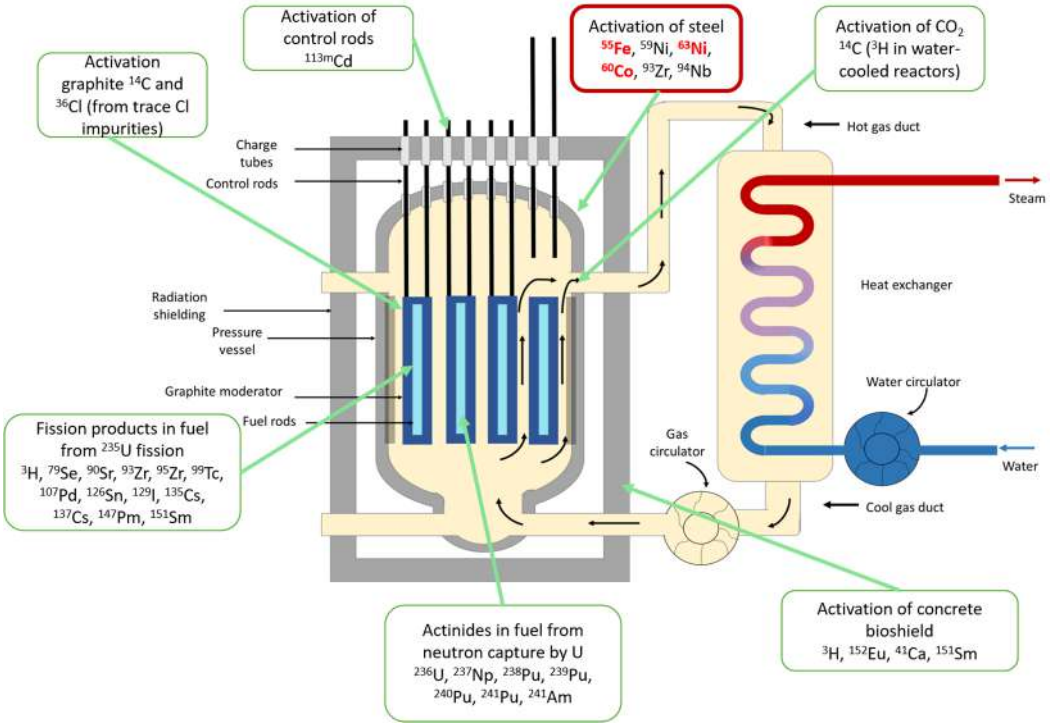

Fig 3.1 . Simplified scheme showing some of the DTM radionuclides produced during the operational life of a nuclear reactor [7].

Key DTM radionuclides produced in nuclear reactors arise from neutron interactions with reactor materials. Some of these DTMs are generated due to the neutron activation of elements present on reactor steel. Moreover, these radionuclides can also migrate to the cooling water or other reactor materials. In particular, this work has been focused on the determination of ^{55}Fe.

^{55}Fe is an electron capture radionuclide with a half-life of 2.74 years, produced by neutron activation of stable iron isotopes, ^{54}Fe and ^{56}Fe, and decaying into ^{55}Mn, emitting characteristic X-rays and Auger electrons. Monitoring ^{55}Fe is critical during decommissioning due to its high production levels associated with the extensive use of iron in nuclear power plant structural components. This radionuclide poses health risks to workers involved in waste handling, classification, and characterization and can potentially spread into environmental media if not correctly stored. While external radiation from ^{55}Fe presents minimal risk, internal exposure is hazardous due to the long biological retention, which can damage blood constituents or bone marrow, increasing leukaemia risk [8]. Consequently, ^{55}Fe analysis is required across multiple matrices,

including steel, graphite, water, and soil, throughout and following the decommissioning process.

Measuring ^{55}Fe is particularly challenging due to its low energy and the presence of numerous interfering species. Classical methods for ^{55}Fe determination consist of a first precipitation at pH 9 using NH_4OH or NaOH solutions to preconcentrate iron. During the process, other interferences are also precipitated such as nickel or cobalt. For that reason, the sample, once reconstructed in 9 M HCl, is passed through an anion exchange column which allows the consequence isolation of iron for the radiometric measure. The primary technique used for its detection is LSC; however, in real samples where the iron content exceeds 200 mg, the maximum detection efficiency achieved is only about 15% [9]. Moreover, the isolation procedure does not always achieve optimal results, as there are currently no resins with selectivity for iron due to the absence of iron-specific extractants.

To address these limitations, a novel scintillating material specific for ^{55}Fe determination was developed in this project, with the aim of providing enhanced selectivity over traditional methods and reducing the colour quenching faced in LSC measurements. This material is based on ion-imprinted polymers, marking the first application of scintillating ion-imprinted polymers for radioactivity determination.

3.1.3. Computational strategy for extractant development

The development of selective resins (scintillating or not) for radionuclide-selective analysis is a multi-stage process. Initially, one or more extractants are selected. If these extractants are not commercially available, they are synthesized in-house. After acquisition or synthesized, the extractants are immobilized on a polymeric surface and subsequently validated across various media and concentrations to evaluate the affinity between the target element and the extractant. This process requires not only considerable time and effort but also significant financial investment.

To mitigate the risk of investing excessive time, effort, and funds in unsuccessful trials, computational techniques can be employed as an initial screening step. Simulations allow for the identification of extractants and conditions with low likelihoods of binding to the target element, enabling focused efforts on more promising

candidates. This computational approach enhances the development process, making it both more efficient and cost-effective.

In this project, a computational strategy was studied and tested for crown ether systems targeting strontium and lead across various working media, including nitric acid, hydrochloric acid, acetic acid, potassium thiocyanate, perchloric acid, and formic acid. This system builds on prior research with CE-PSresin, where similar affinities for Sr^{2+} and Pb^{2+} were observed in nitric acid medium. Thus, the objective of this project extends beyond establishing a computational method for predicting extractant-target radionuclide affinities in a shorter timeframe; it also aims to assess the influence of working media on the interaction affinities between crown ethers and Sr^{2+} or Pb^{2+}.

One of the main techniques used for this is the quantum chemistry-based calculations using DFT. DFT enables the analysis of factors such as cavity size, the influence of electron-withdrawing or electron-donating substituents on structure, and metal-crown ether affinities [10–13]. DFT calculations are highly precise as they account for electronic effects; however, these calculations are typically conducted at 0 K, often disregarding temperature and solvation effects, which limits their accuracy in realistic conditions. In the presence of more realistic conditions (solvent, temperature, etc) the final crown ether conformation might be disrupted by the incorporation of polar solvent molecules thereby weakening the observed crown-metal binding [14].

As an alternative to DFT, this study developed a computational strategy based on MD simulations combined with enhanced sampling methods [15,16]. MD simulations allow for a more realistic sampling and exploration of the thermodynamics of the metal-crown ether complex, considering conformational fluctuations of the crown ether, solvent environment, and thermal effects [17–19]. The results obtained from the simulations for strontium and lead in each working medium were compared with the experimental distribution weight ratios (D_w).

3.2. Results

The results of this chapter are presented into four articles. The first two articles are focused on the development and optimization of a PSresin for alpha-emitting radionuclides and the development of a method for gross alpha parameter determination. The third one is based on the development of the first scintillating ion imprinted polymer for ^{55}Fe (Sc-Fe-IIP) determination. Finally, in the fourth one where a strategy involving molecular dynamics and enhance sampling techniques has been developed to predict the affinity between organic molecules and metals to reduce the steps required for the development of scintillating and non-scintillating resins. Finally, the chapter will finish with a global discussion.

These scientific publications are:

Article #1: **I. Giménez**, H. Bagán, A. Tarancón, J.F. García, PSresin for the analysis of alpha-emitting radionuclides: Comparison of diphosphonic acid-based extractants, Applied Radiation and Isotopes 178 (2021) 109969. https://doi.org/10.1016/J.APRADISO.2021.109969

Article #2: I. Giménez, H. Bagán, A. Tarancón, Fast analysis of gross alpha with a new plastic scintillation resin, Anal Chim Acta 1248 (2023) 340905. https://doi.org/10.1016/j.aca.2023.340905

Article #3: I. Giménez, H. Bagán, A. Tarancón. Scintillating iron imprinted polymers (Sc-Fe-IIP): Novel material for 55Fe selective recognition. Microchemical Journal, 208 (2025), 112268. https://doi.org/10.1016/j.microc.2024.112268

Article #4: I. Giménez.; G. Sormani, A. Rodríguez, A. Hassanali, H. Bagán, A. Tarancón, Design of radionuclide separations based on MD simulations, Anal Chim Acta 1356 (2025) 344047. https://doi.org/10.1016/j.aca.2025.344047

Article #1

PSresin for the analysis of alpha-emitting radionuclides: Comparison of diphosphonic acid-based extractants

Applied Radiation and Isotopes 178 (2021) 109969

Contents lists available at ScienceDirect

Applied Radiation and Isotopes

journal homepage: www.elsevier.com/locate/apradiso

PSresin for the analysis of alpha-emitting radionuclides: Comparison of diphosphonic acid-based extractants

I. Giménez [a], H. Bagán [a], A. Tarancón [a,b,c,*], J.F. García [a,c]

[a] Department of Chemical Engineering and Analytical Chemistry, University of Barcelona, Marti i Franqués, 1-11, ES, 08028, Barcelona, Spain
[b] Serra-Húnter Programme, Generalitat de Catalunya, Barcelona, Spain
[c] Institut de Recerca de l'Aigua, University of Barcelona, Spain

1. ABSTRACT

The analysis of radionuclides is complex, with high economic and time costs. For this reason, there is a need to develop new methods and strategies to reduce these costs. One important group in the analysis of radionuclides is the actinides, which are the main constituents assessed in the total gross alpha together with radium and radon test used to measure radioactivity in drinking water. Moreover, in nuclear dismantling processes, the possible spread of the released radionuclides has to be controlled, which is measured by many techniques, depending on the radionuclides, through scintillation. This work presents a new method to analyse actinides using plastic scintillation resins (PSresins) packed in a solid-phase extraction cartridge. The proposed method combines chemical separation and sample measurement into a single step, reducing the effort, time and reagents required for analysis as well as decreasing the amount of waste generated. The PSresins compared in this study contained three selective extractants based on methylenediphosphonic acid with different radicals, which has a high affinity for tri-, tetra-, and hexavalent actinides in dilute acids. These extractants were immobilised on plastic scintillation microspheres at a ratio of 1/1:6, producing a retention and detection efficiency of 100% for ^{241}Am, ^{230}Th, Uranium and ^{238}Pu. The retention and detection efficiency were 20% and 100%, respectively, for ^{210}Po and low for ^{226}Ra.

1. Introduction

The analysis of radionuclides is complex, with high economic and time costs. This is very evident in decommissioning and environmental monitoring, for which the obtention of appropriate information requires as much analysis as possible. In such situations, the assessment of global or screening parameters may be of help to avoid the use of selective procedures for each radionuclide. For example, the gross beta and alpha parameters are used to measure radioactivity in water intended for human consumption, which are assessed in order to avoid the specific analysis of several alpha and beta emitters if the parametric values do not exceed the limits (España, 2016).

One of the radionuclides group of major concern in radioactivity analysis is the actinides, which include some natural alpha emitters commonly found in natural waters and artificial alpha emitters that indicate nuclear contamination, accidents or terrorist attacks. The quantification of these actinides, regardless of whether alpha spectrometry or liquid scintillation is used, requires previous chemical separation to avoid radiochemical or non-radiochemical interferences. This separation can be achieved through precipitation, liquid-liquid extraction with organic solvents like tributyl phosphate (TBP), or anion-exchange chromatography (M.F. L'Annunziata, 2007). These procedures are usually laborious, long and tedious, and also generate waste. Therefore, they have been replaced by extraction chromatography through solid-phase extraction (SPE) (Horwitz et al., 1993; Zagyvai et al., 2017). This strategy, using a suitable selective extractant in a resin and an appropriate medium, can result in a very good selective extraction of the target radionuclide from the rest of the interferences. Resins that use octyl phenyl diisobutyl carbamoyl methyl phosphine oxide (CMPO) dissolved in TBP as an extractant on an inert support can sorb americium, plutonium and uranium in 1–3 M nitric acid (Triskem, 2015a). The resins based on dipentyl pentylphosphonate show high affinity for uranium(VI) and some tetravalent actinides, such as thorium, neptunium and plutonium, in a nitric acid medium (Triskem, 2015b). Resins based on N,N,N′,N′-tetra-*n*-octyldiglycolamide can sorb americium in 5 M hydrochloric acid and actinium in 1–3 M nitric acid while radium is eluted. Finally, resins based on bis(2-ethylhexyl) methanediphosphonic acid have a high affinity for several alpha emitters (Chiarizia et al., 2007; Rim et al., 2016) and their use has been proposed for the assessment of the total gross alpha parameter (Navarro et al., 2004) due to their high affinity for actinides in 0.1 M hydrochloric acid.

* Corresponding author. Department of Chemical Engineering and Analytical Chemistry, University of Barcelona, Marti i Franqués, 1-11, ES, 08028, Barcelona, Spain.
E-mail address: alex.tarancon@ub.edu (A. Tarancón).

https://doi.org/10.1016/j.apradiso.2021.109969
Received 19 May 2021; Received in revised form 16 September 2021; Accepted 26 September 2021
Available online 28 September 2021

For a fast and simple analysis of alpha-emitting radionuclides, scintillation techniques should be taken into consideration since they combine simplicity with good detection limits. Plastic scintillation resins (PSresins), which are plastic scintillation microspheres (PSm) coated with a selective extractant packed in an SPE cartridge, combine the extraction process and measurement into a single material (Bagán et al., 2011; Coma et al., 2019; Lluch et al., 2016; Sáez-Muñoz et al., 2018). This not only simplifies the analytical method, but it also reduces the number of reagents required, since elution steps are no longer required, and avoids the generation of mixed wastes (hazardous and radioactive) derived from the use of liquid scintillation cocktails (L'Annunziata, 2020; Jay et al., 2020; Tarancón et al., 2021). Extractive scintillating resins has also been used for on-line monitoring of radionuclides (Egorov and O'Hara J. W. 2006; A. F. Seliman et al., 2013; A. F. Seliman et al., 2017).

PSresins have already been mainly developed for the measurement of beta-emitting radionuclides such as ^{90}Sr and ^{99}Tc. In this paper, different PSresins for the selective measurement of alpha-emitting radionuclides have been developed and compared, providing a new methodology for the measurement of alpha emitters that requires less time and fewer reagents. Scintillating resins were tested tested previously for uranium but also for americium, and plutonium (Duval et al. 2016, Duval et al., 2019; Hughes and DeVol, 2003; Roane and DeVol, 2002, 2005). The extractants used in this study are based on diphosphonic acid derivatives (Fig. 1), which have attracted a lot of interest due to their effectiveness as a complexing reagent for metal ions, showing high sorption capacities for actinides that make the stripping of the sorbed actinides difficult (Griffith-Dzielawa et al., 2000; Horwitz et al., 1997; McAlister et al., 2001; Rim, 2013; Rim et al., 2016). This property is of special interest in PSresin measurements since the analyte is not eluted from the resin during analysis.

The interaction between the extractant and the radionuclide is mediated by a diphosphonic group (Rim, 2013; Rim et al., 2016). Therefore, the interaction is expected to be the same for the three extractants assessed in this study. However, a modification of the radicals in the extractant could lead to a better assessment of steric impedance or polarity that could affect the retention capacities of the resin and the quenching effects, which have a direct impact on the detection efficiency and the resolution of the spectrum. These improvements via modifications in the radical chain would benefit the scintillating capacities of the PSresin, thereby improving the detection of scintillation and the discrimination of beta and alpha emitters through pulse shape analysis.

For that reason, the aim of this work was to study different extractants for the extraction of alpha-emitting radionuclides to find the most suitable one for the synthesis of PSresins.

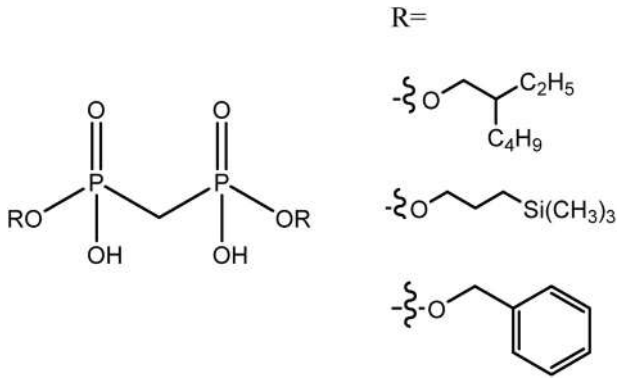

Fig. 1. Core structure of the extractant studied and the different radicals.

2. Experimental

2.1. Reagents and solutions

All the reagents used were of analytical grade. Polystyrene (PS) (MW 250.000 g/mol) was supplied by Acros Organics (Geel, Belgium). Fully hydrolysed polyvinyl alcohol (PVA), 2,5-Diphenyloxazole (PPO), 2,6-diisopropylnaphthalene (DIN) (99% pure), benzyl alcohol, tetrahydrofuran (max. 0.005% H_2O), 3-(trimethylsilyl)-1-propanol (97%) and dichloromethane (99.9% pure) were supplied by Merck (Darmstadt, Germany). 1,4-bis(5-phenyl-2-oxazolyl) benzene (POPOP) was purchased from Carlo Erba Reagents (Chaussée du Vexin, France). Methylenediphosphonic acid (99+%), 2-ethylhexanol and *N,N′*-dicyclohexylcarbodiimide (DCC; 99%) were supplied by Alfa Aesar (Kendal, Germany).

A ^{90}Sr/^{90}Y active stock solution of 38.45 (0.29) Bq/g was prepared from a standard of 4071 (31) Bq/g in a water solution of strontium (100 μg g^{-1}) and yttrium (100 μg g^{-1}) in 0.1 M HCl (Amersham International, Buckinghamshire, England). A natural purified uranium (^{238}U+^{235}U+^{234}U) active stock solution of 2.22 (0.03) Bq/g was prepared from a standard of 101.34 (1.18) Bq/g (Eckert and Ziegle, Berlin, Germany) with 11 years of ingrowth. A ^{238}Pu active stock solution of 46.30 (1.4) Bq/g was supplied by GE Healthcare-Amersham International (Buckinghamshire, England). A ^{230}Th active stock solution of 2.38 (0.07) Bq/g was prepared from a standard of 23.59 (0.27) Bq/g (National Institute of Standards and Technology (NIST), Gaithersburg, USA). A ^{241}Am active stock solution of 47.4 (1.2) Bq/g in 0.5 M HCl was prepared from a standard of 55.4 (1.3) kBq/g (GE Healthcare-Amersham International, Buckinghamshire, England). A ^{226}Ra active stock solution of 4 (0.12) Bq/g in HNO_3 was prepared from a standard of 1.986 (61.5) KBq/g (Ciemat, Madrid, Spain). A ^{210}Pb active stock solution of 160 (4.8) Bq/g was prepared from a standard of 35.5 (1.06) KBq/g (CEA/DAMRI, Gif-sur-Yvette, France). The values in brackets refer to the standard uncertainty.

The OptiPhase Supermix liquid scintillation cocktail from PerkinElmer (Waltham, USA) was used for the liquid scintillation measurements.

2.2. Apparatus

A Quantulus liquid scintillation spectrometer (PerkinElmer, Waltham, USA) with logarithmic amplification, a multichannel analyser (MCA) (4096 channels distributed in four segments of 1024), alpha/beta discrimination and background reduction by an active guard was used for the scintillation measurements.

Secondary electron images were obtained using a JSM-7100F JEOL (Tokyo, Japan) scanning electron microscope at the Scientific and Technological Centres of the University of Barcelona (CCiTUB).

The analysis of stable isotopes was performed using an OPTIMA 8300 ICP-OES detector (PerkinElmer, Waltham, USA) or an ELAN-6000ICP-MS detector (PerkinElmer, Waltham, USA).

A Varian Mercury 400 MHz nuclear magnetic resonance (NMR) system (Oxford, England) was used to confirm the structures of the molecules synthesised.

2.3. Procedure

2.3.1. Preparation of PSresins

PSm were prepared through the extraction-evaporation method, as previously reported (Santiago et al., 2013). Briefly, 250 mL of a solution of polystyrene, diisopropylnaphthalene and the fluors (PPO and POPOP) in dichloromethane were mixed with 2 L of a 1% PVA aqueous solution and stirred for 24 h at 11.6 Hz. The microspheres formed were recovered by filtration and dried in an oven at 40 °C for 24 h.

Three PSresins based on methanediphosphonic acid and with three different radicals were prepared: EH-PSresin; SI-PSresin and BZ-PSresin.

The different extractants were prepared in a similar way, as previously reported for bis(2-ethylhexyl)methanediphosphonic acid (Griffith-Dzielawa et al., 2000; Horwitz et al., 1997; McAlister et al., 2001). Briefly, a 60-ml mixture of THF with methanediphosphonic acid and 2-ethylhexanol (EH-PSresin), benzilic acid (BZ-PSresin) or 3-(trimethylsilyl)-1-propanol (SI-PSresin), depending on the PSresin being prepared, was purged with N_2 and refluxed. Afterwards, an 80-ml solution of DCC in THF was added dropwise. This was left to react for 1 day.

PSresins were prepared by coating the surface of the microsphere with the respective extractant, according to previous studies. A mixed solution of the extractant in isopropanol was stirred with PSm for 45 min and then incubated in a rotary evaporator for 2 h to remove the solvent (Bagán et al., 2011).

2.3.2. PSresin extraction and measurement

One gram of the corresponding PSresin was packed in a 2-mL SPE cartridge (length: 3.2 cm; internal diameter: 1 cm; external diameter: 1.2 cm) from Triskem International (Rennes, France). The cartridge was placed in a vacuum chamber connected to a pump and 10 ml of deionised water was passed through it at a flow rate of 1 ml/min, around 5 inHg. Afterwards, the cartridges were shaken for 180 s at 50 Hz in an IKA MS3 digital vortex (Merck, Darmstadt, Germany) for homogenisation.

Samples were prepared by adding a known amount of the radioactive stock solution and 0.5 M hydrochloric acid made up to 11 ml. The activity added was around 7.5 Bq for ^{241}Am and 3.3 Bq for ^{230}Th, natural uranium, ^{238}Pu, ^{210}Po and ^{226}Ra. Blank samples were prepared by adding deionised water instead of the radioactive stock solution. The ^{90}Sr/^{90}Y sample solution was prepared in 2 M nitric acid and with an activity of around 10 Bq. All solutions were prepared by weight.

The ^{226}Ra sample was subjected to ultrasound for 10 min to remove ^{222}Rn before its passing through the PSresin cartridge.

To perform the sample analysis. The cartridge was first conditioned with 2 ml of 0.5 M HCl. Afterwards, 10 ml of the sample solution were passed through the cartridge. The flow must be around 1 ml/min, which corresponds to a pressure of 3 inHg. Once the sample was loaded, two rinses with 2 ml of 0.5 M HCl or 2 M HNO_3 (in the case of the ^{90}Sr/^{90}Y sample) were performed. Two additional rinses with 2 ml of 6 M lithium nitrate were undertaken for the ^{90}Sr/^{90}Y sample to avoid the chemiluminescence caused by nitric acid.

To ensure the dryness of the cartridge, the pressure was increased to 15–20 inHg for 10 min.

The solutions eluted after passing the sample and rinsing the PSresin cartridge, effluent or effluent solutions, were collected in Corning (New York, USA) 50-ml conical tubes.

Once the extraction process was completed, the cartridge with the PSresin was placed in a 20-mL polyethylene vial and measured in the scintillation counter.

PSresin cartridge effluent were also measured by liquid scintillation to determine the amounts of radionuclides that were not retained. A 6-ml aliquot of efluent was added to a 20-ml polyethylene vial along with 14 ml of the scintillation cocktail. The vials were shaken for 180 s in the vortex at 60 Hz to homogenise the mixture. Blanks were prepared by adding deionised water instead of the effluent solution.

2.3.3. Retention profile of stable metals

Two samples containing 1000 mg L^{-1} of europium(III) and iron(III), respectively, were prepared in 0.5 M HCl. 50 mL of each solution were passed through the cartridge with PSresin and 2-ml fractions of the effluent solution were collected in separate conical tubes to evaluate how is the retention profile of Eu and Fe in the PSresin and to make and estimation of the PSresin capacity. Fractions containing iron(III) were analysed by ICP-OES, whereas ICP-MS was used for those containing europium(III).

2.3.4. Breakthrough volume

400 ml of a 0.5 M-HCl solution were passed through a PSresin cartridge in which ^{241}Am was previously retained. The PSresin cartridge effluent were collected in fractions of 40 ml in a 50-ml conical tube. Each fraction was measured by liquid scintillation, as described before.

2.3.5. Measurement conditions

A "low" coincident bias and a "high-energy" multichannel analyser configuration were used for the scintillation measurements. The counting time for the measurement of the PSresin cartridges was 1 h for ^{241}Am and 3 h for the other radionuclides. LS samples were measured for 1 h. The external quenching parameter (SQP(E)) was measured for 10 min for each vial. The measurement vials were stored in the dark for 2 h before counting, except those containing the ^{226}Ra and ^{210}Po samples that were directly measured after separation to avoid the ingrowth of daughter isotopes.

Alpha/beta discrimination through pulse shape analysis was performed by analysing the PSresin cartridges for 25 min at PSA values of 50, 75, 100, 115, 125, 130, 135, 140, 145, 150, 175, 200, 225 and 250.

2.3.6. Data treatment

The NMR spectra were integrated with the MestReNova software (Mestrelab, Santiago de Compostela, Spain). All the spectra acquired from the scintillation measurements were smoothed using the Savitzky–Golay algorithm with an average window of 21 points, delimitating the range of the windows from 1 to 1024. A net spectrum was obtained by subtracting the spectrum of the equivalent blank solution. The detection efficiency spectrum was obtained as the ratio between the net counts in every channel and the activity in the PSresin cartridge. The detection efficiency was calculated from the integration of the detection efficiency spectrum at the selected energy channel range.

3. Results and discussion

The study of the PSresins was performed in four stages. First, the PSresins were prepared, which included the synthesis of the extractants and the coating of the PSm. Second, the retention and detection efficiencies and the quenching effects for the analyses of several alpha and beta emitters were assessed. Third, the capacity and retention profile were evaluated with stable elements and, fourth, the alpha/beta discrimination capabilities were evaluated.

3.1. PSresin preparation

The correct synthesis of the extractants was confirmed with NMR spectroscopy. The ^{1}H NMR (MD_3OD) signals obtained were:

- EH-PSresin: δ 0.9 (t, 12 H), 1.20 (m, 14 H), 1.47 (m, 4 H), 2.46 (t, 2 H), 3.99 (m, 4 H)
- BZ-PSresin: δ 2.46 (t, 2 H), 4.5 (s, 1 H), 4.9 (s, 4 H), 7.35 (m, 10 H)
- SI-PSresin: δ 0.01 (s, 18 H), 0.53 (m, 4 H), 1.67 (m, 4 H), 2.46 (t, 2 H), 3.99 (m, 4 H)

Three different PSresins were prepared by coating PSm presenting a median diameter of 60 μm with the corresponding extractant. The extractants used were: bis(2-ethylhexyl)methanediphosphonic acid (EH-PSresin), bis(trimethylsilylpropanyl)methanediphosphonic acid (SI-PSresin) and bis(benzylyl)methanediphosphonic acid (BZ-PSresin).

The scanning electron microscopy images (Fig. 2) showed that most of the resins maintained their spherical shape. Furthermore, there were almost no agglomerates present due to the possible softening caused by the solvent used (isopropanol), which could partially dissolve the polystyrene surface of the microspheres after the long contact time. Moreover, it was ensured in a preliminary study that the exposure time conditions in which the immobilisation was performed, were not enough to soften or dissolve the PSm, ensuring that any change observed in the surface could be attributed to the correct immobilisation of the extractant. This indicates that the amount of solvent used for the

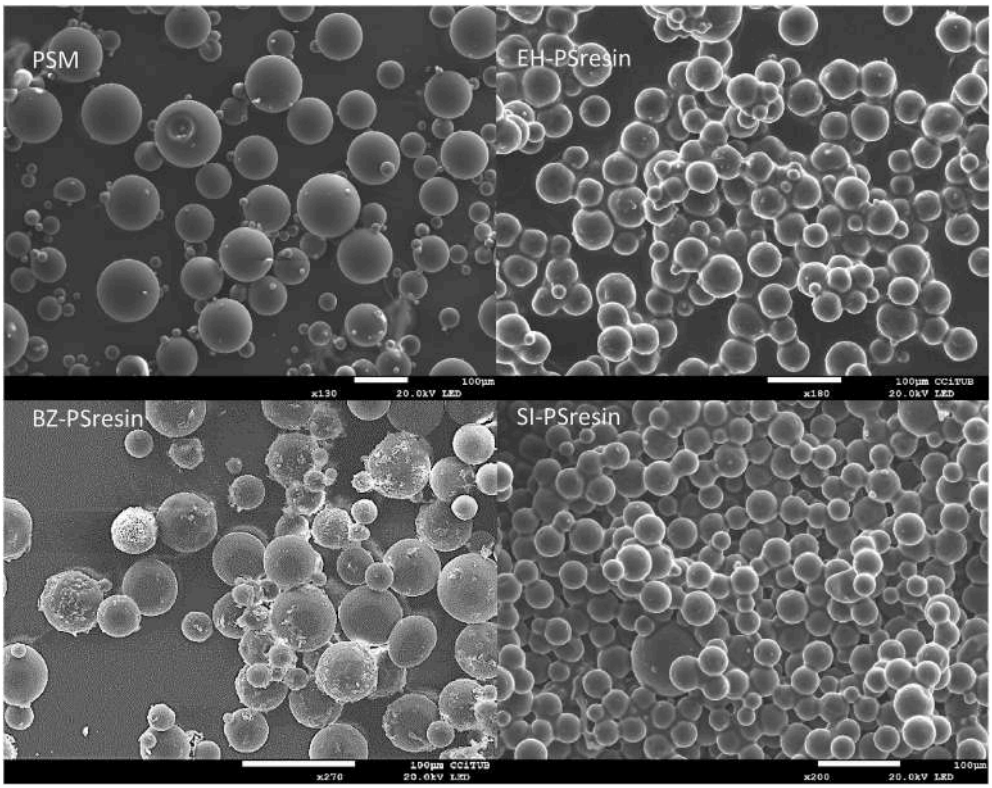

Fig. 2. Secondary electron images for the different PSresins obtained using a scanning electron microscope. EH-PSresin (R = 2-ethylhexyl); BZ-PSresin (R = benzyl); SI-PSresin (R = 3-(trimethylsilyl)-1-propyl).

immobilisation and the time of exposure to it were adequate. The images confirmed that the immobilisation of the extractant on the surface of the scintillation support was performed correctly. The PSm, is the virgin resin, the support without any extractant on it, showing how smooth and plain is the surface, whereas the PSresins had small folds (EH-PSresin), scales (BZ-PSresin) or crystals (SI-PSresin) on the surface, confirming the presence of a superficial layer of the extractant and the presence of extractant between PSm which enhance the retention of the target radionuclide. This difference in appearance was also the first indication of the differences between the PSresins.

Moreover, EH-PSresin and SI-PSresin showed a homogeneous distribution of the extractant on their surface whereas BZ-PSresin does not. These results indicate that the proportion of the PSm:extractant used was adequate at least for EH-PSresin and SI-PSresin. Furthermore, there were some physical differences between them in this regard, since EH-PSresin was stickier than the other two resins.

3.2. Extraction and scintillation detection capabilities

The study was performed using solutions prepared in 0.5 M HCl. This medium was chosen because it was already used in the separation methods involving the non-scintillating diphosphonic acid-based resins (Eichrom, 2014) given the very strong retention of actinides in it.

3.2.1. Background

The background values for the different PSresins were quite similar (0.91 (0.12) cpm, 0.79 (0.11) cpm and 1.14 (0.14) cpm for EH-PSresin, BZ-PSresin and SI-PSresin, respectively). This was expected since all the compounds used for the PSm were organic and the main difference between the PSresins was the radicals of the different extractants, which should not affect the background values.

3.2.2. Americium-241

The first radionuclide that was studied was ^{241}Am since the most stable valence state of americium is (III), which is the one with the highest affinity for diphosphonic acids (Chiarizia et al., 2007). Therefore, it can be assumed that the retention and detection efficiency for the other alpha-emitting radionuclides should be similar to or lower than those for americium.

^{241}Am showed very high retention in EH-PSresin and SI-PSresin, whereas only half of the total americium was retained in BZ-PSresin (Table 1).

The different retention behaviour of BZ-PSresin could be due to the effect of the benzyl group of the lateral chains of the extractant. This group is more polar and more voluminous than the other two, which could affect access and the interaction between the disphosphonic group and the radionuclide in the medium.

The detection efficiency was high for the americium retained in all three PSresins and all the disintegrations are detected. These results are in according to those obtained previously with PSm of 60 μm in similar measurement conditions since all alpha particles are capable to hit the PSresin without being attenuated by the medium (Tarancón et al., 2017). However, the SQP(E) values for BZ-PSresin were lower than those for EH-PSresin and SI-PSresin, which were comparable and similar to those of other PSresins and PSm. Although the SQP(E) for BZ-PSresin indicated that there was not a great quenching effect, the spectrum obtained was broad and shifted to low energies compared to those obtained for EH-PSresin and SI-PSresin, which were not affected by any

Table 1
Retention and detection efficiency for Am-241 in each PSresin. EH-PSresin (R = 2-ethylhexyl); BZ-PSresin (R = benzyl); SI-PSresin (R = 3-(trimethylsilyl)-1-propyl).

	Yield (%)	Detection efficiency (%)	SQP(E)
EH-PSresin	>99.5	100	781
BZ-PSresin	48.4	100	736
SI-PSresin	>99.5	100	779

quenching effect (Fig. 3). This effect is presumed to be associated with the presence of an aromatic ring of the benzyl substituent, which can interfere in the energy transfer process along the polymer chain of the scintillator, causing a decrease in the number of photons emitted by the scintillator.

The broad spectrum obtained with BZ-PSresin will probably hamper alpha/beta discrimination, as well as cause overlapping of the peaks of other potential radionuclides that could be present in a real sample. This and the low retention led to BZ-PSresin being discarded as a candidate for a scintillation resin in subsequent studies.

3.2.3. *Plutonium, thorium and uranium*

EH-PSresin and SI-PSresin were used for the analysis of plutonium (^{238}Pu), thorium (^{230}Th) and natural uranium (^{238}U+^{235}U+^{234}U) standards in 0.5 M HCl. A quantitative retention of ^{238}Pu, ^{230}Th and natural uranium was observed in both PSresins (Table 2), which indicated an optimum interaction between the radionuclides and the extractant, showing no significant differences between them. The valence state in which the analysis was performed was plutonium (IV), thorium (IV) and uranium (VI).

Regarding the scintillation properties, the detection efficiency for ^{238}Pu and ^{230}Th was close to 100%, as expected from the previous analysis of americium. In the case of uranium (^{238}U + ^{235}U + ^{234}U), all the disintegrations were detected, including the short-live decay products in equilibrium, ^{234}Th and ^{234}Pa, which are both high energy beta-emitting radionuclides. As it has been explained in the reagents section, the uranium solution used is a standard from a natural source that has been purified in order to exclude long half-live time radionuclides. Nevertheless, there are also the short half live-time radionuclides formed very fast after purification which are also retained. For that reason, the calculation of the efficiency was done considering the sumatorium of all the uranium isotopes present plus the contribution of ^{234}Th and ^{234}Pa. The detection efficiency and retention were the same for both PSresins. Fig. 4 shows the normalised spectrum for each radionuclide, which was obtained by dividing the count rate spectrum by the total the spectrum area, for SI-PSresin as an example.

Despite organic scintillation is not a technique suited for spectroscopy studies, from a qualitative point of view we can observe that there was a certain correlation between the spectrum position and the energy of the radionuclides studied. Uranium spectrum is the sum of the contribution of ^{238}U and ^{234}U, being their respective energies of 4.27 MeV (^{238}U) and 4.86 MeV (^{234}U), as well as the contribution of the short-lived beta decay products. The spectrum for uranium is located at lower energy channels compared to ^{230}Th due to the ^{238}U contribution which make the spectrum broader together with the presence of the short-lived beta decay products. The spectrum for ^{230}Th, with an energy of 4.77 MeV similar to ^{234}U, is located in the high energy range of the spectrum of the natural uranium, which correspond to the ^{234}U contribution. However, they were not at higher energy than americium. The spectrum for americium, which had an energy of 5.48 MeV, appeared at higher energy channels and showed the narrowest peak of all of them. Lastly, the spectrum for ^{238}Pu, with an energy of 5.59 MeV, appeared at the highest energy channels. Moreover, the shape of the spectrum depended on other factors such as differences in the position and retention inside the PSresin cartridge, which would explain the different shapes of the spectra for ^{241}Am and ^{238}Pu since the former was sharper.

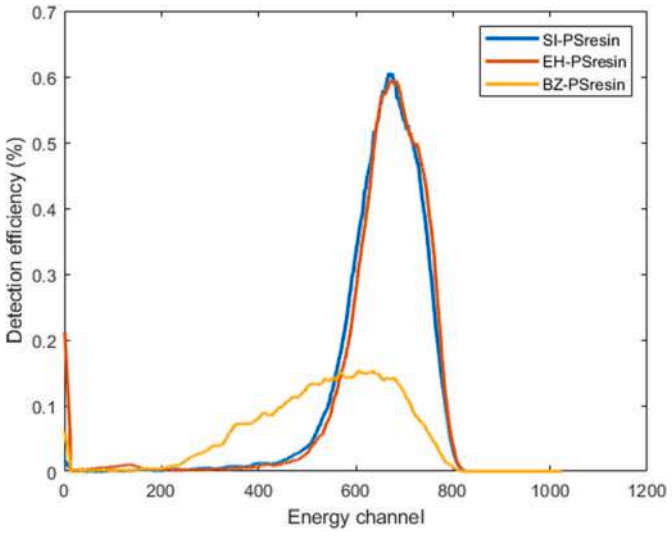

Fig. 3. Detection efficiency spectrum of Am-241 in each PSresin. EH-PSresin (R = 2-ethylhexyl); BZ-PSresin (R = benzyl); SI-PSresin (R = 3-(trimethylsilyl)-1-propyl).

Table 2
Retention and detection efficiency for each type of resin for ^{241}Am, ^{238}Pu, uranium and ^{230}Th. EH-PSresin (R = 2-ethylhexyl); BZ-PSresin (R = benzyl); SI-PSresin (R = 3-(trimethylsilyl)-1-propyl).

	EH-PSresin		SI-PSresin	
	Detection efficiency (%)	Retention (%)	Detection efficiency (%)	Retention (%)
^{241}Am	100 (1)	>99.5	100 (1)	>99.5
^{238}Pu	97.6 (0.6)	>99.3	97 (3)	>99.3
natural U	100 (2)	>98.6	95.9 (0.8)	>98.6
^{230}Th	98 (2)	>97.9	98 (4)	98.2 (0.6)

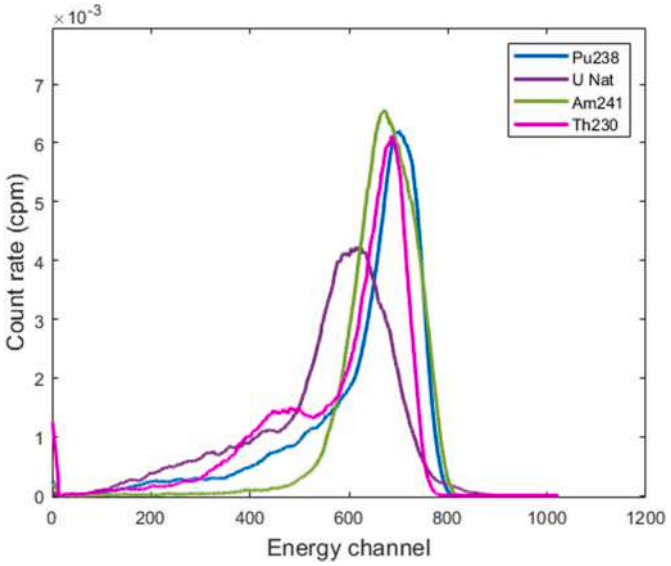

Fig. 4. Normalised spectra for each radionuclide.

No differences were observed in the spectra for EH-PSresin and SI-PSresin (Supplementary Material), demonstrating the similarity of the two extractants used to synthesise the resins.

3.2.4. *Polonium and radium*

Since both resins presented a very good retention of the actinides, their behaviour regarding other common alpha emitters of interest, such as ^{226}Ra and ^{210}Po, was studied.

Retention of polonium was assessed through the measurement of a solution in which ^{210}Pb, ^{210}Bi and ^{210}Po were in secular equilibrium. The spectra obtained (Fig. 5A for the PSresin and 5B for the PSresin cartridge effluent) confirmed the total retention of ^{210}Bi in both PSresins since the peak was broad and located at high energies. By contrast, in the effluent solutions, two clear peaks were identified, one broad peak at low energies corresponding to ^{210}Pb and one sharp peak at high energies

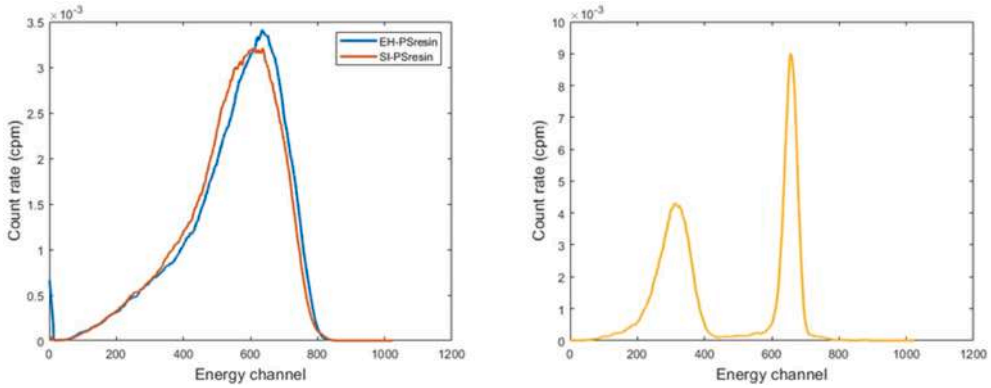

Fig. 5. Normalised spectra of ^{210}Pb, ^{210}Bi and ^{210}Po in the: (A) EH-PSresin and SI-PSresin cartridges; and (B) effluent solution measured through LS.

corresponding to ^{210}Po. This behaviour can be explained by the fact that the oxidation state of bismuth, III, is the one with the highest affinity for this type of diphosphonic acid-based resin in this medium. The retention of polonium was estimated to be around 20%, considering that all bismuth is retained and a 100% detection efficiency in the measurement by LS. No significant differences between the two PSresins were found.

As with uranium, the study of radium was affected by the presence of decay products despite the previous removal of ^{222}Rn before the separation in the PSresin. For this reason just a qualitative analysis of the retention behaviour has been done.

The spectra for ^{226}Ra obtained for EH-PSresin and SI-PSresin (Fig. 6A) were similar, with a broad band indicating that some beta emitters, mainly bismuth radionuclides, were retained in the PSresin cartridge. The spectrum obtained in the measurement of the effluent solution (Fig. 6B) by liquid scintillation indicated that the alpha emitter was weakly retained in both PSresins. In this case, it can be concluded that neither resin presented a good retention of ^{226}Ra in the medium selected, although they presented a good retention of bismuth (^{214}Bi) confirming the results obtained previously for the ^{210}Pb/^{210}Bi/^{210}Po solution.

3.3. Breakthrough volume

Breakthrough volume was studied by the analysis of the PSresin cartridge and the PSresin cartridge effluent after passing 400 mL of 0.5 M HCl through a cartridge which already contained retained ^{241}Am (Table 3).

No differences were observed after passing 400 mL of 0.5 M HCl in terms of retention, detection efficiency and the SQP(E) value for any of the radionuclides and PSresins studied. This, therefore, confirmed that the extractant was strongly adhered to the PSm and the retention of the radionuclide was also very strong.

Table 3
Retention, detection efficiency and the quenching parameter before and after the passing of 400 mL of 0.5 M HCl.

		*Retention (%)		Detection efficiency (%)		SQP(E)	
		Before	After	Before	After	Before	After
^{241}Am	EH-PSresin	>99.5	>99.5	102	102	777	776
	SI-PSresin	>99.5	>99.5	103	104	783	773

*Calculated with the detection limit.

As shown in Fig. 7, the spectrum shifted slightly to lower energy channels after the passing of 400 mL of HCl. This shift can be attributed to a change in the retention pattern along the cartridge, which make the distribution of the radionuclide less homogenous and gave the radionuclide access to areas with worst light emission properties. In spite of that, PSresin demonstrate to be resistant to the pass of 400 mL. For that reason, in case of having a volume sample of several milliliters, the calibration of the detection efficiency and spectrum position might be done under the same condition (same volumes and media for the standards and samples), because as it has been seen, a huge volume of rinse solution or sample modifies the retention pattern along the cartridge.

3.4. Capacity and retention of stable metals

The study of how some stable isotopes are retained in PSresins is of interest as this not only indicates the capacity of the PSresins, but it also provides information about potential stable tracers or stable interferences.

Iron(III) was studied since it is an element commonly found in real samples and its predominant valence state, III, shows affinity for diphosphonic acid-based resins. Europium(III) was also studied as it may

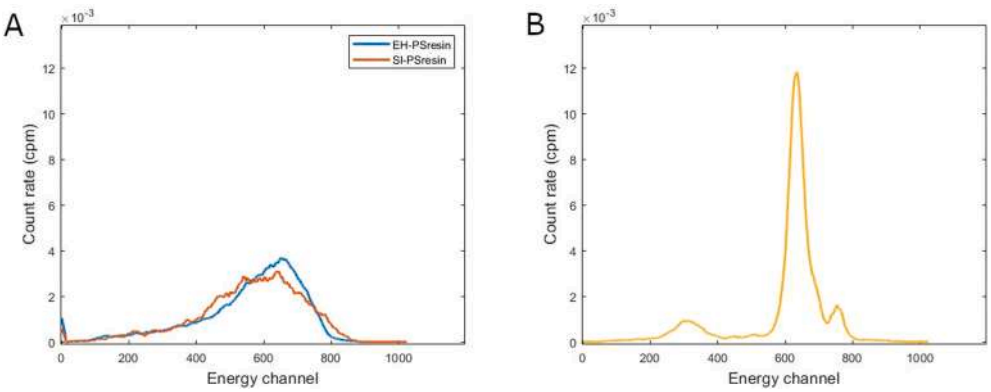

Fig. 6. Normalised spectra of ^{226}Ra in the: (A) EH-PSresin and SI-PSresin cartridges; and (B) effluent solutions measured through LS.

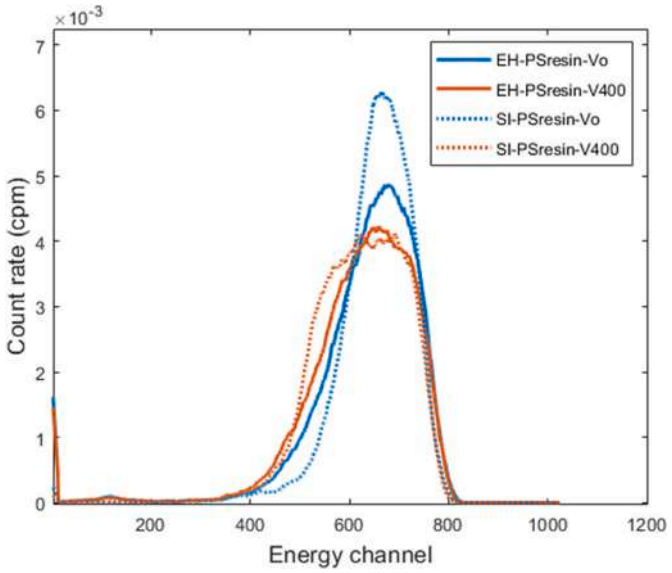

Fig. 7. Normalised spectra for EH-PSresin (continuous line) and SI-PSresin (dashed line) for ^{241}Am. Vo corresponds to the initial spectrum and V400 corresponds to that obtained after passing 400 mL of 0.5 M HCl.

also have a high affinity for the resin and it might be used as a tracer in the extraction process of actinides given its extremely low concentration in samples. Since U, Th, Pu and Am have not stable isotopes, in order to trace its retention in the PSresin in a sample, an element with similar behaviour to them (an analogue) can be used to quantify the yield of the retention. In this situation through a mass balance between the amount of europium spiked in the sample and the amount it is found in the PSresin cartridge effluent, we could know the amount of the analogous radionuclide that has been retained in the PSresin cartridge because all behave similarly in terms of retention into this PSresin. Nevertheless, for its application in real samples, it must be studied further how a non-simple matrix sample could affect the retention and behaviour in the PSresin cartridge of the different actinides and europium.

Both resins for the two elements studied presented similar behaviour since retention profile (supplementary material) and maximum amount of metal retained in each resin (Table 4) are similar. The maximum amount of metal retained was achieved after passing around 2 mg of iron (III) through both resins. For europium (III), EH-PSresin presented a slightly higher capacity than SI-PSresin. This capacity of each resin was relatively low. These results indicated that trivalent metals can become an important interferent in terms of retention, particularly iron(III), which is commonly found in real samples. However, this can be overcome by reducing iron(III) into iron(II) with ascorbic acid. Moreover, despite the relatively low capacities, europium could be used as a stable tracer in the analysis of radionuclides since it is normally not found in real samples and spiking with a low amount (less than 1 mg) would be enough.

However, the low capacity could be improved by increasing the amount of extractant used for the preparation of both PSresins.

3.5. Alpha/beta discrimination

The results obtained in the analysis of the different alpha emitters showed that diphosphonic acid-derived resins were also capable of retaining some beta emitters (e.g., ^{90}Y in 2 M HNO_3). It was therefore worth evaluating the ability of PSresins to discriminate between signals produced by alpha and beta particles, taking advantage of the principle that beta pulses are faster than alpha pulses in organic scintillators. To evaluate alpha/beta discrimination, a ^{90}Sr/^{90}Y solution in 2 M HNO_3 (where ^{90}Y is the beta emitter retained in the PSresin), as well as ^{241}Am and ^{238}Pu solutions in 0.5 M HCl, were passed through a PSresin cartridge and measured at different values of the pulse shape discriminator parameter, PSA, of the Quantulus detector.

Fig. 8 shows the alpha and beta misclassification errors obtained at different PSA values. Both EH-PSresin and SI-PSresin showed similar behaviour (slightly better for EH-PSresin) regarding beta discrimination, with a wrong classification at low PSA values and correct classification at values above 175. For alpha discrimination, a similar behaviour was observed for americium, but not for plutonium, where the misclassification differed slightly, being higher in EH-PSresin than in SI-PSresin. The different behaviour for ^{241}Am and ^{238}Pu can be attributed to the different shapes of the spectra (Fig. 4), since ^{238}Pu had a queue at low energies that tended to be classified as beta. The different behaviour of ^{238}Pu in EH-PSresin and SI-PSresin regarding ^{241}Am can be attributed to factors such as the retention pattern, which can introduce variability in the scintillation process being this variability higher for Pu than for Am.

The values of misclassification at the crossing points are shown in Table 5.

The results demonstrated that alpha/beta discrimination was possible using a compromise PSA value to obtain information about the activity derived from beta and alpha emitters.

Table 4
Capacity of EH-PSresin and SI-PSresin to retain iron(III) and europium(III).

	EH-PSresin	SI-PSresin
Fe (mg/g PSresin)	2.06	1.88
Eu (mg/g PSresin)	2.78	2.13

4. Conclusions

A method for synthesising PSresins to analyse actinides using three diphosphonic acid-based extractants was successfully developed. All three PSresins showed a smooth and homogeneous immobilisation of the extractant. Among the three PSresins, the ones with a 2-ethylhexyl (EH-PSresin) and 3-(trimethylsilyl)-1-propanyl (SI-PSresin) radical chain showed quantitative retention of ^{241}Am, 100% detection efficiencies and no quenching effects, with their spectrum located at high energies. By contrast, the PSresin developed with an extractant containing a benzylic radical chain had a low retention of ^{241}Am and presented a broad spectrum located at low energies. This behaviour was attributed to the steric effects generated by the benzylic radical that affected the interaction between the radionuclide and the extractant as well as the chemical quenching effects caused by the benzyl radical.

EH-PSresin and SI-PSresin presented very similar behaviour in the quantitative retention of ^{241}Am,^{238}Pu, ^{230}Th and ^{NAT}U. Regarding other common alpha emitters such as ^{210}Po and ^{226}Ra, their retention was not quantitative and more studies are required to identify the medium in

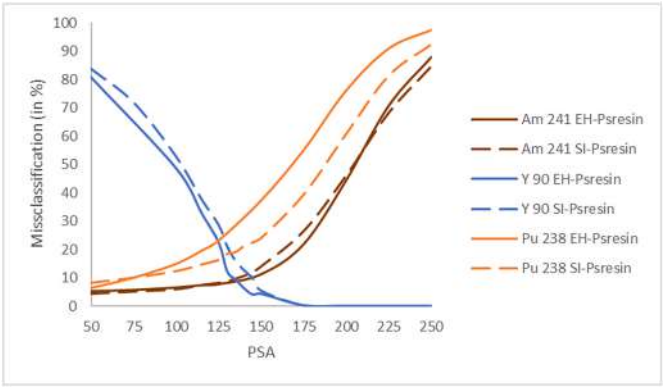

Fig. 8. Alpha and beta classification at different PSA values with EH-PSresin (continuous line) and SI-PSresin (dashed line) for ^{241}Am and ^{238}Pu as the alpha emitters and ^{90}Sr/^{90}Y as the beta emitter.

Table 5
Misclassification error for each PSresin in the crossing points and for the different radionuclides.

	EH-PSresin			SI-PSresin		
	crossing PSA point	Beta (%)	Alpha (%)	crossing PSA point	Beta (%)	Alpha (%)
^{241}Am	150	6	11	150	5	14
^{238}Pu	125	22	30	135	16	19

which these alpha emitters would be retained in order to develop a method for calculating the gross alpha.

The PSresins also showed high retention of beta emitters such as Bi (III) and Y(III), which could lead to the development of applications based on the analysis of these radionuclides.

The capacity of EH-PSresin and SI-PSresin was established to be around 2 mg for Fe(III) and 2.5 mg for Eu(III). Despite the low capacities, these can be used for tracing purposes since the natural concentration of Eu is very low. Moreover, capacity can be improved by increasing the amount of the extractant coating the PSm or by using porous PSm.

Taking everything into consideration, EH-PSresin and SI-PSresin behaved equally in terms of retention yield, detection efficiency, quenching, capacity and alpha/beta discrimination. Both are promising new PSresins that could be used to develop new methods for the total gross alpha test or in actinide analysis.

Declaration of competing interest

The authors declare that they have no known competing financial interests or personal relationships that could have appeared to influence the work reported in this paper.

Acknowledgements

We thank the Spanish Ministerio de Economia, Industria y Competitividad (MINECO) for financial support under award CTM2017-87107-R, and the Catalan Agència de Gestió d'Ajuts Universitaris i de Recerca (AGAUR) for financial support under award 2017-SGR-907.

Appendix A. Supplementary data

Supplementary data to this article can be found online at https://doi.org/10.1016/j.apradiso.2021.109969.

References

Bagán, H., Tarancón, A., Rauret, G., García, J.F., 2011. Radiostrontium separation and measurement in a single step using plastic scintillators plus selective extractants. Application to aqueous sample analysis. Anal. Chim. Acta 686, 50–56. https://doi.org/10.1016/j.aca.2010.11.048.

Chiarizia, R., Horwitz, E.P., Rickert, P.G., Herlinger, A.W., 2007. Acids. Part 1. P,P"-Di(2-Ethylhexyl) methanediphosphonic acid. Solvent Extr. Ion Exch. 14, 773–792. https://doi.org/10.1080/07366299608918368.

Coma, A., Tarancón, A., Bagán, H., García, J.F., 2019. Automated separation of ^{99}Tc using plastic scintillation resin PSresin and openview automated modular separation system (OPENVIEW-AMSS). J. Radioanal. Nucl. Chem. 321, 1057–1065. https://doi.org/10.1007/s10967-019-06659-7.

Duval, Christine E., Devol, Timothy A., Husson, Scott M., 2016. Extractive scintillating polymer sensors for trace-level detection of uranium in contaminated ground water. Anal. Chim. Acta 947. https://doi.org/10.1016/j.aca.2016.09.029. Elsevier Ltd: 1–8.

Duval, C.E., Hardy, teven Pellizzeri, DeVol, Timothy A., Husson, Scott M., 2019. Phosphonic acid and alkyl phosphate-derivatized resins for the simultaneous concentration and detection of uranium in environmental waters. React. Funct. Polym. 137, 133–139. https://doi.org/10.1016/j.reactfunctpolym.2019.01.015.

Egorov, O.B., O'Hara, J.W., M.J., J.W.G., 2006. Equilibration-based preconcentrating minicolumn sensors for trace level monitoring of radionuclides and metal ions in water without consumable reagents. Anal. Chem. 78, 5480–5890.

Eichrom, 2014. Gross Alpha Radioactivity in Water Analytical Procedure, pp. 1–4.

España, 2016. Real Decreto 314/2016. In: BOE-A-2016-7340, vol. 183. Boletin Oficial del Estado, pp. 53106–53126.

Griffith-Dzielawa, J.A., Barrans, R.E., McAlister, D.R., Dietz, M.L., Herlinger, A.W., 2000. Synthesis and characterization of di-[3-(trimethylsilyl)-1-propylene] alkylenediphosphonic acids. Synth. Commun. 30, 2121–2132. https://doi.org/10.1080/00397910008087391.

Horwitz, E.P., Chiarizia, R., Dietz, M.L., Diamond, H., Nelson, D.M., 1993. Separation and preconcentration of actinides from acidic media by extraction chromatography. Anal. Chim. Acta 281, 361–372. https://doi.org/10.1016/0003-2670(93)85194-O.

Horwitz, E.P., Chiarizia, R., Dietz, M.L., 1997. DIPEX: a new extraction chromatographic material for the separation and preconcentration of actinides from aqueous solution. React. Funct. Polym. 33, 25–36. https://doi.org/10.1016/S1381-5148(97)00013-8.

Hughes, L., DeVol, T.A., 2003. On-line gross alpha radiation monitoring of natural waters with extractive scintillating resins. Proc. tenth Symp. Radiat. 505, 435–438. https://doi.org/10.1016/S0168-9002(03)01115-X.

Jay, W., Grate, M.J., Egorov, O.B., 2020. Automated radiochemical separation, analysis, and sensing. In: Handbook of Radioactivity Analysis, vol. 2. Elisever, Amsterdam, pp. 821–879.

L'Annunziata, M.F., 2007. Radioactivity. Introducction and History. Elisever Science B. V., Amsterdam.

Lluch, E., Barrera, J., Tarancón, A., Bagán, H., García, J.F., 2016. Analysis of ^{210}Pb in water samples with plastic scintillation resins. Anal. Chim. Acta 940, 38–45. https://doi.org/10.1016/j.aca.2016.08.004.

L'Annunziata, M.F., 2020. Flow-cell radionuclide analysis. In: Handbook of Radioactivity Analysis, vol. 2. Elisever, Amsterdam, ISBN 9780128143971, pp. 729–820.

McAlister, D.R., Dietz, M.L., Chiarizia, R., Herlinger, A.W., 2001. Metal ion extraction by silyl-substituted diphosphonic acids. I. P,P′-di[3-(trimethylsilyl)-1-propylene] methylene- and ethylenediphosphonic acids. Separ. Sci. Technol. 36, 3541–3562. https://doi.org/10.1081/SS-100108348.

Navarro, N., Rodriguez, L., Alvarez, A., Sancho, C., 2004. Rapid determination of alpha emitters using Actinide resin. Appl. Radiat. Isot. 61, 287–291. https://doi.org/10.1016/j.apradiso.2004.03.023.

Rim, Jung H., 2013. Development of Novel Method for Rapid Extract of Radionuclides from Solution Using Polymer Ligand Film. The Pennsylvania State University, state collage.

Rim, J.H., Armenta, C.E., Gonzales, E.R., Ünlü, K., Peterson, D.S., 2016. Evaluating bis(2-ethylhexyl) methanediphosphonic acid (H2DEH[MDP]) based polymer ligand film (PLF) for plutonium and uranium extraction. J. Radioanal. Nucl. Chem. 307, 2327–2332. https://doi.org/10.1007/s10967-015-4444-3.

Roane, J.E., DeVol, T.A., 2002. Simultaneous separation and detection of actinides in acidic solutions using an extractive scintillating resin. Anal. Chem. 74, 5629–5634. https://doi.org/10.1021/ac026050z.

Roane, J.E., DeVol, T.A., 2005. Evaluation of an extractive scintillation medium for the detection of uranium in water. J. Radioanal. Nucl. Chem. 263 (1), 51–57. https://doi.org/10.1007/s10967-005-0011-7.

Sáez-Muñoz, M., Bagán, H., Tarancón, A., García, J.F., Ortiz, J., Martorell, S., 2018. Rapid method for radiostrontium determination in milk in emergency situations using PS resin. J. Radioanal. Nucl. Chem. 315, 543–555. https://doi.org/10.1007/s10967-017-5682-3.

Santiago, L.M., Bagán, H., Tarancón, A., Garcia, J.F., 2013. Synthesis of plastic scintillation microspheres: evaluation of scintillators. Nucl. Instruments Methods Phys. Res. Sect. A Accel. Spectrometers, Detect. Assoc. Equip. 698, 106–116. https://doi.org/10.1016/j.nima.2012.09.028.

Seliman, A.F., Helariutta, K., Wiktorowicz, S.J., Tenhu, H., Harjula, R., 2013. Stable and selective scintillating anion-exchange sensors for quantification of 99TcO4- in natural freshwaters. J. Environ. Radioact. 126, 156–164. https://doi.org/10.1016/j.jenvrad.2013.07.025.

Seliman, A.F., Bliznyuk, V.N., DeVol, T.A., 2017. Development of stable extractive scintillating materials for real-time quantification of radiostrontium in aqueous solutions. J. Radioanal. Nucl. Chem. 314, 743–751. https://doi.org/10.1007/s10967-017-5420-x.

Tarancón, A., Bagán, H., García, J.F., 2017. Plastic scintillators and related analytical procedures for radionuclide analysis. J. Radioanal. Nucl. Chem. 314 (2), 555–572. https://doi.org/10.1007/s10967-017-5494-5.

Tarancón, A., Bagán, H., García, J.F., 2021. Plastic scintillators in environmental analysis. In: Hamel, M. (Ed.), Plastic Scintillators. Topics in Applied Physics, vol. 140. Springer, Cham.

Triskem, 2015a. PRODUCT SHEET TRU Resin.

Triskem, 2015b. PRODUCT SHEET UTEVA Resin.

Zagyvai, M., Vajda, N., Groska, J., Molnár, Z., Bokori, E., Szeredy, P., 2017. Assay of actinides in human urine by rapid method. J. Radioanal. Nucl. Chem. 314, 49–58. https://doi.org/10.1007/s10967-017-5363-2.

Comparison normalized spectra of EH-PSresin (continuous line) and SI-PSresin (dashed line), for each radionuclide (A: ^{238}Pu; B: ^{241}Am; C: ^{230}Th; D: ^{238}U).

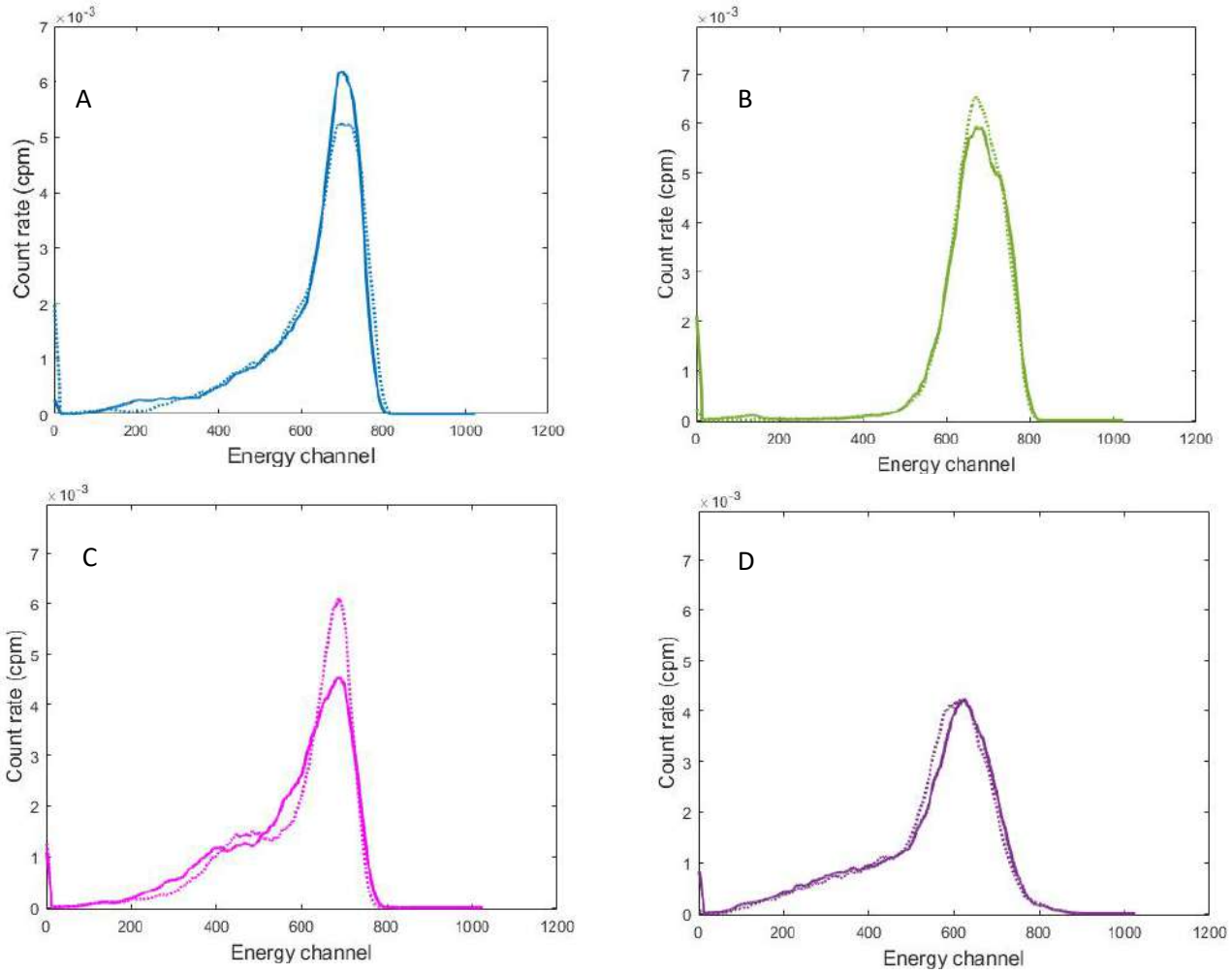

Count data of the measurement of ^{241}Am, ^{232}Th, Uranium and ^{238}Pu with the PSresin.

	EH-Psresin				SI-Psresin			
Radionuclide	**Blank (cpm)**	**Count rate (cpm)**	**Activity added (dpm)**	**Eff (%)**	**Blank (cpm)**	**Count rate (cpm)**	**Activity added (dpm)**	**Eff(%)**
Am-241	0.91	519.06	514.98	101	0.87	543.98	540.1	100.6
		510.34	512.76	99		535.38	522.430	102.3
		515.36	510.25	101		530.41	512.259	103.4
Th-230	0.83	125.91	127.62	98	0.87	128.96	127.523	100.4
		128.84	127.36	101		94.36	98.851	94.6
Nat-U	0.83	197.62	194.24	101	0.87	175.55	185.120	95.3
		190.17	189.87	100		177.2	186.381	94.6
						177.21	188.350	93.6
Pu-238	0.83	400.14	407.44	99	0.87	435.55	431.509	100.7
		407.29	418.56	98		407.8	424.856	95.8
						418.74	438.999	95.2
Y-90	0.83	585.94	584.68	100	0.87	790.5	800.326	98.7

Count data of the breakthrough volume experiment

		Net Count data (cpm)		
	Psresin	Before	After adding 400 mL	Theoretical added cpm
^{241}Am	EH-PSresin	517.4	517.17	504.93
	SI-PSresin	536.78	539.63	519.88

Elution profile of the Fe and Eu capacity experiments.

Fe

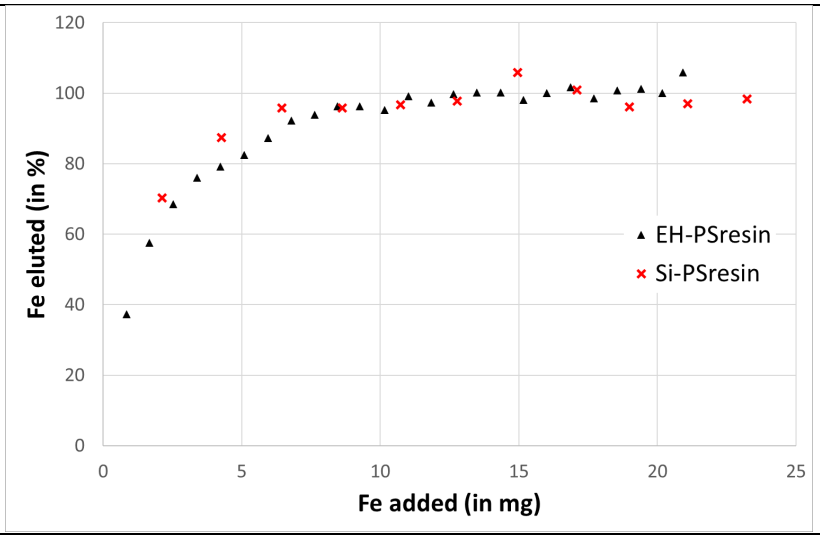

Eu

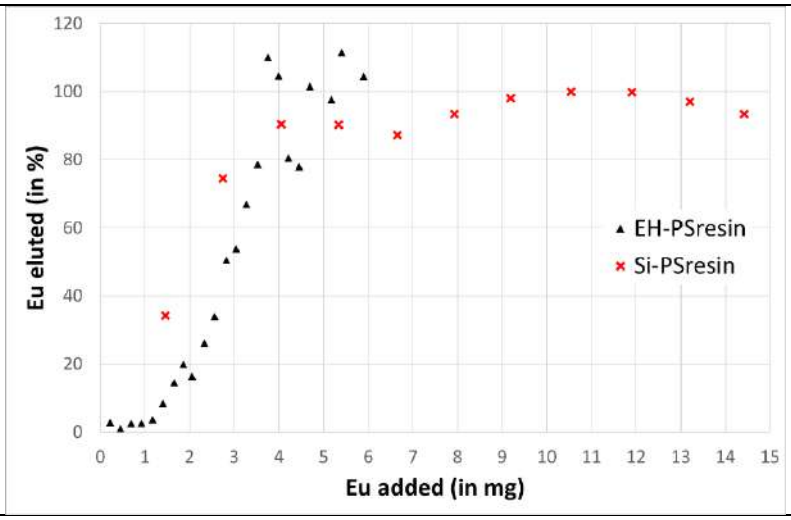

Article #2

Fast analysis of gross alpha with a new plastic scintillation resin

Analytica Chimica Acta 1248 (2023) 340905

Contents lists available at ScienceDirect

Analytica Chimica Acta

journal homepage: www.elsevier.com/locate/aca

Fast analysis of gross alpha with a new plastic scintillation resin

I. Giménez [a], H. Bagán [a,*], A. Tarancón [a,b,c]

[a] Department d'Enginyeria Química i Química Analítica, Universitat de Barcelona, Marti i Franqués, 1-11, ES-08028, Barcelona, Spain
[b] Serra-Húnter Programme, Generalitat de Catalunya, Barcelona, Spain
[c] Institut de Recerca de l'Aigua, Universitat de Barcelona, Montalegre, 6, ES-08001, Barcelona, Spain

HIGHLIGHTS

- New method to measure gross alpha parameter by using a plastic scintillation resin.
- A quantitative retention and 100% detection efficiencies at pH 2 was achieved.
- Gross alpha parameter was measured in less than 5 h.

GRAPHICAL ABSTRACT

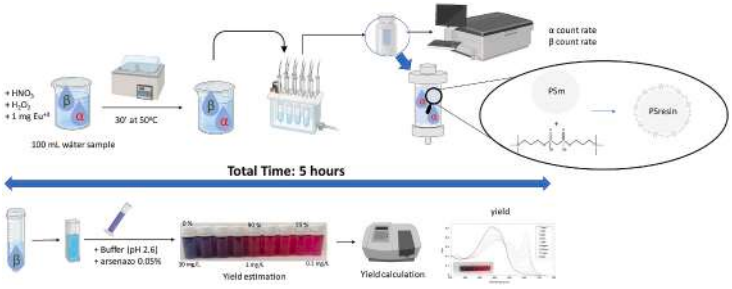

ARTICLE INFO

Handling Editor: Xiu-Ping Yan

ABSTRACT

Radionuclides analysis is a complex task, with high time and economic costs. In decommissioning activities and environmental monitoring, it is very evident, in which, to obtain an appropriate information, it is necessary to perform as many analyses as possible. The number of these analyses can be reduced using screening gross alpha or gross beta parameters. However, the currently used methods cannot give an answer as fast as it would be desired and, moreover, more than 50% of the results reported in the interlaboratory exercises fall outside the acceptance range.

This work presents the development of a new material and method to gross alpha activity determination using a plastic scintillation resin (PSresin) in drinking and river water samples. A specific procedure was developed involving a new PSresin (using bis-(3-trimethylsilyl-1-propyl)-methanediphosphonic acid as an extractant) that is selective for all actinides, radium and polonium. Quantitative retention and 100% detection efficiencies were obtained at pH 2 with nitric acid. PSA value of 135 was used for α/β discrimination. Eu was used to determine or estimate retention in sample analyses. The method developed can measure, in less than 5 h from the reception of the sample, the gross alpha parameter with quantification errors comparable or even lower to those obtained with conventional methods.

1. Introduction

Nuclear energy production is gaining increasing awareness due to its lack of CO_2 emissions and its ability to generate electricity without any greenhouse effect [1]. However, possible accidents and radioactive waste generation pose risks for human beings and the environment,

* Corresponding author.
E-mail address: Hector.bagan@ub.edu (H. Bagán).

https://doi.org/10.1016/j.aca.2023.340905
Received 12 September 2022; Received in revised form 23 January 2023; Accepted 28 January 2023
Available online 2 February 2023

leading to different controversial opinions about its use. On one side, some countries have chosen to break ties with the generation of electricity through nuclear energy. In these countries, many nuclear facilities have reached their operational lifetime. Consequently, radioactivity measurements have to be performed to check if the wastes generated during this decommissioning process can be classified and treated as radioactive residue or not. On the other side, there are some countries that have chosen to rely on nuclear energy to generate electricity, increasing the number of nuclear power plants. In these countries, radioactivity analyses will become commonplace in the laboratories, mainly for environmental surveillance purposes.

Therefore, radioactivity analyses will continue being something needed in the upcoming years, including the determination of specific radionuclides or screening parameters based on gross activity for the assessment of radioactivity content. In general, screening parameters are used to determine if the samples require an exhaustive analysis of specific radionuclides or can be directly classified as non-radioactive. Avoiding the use of complex, laborious and unnecessary selective procedures. The two most important screening parameters for radioactivity assessment are gross alpha and gross beta which are assessed in several situations such as: the classification of wastes generated in normal operations of a nuclear installation or in the dismantling process; first risk evaluation when a disaster (e.g., a nuclear attack or an accident) occurs; assessment of the indicative dose to determine the potability of drinking water. At first sight, it can be seen that these parameters are important in providing a first indication of presence of radionuclides they must be measured reliably and as quickly as possible.

As said before, water intended for drinking purposes must have radioactivity parametric values that comply with national and international standards before being accepted for human consumption [2,3]. The Euratom Drinking Water Directive established gross alpha parameter as one of those of concern for water monitorization. The current parametric limit is 0.1 Bq L^{-1} [4] and encompasses all the alpha-emitting radionuclides once radon has been eliminated (i.e. actinides plus ^{226}Ra and ^{210}Po).

There are some methods for gross alpha activity measurement in water samples. Most of them conduct the measurement with proportional counter or with liquid scintillation counter (LSC) [5,6]. Normally, the pretreatment consists on an evaporation [7] or a co-precipitation [8,9]. These procedures present some problems such as the potential loss of polonium; sample losses during evaporation of salty samples; or non-quantitative precipitation. Moreover, the measurement of gross alpha activity is affected by different factors such as the response of the detector depending on the alpha-emitting radionuclide energy, the radionuclide used as the standard in the calibration, the time delay between the pretreatment and the measurement, the amount of salt (solid residue) in the water sample, the misclassification between alpha and beta signals, and the quenching correction that might be applied for colored samples in the LSC measurements. Due to that, it is commonly accepted that laboratories can present a deviation up to 30% in their measurements [6,9,10]. However, approximately 60–70% of the results obtained in the interlaboratory exercises fall outside the acceptance range. This is because some of the operational parameters mentioned above, particularly the dependence on the calibration radionuclide and the attenuation due to salt content, have a large impact on the final results and, consequently, large differences between laboratories are observed. For that reason, there is still a need to simplify the gross alpha activity determination using a faster method, but also to reduce the variability of this determination.

This work shows the development of a new material and new method to gross alpha activity determination in drinking and river water samples using a plastic scintillation resin (PSresin). A PSresin is composed of plastic scintillation microspheres (PSm) [11] coated with a selective extractant and then packed in a solid-phase extraction (SPE) cartridge, giving as a result a material that unifies the extraction and measurement step. PSresins have been used previously for ^{90}Sr and ^{99}Tc [12,13]. In the present work, a new PSresin, named α-PSresin using bis-(3--trimethylsilyl-1-propyl)-methanediphosphonic acid was developed. The high retention and detection efficiency of α-PSresin make it suitable for a simplified method to measure the gross alpha activity, which would involve only passing the sample through an SPE cartridge containing the PSresin followed by its measurement. Compared to the classical methods based on proportional counters and liquid scintillation, the PSresin methods present the general advantage of having a lower background, as only 1 g of the scintillator is placed on the counter (instead of the 20 mL of sample and scintillator for LSC), leading to equivalent limits of detection with less counting time. Moreover, sample treatment is reduced as the sample only has to be passed through the PSresin. Another potential advantage would be that the extractant does not retain anions or small cations (i.e., K or Na). This implies that autoabsorption of the alpha particles, as happens in proportional counter, would be avoided, and that ^{40}K would not interfere within the measurements, as happens in LSC, reducing misclassification due to beta particles. Another advantage of the use of PSresin for the gross alpha parameter determination is that polonium would be also detected since there is no evaporation step where it could be lost. Moreover, as the method would be faster and easier, more than one sample could be analyzed at the same time. Finally, compared to LS, as no mixed wastes will be generated, the proposed method would be a "green-chemistry" alternative for the gross alpha parameter determination.

2. Experimental section

2.1. Materials

α-PSresin was prepared by coating plastic scintillation microspheres (PSm) with Bis(trimethylsilylpropanyl)methanediphosphonic acid in isopropanol [14]. Extractant was synthesized using 3-(trimethylsilyl)-1-propanol (97%) and *N*,*N*′-diisopropylcarbodiimide (DIC) (98% purity) from Merck (Darmstadt, Germany) and methylenediphosphonic acid (99+%) from Alfa Aesar (Kendal, Germany). PSm were prepared by using the evaporation/extraction method [11].

Non-radioactive standards used include a 1000 mg L^{-1}europium solution from Inorganic Ventures (Christiansburg, USA). Radioactive standards used were: 38.5 (0.3) Bq/g ^{90}Sr/^{90}Y, 46.3 (1.4) Bq/g ^{238}Pu, 47 (1) Bq/g ^{241}Am; 2.22 (0.03) Bq/g uranium (^{238}U + ^{235}U + ^{234}U); 2.38 (0.07) Bq/g ^{230}Th; 4.0 (0.1) Bq/g ^{226}Ra; and 160 (5) Bq/g ^{210}Pb. Radioactive solutions were supplied by different providers. ^{210}Po was obtained by passing the ^{210}Pb solution (containing in equilibrium ^{210}Bi and ^{210}Po) through an Sr-resin (TrisKem International (Rennes, France)) in a 3-M nitric acid medium (retaining ^{210}Pb and ^{210}Po) and then eluting ^{210}Po with 0.1 M nitric acid.

0.05% arsenazo (III) solution was prepared using a buffer solution of pH 2.6–2.8 that was obtained by mixing monochloroacetic acid and sodium acetate in 100 mL of deionized water.

2.2. Procedures

2.2.1. Retention profile of iron

α-PSresin capacity was determined as the plateau of a retention profile curve. This curve was obtained by measuring the Fe(III) in the 2 mL eluted solutions generated after passing 50 mL of a 1000 mg L^{-1} iron (III) solution through 1 g of α-PSresin. Solution medium was 0.5 M HCl and iron (III) was analyzed with a Optima 8300 ICP-OES equipment (PerkinElmer, Waltham, USA).

2.2.2. Batch study

For the batch study, 0.1 g of α-PSresin was weighed in a 14 mL glass cylindric tub together with 3 mL of the corresponding medium containing 1.4–1.6 Bq of the radionuclide under study (^{241}Am, ^{238}Pu, ^{230}Th, ^{236}U, ^{210}Po and ^{226}Ra). For Sr, Y and Pb, the same study was performed, but with the addition of 0.2 mg of the stable isotope instead of the

radioactive. After 24 h of agitation, the resulting supernatant was filtered with disk filters (0.45 μm) and measured together with 2 mL of double-deionized water and 15 mL of OptiPhase Supermix liquid scintillating cocktail in a Quantulus liquid scintillation spectrometer (both from PerkinElmer (Waltham, USA)) for 1 h. In the case of the stable isotopes, the same procedure was followed, but the measurement was performed through ICP-OES in a 1% nitric acid medium.

The media studied were: HNO_3, HCl and H_3PO_4 within the range of 0.5–8 M and at pH 1, 2, 4 and 7.

2.2.3. Standard sample analysis

11 mL samples of known activity were prepared by adding to a 20 mL vial the corresponding radioactive solution, water and nitric acid to a final pH 2. Standard samples were measured with the α-PSresin in a 2 mL cartridge using a the twelve-position vacuum chamber (TrisKem International, Rennes, France) and employing the common procedure for separations with PSresins [14].

After the separation, the dried α-PSresin cartridge was counted in the Quantulus to determine the detection efficiency. The α-PSresin was also measured at several PSA values. An aliquot of the collected wastes was also measured by liquid scintillation (6:14 sample:cocktail proportion) to determine the separation yield.

Ra not retained was determined through secular equilibrium with the descendants following the UNE-EN ISO 13164–4_2020 test method [15].

All the standard samples were analyzed in triplicate.

2.2.4. Sample analysis

100 mL of sample was acidified with nitric acid up to a pH of 2. Hydrogen peroxide was added to reach a 1% concentration. Moreover, the sample was spiked with 1 mg of europium, which is a tracer for alpha-emitting radionuclides. Next, it was treated for 30 min at 50 °C to assure a correct valence adjustment. The resulting solution was then measured with the α-PSresin.

Six real samples (A21/074, A21/031, A21/044, A21/071, A21/118 and Mreal_1) taken from different places in Catalonia (Spain) and 3 interlaboratory samples (JRC-GAB-1, JRC-GAB-2 and IAEA-TEL-2021-03 (sample 5)) were analyzed. One of the real samples (Mreal_1), which had been fully characterized previously and contained naturally occurring radionuclides, and one of the interlaboratory samples (IAEA-TEL-2021-03 (sample 5)), containing artificial radionuclides, were used to define the optimum PSA value for the measurements. Therefore, both were measured at the most promising PSA values: 135, 150 and 175. The other samples were measured at the optimum PSA value of 135. The real samples were previously measured at the Laboratori de Radioactivitate Ambiental (LRA) of the Universitat de Barcelona using the LSC method [6]. Moreover, for the Mreal_1 a determination of all the alpha emitters found in the sample was also done by the LRA.

2.2.5. Retention determination

Two strategies were followed to determine retention: estimation through a visual check and determination with UV–Vis spectrophotometry. Both were based on the formation of a colored complex of Eu with arsenazo (III).

The visual check consisted of taking 10 mL of the effluent solution and adding to it 8 mL of a buffer solution (pH 2.6–2.8) and 1 mL of a 0.05% arsenazo solution. The obtention of a reddish colored solution, similar to that of the arsenazo solution, indicates a retention of Eu higher than 90%, whereas a purple solution indicates that Eu has not been fully retained in the PSresin.

The same solutions were also measured by UV–Vis spectrophotometry at 654 nm. The calibration curve was from 0.1 to 10 mg L^{-1}.

2.2.6. Scintillation measurement conditions

The Quantulus detector was configured at low CB and ^{14}C MCA. α-PSresin and effluent solutions were both counted for 1 h.

The PSresin was also measured in the "PSA" configuration at the following PSA values for 15 min each: 50, 75, 100, 115, 125, 130, 135, 140, 145, 150, 175, 200, 225 and 250.

The PSresin used for the real and interlaboratory samples was measured under the optimum PSA for 2 h each. The effluent solutions were measured for 5 h.

2.2.7. Data treatment

Scintillation spectra were smoothed with the Savitzky–Golay filter (21 points and a first-degree polynomial). Detection efficiency corresponds to the net count rate divided by the activity retained in the α-PSresin.

Alpha misclassification for the alpha standards corresponds to the percentage of the counts in the beta window (1:1024) divided by the total counts. Beta misclassification for the beta was calculated the percentage of the counts in the alpha window (1025:2048) divided by the total counts.

Gross alpha activity (A in Bq L^{-1}) was calculated with the following equation:

$$A = \frac{\frac{CpmA * Effb - CpmB * Intb}{Effa * Effb - Inta * Intb}}{V * 60} \quad (1)$$

where, CpmA the net count rate in the alpha window (in cpm), CpmB the net count rate in the beta window (in cpm), Effa the detection efficiency of the alpha-emitting radionuclides in the alpha window, Effb the detection efficiency of the beta-emitting radionuclides in the beta window, Inta is the misclassification of alphas in the beta window, Intb the misclassification of betas in the alpha window, and V the volume of the sample analyzed (in L).

The combined standard uncertainty was calculated with the following equation using the 20.06.6 version of the wxMaxima free access software:

$$u_c\left(A\left(x_1 - x_{2,\ldots}\right)\right) = \sqrt{\sum \left(\frac{\partial A}{\partial x_i}\right) u(x_i)^2} \quad (2)$$

where A is the function given in Equation (1), xi the different variables on which the value of A depends, and u (xi) the standard uncertainties of each variable.

The detection limit was established theoretically using the Currie equation [16].

3. Results and discussion

A previous study [17] tested the viability of different extractants in the development of a new PSresin. Bis(trimethylsilylpropanyl)methanediphosphonic acid was chosen as the most promising extractant for the development of a new PSresin to measure gross alpha thanks to the actinides high retention and the good α/β discrimination. The development and optimization of this new PSresin, named α-PSresin, and the fast analysis of water samples is described herewith.

3.1. α-PSresin optimization

In order to be able to prepare a PSresin in a bigger scale, the first objective was to improve the synthesis method of the extractant to obtain a purer compound with a high synthesis yield. The main problem was that some sub-products generated during the synthesis (i.e. urea) were partially soluble in organic solvents and water. As consequence, their extraction during the work up was not complete regardless the separation procedure used. Therefore, the synthesis procedure was modified first by changing the reaction solvent from tetrahydrofuran to dichloromethane and the volumes used. On the one hand, the initial volume of solvent in which methanediphosphonic acid and 3-trimethylsilyl-1-propanol were mixed and refluxed was reduced. On the other

hand, the solvent volume in which the coupling agent was dissolved was increased, to obtain a diluted solution that promoted the formation of the disubstituted compound. Moreover, dropwise addition over 3 h promoted the disubstitution reaction. It must be also mentioned that *N*, *N*′-dicyclohexylcarbodiimide (DCC) was replaced with *N*,*N*′-diisopropylcarbodiimide (DIC) as the coupling agent. The main reason for this substitution was that the urea derivative compound occurring as a subproduct of the reaction was easier to extract when DIC was used, making the process easier and producing a purer compound. 3-dimethylamino-propyl-ethyl-carbodiimide (EDC) was also tested due to its lower size compared with DIC and DCC. However, the main product obtained was the tetra-substituted compound instead of the desired disubstituted compound. Finally, an N_2 purge was included in all the synthesis steps. As a result, the extractant obtained had a high purity (>95%) if we consider the RMN spectrum and the yield was 70%, in accordance to the acceptable yield previously obtained for a similar kind of molecule [20].

Once the synthesis of the extractant was optimized, the amount of extractant deposited on the PSm surface was studied. Increase on the extractant amount would lead to the increase of the capacity of the column. However, an excess of it, detectable though visual observation in the scanning electron microscopy (SEM), may cause problems in the pass of the solution through the column bed, affecting retention, or even quenching, due to the attenuation of the alpha particles emitted, affecting detection efficiency. Two different proportions of PSm to extractant were tested: 1:1/6 and 1:1/4. Evaluation of the α-PSresins prepared was done by comparing those parameters for both proportions.

Detection efficiency and retention was determined by analyzing with the PSresin a standard sample of ^{241}Am in a medium of 0.5 M HCl. As can be seen in Fig. 1, there were no significant changes in the spectrum position. Retention and detection efficiency were 100% for both proportions.

Therefore, it was confirmed that there was no significant difference between the two proportions tested and that the extractant layer added on the scintillating support did not generate additional particle quenching effects.

The capacity of the resin was also checked in order to know which is the amount of sample that could be passed through the cartridge This is relevant for the analytical purposes of the α-PSresin as capacity determines the possibility of directly passing a large volume of water sample through the resin without any further treatment. This study was performed with iron as it is known that iron is also retained in this extractant [14]. Table 1 shows the capacities obtained for α-PSresin for both proportions and with the old extractant.

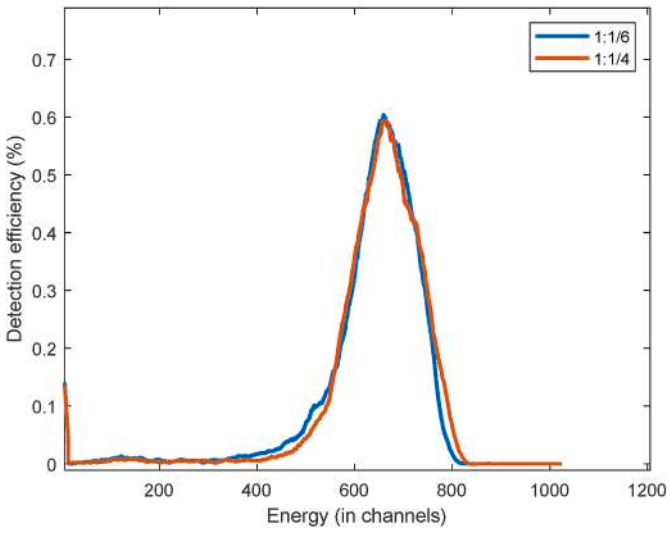

Fig. 1. Comparison of the detection efficiency spectra for different PSm: extractant proportions for a^{241}Am standard measure.

Table 1
Amount of Fe retained in α-PSresin at two immobilization proportions and with the old extractant.

	1:1/6 PSresin (old extractant	1:1/6 α-PSresin	1:1/4 α-PSresin
Fe retained mg/g PSresin	1.88	4.01	5.81

The optimization of the extractant improved the capacity, which was doubled when comparing the same proportions of the old extractant (1:1/6 PSresin) and the new one (1:1/6 α-PSresin). This confirms that increase on the purity of the extractant lead to more binding active sites. Moreover, it is worth to remark that with a proportion of 1:1/4, the amount of iron retained increased and was around 6 mg. This capacity is big enough ensure a correct water analysis involving the PSresin, taking into consideration the amount of possible stable interfering elements that a river or drinking water could contain (e.g. Fe, Ca), and that the affinity of the extractant for actinides is several orders of magnitude higher than for those elements [17].

Finally, morphology was studied by SEM to evaluate the homogeneity of the recovery. The images obtained with a JSM-7100 F JEOL (Tokyo, Japan) scanning electron microscope from the CCiTUB (Fig. 2) showed that α-PSresin was homogenously coated for both proportions. It might seem that a slight excess of extractant occurred when the proportion of the extractant was increased, as the quantity of extractant in the 1:1/4 proportion seems to be more than the necessary to cover the support and some aggregation takes place. Nevertheless, as the 1:1/4 proportion presented a higher capacity, probably due to this excess of extractant; detection efficiency and recovery were unaffected; no extractant losses were detected; and it did not show problem of solution pass throw the column, it was selected for the subsequent experiments.

3.2. Batch study of α- and β-emitters

In order to determine the gross alpha parameter, the retention of all actinides without the retention of the beta emitters, would be desirable. The retention of actinides in bis(trimethylsilylpropanyl)methanediphosphonic acid in 0.5-M HCl was shown to be quantitative in a previous study [17]. However, Ra and Po, both alpha emitters with a natural origin, were not quantitatively retained in this medium. Therefore, a more detailed study of the retention media was performed. The different acid media and their concentrations were chosen based on the previous knowledge on this type of extractants [18–23] and the contact time, 24 h, was selected to ensure enough time for the interaction between the radionuclide and α-PSresin.

The retention curves obtained for several nitric acid concentration is shown in Fig. 3a. The retention profiles obtained with the other acids (HCl and H_3PO_4) were similar and can be checked in detail in the Supplementary Information figures (SI).

In one hand, the retention of all actinides was quantitative in all the concentrations studied which agrees with the very strong affinity of diphosphonic extractants for actinides at different oxidation states described in the literature. On the other hand, the retention of the beta emitters was, in general, low at high acid concentrations, with a small retention of some trivalent beta-emitting radionuclides such as ^{210}Bi or ^{90}Y at HNO_3 8 M. Other alpha emitters, such as polonium and radium, which might be relevant for the measurement of the gross alpha parameter, are not retained at these high acid concentrations, but they are quantitatively retained in low acid concentrations. This means that the extractant is also capable to be linked to divalent elements at low acidic concentrations. As the priority is the retention of all the alpha emitting radionuclides, and the contribution to the scintillation signal of those betta emitter radionuclides retained can be suppressed or corrected through the alpha/beta discrimination analysis, the range of pH between 1 and 7 was studied in more detail (Fig. 3b). In this range, there

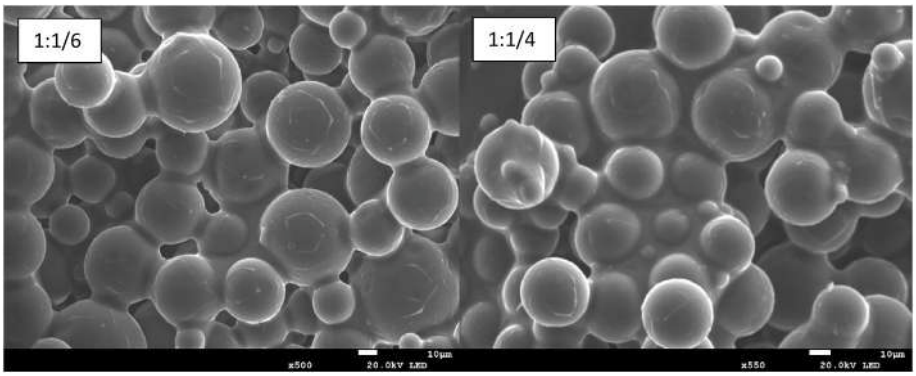

Fig. 2. Comparison of the α-PSresin coating for two different proportions 1:1/6 (left) and 1:1/4 (right) using SEM images.

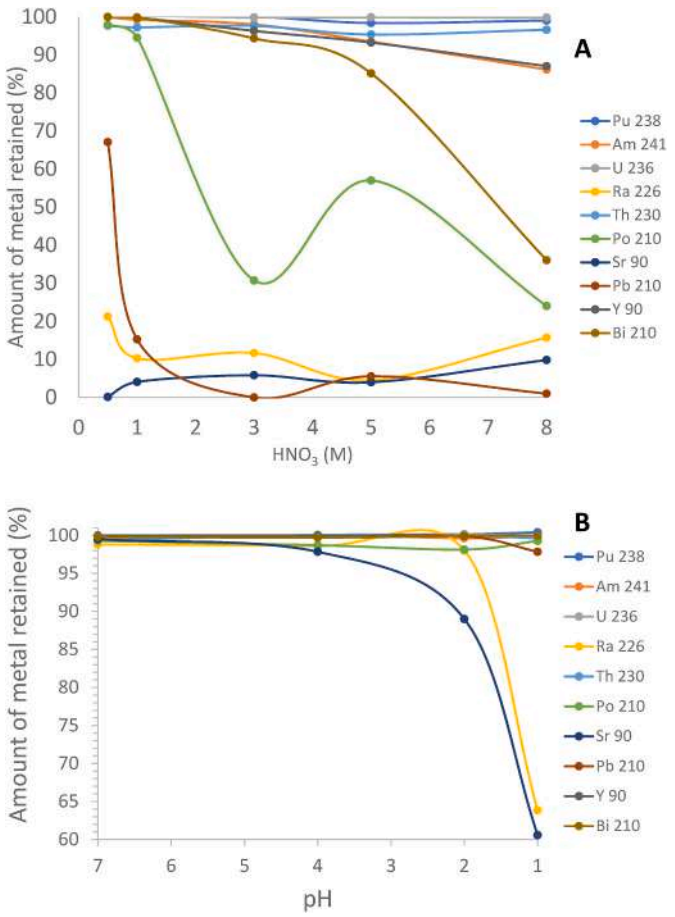

Fig. 3. Results from the batch study. Proportion of metal retention (%) at nitric acid concentrations between 0.5 M and 8 M (A) and at pH values from 1 to 7 (B).

was quantitative retention of radium at pH 2 along with a non-quantitative retention of strontium. Therefore, pH 2 with HNO_3 was chosen as working medium, with the additional advantage that it provided an analytical procedure without the requirement for any further pretreatment, since samples typically arrive acidified at pH 2. It is also important to remark that even in a neutral aqueous medium, without the addition of acid, the retention of all the alpha emitting elements was high.

3.3. Quality parameters of the α-PSresin in a cartridge

The retention of alpha emitters in the α-PSresin cartridge can change from the observed in the batch study because it also depends on the contact time or the pass of the solution through the column. Therefore, the α-PSresin cartridge retention of each radionuclide, in the normal working conditions of a column separation, was studied. This also permitted the determination of the detection efficiency under the chosen working medium, pH 2, for each radionuclide.

In the first trials, all the actinides were quantitatively retained, with a detection efficiency of 100%. However, ^{210}Po showed a non-quantitative retention. This was because its valence state was not adjusted to IV. To ensure the oxidation of all polonium into polonium (IV) hydrogen peroxide was added ot the samples (final concentration of 1%) and they were incubated for 30 min at 50 °C in a water bath. The retention and the detection efficiency of each radionuclide found in these conditions can be seen in Table 2.

The study of the retention of radium in the cartridge was possible to be done due to a previous purification [24] of the ^{226}Ra standard in which all the daughter radionuclides (in particular ^{210}Pb and ^{210}Po) were removed, leaving the solution free of other radionuclides [15]. However, it was not possible to quantify the detection efficiency as some subproducts, probably I_2, from the purification process still remained in the solution. Although the amount was small and did not interfere with the retention of radium, it was enough to produce quenching and disturb the spectrum and the determination of the detection efficiency in the α-PSresin. However, taking into consideration that its energy (4.87 MeV) is between that of ^{236}U (4.57 MeV) and ^{238}Pu (5.59 MeV) and leaving aside other parameters that could also affect the measurement such as retention pattern or oxidation state, it could be estimated that ^{226}Ra detection efficiency and spectrum position would be equivalent to that of ^{236}U and ^{238}Pu.

Going back to Table 2, the retention for all the radionuclides studied was quantitative, except for ^{210}Po, which was almost quantitative (97%). Similarly, the detection efficiency for all of them, except for ^{210}Po, was around 100%. The spectrum for each radionuclide is shown in Fig. 4.

Table 2
Quality parameters for each radionuclide (values in brackets shows the standard deviation between triplicates).

	Retention (%)	Detection efficiency (%)
^{241}Am	>99.5[a]	100 (2)
^{238}Pu	>99.5[a]	100.5 (0.8)
^{236}U	>99.5[a]	101 (1)
^{230}Th	>99.5[a]	97.3 (0.2)
^{226}Ra	>99.5[a]	–
^{210}Po	97 (1)	88 (1)

[a] Activity on the effluent solution below LoD.

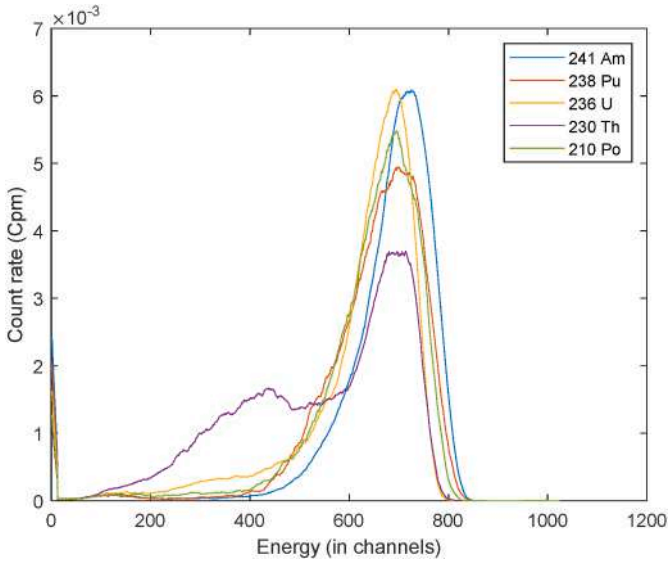

Fig. 4. Normalized count rate spectra for all the alpha-emitting radionuclides measured in the α-PSresin cartridge.

All the spectra appeared at high-energy channels and there were no large differences between radionuclides except for ^{230}Th, which presented a peak at lower energies. One hypothesis to explain this spectra is that, due to its chemistry, Th follows a different retention pattern through the α-PSresin cartridge. This may lead to some precipitation or deposition on the PSm surface [14] during the separation process. As consequence, some attenuation of the alpha particles before reaching the scintillator takes place. Nevertheless, the yield and efficiency for ^{230}Th were also close to 100%.

Regarding the other radionuclides, most of the peaks appeared in a similar position between channels 400 and 850. The small differences can be associated to energy of the α particle, uncertainty of the measurements and differences in the retention pattern on the PSresin [15].

3.4. Alpha/beta discrimination and calibration

As some beta emitting radionuclides could also be retained in the PSresin, their signal could interfere with the one from alpha emitting radionuclides. Therefore, alpha/beta discrimination was studied in order to reduce as much as possible their interference.

Alpha/beta discrimination was studied using ^{90}Sr/^{90}Y in secular equilibrium as a pure beta emitter and ^{241}Am, ^{238}Pu, ^{236}U and ^{210}Po as the alpha-emitting radionuclides, as those present different energies and retention patterns on the PSresin and can therefore have different α/β discrimination behavior. α-PSresin cartridges containing the retained radionuclides were measured using a pulse shape discrimination parameter, measuring at several values of PSA. The aim was to characterize the alpha/beta discrimination capacities of the detection system, as well as to determine which PSA value and which alpha radionuclide were the most suitable to be used as a standard for the calibration of the method. Fig. 5 shows the alpha/beta discrimination for the radionuclides studied.

The misclassification for ^{241}Am was a bit lower than that for the other radionuclides, since it had the thinnest peak and showed a smaller queue at lower energies, as observed in Fig. 4. This improves the classification of particles since low-energy scintillation signals are classified mainly as beta. For the other alpha-emitting radionuclides studied (^{238}Pu,^{236}U and ^{210}Po), the misclassification, as well as the crossing PSA (i.e., the PSA value where alpha and beta misclassifications are equivalent), were similar. Therefore, one of them or a combination of them should be used for the calibration.

^{210}Po was rejected for calibration since it needs to be purified from its parent radionuclides (^{210}Pb and ^{210}Bi) before use, making it not suitable, even though the results were good enough. The selection of ^{238}U/^{234}U, probably the most common in natural waters, was not possible for the presence of short-lived daughter beta emitters in equilibrium (i.e. ^{234}Th, ^{234}Pa) that are also retained in the α-PSresin, thus impeding adequate alpha/beta discrimination calibration. Therefore, the mean between ^{238}Pu and ^{236}U were chosen to determine the working PSA.

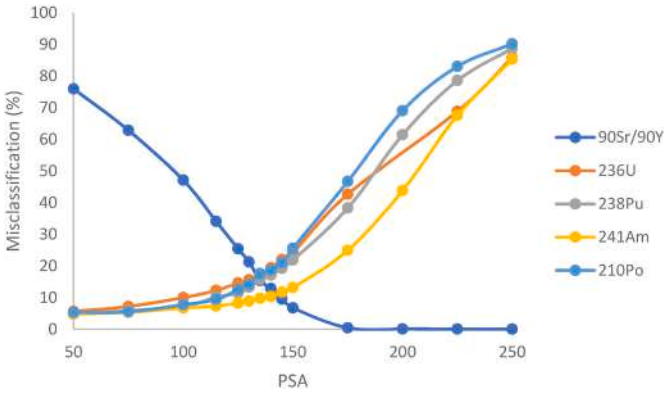

Fig. 5. Misclassification versus the PSA value for ^{236}U, ^{238}Pu,^{241}Am and ^{210}Po.

In order to select the PSA value for the analysis, several factors were taken into account. In one hand, the crossing value of 135 is of interest since alpha and beta misclassifications are compensated. In the other hand, at high PSA values, there will be no interference from the beta-emitting particles in the alpha window, but a lower efficiency of the alpha emitters will be also expected. Therefore, the other PSA values of interest were 150, as the beta misclassification is very low, and 175, because all beta particles are correctly classified and the calculation is simplified. Table 3 shows the alpha and beta misclassification, as well as the detection efficiencies at the different PSA values selected.

These values of detection efficiency and misclassification values were applied in the gross alpha parameter quantification of a real water sample (Mreal_1) and also an interlaboratory sample from IAEA (IAEA-TEL-2021-03 (sample 5)). The objective was to determine which PSA value is the best for the quantification. Mreal_1 is a natural water sample that contains only uranium isotopes at an activity of 1.105 Bq L^{-1}, as provided by the LRA from the Universitat de Barcelona after full characterization by alpha spectrometry. The IAEA-TEL-2021-03 (sample 5) is an interlaboratory sample containing artificial alpha radionuclides. The sample volume was 100 mL and sample treatment only consisted of incubation for 30 min in a water bath at 50 °C after hydrogen peroxide addition to a final concentration of 1%. Moreover, a LSC measurement of the eluted solution was performed to check the retention of all the alpha-emitting radionuclides in the α-PSresin. The values of the quantification deviation at each PSA are shown in Table 4.

For both samples, alpha radionuclides were quantitively retained on the PSresin as no signal was detected on the eluted solutions measured by LSC. The deviations for both samples were lower than 15%

Table 3
Detection efficiency and misclassifications for each PSA studied for the different radionuclides analyzed.

PSA	Detection efficiency (%)				Misclassification (%)			
	^{238}Pu	^{236}U	^{90}Sr	Pu + U	^{238}Pu	^{236}U	^{90}Sr	Pu + U
135	84.2 (3)	82.6 (1)	84.7 (0.1)	85 (4)	16 (3)	17 (2)	12.4 (0.2)	16 (1)
150	78.1 (4)	75.8 (2)	91.9 (0.2)	77 (2)	22 (4)	24 (2)	3.8 (0.2)	23 (2)
175	61.7 (4)	57.3 (0.2)	95.4 (0.1)	59.5 (3)	38 (4)	42.7 (0.2)	0.19 (0.01)	41 (3)

Table 4
Deviation obtained in the quantification of each reference sample at each PSA studied.

PSA	Replicate	Quantification deviation (%)	
		Mreal_1	IAEA-TEL-202-013
135	1	2.0	−14.8
	2	−1.6	6.3
	3	1.6	−10.7
150	1	1.7	−10.9
	2	−7.4	−17.3
	3	−1.4	−11.4
175	1	0.7	−7.2
	2	−10.9	−4.4
	3	3.0	−13.0

irrespective of the PSA value used. These values are highly satisfactory since a deviation of up to 30% [6] is accepted in the gross alpha activity measurement. These results proved that the proposed calibration can be used for both type of sample.

Finally, the deviations were similar for the three PSA studied but slightly lower when using PSA 135. Therefore, PSA 135 was selected for the calibration.

3.5. Retention determination for the alpha-emitting radionuclides

When a separation process is performed, some unknown elements from the sample could modify the retention in the column. Therefore, a tracer has to be used to quantify the retention of radionuclide under analysis. The conventional methods for the gross alpha parameter determination (i.e. LSC or proportional counter) assumed that there are no losses of any of the radionuclides present in the sample when an evaporation or precipitation is performed. It is assumed, for example, that polonium is not lost during evaporation, that all the alpha-emitting radionuclides precipitate or that no splashes take place when the solution is heated until close to dryness.

In this case, using the α-PSresin, the retention of alpha emitters was always quantitative and, therefore, a 100% retention can be assumed in normal conditions. However, the presence of other stable elements in a sample that could be also retained in the α-PSresin, could produce changes in this retention, in particular if their quantity is high. This could be the case of calcium, iron or the organic matter. For a 100 mL sample the amount of iron is lower than the capacity which may be not a problem for the actinide's retention. In the case of calcium, its amount is of the order of the capacity, but it is described that even at high Ca concentrations (0.02–2 M) the retention of actinides in such type of extractants is still very high ($k > 1000$) and unaffected. Regarding organic matter, it has been checked previously in other works that it has no effect in the retention of other radionuclides in a PSresin. For this reason, an easy way to determine the real retention for each sample was proposed. Nevertheless, the proposed method is intended for drinking or river water samples in which the quantities of elements as calcium or iron, that can be retained in the column, are low enough. In addition, organic matter quantities were not enough to change the retention. The tracer has to be non-radioactive to avoid interfering signals in the PSresin and has to be measurable with a non-radioactive technique (e.g., AAS and IPC).

For the α-PSresin europium was used as the non-radiometric surrogate, since it is retained in the α-PSresin in an analog way to that of the actinides and its presence in natural waters is negligible. Europium can be measured in the effluent solution by ICP-OES and ICP-MS. However, a colorimetric assay, in which retention could be estimated by a visual check or quantified by UV–Vis spectrophotometry, was chosen in this case. The ideas was to make easy the application of this method in any laboratory. To perform this, a method based on a colored complex of europium with arsenazo (III) at a pH of 2.6–2.8 was used [25,26]. The organic ligand, at this pH, presents a pink color, whereas within the presence of europium, the solution turns violet (Fig. 6).

Fig. 6 shows the spectra obtained and the color of the calibration standards and the blank (ordered from 10 to 0 mg L^{-1}). The signal produced by the presence of the europium complex was observed at around 654 nm, while the signal corresponding to the pink color of arsenazo without the presence of europium was observed at 525 nm.

From the point of view of an ultra-fast method, a simple visual check based on the absence of the violet color in the separation effluents could be enough to confirm that europium is not present in them and therefore the retention is quantitative. To validate this approach, a detection limit for visual check must be established. From the color of the vials in Fig. 6, it can be seen that at concentrations of 1 mg L^{-1} or lower the solution becomes pink, making not possible to detect the presence of the violet color of the complex. Considering that the sample volume is 100 mL and the amount of europium added is 1 mg, the expected concentration in the column effluents would be of 10 mg L^{-1} if there is no retention of europium. Therefore, the simple visual check can be used to ensure a retention higher than 90% and to assume a quantitative retention, making a more detailed determination unnecessary since the deviations in the calculations would be acceptable.

However, in those cases that a more accurate determination is desired, an accurate determination could be performed by measuring the spectra using UV-Vis spectrophotometry. The absorbance at 654 nm versus the europium concentration was used for the calibration curve fitting (Fig. 7). The absorbance presented a linear correlation with the concentration of europium between 0.1 and 1 mg L^{-1} which is the region of europium concentration expected for the α-PSresin separation effluents in case of quantitative retention. Taking into account the detection limit of the method, a 0.1 mg L^{-1} concentration in the effluent could be clearly detected with UV–Vis spectrophotometry and therefore a retention higher than 99% could be stablished.

3.6. Real sample analysis

Finally, the method proposed for measuring gross alpha activity was validated by analyzing two samples from the interlaboratory programs organized by the European JRC (JRC-GAB-1 and JRC-GAB-2) and five real water samples from the surroundings of Catalonia. In this last case, the results were compared with the ones given by the LRA of the Universitat de Barcelona obtained with the LSC method.

The gross alpha activity quantification was performed in two ways: by estimation of the retention by a visual check, supposing a scenario of an ultra-fast measurement, and by quantification with UV–Vis spectrometry. Regarding the visual check, the effluents obtained after the passing of the sample through the PSresin presented a clear pink color after the addition of the reagents and, therefore, quantitative retention was assumed for the activity calculation (Table 5). When the retention was calculated by UV–Vis spectrometry, values between 95% and 100% were obtained. Results demonstrate that for this kind of samples the

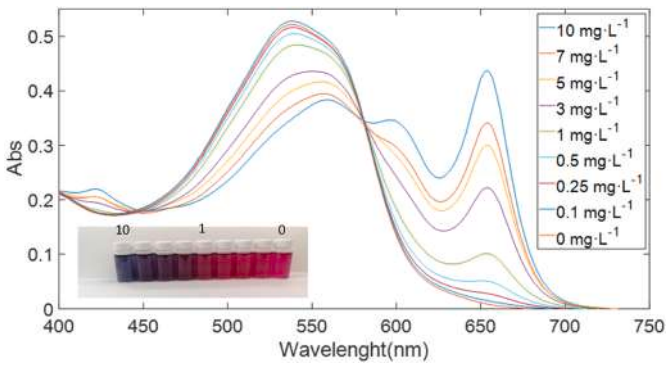

Fig. 6. Standard calibration of the Eu-arsenazo (III) complex measurements with UV–Vis spectrometry.

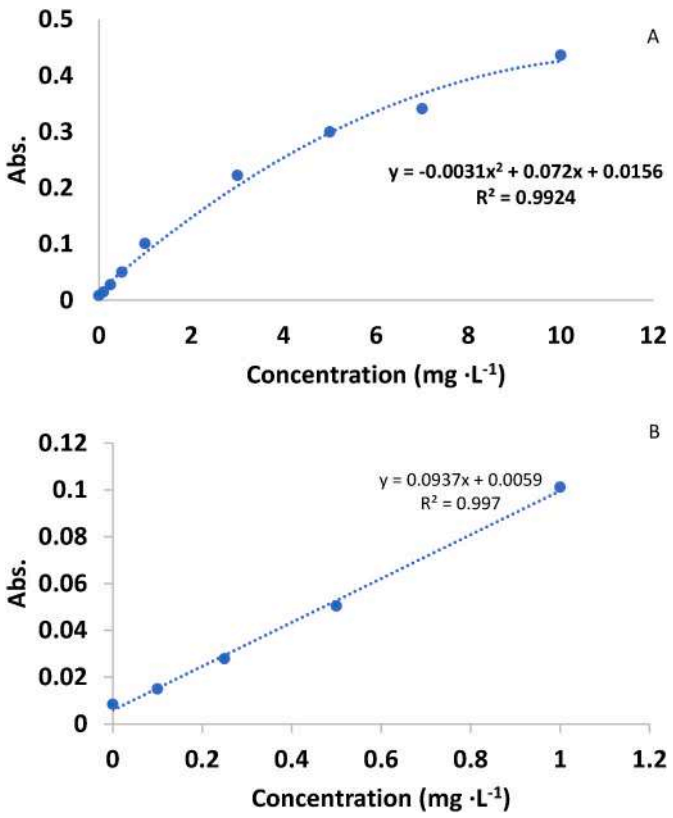

Fig. 7. Calibration curve fitting of absorbance vs concentration of the europium. (A) Complete curve fitting, (B) low-range concentration curve fitting.

Table 5
Retention of europium in each sample that was assessed by a visual check (A) and by UV–Vis spectrometry (B).

Sample	Visual check of color and retention	UV–Vis spectrometry retention
JRC-GAB-1	Pink (100%)	98.3%
JRC-GAB-2	Pink (100%)	99.1%
A21/071	Pink (100%)	98.8%
A21/044	Pink (100%)	97.5%
A21/074	Pink (100%)	95.5%
A21/118	Pink (100%)	99.2%
A21/031	Pink (100%)	95.1%

retention of actinides is almost quantitative and, as expected, potential non-radioactive interferences (e.g., Fe, Ca, organic matter) do not affect their retention.

Focusing on the gross alpha parameter measurement, the results for the two JRC interlaboratory samples analyzed are shown in Table 6.

The results obtained were quite similar to those given as a reference value. Moreover, when the assumption of a 100% retention of alpha-emitting radionuclides was made with the visual check (method A in Table 6), the deviation was low, indicating that the visual check worked correctly. As expected, the deviations obtained with the method determining the real retention of the alpha-emitting radionuclides (method B in Table 6) were slightly lower, suggesting that quantification can be slightly improved if the real retention values are taken into consideration.

The relative uncertainty of the measurement with α-PSresin (expressed as a combined standard uncertainty) was around 10% at this level of activity, which can be considered adequate. The analysis of the different elements contributing to the uncertainty (Fig. 8) showed that the three most important were the alpha count rate, the alpha efficiency and the retention determination. The contribution of the alpha efficiency increased with the increase in sample activity. This is because alpha efficiency, which is the mean of the detection efficiencies for ^{236}U and ^{238}Pu at the PSA value of 135, is independent of sample activity. Furthermore, its variability, RSD, was around 4.9%, which is relatively high as it includes the effect, on the detection efficiency, of the energy of the alpha particles emitted. The contribution of the alpha count rate to the uncertainty depended on sample activity, as observed with the other count rate variables, becoming important as the activity decreased. Finally, the contribution of the retention, with an RSD of 2.9%, was also independent of sample activity and was lower than that of the alpha efficiency.

Finally, the results obtained for the real water samples are shown in Table 7.

Moreover, for the JRC interlaboratory samples, the color was always pink during the visual check, indicating that more than 90% of europium had been retained. The results of the UV–Vis measurements confirmed these findings, showing retentions higher than 95% for all the samples (Table 7). Consequently, there were no significant differences between the results from both strategies.

Therefore, it can be concluded that the α-PSresin is capable to measure the gross alpha parameter with similar results and that the colorimetric UV–Vis determination could be useful in calculating the real retention for each sample. However, if it is requires a fast measurement to assess the gross alpha content of one or more samples, performing a visual check might be a straightforward option.

Regarding the limit of detection it has to be pointed out that the background of the PSresin is lower than that of the LSC due to the use of a lower amount of the scintillating material (1 g in α-PSresin vs 20 mL in the LSC vial). As consequence the minimum activity detection levels required for water monitoring can be achieved in only 2 h of counting time. The minimum detectable activity was 0.025 Bq L^{-1}, considering of 100 mL sample, 0.063 cpm of background and 2 h of measurement.

Comparing the methods proposed with the conventional ones, its main advantage is that it can give reliable results in less time and with a deviation equivalent to the ones obtained in laboratories currently. It is capable to give the result in just 5–6 h since the sample reception, since the conventional methods last up to 24–48 h to give a response since the sample reception.

Moreover, with the method proposed there are no losses of polonium as heating at high temperatures is avoided. Detection is less influence by salt content of the sample as our method has no salt autoabsorption and ^{40}K influence is avoided, leading to an improvement in the quantification. Color quenching is also avoided. If desired, more than one sample can be easily analyzed at the same time depending on the capacity of the vacuum box used (from 4 to 24 positions). Finally, there is also no need for liquid scintillation cocktails for the measurements, thereby reducing the generation of mixed wastes.

4. Conclusions

The preparation of the α-PSresin extractant was successfully

Table 6
Comparison of the results obtained by a visual check (A) and UV–Vis spectrometry (B) versus the reference values.

	Reference value (Bq/L)	PSresin value (Bq/L) (A)	PSresin value + UV–Vis (Bq/L) (B)	Deviation (%) (A)	Deviation (%) (B)
JRC-GAB-1	0.37 (0.01)	0.35 (0.03)	0.35 (0.04)	7.4	5.6
JRC-GAB-2	0.73 (0.02)	0.70 (0.06)	0.71 (0.06)	4.3	3.3

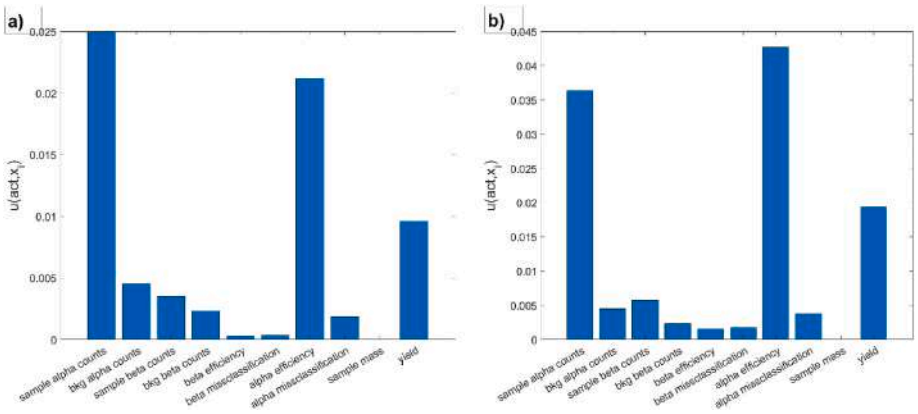

Fig. 8. Analysis of the uncertainty associated with each component for the JRC-GAB-1 (a) and JRC-GAB-2 (b) samples.

Table 7
Comparison of the results obtained with the visual check (A) and by UV–Vis spectrometry (B) versus the values obtained with the LSC conventional method.

	Activity Bq L^{-1}		
Sample	LSC	PSresin (A)	PSresin + UV–Vis (B)
A21/071	< LoD	< LoD	< LoD
A21/044	0.07 (0.02)	0.06 (0.01)	0.06 (0.02)
A21/074	0.53 (0.09)	0.46 (0.04)	0.48 (0.05)
A21/118	0.9 (0.2)	0.65 (0.07)	0.66 (0.07)
A21/031	1.4 (0.3)	1.26 (0.09)	1.3 (0.1)

The activity values obtained were similar to those obtained with the LSC method, with some discrepancies observed only in one sample (A21/118).

optimized, improving yield and purity. The new α-PSresin has a capacity of 5.8 mg, which is suitable for analyzing alpha radionuclides without effect of non-radioactive interferences. Several separation media were studied, which demonstrated that low acid concentrations were the best option for the total retention of alpha-emitting radionuclides (actinides, radium and polonium). pH 2 was selected as optimum medium for the development of a new procedure that can quickly measure the gross alpha parameter.

A new optimal method for measuring gross alpha activity has been developed, reducing the amount of effort and reagents needed compared to currently used methods. This procedure consists of adjusting the sample medium to a pH of 2 with nitric acid, adding H_2O_2 to a final concentration of 1%, heating the solution at 50 °C in a water bath for 30 min, passing the solution through α-PSresin, performing a scintillation measurement of α-PSresin, and estimating or calculating the retention. The procedure avoids potential Po losses, while the retention or loss of alpha particles can be determined. Europium is a good tool for estimating and determining the retention of alpha-emitting radionuclides. The formation of the colored arsenazo-europium complex can be precisely measured with UV–Vis spectrophotometry or estimated by a visual check, enabling an ultra-fast measurement. In the latter case, 100% retention can be assumed if the color of the Eu-arsenazo complex is not obtained. PSA calibration was evaluated with a fully characterized real sample and with an interlaboratory sample, providing satisfactory results at a PSA value of 135.

The whole methodology worked correctly in the analysis of two JRC interlaboratory samples (JRC-GAB-1 and JRC-GAB-2) and 5 real samples. Results obtained were comparable to the references values and to those obtained with the standard LSC method with an equivalent uncertainty.

Finally, the new method developed has a limit of detection of 0.025 Bq L^{-1} with an analysis time of less than 5 h (including sample treatment and measurement), which is much faster than conventional methods today used (around 24–48 h to give a response).

CRediT authorship contribution statement

I. Giménez: Methodology, Validation, Formal analysis, Investigation, Writing – original draft, Writing – review & editing. **H. Bagán:** Software, Resources, Writing – review & editing, Supervision, Funding acquisition. **A. Tarancón:** Software, Formal analysis, Resources, Writing – review & editing, Supervision, Funding acquisition.

Declaration of competing interest

The authors declare that they have no known competing financial interests or personal relationships that could have appeared to influence the work reported in this paper.

Data availability

Data will be made available on request.

Acknowledgments

This work is financed by the research project PID2020-114551RB-I00 financed by MCIN/AEI/10.13039/501100011033 and the Catalan Agència de Gestió d'Ajuts Universitaris i de Recerca (AGAUR) under 2017-SGR-907. I. Giménez also thanks the University of Barcelona for the PREDOCS-UB grant.

Appendix A. Supplementary data

Supplementary data to this article can be found online at https://doi.org/10.1016/j.aca.2023.340905.

References

[1] Official Journal of the European Union, Delegated Regulation (EU) 2021/2139 as regards economic activities in certain energy sectors and Delegated Regulation (EU) 2021/2178 as regards specific public disclosures for those economic activity [Online]. Available": https://ec.europa.eu/info/sites/default/files/business_economy_euro/banking_and_finance/documents/, 2022.
[2] World Health Organization, Guidelines for Drinking-Water Quality: Fourth Edition Incorporating the First Addendum, Geneva, 2017. Licence: CC BY-NC-SA 3.0 IGO.
[3] Official Journal of the European Union, Council Directive 2013/51/Euratom of 22 October 2013 Laying Down Requirements for the Protection of the Health of the General Public with Regard to Radioactive Substances in Water Intended for Human Consumption, 2013.
[4] REAL DECRETO, B. España, criterios sanitarios de la calidad del agua de consumo humano, real decreto 1798/2010 [Online], 2011. Available: http://www.boe.es.
[5] J.A. Corbacho, et al., Procedimiento para la determinación del Procedimiento para la determinación del índice de actividad alfa total en aguas potables mediante la metodología de desecación y medida en detectores de ZnS(Ag) o en contador proporcional, Colección de informes técnicos, Consejo de Seguridad Nuclear(CSN), 2014 ref: INT-04.07.
[6] J. Fons, et al., Procedimiento para la determinación de los índices de actividad alfa total y beta total en aguas potables mediante el método de concentración y

detección por centelleo líquido, Colección de informes técnicos, Consejo de Seguridad Nuclear(CSN), 2014 ref: INT-04.07.
[7] U.S. EPA, EMSL, Office of Water (MS-4606), Analytical methods approved for drinking water compliance monitoring of radionuclides naturally occurring radionuclides EPA 815-B-19-004 EPA, Environ. Prot. Agency (2019) 1–28.
[8] U.S. EPA, EMSL. "Method 900.0: Gross Alpha and Gross Beta Radioactivity in Drinking Water, Prescribed Procedures for Measurement of Radioactivity in Drinking Water, EPA/600/4/80/032, 1980.
[9] V. Jobbágy, U. Wätjen, J. Meresova, Current status of gross alpha/beta activity analysis in water samples: a short overview of methods, J. Radioanal. Nucl. Chem. 286 (2) (2010) 393–399, https://doi.org/10.1007/s10967-010-0709-z.
[10] M. Montaña, et al., A comparative experimental study of gross alpha methods in natural waters, J. Environ. Radioact. 118 (Apr. 2013) 1–8, https://doi.org/10.1016/J.JENVRAD.2012.10.009.
[11] L.M. Santiago, H. Bagán, A. Tarancón, J.F. Garcia, Synthesis of plastic scintillation microspheres: evaluation of scintillators, Nucl. Instrum. Methods Phys. Res. 698 (2013) 106–116, https://doi.org/10.1016/j.nima.2012.09.028.
[12] J. Barrera, A. Tarancón, H. Bagán, J.F. García, A new plastic scintillation resin for single-step separation, concentration and measurement of technetium-99, Anal. Chim. Acta 936 (2016) 259–266, https://doi.org/10.1016/j.aca.2016.07.008.
[13] H. Bagán, A. Tarancón, G. Rauret, J.F. García, Radiostrontium separation and measurement in a single step using plastic scintillators plus selective extractants. Application to aqueous sample analysis, Anal. Chim. Acta 686 (1–2) (2011) 50–56, https://doi.org/10.1016/j.aca.2010.11.048.
[14] I. Giménez, H. Bagán, A. Tarancón, J.F. García, PSresin for the analysis of alpha-emitting radionuclides: Comparison of diphosphonic acid-based extractants, Appl. Radiat. Isot. 178 (Dec. 2021), 109969, https://doi.org/10.1016/J.APRADISO.2021.109969.
[15] CEN/TC 230, European Standard, Water Quality -Radon-222 -Part 4: Test Method Using Two-phase Liquid Scintillation Counting (ISO 13164-4:2015)), 2020.
[16] L.A. Currie, Limits for qualitative detection and quantitative determination. Application to radiochemistry, Anal. Chem. 40 (3) (1968) 586–593, https://doi.org/10.1021/ac60259a007.
[17] E.P. Horwitz, R. Chiarizia, M.L. Dietz, DIPEX: a new extraction chromatographic material for the separation and preconcentration of actinides from aqueous solution, React. Funct. Polym. 33 (1) (1997) 25–36, https://doi.org/10.1016/S1381-5148(97)00013-8.
[18] T.International, Product Sheet, "DGA Resin (Normal and Branched), vol. 33, 2015, pp. 5–9.
[19] E.P. Horwitz, et al., DIPEX: a new extraction chromatographic material for the separation and preconcentration of actinides from aqueous solution, React. Funct. Polym. 33 (1997) 25–36.
[20] N. Navarro, L. Rodriguez, A. Alvarez, C. Sancho, Rapid determination of alpha emitters using Actinide resin, Appl. Radiat. Isot. 61 (2–3) (2004) 287–291, https://doi.org/10.1016/j.apradiso.2004.03.023.
[21] LLC Eichrom Technologies, Strontium-89/90 in Water, Analytical Procedure, 2014.
[22] T.International, Product Sheet "UTEVAresin", vol. 33, 2015, pp. 3–6. Iv.
[23] T.International, Product Sheet, "TEVA Product Sheet, vol. 33, 2015, pp. 1–4. September.
[24] M. Havelka, R. Bluďovský, Activity standardisation of 226Ra by 4πα liquid scintillation counting method, Appl. Radiat. Isot. 81 (Nov. 2013) 216–220, https://doi.org/10.1016/j.apradiso.2013.03.034.
[25] J. Uhrovďík, M. Gyeváthová, J. Lesný, Possibility of the spectrophotometric determination of europium by means of arsenazo III, Nova Biotechnologica et Chimica 12 (2) (2013) 93–99, https://doi.org/10.2478/nbec-2013-0011.
[26] Optimization and validation of the spectrophotometric method for quantification of europium in aqueous reprocessing streams, J. Radiat. Nucl. Appl. 5 (3) (Sep. 2020) 227–233, https://doi.org/10.18576/jrna/050310.

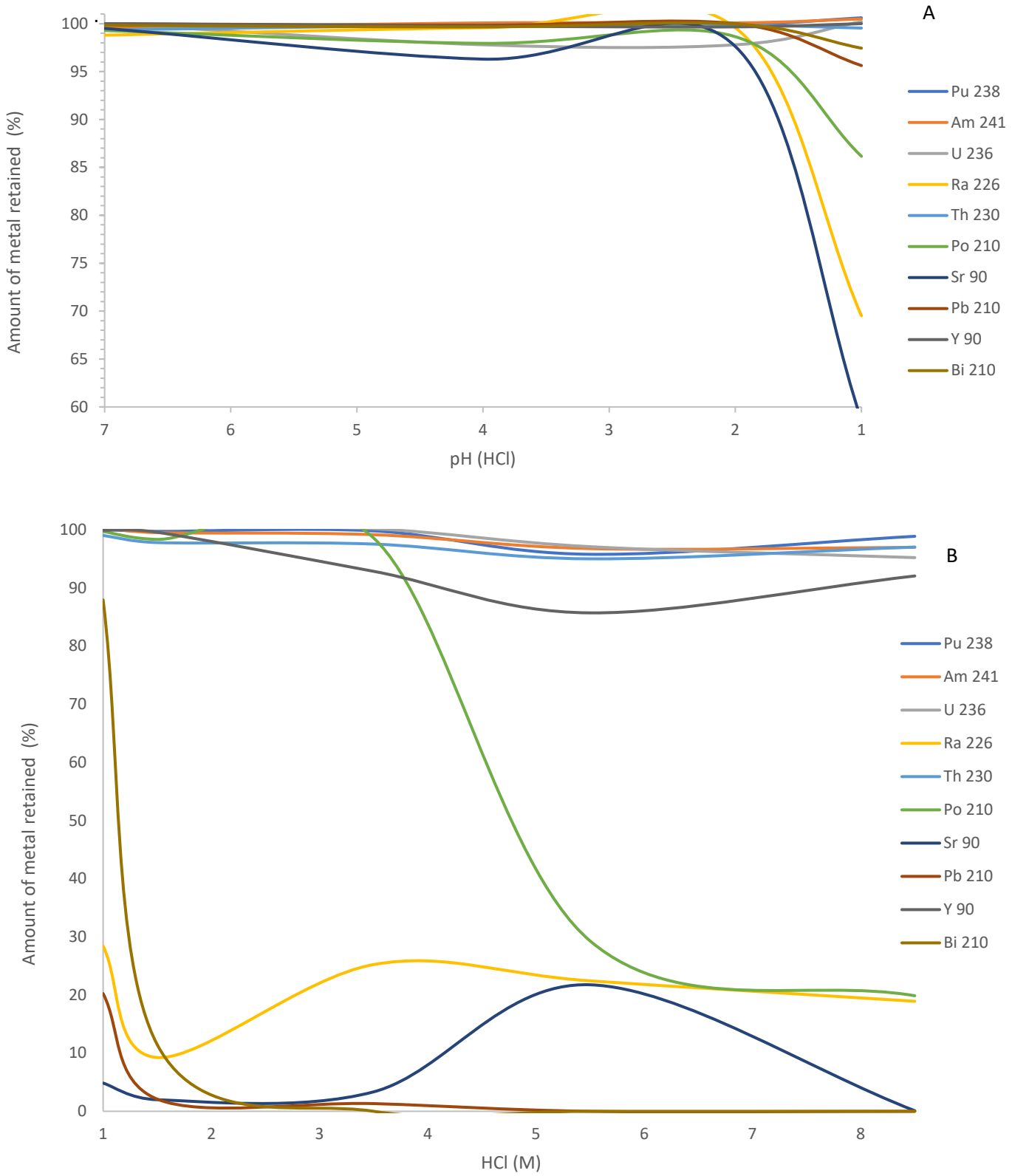

SI.1. Batch study for hydrochloric acid media where it is representing the yield (%) retention in front (A) the pH from 1 to 7 and (B) with the acidic concentration

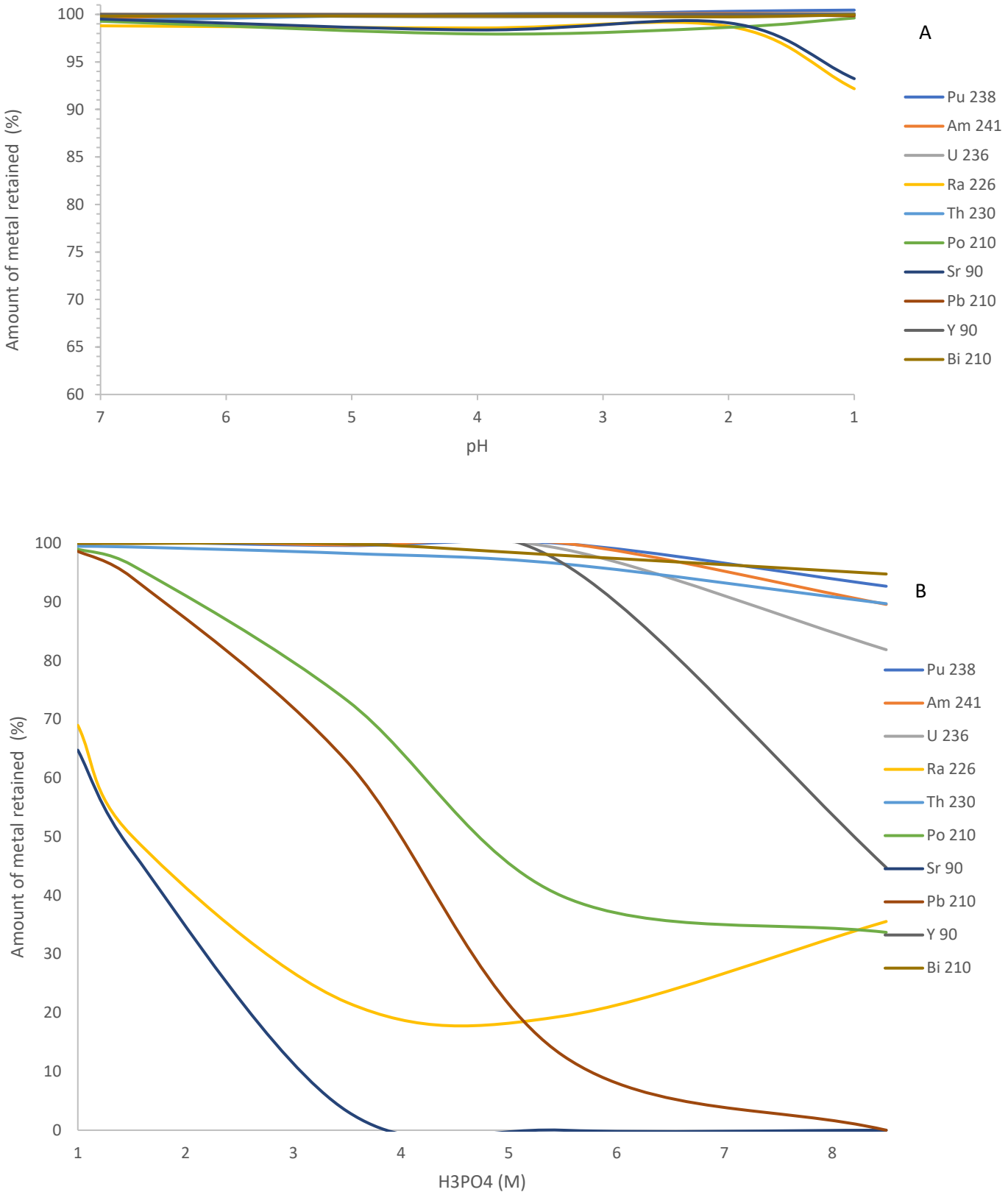

SI.2. Batch study for Orto-phosphoric acid media where it is representing the yield (%) retention in front (A) the pH from 1 to 7 and (B) with the acidic concentration

Article #3

Scintillating Iron Imprinted Polymers (Sc-Fe-IIP): Novel material for ^{55}Fe selective recognition

Microchemical Journal 208 (2025) 112268

Contents lists available at ScienceDirect

Microchemical Journal

journal homepage: www.elsevier.com/locate/microc

Scintillating iron imprinted polymers (Sc-Fe-IIP): Novel material for ^{55}Fe selective recognition

I. Giménez [a], H. Bagán [a,*], A. Tarancón [a,b,c]

[a] Departament d'Enginyeria química i química analítica, Universitat de Barcelona, Marti i Franqués, 1-11, ES-08028, Barcelona, Spain
[b] Serra-Húnter Programme, Generalitat de Catalunya, Barcelona, Spain
[c] Institut de Recerca de l'Aigua, Universitat de Barcelona, Spain

A B S T R A C T

In the coming years, numerous nuclear power plants are expected to reach the end of their operational lifespans, leading to a substantial increase in the demand for analyses during the decommissioning process. Of particular concern is ^{55}Fe, a fission product originating from neutron activation of stable iron. The conventional methods for determining ^{55}Fe using liquid scintillation are known for being time-consuming, complex, and involving multiple steps to eliminate interferences. In this work, the first scintillating imprinted polymer for ^{55}Fe has been developed (Sc-Fe-IIP). Several tests have been conducted to define the polymerization procedure, the components of the polymer, and their proportions, making it possible to combine selective retention and scintillation capabilities for ^{55}Fe determination in one material. The optimum Sc-Fe-IIP is composed of styrene, divinylbenzene, and vinyl phosphonic acid, together with a complex of Fe with acrylic acid and scintillation fluorescence solutes. The iron capacity is up to 17 mg per gram of Sc-Fe-IIP, and the selectivity is 95 %, with reduced retention of copper (4 %) and no retention of nickel or cobalt. Regarding scintillation capabilities, the Sc-Fe-IIP showed a detection efficiency of 4.90 %.

1. Introduction

During the dismantling of nuclear power plants (NPPs), the accurate measurement of the radionuclides present in a large number of samples is crucial to adequately plan waste management, classifying them according to the activity and half-life of the radionuclides present. Gamma emitting radionuclides are considered usually easy to measure. However, there are others, usually pure alpha or beta emitters, called difficult-to-measure (DTM) radionuclides, that are of interest in the NPP waste characterization, but their measurement still requires the development of new methodologies, especially for its separation from interferences and preconcentration. DTM radionuclides include fission products such as ^{126}Sn,^{99}Tc, ^{79}Se, etc. as well as activation products such as ^{36}Cl,^{63}Ni,^{55}Fe, etc. which are generated through neutron interactions with the reactor materials.

Leskinen et al. and Hou et al. have studied the challenges associated with quantifying DTM radionuclides in decommissioning samples. These challenges include the lack of commercially available reference materials, sample heterogeneity, low activity levels, low-energy emissions, and the need to isolate target radionuclides from various interfering elements. These interfering elements often exhibit higher activity levels and chemical similarities to the target radionuclides, complicating separation. As a result, the separation process becomes lengthy and labor-intensive prior to radiometric measurement [1,2].

This work addresses the challenges of determining one of these DTM radionuclides, ^{55}Fe, one of the most abundant radionuclides in materials in the first years after the shutdown. ^{55}Fe is an electron capture radionuclide with a half-life of 2.74 years which decays into ^{55}Mn, emitting characteristic X-rays and Auger electrons [3]. It is usually measured by liquid scintillation counting (LSC), due to the technique's inherent high detection efficiency and simplicity, despite the generation of mixed hazardous and radioactive wastes [4]. However, its determination has two challenges: the isolation of ^{55}Fe from other radionuclides such as ^{60}Co, usually present in similar activity levels or two orders of magnitude higher, depending on the time passed after the shutdown; and the decrease of the detection efficiency in the scintillation measurement, due to the colour quenching caused by the iron salts present in the counting sample [5].

The lack of selectivity is usually overcome by applying conventional strategies such as iron precipitation as hydroxide and subsequent separation through anion exchange chromatography (Dowex AG-1X4). However, this lengthy and tedious process does not permit the processing of many samples. Alternatively, commercial resins like TRU® resin [6–8] can be used. In addition, phosphoric acid is often used as a masking agent to reduce the colour quenching caused by red iron species [9 10].

* Corresponding author.
E-mail address: hector.bagan@ub.edu (H. Bagán).

https://doi.org/10.1016/j.microc.2024.112268
Received 3 June 2024; Received in revised form 8 November 2024; Accepted 21 November 2024
Available online 26 November 2024

This work presents a novel selective scintillating material, based on ion-imprinted polymers, addressed to enhance ^{55}Fe analysis, overcoming the drawbacks described before (Sc-Fe-IIP). This approach integrates the selective separation and measurement steps into a single material, reducing the time, cost, and reagents required. Extractive scintillating polymers have been already developed previously using impregnation of linear polystyrene, however, for ^{55}Fe, the lack of a selective extractant, regarding main interferences, makes this strategy not valid and new extractive strategies, like ion/molecularly imprinted polymers, need to be explored. Ye et al. demonstrated the feasibility of this concept by developing a material for (^{32}S)-propanol recognition based on fluorescent properties, but with an extremely low detection efficiency [11].

Ion/molecularly imprinted polymers are materials with specific cavities on the surface of the polymeric network, which confer selectivity towards the target element. This element can be an ion, in the case of ion-imprinted polymers (IIP) [12], or a molecule, as in molecular-imprinted polymers (MIP) [13,14]. Generally, ion/molecularly imprinted polymers are known for their specific binding sites, good stability, and easy synthesis [15].

Various IIPs have already been developed for elements such as lead, cadmium, iron, etc. [16–19], including radionuclides like uranium, thorium, or strontium [20] as a tool for their preconcentration or removal.

Specifically for iron, a wide range of Fe-IIPs have been developed. These include the use of different compositions, including styrene (St) and methacrylate derivatives as monomers and divinylbenzene (DVB) and ethylene glycol dimethacrylate (EGDMA) as crosslinkers; the preparation through different polymerization techniques as bulk, precipitation, or suspension polymerization; and the target of different samples types such as drinking water, human plasma samples, etc [12,15,21]. As an example, Singh and Misra reported the development of a Fe-IIP based on acrylic acid (AAC), St and DVB with a maximum iron capacity of 62.4 mg·g^{-1} aimed at water samples analysis [22]. Ara et al, developed a Fe-IIP for iron analysis in drinking water using 8-hydroxyquinoline as a chelating agent, methacrylic acid (MAA) and DVB with a maximum iron capacity of 9.5 mg·g^{-1} [23]. Zhu et al, reported a Fe-IIP using bis(2-methacryloxyethyl)phosphate (EGPO4) as a functional monomer and EGDMA for the separation of iron from highly concentrated basic chromium sulphate solutions [24]. Fe-IIPs for more complex samples have been developed. Ozkara et al, developed a Fe-IIP, using N-methacryloyl-(L)-cysteine methyl ester and 2-hydroxyethyl methacrylate for iron removal from human plasma with beta thalassemia, achieving an iron capacity of 0.15 mg·g^{-1} [25]. Yavuz et al, developed a Fe-IIP for iron removal from human plasma samples using N-methacryloly-(L)-glutamic acid as a complexing monomer and 2-hydroxyethyl methacrylate, with a capacity of 5.2 mg per gram of particles [26].

However, none of the previously developed Fe-IIPs included the components necessary for scintillation, thus limiting their application for the separation and measurement of ^{55}Fe in analytical contexts. The scintillating ion-imprinted polymer developed in this study for ^{55}Fe builds on prior experience with scintillating polymers [27–30] incorporating St as a scintillating monomer. According to existing literature, acrylic compounds are particularly effective as polymerizable Fe-complexing agents [22,31–33]. Crosslinkers, such as DVB and EGDMA, with or without aromatic rings, are required to impart rigidity and ensure selectivity. However, their proportions must be carefully balanced, as excessive crosslinking can interfere with scintillation. Additionally, fluorescent molecules are essential to facilitate light emission within the detection range of the PMT.

2. Experimental section

2.1. Reagents and solutions

Styrene (St) (99 %), 1,2- and 1,4- isomeric mixture divinylbenzene (DVB) (80 %), sodium chloride and 2,5–diphenyloxazole (PPO) (99 %) were obtained from Acros Organics (Geel, Belgium); aluminium oxide (α-phase) and iron(III) nitrate (9·H_2O) were obtained from Alfa Aesar (Kandel, Germany); 1,4–bis(5-phenyl-2-oxazolyl) benzene (POPOP), 2,2′-Azobis(2-methylpropionitrile) (AIBN), vinylphosphonic acid (VPA), bis(2-methacryloxyethyl)phosphate (EGPO4), methyl methacrylate (MMA), vinyl biphenyl (v-Biph), methylacrylic acid (MAA), acrylic acid (AAC), 60 % 1,2- and 40 % 1.4- isomeric mixture methyl styrene (Vt), ethylene glycol dimethacrylate (EGDMA), 3-aminopropyl trimethoxy silane (APS), polyvinyl alcohol (PVA) partially hydrolyzed (30.000 MW), methanol, triethylamine, toluene and nickel, cobalt and copper ICP standards were supplied by Merck (Darmstadt, Germany); iron ICP standard (10000 mg·L^{-1}) was obtained from Inorganic Ventures (Christiansburg, USA). Acryloyl-2,5-diphenyloxazole (p-PPO) was synthesized following the literature [34].

Radioactive solutions used include a ^{14}C active stock solution of 136 (3) Bq·g^{-1} from Cerca Framatome (Paris, France) and a ^{55}Fe active stock solution of 406(7) Bq·g^{-1} in HCl 0.1 M from Eckert and Ziegler (Berlin, Germany).

OptiPhase Supermix liquid scintillation cocktail from PerkinElmer (Waltham, USA) was used for the liquid scintillation measurements. 2 mL solid phase extraction (SPE) cartridge was supplied by TrisKem International (Rennes, France).

2.2. Apparatus

Scintillation measurements were performed using a Quantulus liquid scintillation spectrometer (PerkinElmer, Waltham, USA) and a HIDEX 300 SL super low-level detector (Hidex, Turku, Finland).

Secondary electron images were obtained using a JSM-7100FE JEOL (Tokyo, Japan) scanning electron microscope at the Scientific and Technological Centres of the Universitat de Barcelona (CCiTUB).

The analysis of stable elements was performed using an Optima 8300 ICP-OES or an ELAN-6000 ICP-MS, both from PerkinElmer (Waltham, USA), at the Scientific and Technological Centres of the Universitat de Barcelona (CCiTUB).

N_2 adsorption/desorption isotherms were used to study the surface area and pores of the synthesized polymers using a TriStar 3000 (Micromeritics, USA) at the Scientific and Technological Centres of the Universitat de Barcelona (CCiTUB).

2.3. Procedures

2.3.1. Suspension polymerization

An organic phase, containing all the organic reagents, the iron complex and the initiator (0.1 g of AIBN), was dispersed into an aqueous phase containing a surfactant (PVA) through stirring. The mixture was then subjected to thermal polymerization at 65 °C for 4 h, followed by 90 °C for 20 h. The resulting particles were filtered and washed with water and ethanol to remove the solvents and any non-reactive compounds.

Tables 1 and 2 show the composition of each prepared polymer.

All polymers incorporated 0.4 g of the primary fluorescent solute (PPO, p-PPO, or v-Byph) and 0.05 g of POPOP. Before the addition of the organic phase, the aqueous phase was purged with nitrogen for 30 min.

For polymers, SuS_1 to 11, 100 mL of aqueous phase was used, with the organic phase containing 12 mL of toluene and 2 mL of methanol as porogens. The monomer-to-crosslinker ratio was 70:30, resulting in approximately 12–14 g of final polymer. The ratio of iron to chelating agent was based on prior studies [22].

In the case of polymers SuS_12 to 24, the concentration of PVA solution was increased from 0.5 % to 10 %, and 1 % of NaCl was added. Additionally, 0.4 g of VPA and 4 g of EGPO4 were used, respectively, as bleaching agents. EGPO4 served dual roles as both a crosslinker and bleaching agent. The monomer-to-crosslinker mass ratio was adjusted to 40:60 and the amount of porogen was reduced to 6 mL of toluene and 1

Table 1
Summary of the different IIP synthesised without NaCl in the aqueous phase.

CODE	Monomer:Crosslinker (mass ratio 70:30, 14 g)	Chelating Agent	Fluorescent solutes
SuS_1	St:DVB	AAC	PPO + POPOP
SuS_2	St:EGDMA	AAC	PPO + POPOP
SuS_3	MMA:DVB	AAC	PPO + POPOP
SuS_4	MMA:EGDMA	AAC	PPO + POPOP
SuS_5	St:DVB	APS	PPO + POPOP
SuS_6	St:EGDMA	APS	PPO + POPOP
SuS_7	MMA:DVB	APS	PPO + POPOP
SuS_8	St:DVB	MAA	PPO + POPOP
SuS_9	St:EGDMA	MAA	PPO + POPOP
SuS_10	MMA:DVB	MAA	PPO + POPOP
SuS_11	MMA:EGDMA	MAA	PPO + POPOP

Aqueous solution: 100 mL 0.5 % PVA.
Fe-chelating agent: 1 g of a 1:14 M ratio.
Porogens: 12 mL of toluene + 2 mL of methanol.
Fluorescent solutes: 0.4 g of PPO and 0.05 g of POPOP.

mL of methanol, yielding approximately 6 g of the final polymer.

Additionally, polymers SuS_16 to 24 were prepared using 150 mL of aqueous phase instead of 100 mL and a 1:1 iron-to-chelating agent molar ratio. Additionally, 1.5 equivalents of triethylamine, relative to the amount of chelating agent, were added.

Non-ion imprinted polymers (nIIPs) were prepared following the same procedure but without the addition of iron.

2.3.2. Template removal

Template removal was conducted by stirring the resulting Sc-IIP in 1 L of 3 M nitric acid solution for 2 to 3 h to eliminate the iron [35]. Sc-IIP was then filtered and the filtrated solution was checked to determine if iron was present or not. The removal process was repeated until no iron was present in the filtrate solution, indicating the complete removal of the available iron on the polymer. To check the presence of iron in the filtrate solution, a 10 mL aliquot was mixed with a 6 M KSCN solution and if the solution turned red (indicating the presence of iron with a concentration above 0.5 $mg{\cdot}L^{-1}$) the Sc-IIP was cleaned again. Each polymer prepared needed from 8 to 12 iterations to remove all iron from the polymer. Additionally, EDS analysis was performed on each polymer before and after template removal to verify both, the initial presence of the iron and its complete removal.

2.3.3. Batch studies

Batch studies were performed to test the capacity and selectivity of iron against potential interferences (Ni, Co and Cu).

For capacity studies, 0.5 g of the Sc-Fe-IIP, 20 mL of a solution containing 20 mg of the metal (Fe^{3+}, Ni^{2+}, Cu^{2+} or Co^{2+}) and 5 mL of a acetate solution (pH 4 or pH 6) were added to a 50 mL Corning (New York, USA) conical tube.

For selectivity studies, 0.5 g of the Sc-Fe-IIP, 20 mL of double deionised water, 0.05 g of each metal (Fe^{3+}, Ni^{2+}, Cu^{2+} and Co^{2+}) and 5 mL of pH 6 acetate solution were added to a 50 mL conical tube.

In both cases, the mixture was left to interact for 24 h in an end-over-end shaker. Afterward, the solution was filtered with disk filters (0.45 μm) and analysed by ICP-OES and ICP-MS.

2.3.4. Scintillating capacity characterization

0.5 g of Sc-Fe-IIP was placed in a 6 mL polyethylene vial together with 0.2 mL of the active solution (^{14}C or ^{55}Fe). Afterward, the vials were placed in an IKA MS3 digital vortex (Merck, Darmstadt, Germany) at 3000 rpm for 3 min for homogenization and then measured in a scintillator detector. Previously to starting the measurement, the vials were stored in the dark for 2 h to get rid of luminescence effects. ^{14}C and ^{55}Fe samples were measured for 1 h and 3 h, respectively, with 10 min of SQP(E).

2.3.5. Column studies

Sc-Fe-IIP was packed in a 2 mL SPE cartridge and placed in a vacuum chamber connected to a pump where 10 mL of deionised water was passed through it at a flow rate of 1 $mL{\cdot}min^{-1}$, around 5 inHg, to compact the polymer. Afterward, the cartridges were shaken for 180 s at 50 Hz in a vortex for homogenization. The cartridges were first conditioned with 5 mL of pH 6 solution, then 10 mL of the sample containing 13 Bq of ^{55}Fe and 1 mg of Fe^{3+} in pH 6 solution were passed through it at a flow rate of 1 $mL{\cdot}min^{-1}$. Afterwards, two 2 mL rinses with pH 6 solution were performed, followed by an increase of the pressure to ensure the dryness of the polymer. The column was then disconnected, placed on a scintillation vial and measured. The counting time was 3 h.

2.3.6. Data treatment

All acquired spectra were smooth using the Savitzky-Golay filter, employing an average window size of 21 points and a first-degree polynomial. The net spectrum was obtained by subtracting the spectrum of the corresponding blank solution.

To determine the detection efficiency, the net counts in each channel

Table 2
Summary of the different IIPs synthesised with NaCl in the aqueous phase.

CODE	Base Monomer	Crosslinker monomer	Iron-chelating agent molar ratio	Fe-complex	Aqueous solution volume	Bleaching agent	Primary Fluorescent solutes
SuS_12	St	DVB	1:14	1 g	100 mL	0.4 g VPA	PPO
SuS_13	St	–	1:14	1 g	100 mL	4 g $EGPO_4$	PPO
SuS_14	MMA	DVB	1:14	1 g	100 mL	0.4 g VPA	PPO
SuS_15	MMA	DVB	1:14	1 g	100 mL	–	PPO
SuS_16	St	DVB	1:1	1 g	150 mL	0.4 g VPA	PPO
SuS_17	MMA	DVB	1:1	1 g	150 mL	0.4 g VPA	PPO
SuS_18	St	DVB	1:1	1 g	150 mL	0.4 g VPA	p-PPO
SuS_19	St	DVB	1:1	0.5 g	150 mL	0.4 g VPA	p-PPO
SuS_20	St	DVB	1:1	0.5 g	150 mL	0.4 g VPA	PPO
SuS_21	St	DVB	1:1	1 g	150 mL	0.4 g VPA	v-Biph
SuS_22	St	DVB	1:1	0.5 g	150 mL	0.4 g VPA	v-Biph
SuS_23	Vt	DVB	1:1	1 g	150 mL	0.4 g VPA	PPO
SuS_24	Vt	DVB	1:1	0.5 g	150 mL	0.4 g VPA	PPO

Aqueous solution: 10% PVA and 1% NaCl.
Chelating agent: AAC.
In equivalents regarding the Fe-chelating agent.
Porogens: 6 mL of toluene + 1 mL of methanol.
Sus_16 to 24 include 1.5 Equivalent of triethylamine.
Secondary fluorescent solute POPOP.

were divided by the activity in the Sc-Fe-IIP vial or cartridge. The overall detection efficiency was then obtained by integrating the detection efficiency spectrum across the whole spectra.

Adsorption capacity and selectivity (retention percentage of each metal, when the polymer is exposed to a low concentration mixture of all the metals studied) were obtained using the following equations:

$$C = \frac{V(mct - mc)}{mp} \quad (1)$$

$$S = \frac{(mct - mc)}{mct} * 100 \quad (2)$$

Where C is the capacity (metal mg·g Sc-Fe-IIP $^{-1}$) and S is the Selectivity (%), mct is the initial concentration of metal added (in mg·L^{-1}), mc is the metal concentration in solution after the experiment (in mg·L^{-1}), obtained from the ICP measurements, V is the volume of the loading solution (L) and mp is the mass of Sc-Fe-IIP used in grams.

3. Results and Discussion

3.1. First composition evaluation

The primary goal of this stage was to evaluate various combinations of monomers, crosslinkers, and chelating agents to determine the most effective configuration. Based on literature and preliminary studies, eleven polymers were synthesized, using bulk polymerization, to assess the compatibility of the different monomers. From the successful combinations, the following components were selected: St and MMA as monomers, EGDMA and DVB as crosslinkers and AAC and MAA as polymerizable chelating agents. Additionally, APS was selected as a non-polymerisable chelating agent [36,37].

In the initial stage, Sc-IIPs were prepared by suspension polymerization using a 0.5 % PVA aqueous solution and an organic phase containing the monomer and crosslinker in a 30:70 ratio. The organic phase also included 1 g of iron complex (with a 1:14 iron-to-chelating agent ratio [18 31]), along with 12 mL of toluene and 2 mL of methanol as porogens to stabilise the solution.

All synthesized polymers initially displayed a red colour, indicating the presence of the iron template in the structure. After iron removal, the red colour disappeared and polymers with AAC and APS as chelating agents were colourless, while those with MAA appeared beige. Figure S1 in the supplementary material, shows EDS spectra for SuS_1 before and after template removal as an example of how the initial iron signal disappeared after rinsing the polymer.

All polymers had a spherical shape with a size range between 0.5 and 2 mm (Fig. 1, SuS_1 as an example).

Next, the scintillating properties of the polymer were tested using a ^{14}C standard instead of a ^{55}Fe, as the low energy of ^{55}Fe would not allow for proper identification of small improvement in scintillation capabilities (Table 3).

The detection efficiencies for all polymers were low, as ^{14}C detection efficiency using plastic scintillators typically ranges around 50–60 % [38]. This low detection efficiency could be attributed to different factors. First, the presence of large quantities of crosslinker agents and too much rigidity, as the energy transfer between solvent molecules during the scintillating process requires certain chain mobility. In the second term the particle diameter, as it is too high compared to the optimum for plastic scintillation microspheres, between 40 and 70 μm, balancing particle quenching and optical quenching [29]. And third, the chemical quenching effect caused by iron encapsulated in the polymer.

If the different polymers are compared, the chelating agent used played a crucial role in the scintillation capabilities, as polymers containing MAA did not exhibit any scintillation, while those using AAC or APS had a detection efficiency ranging from 2 to 9.6 %. This effect can be attributed to the colour of the polymer after template removal.

Iron capacity was then studied in two different media, pH 4 and 6. In all cases, the resulting iron capacity was higher at pH 6 than at pH 4. This performance is attributed to the effective deprotonation of AAC at pH 6. The iron complex formed with the acrylate groups, once they are deprotonated, results in an octahedral geometry for Fe (III) with three molecules of AAC. Each Fe (III) ion is surrounded by six donor atoms (oxygens from the carboxylate groups). This explanation also applies to MAA. AAC has a pKa of 4.25 and an MAA of 4.65, therefore a working medium with a pH equal or higher than 6 ensures complete

Table 3
Detection efficiency, quenching parameter, and iron capacity, at two media, for the different iron imprinted polymers obtained by suspension polymerization. N = 2.

CODE	Chelating agent	Monomer composition	*^{14}C detection efficiency (%)*	SQP (E)	iron capacity (mg Fe·g Sc-Fe-IIP^{-1})*	
					pH 4	pH 6
SuS_1	AAC	St:DVB	2.16(0.04)	490	>0.1	>0.1
SuS_2		St:EGDMA	5.31(0.07)	586	3.58	7.24
SuS_3		MMA:DVB	9.36(0.09)	470	5.36	23.05
SuS_4		MMA: EGDMA	5.05(0.07)	475	3.34	16.00
SuS_5	APS	St:DVB	3.04(0.05)	473	>0.1	1.09
SuS_6		St:EGDMA	9.65(0.08)	588	0.68	0.62
SuS_7		MMA:DVB	4.09(0.06)	508	0.52	3.16
SuS_8	MAA	St:DVB	<0.05	510	0.62	0.78
SuS_9		St:EGDMA	<0.05	532	1.21	3.36
SuS_10		MMA:DVB	<0.05	504	1.66	3.09
SuS_11		MMA: EGDMA	<0.05	489	1.34	13.84

*N = 1.

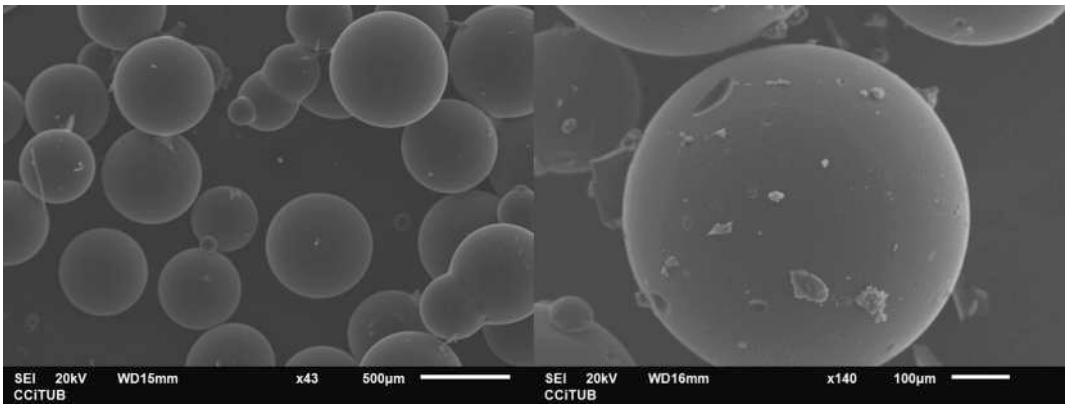

Fig. 1. Polymers obtained through suspension polymerization (SuS_1 as an example).

deprotonation of the acrylate groups. MAA and AAC demonstrated higher iron capacities compared to APS, likely due to poor incorporation of the APS complex in the polymer or its extraction during template removal, as it was not polymerized.

The obtained results conclude that AAC was the chelating agent with the best performance, using St or MMA as monomers and DVB as the crosslinker to ensure the presence of aromatic rings.

To improve scintillating and iron capacity performance, two main issues were addressed. First, a reduction in particle size was targeted, as this would enhance scintillating properties by reducing the distance beta particles travel before interacting with the polymer. Second, the introduction of a polymerizable bleaching agent capable of suppressing the red coloration of the polymer in the presence of iron.

3.2. Addition of bleaching agents and particle size reduction

The reduction in particle size can be achieved by increasing the concentration of PVA in the aqueous phase to 10 % and including 1 % sodium chloride. Both changes affect the droplet formation when organic and aqueous phases are mixed. The addition of sodium chloride increases the ionic strength of the solution, resulting in a thinner interface and better droplet formation, whereas an increase in PVA concentration leads to the formation of small droplets.

Conventional methods for ^{55}Fe measurement by LSC typically employ phosphoric acid to reduce or suppress the red coloration intensity caused by iron species, thereby avoiding colour quenching. This approach was implemented in the Sc-Fe-IIP by introducing a polymerizable phosphate monomer, referred to as a bleaching agent, into the polymer structure. Two types of monomers were tested as bleaching agents: VPA, which acts as a chelating agent, and EGPO4, which acts as both a chelating agent and a crosslinker. These compounds replace one or two of the acrylate groups in the iron complex, eliminating the red colour while keeping the octahedral geometry with six oxygen donor atoms.

Four different types of polymers were prepared, all containing AAC as a chelating agent. The first two polymers (SuS_12 and 13) consisted of St as a monomer, the first one with DVB as the crosslinker and VPA as the bleaching agent, and the second with EGPO4 as the crosslinker and bleaching agent. The third polymer (SuS_14) used MMA as a monomer, aiming to improve iron capacity, along with DVB as a crosslinker and VPA as the bleaching agent. The fourth polymer (SuS_15) was the same composition as SuS_3, as it had the best parametric values in the previous tests, and allowed to study the effect of particle size reduction on scintillation properties. EGPO4 was not tested alone with MMA because it would not produce any scintillation due to the absence of aromatic rings.

All polymers containing a bleaching agent exhibited a white appearance before and after template removal, whereas the one without a bleaching agent had a reddish colour before removal. Figure S2 in the supplementary material shows this difference in coloration before iron removal. This confirmed that the bleaching agent acted as expected, complexing iron and reducing the red colour. The particle size reduction was successfully achieved (Fig. 2), resulting in perfect microspheres, ranging from 30 to 60 μm, except for SuS_13, that formed a fragile block that could be disaggregated into particles, attributed to the use of EGPO4 as a crosslinker.

This size reduction significantly improved the detection efficiency for ^{14}C (Fig. 3A) as comparing SuS_15 and SuS_3 (Table 3), the detection efficiency increased from 9.36 % to 12 %. Additionally, the size reduction, together with the VPA addition to the St and DVB combination, increased the detection efficiency from 2 % to 18 %.

^{55}Fe detection efficiency (Fig. 3B) was also measured to assess the real effect of the bleaching agent once an adequate particle diameter was achieved. The detection efficiencies obtained were low, as expected, due to the quenching effects mentioned before and the low energy of ^{55}Fe emission, which is comparable in scintillation terms to ^{3}H, for which a 1.5 % detection efficiency is typically achieved [29]. Comparing SuS_14 and SuS_15, the detection efficiency of SuS_14, containing VPA, was twice that of SuS_15, without VPA. Again, SuS_12 shows the highest detection efficiency.

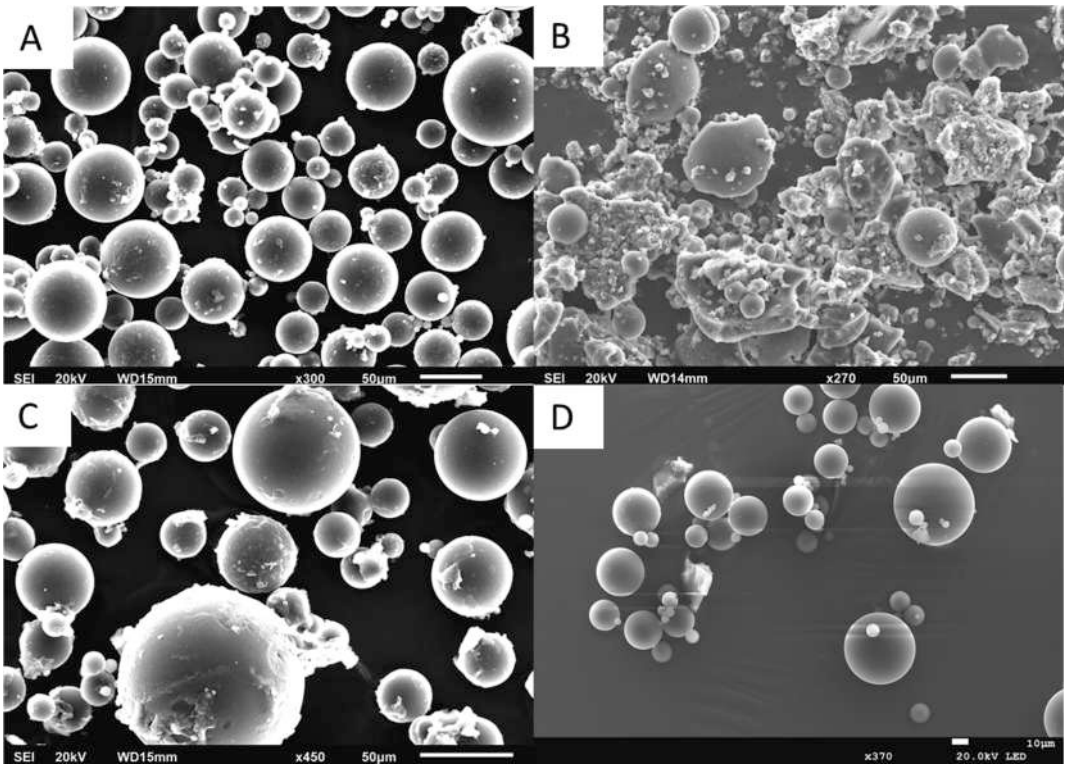

Fig. 2. SEM images for each Sc_Fe_IIP prepared. SuS_12 (A), SuS_13 (B), SuS_14 (C) and SuS_15 (D).

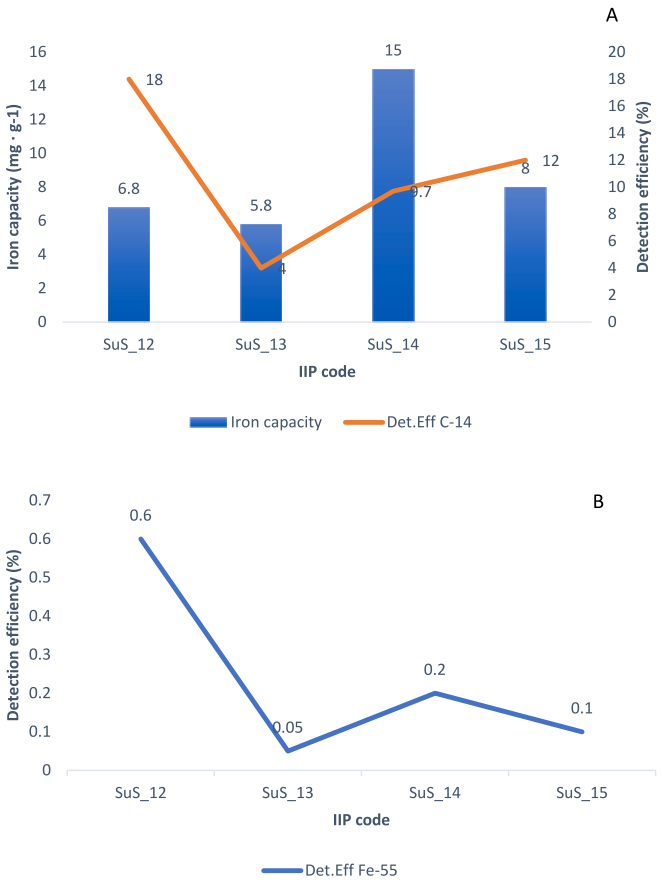

Fig. 3. Detection efficiency for ^{14}C (A) and ^{55}Fe (B) and iron capacity (A) for the optimized iron imprinted polymers obtained by suspension polymerization, after size reduction.

Regarding the iron capacity (Fig. 3A), the values of the polymers remained on similar values, except for SuS_12, where the capacity increased up to 7 mg Fe·g^{-1} with the addition of VPA and particle size reduction for the St and DVB composition. Results suggested that no big changes were caused by the inclusion of the bleaching agent (Table S1 in supplementary information presents the data with the mean and standard deviations).

To assess the potential use of each polymer in real conditions, iron selectivity was studied, as well as the non-imprinted version of the polymer. Selectivity was studied against potential chemical or radioactive interferents: copper, cobalt, and nickel. ^{60}Co and ^{63}Ni are activation products and are generated in large amounts at the nuclear reactors, therefore interfering with the detection as their signals overlap with that of ^{55}Fe. Copper was studied because of the large amount in which can be found in a real sample, potentially saturating the polymer and preventing the retention of iron.

The non-imprinted polymers presented the same size and shape as the imprinted polymers for SuS_12, 14 and 15, but not for SuS_13 which led to a hydrogel formation, not enabling its study. Fig. 4 shows the selectivity for the imprinted and non-imprinted versions of each polymer (Table S2 in supplementary information presents the data with the mean and standard deviations).

In all cases, iron selectivity was higher than for any of the other studied metals, indicating that the polymer has a higher affinity for iron. However, the non-imprinted polymer presented very similar selectivity. The 1:14 proportion between iron and AAC, selected based on the literature [22], may efficiently lead to an increase in iron capacity, as proven, but it appeared to limit the selectivity against other metals. The explanation relies on the non-complexed acrylate groups located on the surface or in non-specific cavities, which interact with other metals in the solution, thus reducing the selectivity of the ion-imprinted polymer.

3.3. Selectivity improvement

The lack of selectivity due to non-specific sites was addressed by increasing the amount of iron added during the complex preparation to a 1:1 ratio, ensuring that all AAC would be complexed with iron. To further enhance the complex formation, triethylamine was added to the organic phase to fully deprotonate the AAC, making it more available for complexation with iron. Adding 1.5 equivalents of triethylamine, concerning the AAC, resulted in a neutral pH, preventing the precipitation of iron hydroxide. The exothermic nature of the neutralization process,

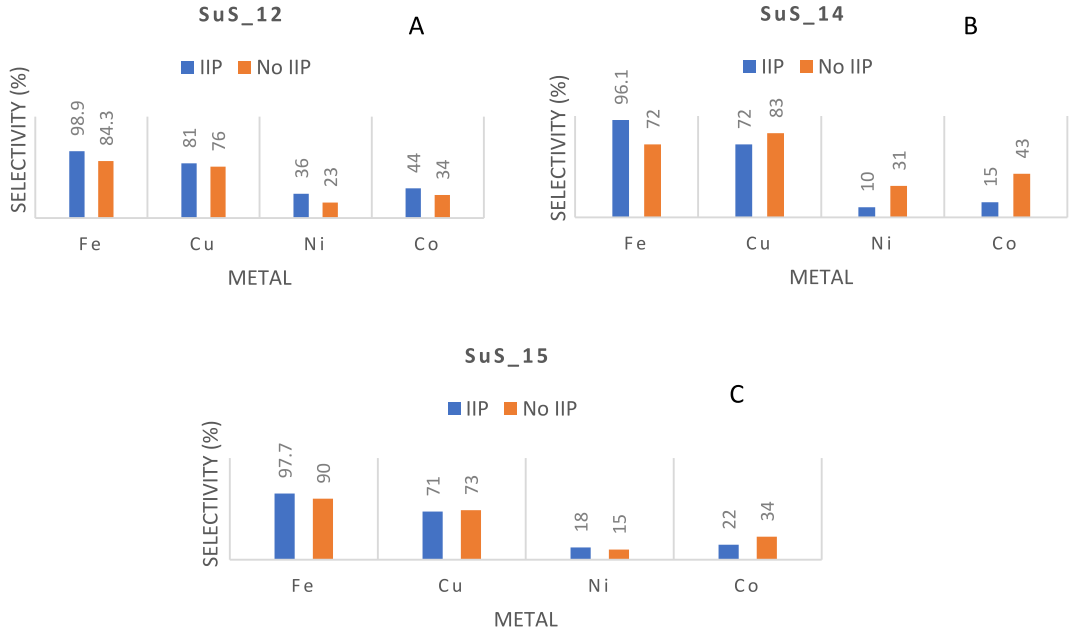

Fig. 4. Selectivity of the different optimised iron polymers (imprinted (Blue) and non-imprinted (Orange)), obtained after size reduction. A polymer SUS_12, B polymer SUS_14 and C polímer SUS_15. (For interpretation of the references to colour in this figure legend, the reader is referred to the web version of this article.)

which could potentially initiate the polymerization of AAC before the complexation step, was mitigated by preparing the iron complex at 0 °C in an ice bath.

Two polymers were prepared, one including St, DVB and VPA (SuS_16) and the other MMA, DVB and VPA (SuS_17). AAC was the chelating agent in both, as this composition had shown the best performance in terms of detection efficiency, iron capacity and selectivity in the previous section.

Fig. 5 and Figure S3, in supplementary material, show SEM images for SuS_16 and SuS_17 polymers and their surfaces, respectively. Additionally, Figure S4, in supplementary material, shows the X-ray spectra for SuS_16 as an example of the successful iron removal after template extraction. The images revealed that altering the iron:AAC ratio and adding triethylamine did not result in significant changes to the polymer surface structure or morphology. Figure S5 in the supplementary material confirms this by comparing the BET-specific surface areas for SuS_1 (without VPA or triethylamine), SuS_12 (with VPA and without triethylamine), and SuS_16 (with VPA and triethylamine) alongside the iron capacity of each. The BET surface areas of SuS_12 and SuS_16 were nearly identical (241.19 and 240.69 $m^2 \cdot g^{-1}$, respectively), indicating that triethylamine addition did not substantially alter the polymer surface area, and they are notably higher than in SuS_1, which had no measurable surface area or porosity, underscoring its lack of iron capacity during initial testing and demonstrating the effectiveness of the implemented modifications. The only observed effect of triethylamine addition was an increase in pore size, from 24.78 Å in SuS_12 to 74.42 Å in SuS_16, indicating that the changes in capacity of those polymers are not attributable to changes on the surface structure.

Modifications done improved both iron capacity and selectivity, as shown in Table 4. SuS_16 showed higher capacity for iron and significantly lower for the interfering metals, as well as a high iron selectivity with almost no selectivity for Cu, Co, or Ni, representing a significant improvement over the previous polymer version. For SuS_17, the capacity is similar to that obtained for SuS_16, but is less selective, as the decrease in the selectivity of the interferences was only observed for Co.

Comparing these polymers to the non-imprinted version, SuS_16 showed significantly better iron capacity and selectivity, indicating that changes lead to the generation of iron-specific sites. SuS_17 also had higher iron capacity and reduced capacity for interfering metals. However, in terms of selectivity, similar affinities for copper and nickel, compared to the non-imprinted version, were observed, indicating that MMA produces less selectivity than St.

3.4. Scintillation improvement

To increase the scintillation capabilities of the polymers, three different strategies were followed. In the first strategy, PPO, the primary fluorescent solute, was substituted with p-PPO or v-Byph, which are polymerizable fluorescent solutes, to avoid improper trapping of the fluorescent solutes during polymer preparation that could lead to a decrease in scintillation performance. The second strategy involved reducing the amount of iron complex added to the polymer from 1 g to 0.5 g as the iron complex encapsulated inside the polymer may affect the scintillation through chemical or colour quenching. The third strategy involved replacing St with Vt to enhance the energy transfer process as methyl groups or aliphatic chains directly attached to an aromatic system can improve the quantum yield of the molecule by increasing the fluorescence rate constant while decreasing the intersystem crossing rate constant. This effect arises from a symmetry decrease, leading to partial relaxation of forbidden transition bands [39].

All newly synthesized polymers consistently exhibited a spherical shape with diameters ranging from 30 to 60 μm, except in the cases of SuS_23 and SuS_24, where the substitution of St with Vt resulted in the formation of aggregates rather than microspheres (Figure S6 in the supplementary material). Metal capacity and selectivity data for these polymers are presented in Table 5.

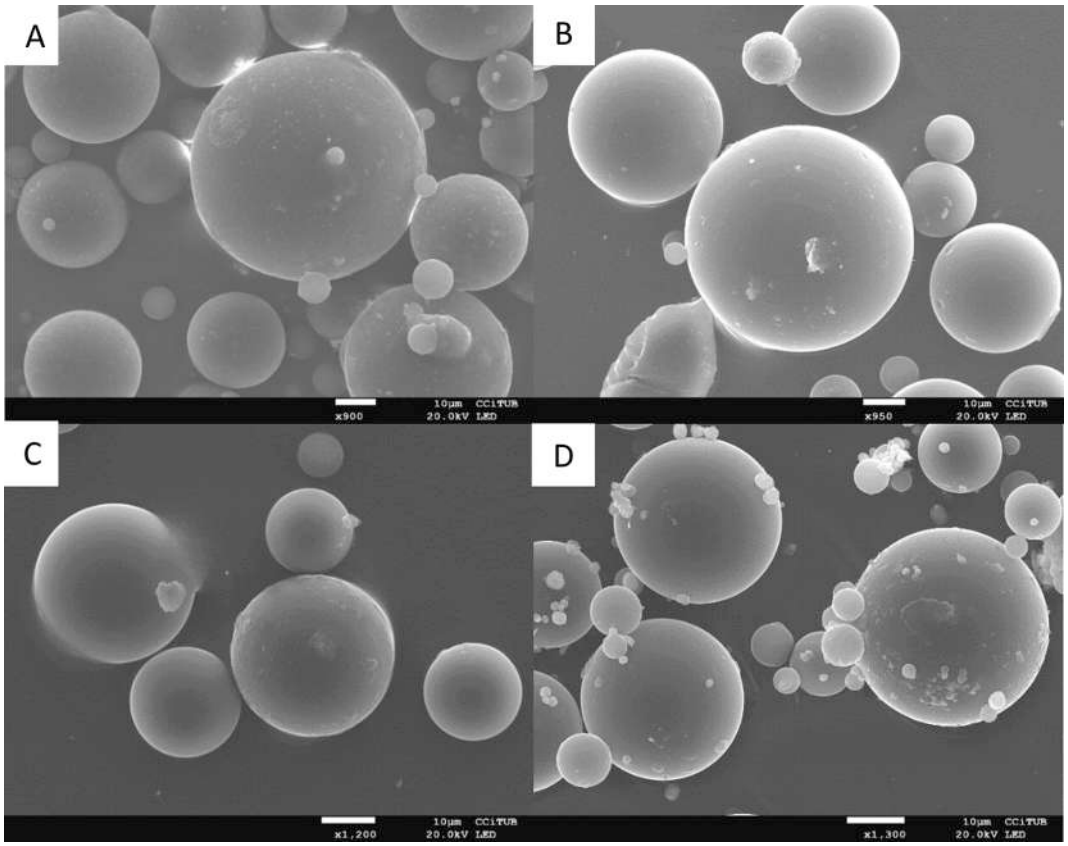

Fig. 5. SEM images for each Sc_Fe_IIP prepared involving triethylamine. SuS_16 (A and C), SuS_17 (B and D).

Table 4
Iron adsorption capacity and selectivity of the different iron imprinted polymers obtained after increasing the amount of iron in the complex. N = 2.

	CODE	Capacity (mg metal·g Sc-Fe-IIP^{-1})				Selectivity (%)			
		Fe	Cu	Ni	Co	Fe	Cu	Ni	Co
Imprinted	SuS_16	18(2)	0.9(0.7)	<0.10	0.5(0.2)	98(2)	7.8(0.1)	4.0(5)	<1
	SuS_17	19(2)	3.0(0.8)	<0.1	5(5)	95(1)	75(3)	26(4)	9(7)
Non imprinted	SuS_nIIP_16	10(2)	9(1)	1(1)	2.6(0.4)	84.3(0.8)	76(8)	23(4)	34(8)
	SuS_nIIP_17	16.9(0.3)	16(2)	3.7(0.9)	6(1)	72(3)	83(5)	31(4)	43(16)

Based on the results, the changes made do not have a significant impact on the selectivity or capacity of the polymers, as these properties remain consistent. Additionally, no clear correlation was found between the amount of iron complex added and the polymer's capacity, suggesting that the synthesis solution may reach a saturation point. At this stage, the polymers incorporate a limited amount of the iron complex, while any excess remains in a non-polymerizable or inaccessible form.

Scintillation performance was evaluated for both ^{14}C and ^{55}Fe using two detectors: a Quantulus 1220 and a Hidex 300SL. The obtained results are shown in Table 6.

The detection efficiency was significantly better in the Hidex than in the Quantulus detector. This can be attributed to the age of the detector (a new Hidex compared to an old Quantulus) and the potential loss of sensitivity of the PMT's of the Quantulus detector at low energies. Resulting in lower detection efficiencies.

Regarding the scintillating properties, the reduction of the iron complex used (polymers SuS_19, 20, 22, and 24) led, in all cases, to higher detection efficiencies, likely due to a decrease in acrylate groups, that affected the scintillation energy transfer process causing quenching.

The substitution of St with Vt (SuS_23 and 24), as expected, improved the energy transfer mechanism, resulting in higher ^{55}Fe detection efficiencies.

The addition of polymerizable fluorescent solutes (polymers SuS_18, 19, 21, and 22) did not make a significant difference, indicating that the previously used non-polymerizable solutes were successfully trapped in the polymer structure.

Polymers SuS_16 and 20 with St:DVB:VPA composition and PPO and POPOP as fluorescent solutes, showed the most favourable results in terms of detection efficiency for ^{55}Fe, as well as capacity and selectivity, making them the most promising candidates for ^{55}Fe analysis. Specifically, SuS_16, which exhibited the highest iron capacity with suitable scintillating conditions (2.2 % ^{55}Fe detection efficiency).

3.5. Cartridge test

A final real-use test was performed with one gram of SuS_16 polymer packaged into an SPE cartridge, for the analysis of a ^{55}Fe standard solution. The cartridge was loaded with 10 mL of a solution containing 750 dpm of ^{55}Fe and 1 mg of stable iron at pH 6. After passing the sample and drying the column, the cartridge was measured in both detectors.

Table 6
Detection efficiency for ^{14}C and ^{55}Fe in Quantulus 1220 and Hidex 300SL detectors using the different scintillating iron imprinted polymers obtained after the modifications aiming to improve the scintillation capacities. N = 2.

CODE	Monomers composition	*^{55}Fe detection efficiency (%)*		*^{14}C detection efficiency (%)*	
		Quantalus	Hidex	Quantalus	Hidex
SuS_16	St:DVB:VPA_1	0.73(0.01)	2.3(0.2)	28(2)	72(1)
SuS_20	St:DVB:VPA_05	0.76(0.02)	4.7(0.2)	39(1)	77(1)
SuS_18	p-PPO:St:DVB:VPA_1	0.24(0.02)	1.07 (0.03)	20(1)	57(2)
SuS_19	p-PPO:St:SVB:VPA_05	0.53(0.02)	3.17 (0.01)	27.2(0.4)	55.7 (0.6)
SuS_21	v-Biph:St:DVB:VPA_1	0.11(0.09)	0.23 (0.03)	16(4)	37(2)
SuS_22	v-Biph:St:DVB:VPA_05	0.3(0.1)	2.1(0.2)	24.5(0.5)	50(1)
SuS_23	Vt:DVB:VPA_1	0.9(0.1)	3.7(0.2)	44(1)	67(3)
SuS_24	Vt:DVB:VPA_05	0.77(0.08)	4.9(0.3)	29.4(0.6)	59(5)

Table 7
Iron yield and detection efficiency for the Sc-Fe-IIP as a cartridge.

Sc-Fe-IIP	Yield (%)	^{55}Fe detection efficiency (%)	
		Quantalus	Hidex
SuS_16	30(2)	0.8(0.1)	4.9(0.4)

The yield obtained was around 30 % (Table 7), which is somewhat low for routine separations and lower also than the value obtained in batch tests. However, this is very promising for a first approach of a scintillating imprinted polymer, especially considering that several optimizations can still be performed, particularly regarding the retention medium. The detection efficiency, in both detectors, surpassed the values obtained in solution with vials. This improvement can be attributed to the radionuclide's retention on the polymer's surface and the removal of the solution between the polymer, thereby reducing the attenuation caused by the medium. Additionally, the positioning of the scintillator in the mid-part of the PMT facilitates the detection. The results obtained demonstrate that the developed material is promising but requires further development.

Table 5
Capacity and selectivity of the different iron imprinted polymers obtained after the modifications aiming to improve the scintillation capacities. N = 2.

CODE	Monomers composition	Capacity (mg metal·g Sc-Fe-IIP^{-1})				Selectivity (%)			
		Fe	Cu	Ni	Co	Fe	Cu	Ni	Co
SuS_16	St:DVB:VPA_1	18(2)	0.9(0.7)	<0.10	0.5(0.2)	98(2)	7.8(0.1)	4.0(5)	<1
SuS_20	St:DVB:VPA_05	5.4(0.3)	1.0(0.2)	<0.13	<0.2	95(2)	4(2)	<0.5	<1
SuS_18	p-PPO:St:DVB:VPA_1	5(2)	0.8(0.1)	<0.13	<0.2	97(1)	<2	9(4)	<1
SuS_19	p-PPO:St:SVB:VPA_05	7(2)	1.16(0.09)	<0.13	<0.2	98.2(0.3)	7(6)	<0.5	<1
SuS_21	Biph:St:DVB:VPA_1	3(1)	1.0(0.8)	<0.15	<0.2	97(1)	6(1)	2(1)	<1
SuS_22	Biph:St:DVB:VPA_05	3.3(0.7)	0.8(0.3)	<0.10	<0.2	98(1)	6(1)	<0.5	<1
SuS_23	Vt:DVB:VPA_1	2.8(0.6)	0.5(0.2)	<0.15	0.5(0.2)	98(3)	12(3)	4(2)	<1
SuS_24	Vt:DVB:VPA_05	8(2)	1.7(0.7)	<0.16	0.9(0.2)	98(1)	27.8(0.1)	12(7)	<1

4. Conclusion

The extensive evaluation of the different scintillating imprinted polymers prepared has led to the following specific conclusions regarding composition and synthesis strategies: AAC exhibited superior performance among the tested chelating agents; particle size has to be reduced to 30–40 μm to achieve acceptable values of detection efficiency. The addition of triethylamine and the adjustment of the iron: AAC ratio to 1:1 were crucial for ensuring the complete complexation of iron and AAC, thereby reducing the formation of non-specific binding sites. Monomer combinations solely involving EGDMA and MMA were excluded due to the necessity of aromatic rings for effective scintillation; the introduction of a bleaching agent, VPA, enhanced scintillation performance by mitigating colour quenching caused by iron.

Among the various compositions studied, the St:DVB combination with 1 g of Fe-AAC complex emerged as the most promising Sc-Fe-IIP across key parameters: capacity, selectivity, and scintillation performance. The Sc-Fe-IIP demonstrated the ability to detect ^{55}Fe with a detection efficiency of up to 5 %, an iron capacity exceeding 15 mg and high iron selectivity. This promising Sc-Fe-IIP was successfully tested in an SPE cartridge, yielding favourable results: a detection efficiency of 5 % and a retention yield of 30 %. This supposes great progress regarding previous scintillating imprinted polymer described in the literature, where detection efficiency was significantly lower and no real separation test was performed.

However, while the retention and the detection efficiency obtained are acceptable for this initial prototype, the scintillating imprinted polymer needs improvement to be comparable to classical SPE separation and measurement with LSC or classical PSresin where retention above 50 % and efficiencies above 30 % could be expected for ^{55}Fe. Future work to achieve a viable material for routine laboratory analysis, should focus then on optimizing the scintillating imprinted polymer to achieve higher retention yield and detection efficiency. This can be accomplished, for example, by increasing the amount of fluorescent solutes added, optimizing the working media used for SPE separation, adjusting the bleaching to chelating agent ratio, evaluating new iron: chelating agent ratios or developing a scintillating support on which the IIP would be polymerized on the surface.

Declaration of competing interest

The authors declare the following financial interests/personal relationships which may be considered as potential competing interests: The authors reports financial support was provided by Spain Ministry of Science and Innovation.

Acknowledgments

This work was carried out in a Generalitat de Catalunya Research Group (2021 SGR 01342) and has received funding from the Ministerio de Ciencia, Innovación y Universidades (MICIU) de España through project PID2020-114551RB-I00 funded by MICIU/AEI/10.13039/501100011033. I. Giménez thanks the Universitat de Barcelona for the PREDOCS-UB grant.

Appendix A. Supplementary data

Supplementary data to this article can be found online at https://doi.org/10.1016/j.microc.2024.112268.

Data availability

Data will be made available on request.

References

[1] A. Leskinen, S. Salminen-Paatero, C. Gautier, A. Räty, M. Tanhua-Tyrkkö, P. Fichet, T. Kekki, W. Zhang, J. Bubendorff, E. Laporte, G. Lambrot, R. Brennetot, Intercomparison exercise on difficult to measure radionuclides in activated steel: statistical analysis of radioanalytical results and activation calculations, J. Radioanal. Nucl. Chem. 324 (2020) 1303–1316, https://doi.org/10.1007/s10967-020-07181-x.
[2] X. Hou, Radiochemical analysis of radionuclides difficult to measure for waste characterization in decommissioning of nuclear facilities, J. Radioanal. Nucl. Chem. 273 (2007) 43–48, https://doi.org/10.1007/s10967-007-0708-x.
[3] U. Schötzig, Half-life and X-ray emission probabilities of 55Fe, Appl. Radiat. Isot. 53 (2000) 469–472, https://doi.org/10.1016/S0969-8043(00)00166-4.
[4] X. Hou, Liquid scintillation counting for determination of radionuclides in environmental and nuclear application, J. Radioanal. Nucl. Chem. 318 (2018) 1597–1628, https://doi.org/10.1007/s10967-018-6258-6.
[5] International Atomic Energy Agency, Radiological Characterization of Shut Down Nuclear Reactors for Decommissioning Purposes, IAEA Vienna (1998) 184. https://www-pub.iaea.org/MTCD/publications/PDF/TRS389_scr.pdf.
[6] Triskem International, A. Procedure, Iron-55 in water, (2014) 1–7.
[7] Ž. Grahek, M.R. Mačefat, Isolation of iron and strontium from liquid samples and determination of 55Fe and 89,90Sr in liquid radioactive waste, Anal. Chim. Acta 511 (2004) 339–348, https://doi.org/10.1016/j.aca.2004.01.049.
[8] C. Augeray, M. Magalie, B. Nathalie, P. Marie-France, L. Chloé, L. Jeanne, F. Corinne, P. Jean-Louis, Development of a protocol to measure iron-55 in solid matrices in the environment, J. Environ. Radioact. 141 (2015) 164–173, https://doi.org/10.1016/j.jenvrad.2014.11.016.
[9] ISO, 22515: 2021 Water Quality-Iron-55-Test Method Using Liquid Scintillation Counting, International Organization for Standardization, Geneva (2021).
[10] X. Hou, L.F. Østergaard, S.P. Nielsen, Determination of 63Ni and 55Fe in nuclear waste samples using radiochemical separation and liquid scintillation counting, Anal. Chim. Acta 535 (2005) 297–307, https://doi.org/10.1016/j.aca.2004.12.022.
[11] L. Ye, I. Surugiu, K. Haupt, Scintillation proximity assay using molecularly imprinted microspheres, Anal. Chem. 74 (2002) 959–964, https://doi.org/10.1021/ac015629e.
[12] M. Budnicka, M. Sobiech, J. Kolmas, P. Luliński, Frontiers in ion imprinting of alkali- and alkaline-earth metal ions – Recent advancements and application to environmental, food and biomedical analysis, TrAC - Trends in Analytical Chemistry 156 (2022) 116711, https://doi.org/10.1016/j.trac.2022.116711.
[13] M. Sobiech, P. Luliński, Molecularly imprinted solid phase extraction – recent strategies, future prospects and forthcoming challenges in complex sample pretreatment process, TrAC - Trends in Analytical Chemistry 174 (2024) 117695, https://doi.org/10.1016/j.trac.2024.117695.
[14] Y. Liu, L. Wang, H. Li, L. Zhao, Y. Ma, Y. Zhang, J. Liu, Y. Wei, Rigorous recognition mode analysis of molecularly imprinted polymers—Rational design, challenges, and opportunities, Prog. Polym. Sci. 150 (2024) 101790, https://doi.org/10.1016/j.progpolymsci.2024.101790.
[15] F. Shakerian, K.H. Kim, E. Kwon, J.E. Szulejko, P. Kumar, S. Dadfarnia, A.m., Haji Shabani, Advanced polymeric materials: Synthesis and analytical application of ion imprinted polymers as selective sorbents for solid phase extraction of metal ions, TrAC - T, Trends Anal. Chem. 83 (2016) 55–69, https://doi.org/10.1016/j.trac.2016.08.001.
[16] A. Abdullah, F.N. Balouch, A. Talpur, M.T. Kumar, A.M. Shah, Mahar, Amina, Synthesis of ultrasonic-assisted lead ion imprinted polymer as a selective sorbent for the removal of Pb 2+ in a real water sample, Microchem. J. 146 (2019) 1160–1168, https://doi.org/10.1016/j.microc.2019.02.037.
[17] L.L.G. de Oliveira, F.A.C. Suquila, E.C. de Figueiredo, M.G. Segatelli, C.R.T. Tarley, Restricted access material-ion imprinted polymer-based method for on-line flow preconcentration of Cd2+ prior to flame atomic absorption spectrometry determination, Microchem. J. 157 (2020) 105022, https://doi.org/10.1016/j.microc.2020.105022.
[18] T. Yordanova, I. Dakova, K. Balashev, I. Karadjova, Polymeric ion-imprinted nanoparticles for mercury speciation in surface waters, Microchem. J. 113 (2014) 42–47, https://doi.org/10.1016/j.microc.2013.11.008.
[19] M. Mitreva, I. Dakova, I. Karadjova, Iron(II) ion imprinted polymer for Fe(II)/Fe (III) speciation in wine, Microchem. J. 132 (2017) 238–244, https://doi.org/10.1016/j.microc.2017.01.023.
[20] V.V. Kusumkar, M. Galamboš, E. Viglašová, M. Daňo, J. Šmelková, Ion-imprinted polymers: Synthesis, characterization, and adsorption of radionuclides, Materials 14 (2021) 1083, https://doi.org/10.3390/ma14051083.
[21] X. Zhou, B. Wang, R. Wang, Insights into ion-imprinted materials for the recovery of metal ions: Preparation, evaluation and application, Sep. Purif. Technol. 298 (2022) 121469, https://doi.org/10.1016/j.seppur.2022.121469.
[22] D.K. Singh, S. Mishra, Synthesis and characterization of Fe(III)-ion imprinted polymer for recovery of Fe(III) from water samples, J.Sci. Ind. Res. 69 (2010) 767-772. ISSN 0975-1084.
[23] B. Ara, M. Muhammad, M. Salman, R. Ahmad, N. Islam, T. ul H. Zia, Preparation of microspheric Fe(III)-ion imprinted polymer for selective solid phase extraction, Appl Water Sci 8 (2018) 41. https://doi.org/10.1007/s13201-018-0680-3.
[24] G. jin Zhu, H. yan Tang, P. hui Qing, H. ling Zhang, X. chuan Cheng, Z. hua Cai, H. bin Xu, Y. Zhang, A monophosphonic group-functionalized ion-imprinted polymer for a removal of Fe3+ from highly concentrated basic chromium sulfate solution, Korean Journal of Chemical Engineering 37 (2020) 911–920. https://doi.org/10.1007/s11814-020-0485-6.

[25] S. Özkara, R. Say, C. Andaç, A. Denizli, An ion-imprinted monolith for in vitro removal of iron out of human plasma with beta thalassemia, Ind. Eng. Chem. Res. 47 (2008) 7849–7856, https://doi.org/10.1021/ie071471y.
[26] H. Yavuz, R. Say, A. Denizli, Iron removal from human plasma based on molecular recognition using imprinted beads, Mater. Sci. Eng. C 25 (2005) 521–528, https://doi.org/10.1016/j.msec.2005.04.005.
[27] I. Giménez, H. Bagán, A. Tarancón, Fast analysis of gross alpha with a new plastic scintillation resin, Anal. Chim. Acta 1248 (2023) 340905, https://doi.org/10.1016/j.aca.2023.340905.
[28] A. Tarancón, H. Bagán, J.F. García, Plastic scintillators and related analytical procedures for radionuclide analysis, J. Radioanal. Nucl. Chem. 314 (2017) 555–572, https://doi.org/10.1007/s10967-017-5494-5.
[29] L.M. Santiago, H. Bagán, A. Tarancón, J.F. Garcia, Synthesis of plastic scintillation microspheres: Evaluation of scintillators, Nucl Instrum Methods Phys Res A 698 (2013) 106–116, https://doi.org/10.1016/j.nima.2012.09.028.
[30] A. Coma, H. Bagán, A. Tarancón, Preparation and evaluation of crosslinked plastic scintillation microspheres (CPSm), Polym. Test. 137 (2024) 108514, https://doi.org/10.1016/j.polymertesting.2024.108514.
[31] R.E. Dey, X. Zhong, P.J. Youle, Q.G. Wang, I. Wimpenny, S. Downes, J.A. Hoyland, D.C. Watts, J.E. Gough, P.M. Budd, Synthesis and Characterization of Poly (vinylphosphonic acid-co-acrylic acid) Copolymers for Application in Bone Tissue Scaffolds, Macromolecules 49 (2016) 2656–2662, https://doi.org/10.1021/acs.macromol.5b02594.
[32] C. Lin, M. Liu, H. Zhan, Pb(II)-imprinted polymer prepared by graft copolymerization of acrylic acid onto cellulose, Adv. Mat. Res. (2011) 2045–2048, https://doi.org/10.4028/www.scientific.net/AMR.295-297.2045.
[33] X. Cai, J. Li, Z. Zhang, F. Yang, R. Dong, L. Chen, Novel Pb2+ ion imprinted polymers based on ionic interaction via synergy of dual functional monomers for selective solid-phase extraction of Pb2+ in water samples, ACS Appl. Mater. Interfaces 6 (2014) 305–313, https://doi.org/10.1021/am4042405.
[34] I. Hamerton, J.N. Hay, J.R. Jones, S.Y. Lu, Covalent incorporation of 2,5-diphenyloxazole in sol-gel matrices and their application in radioanalytical chemistry, Chem. Mater. 12 (2000) 568–572, https://doi.org/10.1021/cm991157x.
[35] J.E. Novianty, K. Jorena, A.A. Saleh, E. Bama, M. Koriyanti, I.R. Ariani, Synthesis of Fe(III)-IIPs (Ion Imprinted Polymers): Comparing Different Concentrations of HCl and HNO3 Solutions in the Fe(III), in: Polymer Extraction Process for Obtaining the Largest Cavities in Fe(III)-IIPs, Science and Technology Indonesia 8, 2023, pp. 361–366.
[36] X. Chang, N. Jiang, H. Zheng, Q. He, Z. Hu, Y. Zhai, Y. Cui, Solid-phase extraction of iron(III) with an ion-imprinted functionalized silica gel sorbent prepared by a surface imprinting technique, Talanta 71 (2007) 38–43, https://doi.org/10.1016/j.talanta.2006.03.012.
[37] Ö. Saatçilar, N. Şatiroğlu, R. Say, S. Bektaş, A. Denizli, Binding behavior of Fe3+ ions on ion-imprinted polymeric beads for analytical applications, J. Appl. Polym. Sci. 101 (2006) 3520–3528, https://doi.org/10.1002/app.24591.
[38] M. Hamel Editor, Plastic Scintillators, Chemistry and Applications, Springer Nature 140 (2021). ISBN : 978-3-030-73487-9.
[39] N. Nijegorodov, V. Vasilenko, P. Monowe, M. Masale, Systematic investigation of the influence of methyl groups upon fluorescence parameters and the intersystem crossing rate constant of aromatic molecules, Spectrochim. Acta A Mol. Biomol. Spectrosc. 74 (2009) 188–194, https://doi.org/10.1016/j.saa.2009.06.003.

Supplementary material:

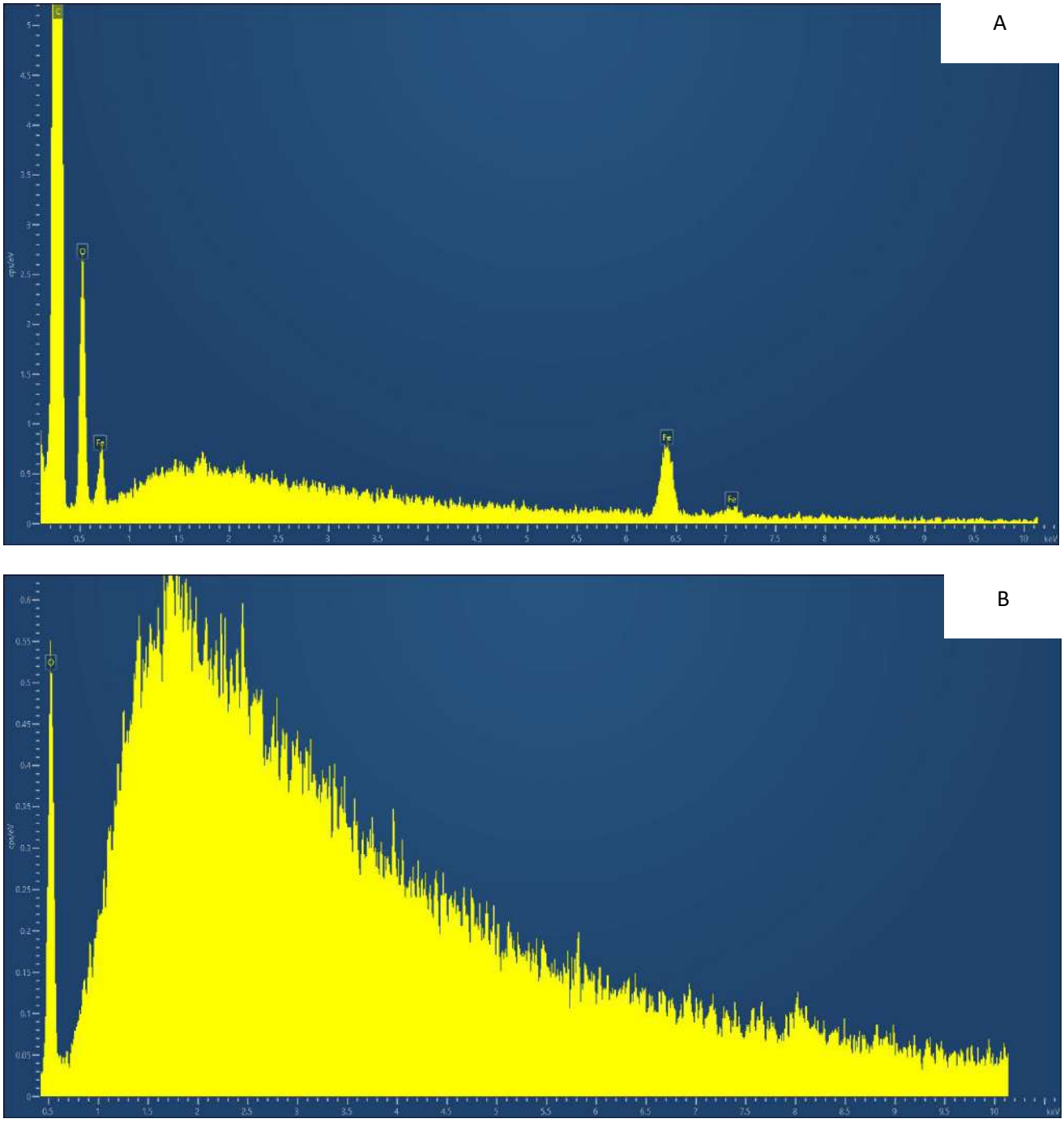

Figure S.1 EDS spectra for polymer SUS_1. First spectrum (A) refers to the polymer before template removal and second spectrum (B) to the polymer after template removal

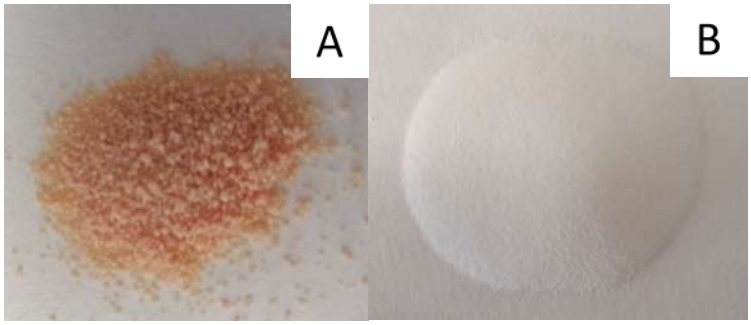

Figure S.2 Sc-Fe-IIP prepared without (A) and with (B) addition of VPA (iron has not been still removed)

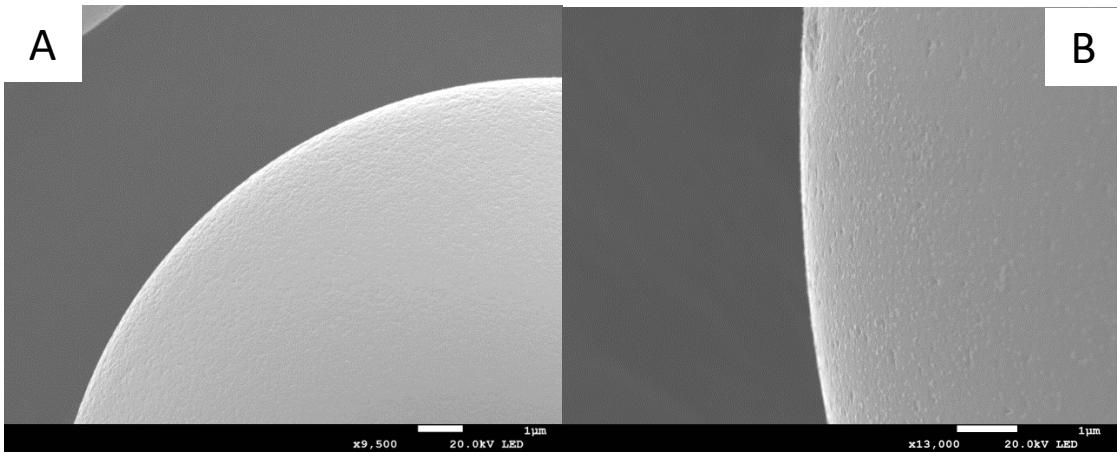

Figure S 3 Close SEM image for SuS_16 (A) and SuS_17 (B)

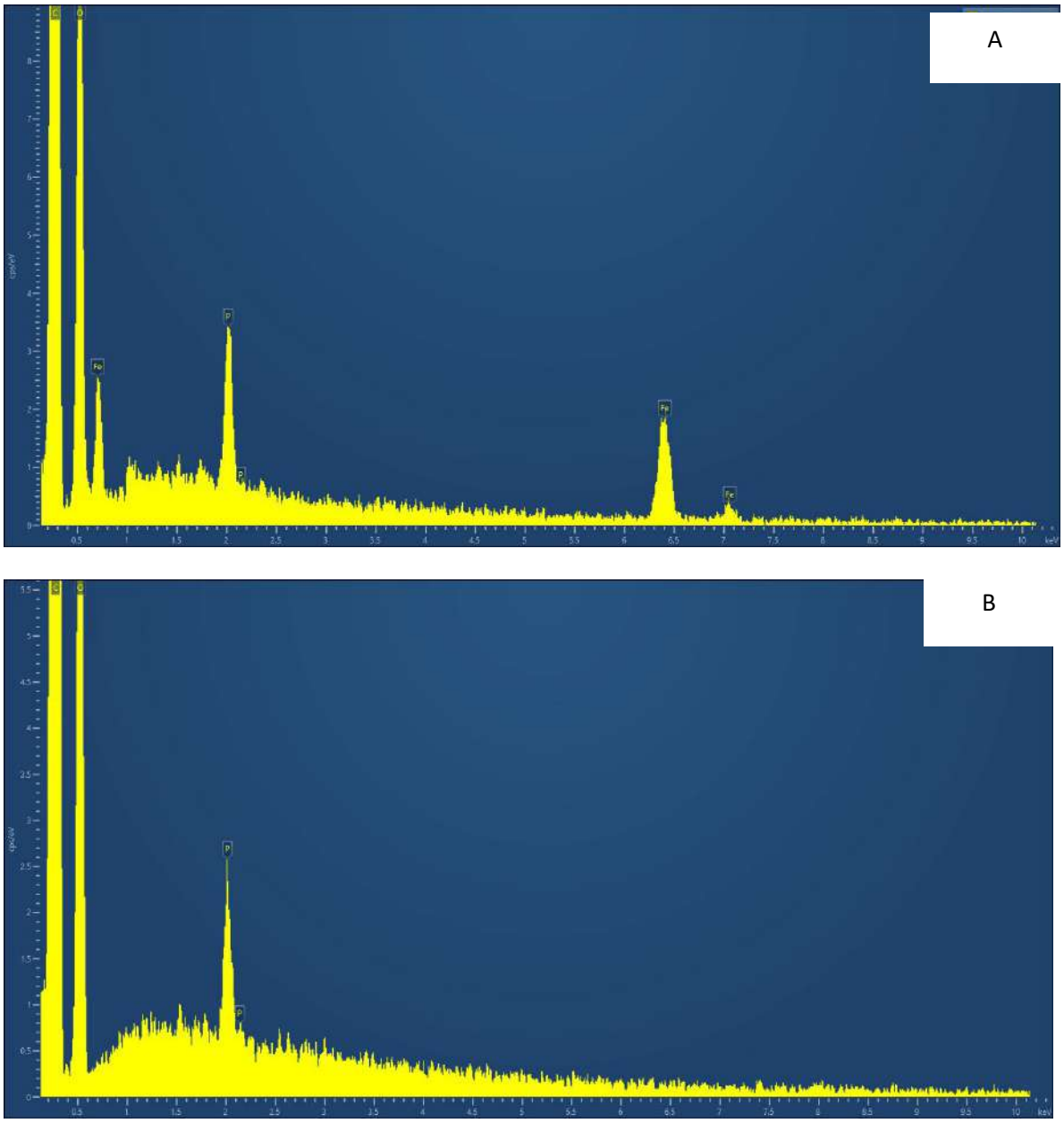

Figure S. 4 EDS spectra for polymer SUS_16. First spectrum (A) refers to the polymer before template removal and second spectrum (B) to the polymer after template removal

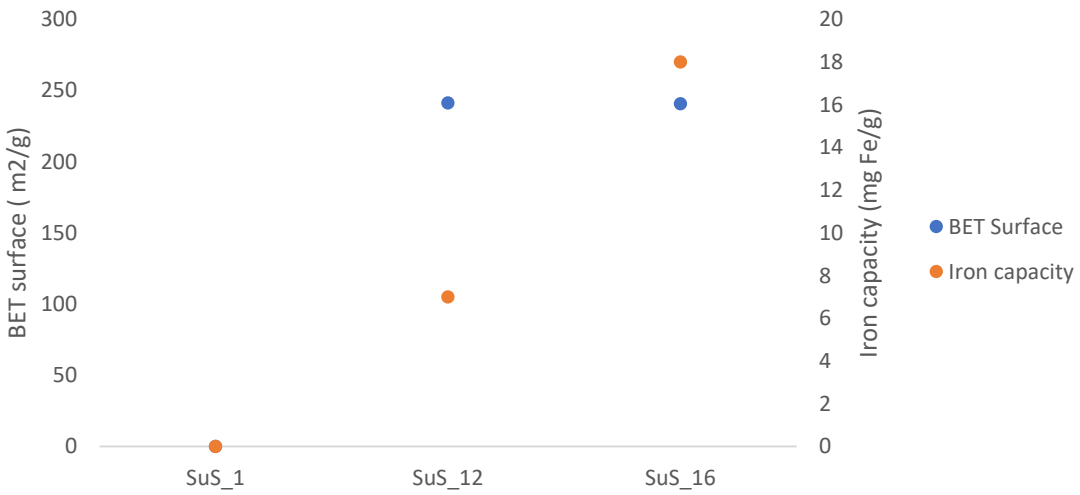

Figure S. 5 Comparation between the BET surface and the iron capacity for SuS_1, SuS_12 and SuS_16.

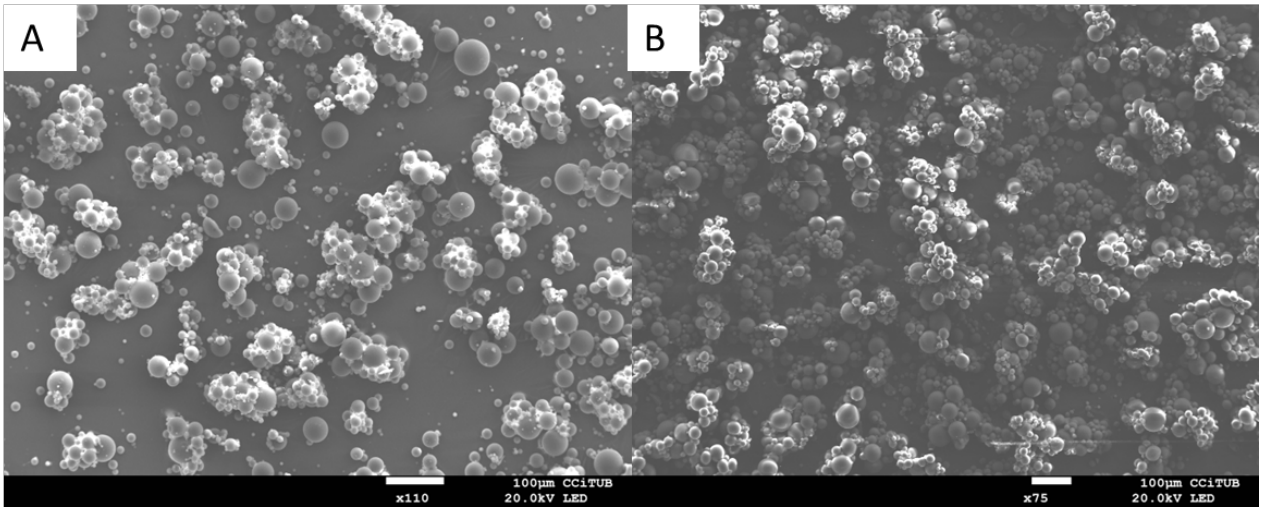

Figure S. 6 SuS_23(A) and SuS_24 (B)

Table s. 1 Size, detection efficiency for 14C and 55Fe and iron adsorption capacity for the optimised iron imprinted polymers obtained by suspension polymerization, after size reduction. Corresponding to the data shown in Figure 3.

CODE	Monomers composition	Size (µm)	^{14}C *detection efficiency (%)*	^{55}Fe *detection efficiency (%)*	Capacity (mg Fe · g Sc-Fe-IIP^{-1})
SuS _12	St:DVB:VPA	30-44	18(1)	0.60(0.1)	6.8(1)
SuS _13	ST:EGPO4	particles	4(3)	0.05(0.01)	5.8(6)
SuS_14	MMA:DVB:VPA	30-55	9.7(0.5)	0.20(0.08)	15.0(0.6)
SuS _15	MMA:DVB	45-60	12(2)	0.10(0.05)	8(2)

Table s. 2 Selectivity of the different optimized iron polymers (imprinted and non-imprinted), obtained after size reduction. Corresponding to the data shown in Figure 4.

Type	CODE	Monomers composition	Selectivity (%)			
			Fe	Cu	Ni	Co
Imprinted	SuS _12	St:DVB:VPA	98.9(0.8)	81(8)	36(10)	44(7)
	SuS_14	MMA:DVB:VPA	96.1(0.3)	72(4)	10(11)	15(8)
	SuS_15	MMA:DVB	97.7(0.7)	71(12)	18(6)	22(10)
Non imprinted	SuS_12	St:DVB:VPA	84.3(0.8)	76(8)	23(4)	34(8)
	SuS_14	MMA:DVB:VPA	72(3)	83(5)	31(4)	43(16)
	SuS_15	MMA:DVB	90(2)	73(11)	15(20)	34(24)

Article #4

Design of radionuclide separations based on MD simulations

Analytica Chimica Acta 1356 (2025) 344047

Contents lists available at ScienceDirect

Analytica Chimica Acta

journal homepage: www.elsevier.com/locate/aca

Design of radionuclide separations based on MD simulations

I. Giménez [a], G. Sormani [b], A. Rodríguez [c], A. Hassanali [b], H. Bagán [a], A. Tarancón [a,d,e,*]

[a] Departament d'Enginyeria química i química Analítica, Universitat de Barcelona, Marti i Franqués, 1-11, ES-08028, Barcelona, Spain
[b] The "Abdus Salam" International Centre for Theoretical Physics, I-34151, Trieste, Italy
[c] Dipartimento di Matematica e Geoscienze, University of Trieste, 34127, Trieste, Italy
[d] Serra-Húnter Programme, Generalitat de Catalunya, Barcelona, Spain
[e] Institut de Recerca de l'Aigua, Universitat de Barcelona, Spain

HIGHLIGHTS

- New methodology for radionuclide separation desing.
- MD simulations for ^{90}Sr and ^{210}Pb separation with crown-ether resins.
- Thermodynamic understanding of the anion affinity effect.

GRAPHICAL ABSTRACT

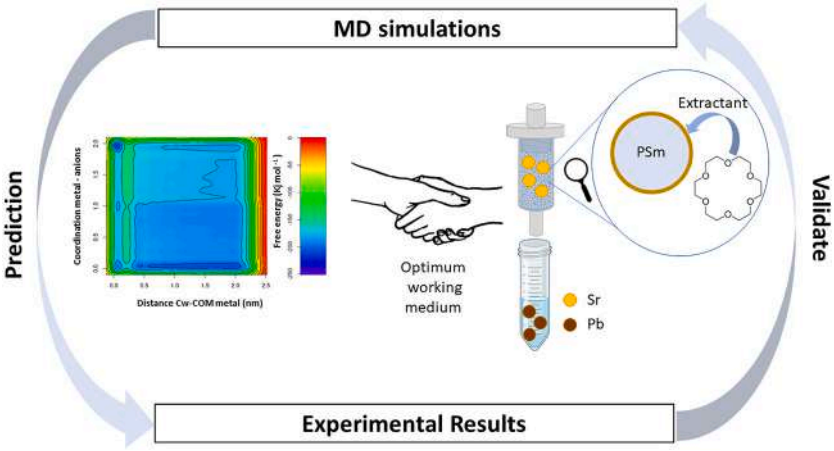

ABSTRACT

Background: The development of selective materials for radionuclide separation is often a long and costly process, requiring labor-intensive chemical separations and extensive optimization. To streamline the development of selective materials, this study explores MD simulations to accelerate the identification of optimal separation conditions, extractant-radionuclide affinity, reducing the need for extensive experimental trials.
Results: We assessed the effectiveness of MD simulations using the challenging system of Sr^{2+} and Pb^{2+} with 18-crown-6 crown ether, focusing on the influence of different working media, including nitric, hydrochloric, formic, acetic, and perchloric acids, as well as potassium thiocyanate. The simulation results were validated experimentally by measuring the distribution weight ratios (D_w) of Sr^{2+} and Pb^{2+} using crown ether immobilized on a polymeric surface. Our findings demonstrate a strong correlation between MD predictions and experimental data, particularly highlighting acetic acid as a medium where Sr^{2+} forms stable complexes, while Pb^{2+} does not.
Significance: This study confirms the suitability of MD simulations as a reliable tool for predicting the selectivity of extractants, enabling faster development of new scintillating and non-scintillating resins. By reducing the time and resources needed for experimental optimization, this approach offers a more efficient pathway for the development of advanced materials for radionuclide separation.

* Corresponding author. Departament d'Enginyeria química i química Analítica, Universitat de Barcelona, Marti i Franqués, 1-11, ES-08028, Barcelona, Spain
E-mail address: alex.tarancon@ub.edu (A. Tarancón).

https://doi.org/10.1016/j.aca.2025.344047
Received 13 February 2025; Received in revised form 8 April 2025; Accepted 8 April 2025
Available online 8 April 2025

1. Introduction

Liquid scintillation counting (LSC) is one of the primary techniques used for the determination of radionuclides, especially for beta and alpha emitters [1,2]. LSC is highly valued for its simplicity and high detection efficiencies. However, it lacks selectivity, requiring labour-intensive, costly, and time-consuming chemical separation processes to isolate the target radionuclide from interfering species present in the sample. These separation procedures frequently involve solid-phase extraction using chromatographic resins, which, under optimized conditions, can selectively isolate the radionuclide of interest [3–8]. After separation, the solution containing the isolated radionuclide is mixed with a scintillation cocktail for measurement in the detector.

Despite the existence of well-established procedures for the accurate isolation and quantification of many radionuclides, there remain challenges in determining certain radionuclides due to the absence of effective separation procedures and selective materials. Examples of these challenging systems include the separation of ^{55}Fe from ^{60}Co or ^{63}Ni, ^{90}Sr from ^{210}Pb, and ^{241}Am from ^{152}Eu or ^{244}Cm. Furthermore, conventional LSC methods generate mixed hazardous and radioactive wastes which are difficult and costly to manage, posing significant environmental concerns.

To address these limitations and develop more efficient analytical strategies, plastic scintillation resins (PSresins) have emerged over the past decade [9,10]. PSresins consist of a selective extractant immobilized on the surface of plastic scintillation microspheres (PSm) [11]. These resins integrate the chemical separation and measurement steps into a single process, eliminating the need for elution and thus reducing sample preparation complexity and eliminating the mixed waste generation. However, potential interferences have to be completely removed from the cartridge performing rinses to avoid activity overestimation, meaning that separation steps must be adapted to the PSresin working mode. Nevertheless, PSresins, as well as standard resins, are not available for all radionuclides of interest, meaning that challenges related to chemical separation persist despite the reduction in waste generation.

The development of new selective materials and new chemical separation procedures involves multiple stages, each requiring significant time, labour, and resources. Initially, the extractant, must be synthesized with enough yield and purity, and immobilized on an inert or scintillating support, in the optimal proportion, to produce the selective material. Subsequently, the interaction between the radionuclide and the extractant is studied to determine its affinity. The efficacy of the target radionuclide's extraction is influenced by the composition of the working medium, requiring extensive batch studies to identify optimal conditions. Once an effective working medium is established, potential interferences are studied to evaluate the selectivity of the material and determine the achievable decontamination factors [9,12–16]. Following these analyses, the separation process is optimized by determining the appropriate loading medium and additional rinses needed to retain the target radionuclide while removing interferences. This process can take several months or even years due to the long duration of required experiments and their inability to be conducted in parallel, some of them.

To streamline this development process, computational simulations can be employed to explore extractant molecules, understand interaction mechanisms, and assess the influence of different working media before initiating experimental work, thereby saving time and reducing costs. Techniques such as Density Functional Theory (DFT) and Molecular Dynamics (MD) simulations are particularly valuable in this regard. DFT provides detailed insights into the electronic interactions between radionuclides and extractants, helping to predict binding affinities and selectivity. However, DFT is limited to static, idealized conditions without accounting for temperature, pressure, or solvent effects. In contrast, MD simulations can model the dynamic behaviour of these systems, including the impact of temperature and solvent interactions, which are crucial for realistic separation processes. Consequently, in this work, the suitability and accuracy of MD simulations for the development of selective resins are assessed by predicting the affinity of an extractant for a radionuclide, in various working media, and validating the results experimentally. The study focuses on the separation of Sr^{2+} and Pb^{2+} using crown ethers. This system is very well known, with the Sr-resin being widely used for the separation of ^{90}Sr from common interferences in strong HNO_3 [17]. While Pb^{2+} is more strongly retained than Sr^{2+}, this does not pose an issue, as ^{90}Sr can be selectively eluted in low HNO_3 conditions. ^{90}Sr analysis with crown ether PSresin is also feasible with the advantages of no mixed waste generation [10,18]. However, when ^{210}Pb is also present, it cannot be rinsed without removing ^{90}Sr. Consequently, the measurement of ^{90}Sr in the presence of ^{210}Pb is not possible unless a previous precipitation separation is applied [19]. The theoretical study of the interaction of Sr^{2+} and Pb^{2+} using crown ethers in different media will be not only useful to determine in which medium ^{90}Sr can be separated from ^{210}Pb in a crown ether PSresin, aiming for environmental waste samples such as contaminated water, soil, and effluents from nuclear power plants, but also to evaluate if this strategy could be valid for the design of new extractants and methods for radionuclide separation as well as to understand the mechanism of interaction between extractant and radionuclides.

Previous computational studies using DFT have explored the stability of crown ethers within various alkaline elements, focusing on the influence of cavity size and electron-withdrawing effects on their structures [20–23]. While these approaches provide precise electronic insights, they are typically conducted at 0 K, neglecting critical factors such as water solvation and entropic contributions. These factors are essential for a complete understanding, as they significantly impact stability and reactivity at non-zero temperatures. Thus, the final ion-crown ether conformation predicted by DFT may not accurately reflect the behaviour under more realistic conditions that include solvent and temperature effects.

Therefore, the present study uses MD simulations to evaluate the binding affinities of Sr^{2+} and Pb^{2+} with 18-crown-6 ether across different working media. This approach provides a more realistic representation of the interactions, accounting for solvent environments, conformational flexibility, and thermal effects. Six working media (nitric acid, hydrochloric acid, formic acid, acetic acid, perchloric acid, and potassium thiocyanate) have been simulated and subsequently validated experimentally using the 18-crown-6 ether immobilized on an inert polymeric surface. The simulation results are compared with experimental distribution weight ratios (D_w), a widely used metric for assessing the affinity of metals for resins in specific media.

2. Results & discussion

2.1. Studied system

We investigate the stability of the complexes formed between the 18-crown-6 crown ether and Sr^{2+} or Pb^{2+} in six different working media that are of common use in laboratories: nitric acid (HNO_3) the common working media for ^{90}Sr separations with crown ethers, hydrochloric acid (HCl), formic acid (HCOOH), acetic acid (CH_3COOH), perchloric acid ($HClO_4$), and potassium thiocyanate (KSCN).

18-crown-6 is the core section of the crown ether commonly used in strontium selective resins, (4,4′(5')-di-*t*-butylcyclohexano-18-crown-6). This section is selected since it constitutes the essential binding component with the ion (refer to the top panel of Fig. 1). The presence of substituents on the crown ether can influence the binding affinity, depending on the functional groups of the substituents, but the general trend will remain the same, especially if the substituents are based on alkenes chains [24,25]. In a similar manner, to simplify the simulation, no diluents were considered in spite that it may have also some influence. By this way, focusing only on the essential part of the crown ether, the computational cost of the assessment of the theoretical procedure

may be reduced, providing a simple but efficient tool to study extractant-metal interaction in aqueous medium in presence of anions.

18-crown-6 consists of a cyclic arrangement of six ethylene oxide (–CH_2CH_2O–) units, forming a flexible macrocyclic ligand. The six oxygen atoms in the ring, each with lone pairs of electrons, are strategically positioned to coordinate with a central cation via ion-dipole interactions (see the middle panel of Fig. 1). The cavity size of 18-crown-6, defined by the effective internal diameter of the macrocyclic ring, is approximately 2.6–3.2 Å. The geometrical compatibility between the cation and the cavity, coupled with the optimal alignment of the oxygen atoms' electron lone pairs, results in the formation of highly stable complexes.

In general, crown ethers are known for their inherent flexibility, which allows them to adapt their cavity size to accommodate ions of varying sizes. This flexibility has been studied extensively, particularly through DFT simulations, which have shown that crown ethers can modify their structure to host ions ranging in size from small lithium ions to larger cesium ions. In the case of 18-crown-6, its flexible backbone enables it to fold and adjust in response to the ionic radius of the guest cation, effectively trapping it within the cavity. Studies in the gas phase have demonstrated that this unrestricted flexibility allows crown ethers to achieve optimal conformations for ion binding, resulting in a strong complexation affinity for ions across a wide range of radii [26,27].

However, the flexibility of 18-crown-6 is influenced by environmental conditions, such as solvent and temperature. In solution, the presence of solvent molecules and thermal motion introduces some restrictions on the crown ether's ability to fold, slightly limiting the extent to which it can adapt its structure [26]. Even with these restrictions, 18-crown-6 retains enough conformational adaptability to form stable complexes with ions of similar ionic radii, such as Sr^{2+} and Pb^{2+}, as demonstrated in various studies [21,23,28–32].

2.2. Free energies landscapes of crown ether-metal complexes in solvent

Free energy calculations are used to estimate the Gibbs free energy change associated with a specific process. In this case, the binding of metal ions (like Pb^{2+} or Sr^{2+}) with crown ethers in the presence of anions in the solvent, provides a measure of the binding strength between molecules. A negative value for the Gibbs free energy change indicates that the process is thermodynamically favorable (the metal ion and the crown ether form a stable complex). The larger the absolute value obtained the stronger and more stable the interaction is, suggesting strong binding affinities. In practical terms, a higher binding energy makes the metal-crown ether complex more stable, which can influence its behavior in processes such as separation or purification. The presence of counter anions due to the working media, can enhance or not this binding by stabilizing the complex, further increasing or decreasing the affinity between the crown ether and the metal ion [29]. Therefore, by understanding these free energy values, we can predict how different the crown ethers will behave in practical applications.

2.2.1. Simulation process definition: nitrates as counterion

We initially conducted a 400 ns molecular dynamics (MD) simulation of Sr^{2+} or Pb^{2+} together with 18-crown-6 and two nitrate molecules, solvated with approximately 2500 SPC/E water molecules. The 12-6 Lennard-Jones is a widely used potential model for nonbonded interactions, however, when dealing with highly charged metal ions, it faces significant limitations, as it does not account for ion-induced dipole interactions, underestimating the strength of ion-water interactions and, as a consequence, lacking in accuracy for hydration free energy (HFE), ion-oxygen distance (IOD) and coordination number (CN). For that reason, Mertz and co-workers [33] developed the 12-6-4 Lennard-Jones potential, which corrects the classical model with the inclusion of an extra attractive term which provides a more realistic representation of highly charged metal ions. For Sr^{2+} and Pb^{2+}, switching to the 12-6-4 model can improve accuracy in specific areas such as hydration energies and ion coordination, but the differences may not be as large as those observed with M^{3+} or M^{4+} ions. Therefore, given their availability, 12-6-4 LJ potentials were used.

The temporal evolution of the coordination between the metal ions (Sr^{2+} or Pb^{2+}) and the crown ether was studied using the PLUMED plugin to calculate the distance between the centers of mass (COM) of the crown ether and the metal ion. Fig. S1 in Supplementary Information indicate that during this 400 ns period, the Sr^{2+} ion does not approach the crown ether within the expected binding distance (~0.05 nm COM separation). This suggests that binding did not occur, likely due to insufficient sampling; the system may be trapped in high-energy states separated by large energy barriers. Given this lack of sampling, we concluded that unbiased simulations alone could not provide a converged picture of the Sr^{2+}-crown ether interaction. Metadynamics was therefore employed as a way to accelerate sampling of rare events and overcome high-energy barriers. By adding a history-dependent bias to the system, metadynamics allows us to explore configurations that are

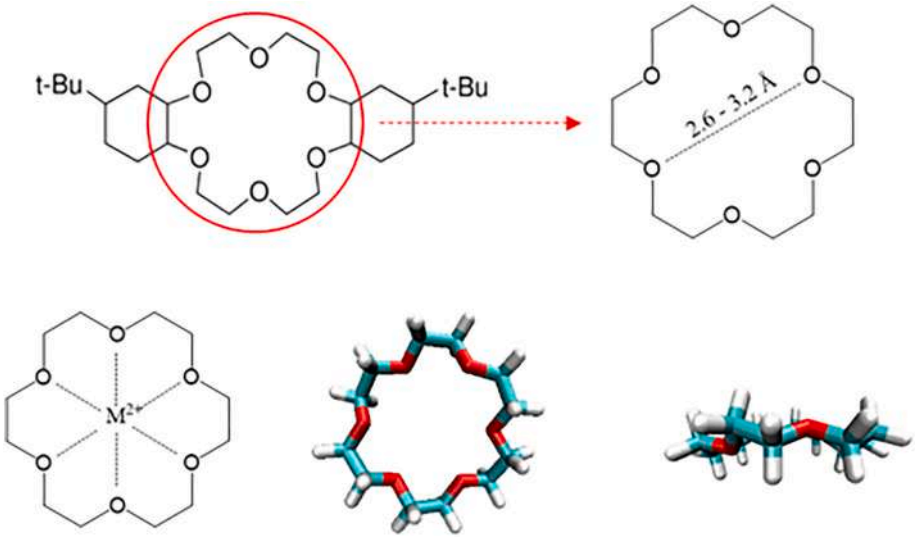

Fig. 1. Top panel, representation of the crown ether used in CE-PSresin, and the core crown ether used in the simulation. Middle panel interaction of the metal with the oxygen of the crown ether and the geometry of the 18-crown-6 from upper and side view.

rarely accessed in unbiased MD.

To have a complete exploration of the phase space of the system, we performed a 2 μs metadynamics simulation, based on the configurations obtained from the initial MD production run. To evaluate the affinity of each metal and the influence of the anions, we analyzed two collective variables: the distance between the centers of mass of the crown ether and the metal ion, and the coordination number between the metal ion and the two nitrate anions.

The free energy landscape was reconstructed using RStudio with the MetadynMiner and MetadynMiner3 libraries [34]. The middle panel of

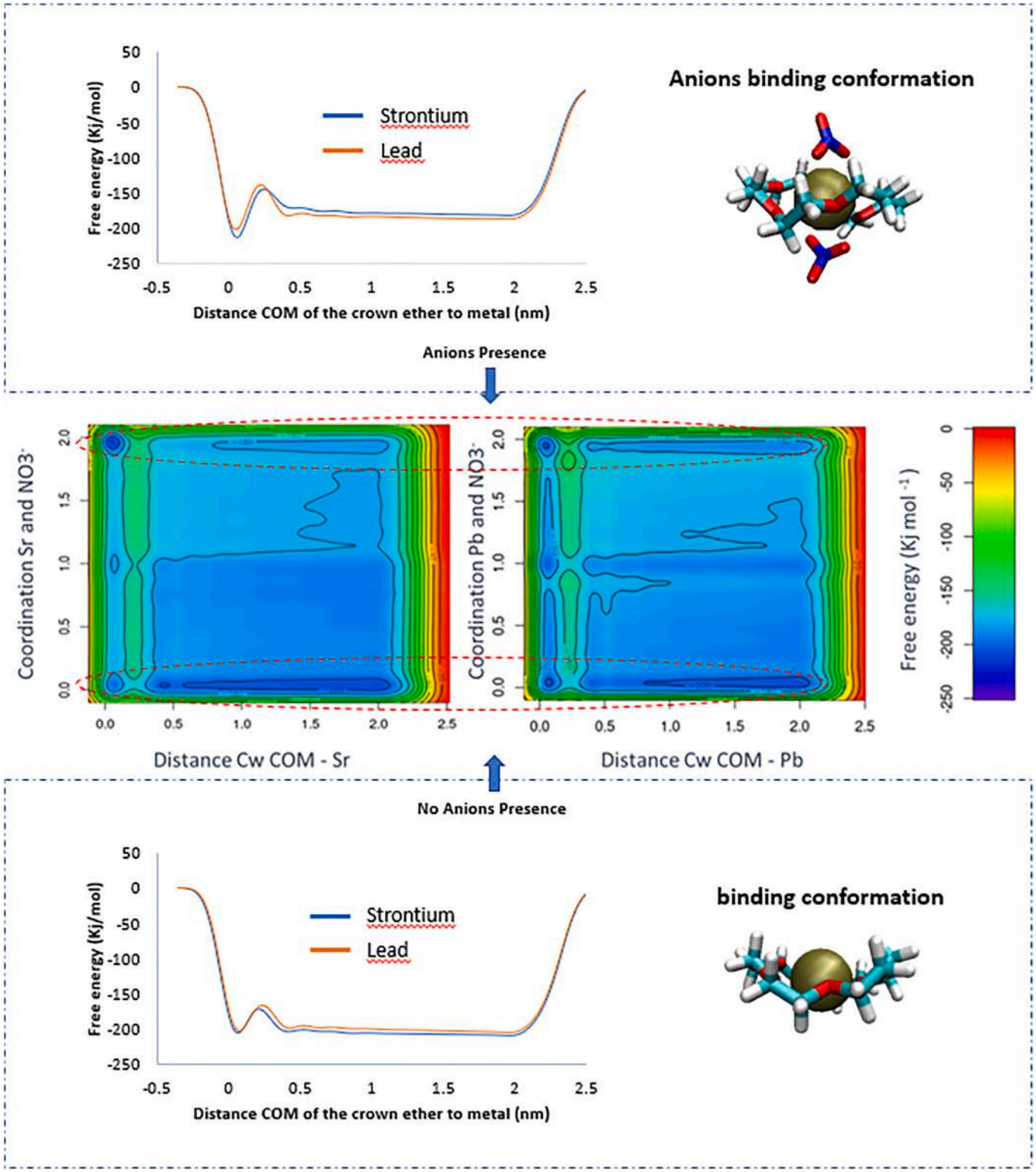

Fig. 2. Top panel, evolution of the free energy at presence of nitrates in the bonding of the metal with the 18-crown-6, along with the snapshot of the conformation of the complex in the bounding situation. Middle panel, free energy landscape for strontium and lead considering the coordination of the metal and the nitrates and the distance between the center of masses of the 18-crown-6 and the metal. Bottom panel, evolution of the free energy without the presence of nitrates in the bonding of the metal with the 18-crown-6.

Fig. 2 shows the free energy profiles obtained for strontium and lead, respectively. To provide a clearer interpretation, we extracted the data corresponding to two specific coordination states: coordination number 2 (presence of anions) and coordination number 0 (absence of anions). The resulting 1-D profiles are presented in the top panel (presence of anions) and bottom panel (absence of anions) of Fig. 2.

In both scenarios, Sr^{2+} and Pb^{2+} exhibit similar affinities for 18-crown-6, consistent with their known strong retention in crown ether-based resins. Additionally, the presence of nitrate anions was found to enhance the affinity between the metal ions and the crown ether and do not compete with the crown ether for direct coordination with the metal ion. Instead, their presence serves to balance the charge and support the solvation environment [29,35]. Both systems showed similar complex conformations as depicted in the structures extracted from the simulation, with the metal ion positioned centrally within the crown ether and nitrates axially co-complexing the cation, proving the reported stable complex conformation. Concluding that metadynamics simulations, under the chosen description of the system, accurate describes the system in concordance with literature for what reported theoretically and experimentally regarding the complex conformation shape and stability in the presence of nitrate anions.

2.2.2. FES of metal-crown ether complexes using different counterions

Given the difficulties in separate Sr^{2+} and Pb^{2+} using nitrates as counterions and motivated to study the effects of the anion's presence, we analyzed the free-energy landscape of the cation-crown ether compounds with five more working media (chloride, perchlorate, acetate, formate and thiocyanate) for Sr^{2+} and Pb^{2+}, these ions were selected according to the literature, based on their capability of enhance the binding of Sr^{2+} or Pb^{2+} with crown ether, among those that present a reasonable cost, safety and their solutions are colourless [2–4].

Anions help to balance the positive charge of the metal ion, thereby reducing electrostatic repulsion within the complex, also, the size and polarizability of the anions can affect the solvation environment. Larger, more polarizable, anions can disrupt the solvation shell more effectively, and can enhance the complex's overall stability by lowering the free energy of the system. Additionally, geometric factors play a role in how anions interact with the metal ion-crown ether system. Finally, the geometry of anions, can influence the final complex as it affects the previously mentioned flexibility of the crown ether, thus affecting its binding affinity and selectivity [36,37].

Fig. 3 shows the 2-D profiles of the free energy landscape, for all the considered anions, focusing on the anion presence (the CN = 2 section). The left panel corresponds to the strontium system and the right panel to the lead system. For strontium the global minimum is found in all cases in the bonding situation (0.03 nm), while the lead system, only has a favorable binding with nitrate and formate. Given the obtained results, the separation of Sr^{2+} and Pb^{2+} could be achieved by retention of the Sr^{2+} and elution or directly not retention of Pb^{2+} in a crown ether-based resin in acetate medium.

2.3. Experimental validation

In order to test the effectiveness of the proposed theoretical procedure for the prediction of the interaction between a metal (or radionuclide) and an extractant (typically organic molecules) in different working media, we compared the agreement between the binding affinities predicted in simulations with the experimental ones, obtained through batch studies.

The free energy difference (ΔF) between the unbound and the bound situations, for each metal-crown ether complex in each anionic medium (NO_3^-, Cl^-, $HCOO^-$, CH_3COO^-, ClO_4^-, and SCN^-), was used to quantify the simulated binding affinity. A more negative ΔF value indicates a more favorable binding interaction. On the other hand, to get an experimental measure of the binding affinity, we performed batch studies for all the systems which were analyzed theoretically and we measured the distribution weight ratio (D_w). This experimental parameter is a measure of the affinity between the target cation (Sr^{2+} or Pb^{2+} in this case) and the crown ether within the studied medium. A high D_w value indicates strong affinity between the target metal and the extractant under specific conditions.

Fig. 4 presents a comparison between the computed free energy differences and the experimentally determined D_w values. A strong inverse correlation was observed for both metals: a negative ΔF (indicating a more favorable binding interaction) corresponds to a positive D_w indicating a strong affinity between the metal and the crown-ether in both cases. The overall trends observed in the simulations were consistently reflected in the experimental results, demonstrating the effectiveness of simulations of predicting the experimental behavior.

The single exception to this correlation was observed for the lead-crown ether complex using perchlorate as counterion, where simulations predicted an unfavorable binding interaction, but, experimental results indicated the presence of weak binding. Nevertheless, both values are small and discrepancy can be interpreted as a consequence of a weak interaction and the uncertainty of both determinations.

Although a clear correlation was observed between the experimental and simulation results, the D_w values obtained in this study are relatively low compared to those of fully optimized resins, where a D_w value greater than 10^2 is indicative of high affinity.

Another important observation is that it is experimentally confirmed that the crown ether has the highest affinity for Sr^{2+} when acetate is used as counterion, while there are no evidences of experimental binding between the Pb^{2+} and the crown-ether confirming the lack of affinity.

Acetate could thus be the optimal medium in which Sr-selective retention can be achieved using a PSresins. It should be noted that this

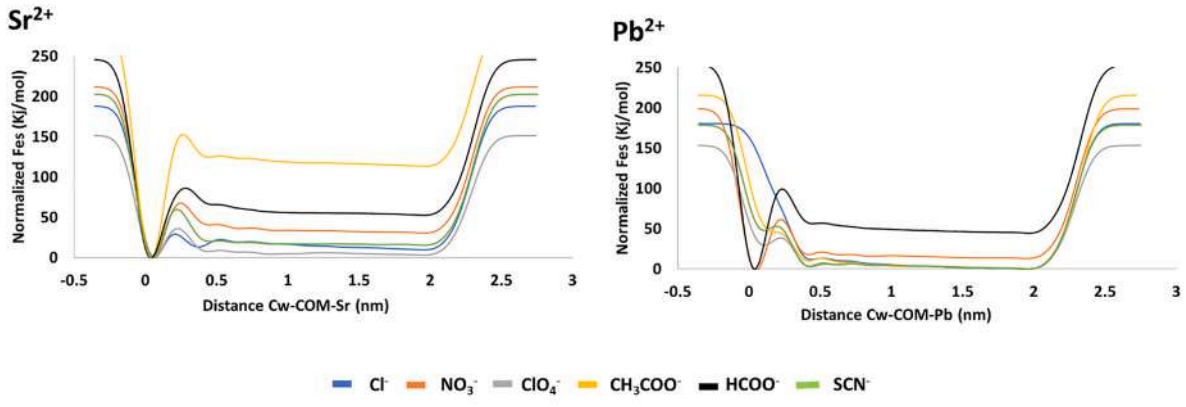

Fig. 3. Free energy profile for each system studied in presence of anions. Left panel refers to strontium and right panel to lead.

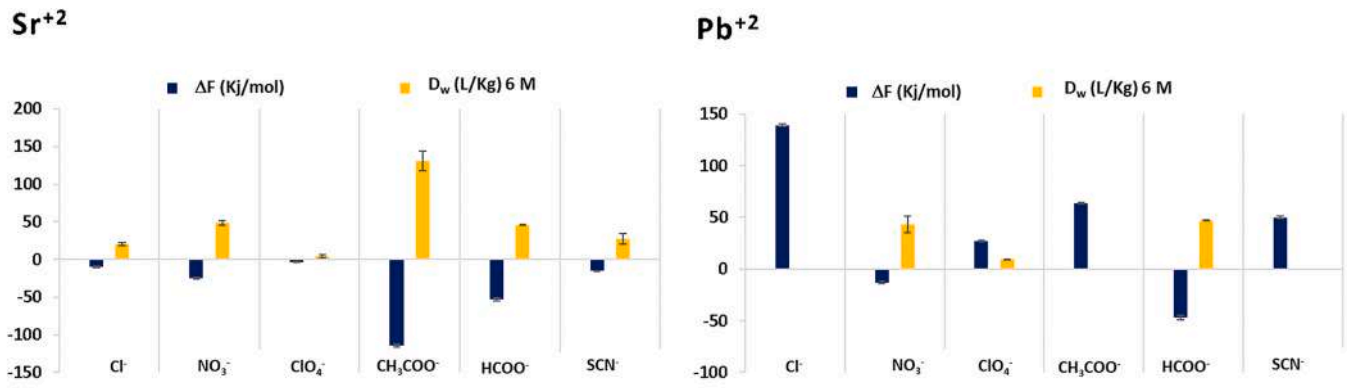

ΔF (Kj/mol)	Cl^-	NO_3^-	ClO_4^-	CH_3COO^-	$HCOO^-$	SCN^-
Strontium	-10(1)	-25(1)	-3.5(0.9)	-114(2)	-53(2)	-15.4(0.9)
Lead	139.24(0.8)	-19.1(0.9)	26.9(0.9)	64(1)	-47(2)	50(1)

D_w (L/Kg)	Cl^-	NO_3^-	ClO_4^-	CH_3COO^-	$HCOO^-$	SCN^-
Strontium	20 (2)	47(3)	4(2)	131(13)	45.8(0.8)	27(7)
Lead	<0.5	43(8)	9.1(0.6)	<0.5	47.0(0.6)	<0.5

Fig. 4. Correlation between the differences in free energy and the experimental Dw for strontium (left panel) and lead (Right panel). Left table differences in free energy for strontium and lead. Right table Dw for Strontium and lead.

trend could be affected by the typical diluents and polymers used with the crown ethers in selective resins, and therefore, it has to be tested in a more realistic system.

2.4. Thermodynamic analysis on the acetate system

To understand why strong binding is observed with strontium when using acetate as the anion, but not with lead, we analyzed the free energy, internal energy and entropy of the systems. The thermodynamic parameters have been calculated for each system, taking as a reference point the non-bounding non-acetate situations, moving to the metal-crown ether binding in absence of acetate, and finally studying the effect of the acetate in the complex formation (Table 1).

The binding of the metal ion to the crown ether alone resulted in an unfavorable condition, characterized by a positive free energy difference. However, when acetate anions are introduced into the system, there is a noticeable internal energy penalty in both cases, accompanied by an increase in entropy.

In the strontium system, the increase in entropy compensates for the internal energy penalty, leading to a favorable overall free energy change. In contrast, in the lead system, the entropy gain is insufficient to overcome that penalty, resulting in an unfavorable situation. This explains why, in an acetate medium, lead does not bind to the resin, whereas strontium does.

The addition of acetate anions to the Sr^{2+}-crown ether complex leads to a favorable increase in entropy due to the release of water molecules from the solvation shells of strontium and the acetates. This entropy gain offsets the moderate internal energy penalty, resulting in a favorable free energy change. In the case of lead, the strong initial binding to the crown ether and the significant structural reorganization required to accommodate the acetates incur a large internal energy penalty. The entropy gain from desolvation is insufficient to compensate the internal energy cost, leading to an unfavorable overall free energy change. Therefore, the formation of a stable Sr^{2+}-crown ether-acetate complex is more favored due to the flexible coordination environment of strontium compared to the Pb^{2+}-crown ether-acetate complex, which is hindered by lead's substantial internal energy penalty [35,38]. These observations suggest that temperature plays a critical role in modulating the stability of these metal-crown ether complexes. For strontium, the favorable entropy gain indicates that higher temperatures could enhance the stability of the Sr^{2+}-crown ether-acetate complex, as increased temperature amplifies the entropic contribution. In contrast, for lead, the significant internal energy penalty remains dominant at elevated temperatures. Since the entropy change for the Pb^{2+}-crown ether-acetate complex is insufficient to offset the positive change, increasing the temperature will not improve its stability, resulting in either unfavorable or only weakly favorable complex formation.

Checking the metal-crown ether-acetate binding conformation, the Sr^{2+}-crown ether-acetate system showed an expected complex conformations as depicted in the structures extracted from the simulation (Left panel, Fig. 5), with the Sr^{2+} ion positioned centrally within the crown ether and acetates axially co-complexing the cation. However, in the case of lead, the acetates are in cis conformation (both acetates from the same side) co-complexing the cation (right panel, Fig. 5). This resulting binding conformation for Pb^{2+}-crown ether-acetate is thermodynamically less stable as it has been seen and this could be explained due to repulsion and steric hindrance effects between both acetates molecules not leading to a very stable compound.

From the coordination point of view, strontium ions typically prefer higher coordination numbers, usually around 7 to 8, which allows for a more flexible coordination environment [39]. This flexibility allows the interaction of the metal both with the crown ether and with the acetate anions without significant disruption of the overall complex. Additionally, the strontium and acetate interactions are mainly ionic; reason why they can integrate into the coordination sphere without causing major distortions or coordination competition [40,41]. In contrast, lead ions generally prefer lower coordination numbers, around 4 to 6, even though can get to larger coordination numbers [42–44], and can have a more covalent interactions than strontium, due to the inert pair effect. This preference might result into a less flexible coordination sphere. When acetates attempt to coordinate with lead, they can disrupt the Pb^{2+}-crown ether interactions, introducing significant steric and electronic strain. In addition, lead ions can have a stronger interaction with acetates, which can thus compete directly with the interactions between lead and the crown ether [45–48], not leading to a stable conformation.

Table 1
ΔF, ΔU and -T ΔS for strontium and lead, taking as a reference point the non-bounding non-acetate situations with the crown ether (Cw), moving to the metal-crown ether binding in absence of acetate, and to the metal-crown ether-acetate binding. In Kj/mol.

	No acetate			Acetate		
	ΔF	ΔU	-TΔS	ΔF	ΔU	-TΔS
Sr^{2+}-Cw	26 (3)	−33 (8)	59 (9)	−110 (2)	6 (3)	−116 (4)
Pb^{2+}-Cw	62 (2)	24 (7)	38 (7)	42 (3)	82 (5)	−40 (6)

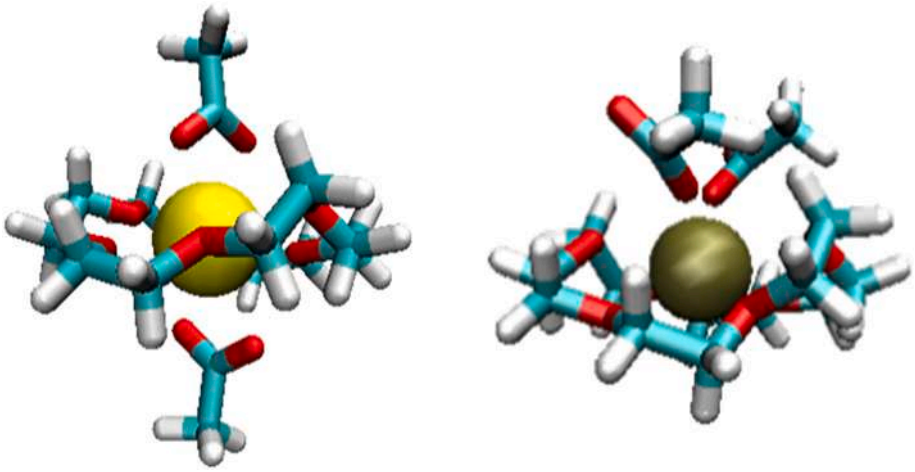

Fig. 5. Snapshots in binding situation in presence of acetate. Left-panel for strontium and right panel for lead.

3. Conclusions

The use of all-atoms MD simulations provides a useful support in understanding the medium effect on the stability of the metal-crown ether complex. Metadynamics, in particular, allows the identification of a suitable working medium where the highest affinity between the target element and extractant is achieved.

The correlation between experimental and simulation results confirms that molecular dynamics is an effective tool for predicting experimental binding affinities. Compared to other simulation strategies, the MD is more realistic as it includes the water molecules, allowing to consider the effect of solvation they caused.

The results obtained are also in agreement with literature in what regards nitric acid, the medium in which both cations are complexed with the crown-ether. Regarding the other anions studied, all present similar behavior for both cations, except in acetic medium. In the system formed by Sr^{2+} or Pb^{2+} with 18-crown-6, when using acetate as counterions, the Sr^{2+}-crown ether complex has the highest stability while the Pb^{2+}-crown ether compound is not stable. This result suggests the possibility to use acetate as medium to remove Pb^{2+} from crown-ether PSresins making possible the measurement of ^{90}Sr in the presence of ^{210}Pb in the sample.

The established methodology is a straightforward strategy that considers the main parameters affecting the affinity between a target element and extractant with low statistical errors. It can be used as a screening tool in the preliminary selection of promising extractant candidates and separation media likely to meet the separation of radionuclides, enabling a future faster development of scintillating and non-scintillating resins with reduced time and economic investment.

CRediT authorship contribution statement

I. Giménez: Writing – review & editing, Writing – original draft, Investigation, Formal analysis, Data curation, Conceptualization. **G. Sormani:** Writing – review & editing, Writing – original draft, Visualization, Validation, Supervision, Methodology, Investigation, Formal analysis, Data curation, Conceptualization. **A. Rodríguez:** Writing – review & editing, Supervision, Project administration, Methodology, Investigation, Conceptualization. **A. Hassanali:** Writing – review & editing, Validation, Supervision, Resources, Project administration, Methodology, Funding acquisition, Conceptualization. **H. Bagán:** Writing – review & editing, Supervision, Funding acquisition. **A. Tarancón:** Writing – review & editing, Supervision, Project administration, Funding acquisition.

Declaration of competing interest

The authors declare that they have no known competing financial interests or personal relationships that could have appeared to influence the work reported in this paper.

Acknowledgements

This work was carried out in a Generalitat de Catalunya Research Group (2021 SGR 01342) and has received funding from the Ministerio de Ciencia, Innovación y Universidades (MICIU) de España proyecto PID2020-114551RB-I00 financiado por MICIU/AEI/10.13039/501100011033. I. Giménez thanks the Universitat de Barcelona for the PREDOCS-UB grant. A.H. acknowledges the funding received by the European Research Council (ERC) under the European Union's Horizon 2020 research and innovation programme (grant number 101043272 - HyBOP). Views and opinions expressed are however those of the author (s) only and do not necessarily reflect those of the European Union or the European Research Council Executive Agency. Neither the European Union nor the granting authority can be held responsible for them.

Appendix A. Supplementary data

Supplementary data to this article can be found online at https://doi.org/10.1016/j.aca.2025.344047.

Data availability

Data will be made available on request.

References

[1] X. Hou, Liquid scintillation counting for determination of radionuclides in environmental and nuclear application, J. Radioanal. Nucl. Chem. 318 (2018) 1597–1628, https://doi.org/10.1007/s10967-018-6258-6.
[2] X. Hou, X. Dai, Environmental liquid scintillation analysis, in: Handbook of Radioactivity Analysis: Volume 2: Radioanalytical Applications, Elsevier, 2020, pp. 41–136, https://doi.org/10.1016/B978-0-12-814395-7.00002-7.
[3] S.L. Maxwell, B.K. Culligan, Rapid separation method for emergency water and urine samples, J. Radioanal. Nucl. Chem. 279 (2009) 901–907, https://doi.org/10.1007/s10967-008-7387-0.
[4] N.A. Bezhin, I.I. Dovhyi, S.V. Kapranov, N.I. Bobko, V.V. Milyutin, V.O. Kaptakov, E.A. Kozlitin, I.G. Tananaev, Separation of radiostrontium from seawater using various types of sorbents, J. Radioanal. Nucl. Chem. 328 (2021) 1199–1209, https://doi.org/10.1007/s10967-021-07718-8.
[5] E.P. Horwitz, R. Chiarizia, M.L. Dietz, H. Diamond, D.M. Nelson, Separation and preconcentration of actinides from acidic media by extraction chromatography, Anal. Chim. Acta 281 (1993) 361–372, https://doi.org/10.1016/0003-2670(93)85194-O.

[6] D.L. Stoliker, N. Kaviani, D.B. Kent, J.A. Davis, Evaluating ion exchange resin efficiency and oxidative capacity for the separation of uranium(IV) and uranium (VI), Geochem. Trans. 14 (2013), https://doi.org/10.1186/1467-4866-14-1.
[7] B. Liu, K. Shi, G. Ye, Z. Guo, W. Wu, Method development for plutonium analysis in environmental water samples using TEVA microextraction chromatography separation and low background liquid scintillation counter measurement, Microchem. J. 124 (2016) 824–830, https://doi.org/10.1016/j.microc.2015.10.007.
[8] Ž. Grahek, N.Z. Zečević, S.L. Lulić, Possibility of rapid determination of low-level 90 Sr activity by combination of extraction chromatography separation and cherenkov counting. https://doi.org/10.1016/S0003-2670(99)00469-9, 1999.
[9] I. Giménez, H. Bagán, A. Tarancón, Fast analysis of gross alpha with a new plastic scintillation resin, Anal. Chim. Acta 1248 (2023) 340905, https://doi.org/10.1016/j.aca.2023.340905.
[10] H. Bagán, A. Tarancón, G. Rauret, J.F. García, Radiostrontium separation and measurement in a single step using plastic scintillators plus selective extractants. Application to aqueous sample analysis, Anal. Chim. Acta 686 (2011) 50–56, https://doi.org/10.1016/j.aca.2010.11.048.
[11] L.M. Santiago, H. Bagán, A. Tarancón, J.F. Garcia, Synthesis of plastic scintillation microspheres: evaluation of scintillators, Nucl. Instrum. Methods Phys. Res. 698 (2013) 106–116, https://doi.org/10.1016/j.nima.2012.09.028.
[12] E. Philip Horwitz, R. Chiarizia, M.L. Dietz, A novel strontium-selective extraction chromatographic resin, Solvent Extr. Ion Exch. 10 (1992) 313–336, https://doi.org/10.1080/07366299208918107.
[13] R. Chiarizia, A.W. Herlinger, E.P. Horwitz, Metal extraction by alkyl substituted diphosphonic acids. Part 3. P,P'-DI(2-ethylhexyl) ethanediphosphonic acid solvent extraction study, Solvent Extr. Ion Exch. 15 (1997) 417–431, https://doi.org/10.1080/07366299708934486.
[14] R. Chiarizia, E.P. Horwitz, P.G. Rickert, A.W. Herlinger, Acids. Part 1. P,P"-Di(2-Ethylhexyl) Methanediphosphonic Acid, vol. 14, Solvent Extraction and Ion Exchange, 1996, pp. 773–792, https://doi.org/10.1080/07366299608918368.
[15] E.P. Horwitz, R. Chiarizia, M.L. Dietz, DIPEX: a new extraction chromatographic material for the separation and preconcentration of actinides from aqueous solution, React. Funct. Polym. 33 (1997) 25–36, https://doi.org/10.1016/S1381-5148(97)00013-8.
[16] I. Giménez, H. Bagán, A. Tarancón, J.F. García, PSresin for the analysis of alpha-emitting radionuclides: comparison of diphosphonic acid-based extractants, Appl. Radiat. Isot. 178 (2021) 109969, https://doi.org/10.1016/J.APRADISO.2021.109969.
[17] Triskem international, Product Sheet, SR Resin, vol. 33, 2015, pp. 3–6.
[18] M. Sáez-Muñoz, H. Bagán, A. Tarancón, J.F. García, J. Ortiz, S. Martorell, Rapid method for radiostrontium determination in milk in emergency situations using PS resin, J. Radioanal. Nucl. Chem. 315 (2018) 543–555, https://doi.org/10.1007/s10967-017-5682-3.
[19] I. Giménez, J. Rotger, E. Apellániz, H. Bagán, J. Tent, A. Rigol, A. Tarancón, A new method based on selective fluorescent polymers (PSresin) for the analysis of 90Sr in presence of 210Pb in environmental samples, Appl. Radiat. Isot. 199 (2023), https://doi.org/10.1016/j.apradiso.2023.110879.
[20] I.A. Bagatur, Ay Freidzon, M. Al, E. Baerends, J. Howard, L. Kuz, DFT calculations on the electronic and geometrical structure of 18-crown-6 complexes with Ag+, Hg2+, Ag0, Hg+, Hg0, AgNO3, and HgX2 (X= Cl, Br, and I), J. Mol. Struct.: THEOCHEM 588 (1–3) (2002) 55–69, https://doi.org/10.1016/S0166-1280(02)00119-7.
[21] S. Hadisaputra, H. Dwi Pranowo, R. Extraction, Of strontium (II) by crown ether: insights from density functional calculation, Indones. J. Chem. 12 (3) (2012) 207–216, https://doi.org/10.22146/ijc.21332.
[22] E.D. Glendening, D. Feller, An Ab initio investigation of the structure and alkaline Earth divalent cation selectivity of 18-Crown-6. https://doi.org/10.1021/ja960469n, 1996.
[23] B. Martínez-Haya, P. Hurtado, A.R. Hortal, S. Hamad, J.D. Steill, J. Oomens, Emergence of symmetry and chirality in crown ether complexes with alkali metal cations, J. Phys. Chem. A 114 (2010) 7048–7054, https://doi.org/10.1021/jp103389g.
[24] S.V. Nesterov, Crown ethers in radiochemistry. Advances and prospects, Russ. Chem. Rev. 69 (2000) 769–782, https://doi.org/10.1070/RC2000v069n09ABEH000586.
[25] C.J. Pedersen, Cyclic polyethers and their complexes with metal salts, J. Am. Chem. Soc. 89 (1967) 2495–2496, https://doi.org/10.1021/ja00986a052.
[26] Z. Jing, G. Wang, Y. Zhou, D. Pang, F. Zhu, H. Liu, Selectivity of 18-crown-6 ether to alkali ions by density functional theory and molecular dynamics simulation, J. Mol. Liq. 311 (2020), https://doi.org/10.1016/j.molliq.2020.113305.
[27] Y. Liu, A.T. Ta, K.C. Park, S. Hu, N.B. Shustova, S.R. Phillpot, Binding of radionuclides and surrogate to 18-crown-6 ether by density functional theory, Microporous Mesoporous Mater. 364 (2024), https://doi.org/10.1016/j.micromeso.2023.112882.
[28] H. Arabzadeh, B. Walker, J.M. Sperling, O. Acevedo, P. Ren, W. Yang, T. E. Albrecht-Schönzart, Molecular dynamics and free energy calculations of Dicyclohexano-18-crown-6 diastereoisomers with Sm2+, Eu2+, Dy2+, Yb2+, Cf2+, and three halide salts in tetrahydrofuran and acetonitrile using the AMOEBA force field, J. Phys. Chem. B 126 (2022) 10721–10731, https://doi.org/10.1021/acs.jpcb.2c04613.
[29] P. Vayssière, G. Wipff, Importance of counter-ions in alkali and alkaline-earth cation extraction by 18-crown-6: molecular dynamics studies at the water/sc-CO2 interface, Phys. Chem. Chem. Phys. 5 (2003) 2842–2850, https://doi.org/10.1039/b303058j.
[30] I.A. Kuz'mina, M.A. Volkova, K.I. Kuz'mina, T.R. Usacheva, V.A. Sharnin, G. Arena, Effect of reactant solvation on the stability of complexes of silver(I) with 18-crown-6 in ethanol-dimethyl sulfoxide mixtures, J. Mol. Liq. 276 (2019) 78–82, https://doi.org/10.1016/j.molliq.2018.11.097.
[31] K. Horn, H. Yamada, T. Yamabe, Theoretical study on the nature of the interaction between crown ethers and alkali cations : relation of interaction energy and ion selectivity, Tetrahedron 39 (1983) 67–73, https://doi.org/10.1016/S0040-4020(01)97631-8.
[32] G.W. Gokel, W.M. Leevy, M.E. Weber, Crown ethers: sensors for ions and molecular scaffolds for materials and biological models, Chem. Rev. 104 (2004) 2723–2750, https://doi.org/10.1021/cr020080k.
[33] P. Li, L.F. Song, K.M. Merz, Parameterization of highly charged metal ions using the 12-6-4 LJ-type nonbonded model in explicit water, J. Phys. Chem. B 119 (2015) 883–895, https://doi.org/10.1021/jp505875v.
[34] D. Trapl, V. Spiwok, Analysis of the Results of Metadynamics Simulations by Metadynminer and metadynminer3d, 2020. ArXiv Preprint ArXiv:2009.02241.
[35] J.W. Steed, J.L. Atwood, Anion binding, in: Supramolecular Chemistry, second ed., John Wiley & Sons, 2009, pp. 223–284.
[36] G.W. Gokel, L. Echegoyen, M.S. Kim, E.M. Eyring, S. Petrucci, Influence of solvent, anion and presence of nitrogen in the ring structure on the mechanism of complexation of alkali metal cations with crown ethers, Biophys. Chem. 26 (1987) 225–233, https://doi.org/10.1016/0301-4622(87)80025-X.
[37] S. Han, Anionic effects on the structure and dynamics of water in superconcentrated aqueous electrolytes, RSC Adv. 9 (2019) 609–619, https://doi.org/10.1039/c8ra09589b.
[38] B.G. Cox, P. Firman, H. Schneider, Thermodynamic and kinetic studies on complex formation of alkaline Earth metal ions with diaza-crown ethers in methanol, Inorg. Chim. Acta. 69 (1983) 161–166, https://doi.org/10.1016/S0020-1693(00)83567-7.
[39] O.W. Wheeler, D.R. Carl, P.B. Armentrout, Second–shell thermochemistry for hydration of strontium dications as determined by threshold collision-induced dissociation and computations, Int. J. Mass Spectrom. 429 (2018) 76–89, https://doi.org/10.1016/j.ijms.2017.05.009.
[40] I.V. Pletnev, in: K. Gloe (Ed.), Macrocyclic Chemistry: Current Trends and Future Perspectives, Springer, Dordrecht, 2006, 2005, 450 pp., ISBN-10 1-4020-3364-8.
[41] K.M. Fromm, Coordination polymer networks with s-block metal ions, Coord. Chem. Rev. 252 (2008) 856–885, https://doi.org/10.1016/j.ccr.2007.10.032.
[42] C. Lapouge, J.P. Cornard, Theoretical study of the Pb(II)-catechol system in dilute aqueous solution: complex structure and metal coordination sphere determination, J. Mol. Struct. 969 (2010) 88–96, https://doi.org/10.1016/j.molstruc.2010.01.047.
[43] W. Zhao, W. Tan, X. Feng, F. Liu, Y. Xie, Z. Xie, XAFS studies on surface coordination of Pb2+ on birnessites with different average oxidation states, Colloids Surf. A Physicochem. Eng. Asp. 379 (2011) 86–92, https://doi.org/10.1016/j.colsurfa.2010.11.040.
[44] R.L. Davidovich, V. Stavila, D.V. Marinin, E.I. Voit, K.H. Whitmire, Stereochemistry of lead(II) complexes with oxygen donor ligands, Coord. Chem. Rev. 253 (2009) 1316–1352, https://doi.org/10.1016/j.ccr.2008.09.003.
[45] I. Persson, K. Lyczko, D. Lundberg, L. Eriksson, A. Pjaczek, Coordination chemistry study of hydrated and solvated lead(II) ions in solution and solid state, Inorg. Chem. 50 (2011) 1058–1072, https://doi.org/10.1021/ic1017714.
[46] K.W. Whitten, R.E. Davis, L. Peck, G.G. Stanley, *Chemistry*. Cengage Learning, 10 edition, 2013. ISBN 9781133610663/1133610668.
[47] Y. Hanifehpour, B. Mirtamizdoust, B. Khomami, S.W. Joo, Effects of halogen bonding in chemical activity of Lead(II) electron pair: sonochemical synthesis, structural studies, and thermal analysis of novel Lead(II) nano coordination polymer, Z. Anorg. Allg. Chem. 641 (2015) 2466–2472, https://doi.org/10.1002/zaac.201500250.
[48] T. Bala, B.L.V. Prasad, M. Sastry, M.U. Kahaly, U.V. Waghmare, Interaction of different metal ions with carboxylic acid group: a quantitative study, J. Phys. Chem. A 111 (2007) 6183–6190, https://doi.org/10.1021/jp067906x.

Supplementary Material

Design of radionuclide separations based on MD simulations

Giménez, I.[1*]; Sormani.G [2], Rodríguez. A [3], Hassanali. A [2], Bagán, H.[1] Tarancón, A.[1,4,5]

[1]Departament d'Enginyeria química i química analítica, Universitat de Barcelona, Marti i Franqués, 1-11, ES-08028, Barcelona, Spain.

[2] The "Abdus Salam" International Centre for Theoretical Physics, I-34151 Trieste, Italy

[3] Dipartimento di Matematica e Geoscienze, University of Trieste, 34127 Trieste, Italy

[4]Serra-Húnter Programme, Generalitat de Catalunya, Barcelona, Spain.

[5]Institut de Recerca de l'Aigua, Universitat de Barcelona

This file includes:

Section 1: Unbiased simulation Sr^{2+}-crown ether-nitrates system Page 2

Fig. S1. Temporal evolution of the distance between the

center of masses (COM) of the crown ether and strontium along 400ns Page 2

Section 2: Computational methods & experimental section Page 3

1.Computational methods Page 3

1.1. Free energy calculation Page 4

1.2. Entropy evaluation Page 5

2. Experimental section Page 5

2.1. Reagents and equipment's Page 5

2.2. Crown ether immobilization Page 6

2.3. Batch studies Page 6

2.4. Data treatment Page 7

2.5. References Page 7

Section 3: Force field parameters Page 9

Section 1. Unbiased simulation Sr^{2+}-crown ether-nitrates system

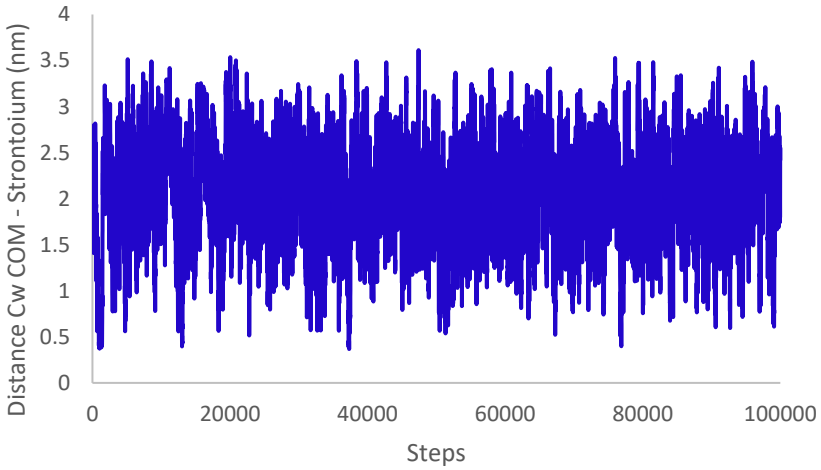

Fig. S1 Temporal evolution of the distance between the center of masses (COM) of the crown ether and strontium along 400ns

Section 2. COMPUTATIONAL METHODS & EXPERIMENTAL SECTION

1. Computational methods

Initial structures files for crown ether molecules and anions are obtained from the Automated Topology Builder (ATB) repository [1]. The Generalized Amber Force Field (GAFF) [2] for organic molecules is used to construct interaction potentials for 18-crown-6 and anion molecules [3] through the Antechamber package. The charges are calculated using the AM1-BCC charge model [4]. For Pb^{2+} and Sr^{2+} a potential specifically developed for transition metals is used [5]. In detail, Mertz and co-workers have shown in Ref. [5] that in order to obtain both accurate structural and thermodynamic properties associated with the binding of transition metal ions to proteins, classical force fields can be corrected via the inclusion of an extra attractive term ($\propto 1\frac{1}{r^4}$) which mimics charge-induced dipole interactions, leading to the nonbonded interaction potential shown in Eq.1.

$$U_{ij} = \frac{e^2 Q_i Q_j}{r_{ij}} - \frac{c_4^{ij}}{r_{ij}^4} + \frac{c_{12}^{ij}}{r_{ij}^{12}} - \frac{c_6^{ij}}{r_{ij}^6} \quad \text{(Eq.1)}$$

All MD simulations are run using the Amber2023 package. The metal–18-crown-6 complexes is placed in a cubic box containing around 2500 SPC/E water molecules [6]. This water model is rigid body and non-dissociable, therefore speciation events for example between strontium or lead and water ionic products coming from hydrolysis are not considered. Two of the studied anions are then added in each simulation. For all systems, an equilibration procedure is conducted before moving to production runs. First, a minimization step is performed using the steepest descent algorithm [7], then the temperature is gradually brought from 0 to 300 K along a NVT simulation of 20 ps, and finally, the density is equilibrated through a simulation in the NPT ensemble for 2 ns using a Berendsen barostat [8] fixed at 1 bar. This equilibration phase is followed by a 400 ns simulation in the NVT ensemble at a temperature of 300 K. The box sizes along the x, y, and z are 46.6, 47.7, and 48.09 Å, respectively. In all MD simulations, the time step is set to 2 fs and the temperature is controlled using a BUSSI thermostat [9] with a time constant of γ = 2 ps^{-1}. A cutoff of 11 Å is used for the nonbonded interactions. Long-range corrections to the Van der Waals are included. The particle mesh Ewald (PME) [10] is used to treat the long-range part of the Coulomb interactions.

Metadynamics simulations [11] are used to improve the state sampling of the system. Metadynamics simulations are run with the PLUMED plugin [12]. Two collective variables (CVs) are studied, the distance between the metal and the center of masses (COM) of the crown ether

and the coordination between the anions and the metal. The Free Energy Profile (FES) as a function of these two CVs is thus obtained. Gaussian hills with a height of 1.2 Kj · mol $^{-1}$ and a width of 0.1 for each collective variable are deposited every 500 simulation steps. Well-tempered metadynamics is employed with a bias factor of 10. The simulation is performed over 2 µs. An upper wall, with a force constant of 1000 Kj·mol^{-1}, is applied to the distance collective variable to prevent it from exceeding 2 nm. Data are treated in Rstudio using metadynminer and metadynminer3d libraries [13] to obtain the free energy landscapes, and reweighing to obtain the statistical error of the simulation using average block analysis.

1.1. Free energy calculation

For the free energy calculation, the packages metadynminer and metadynminer3d were used. At the end of simulation, the free energy surface can be estimated as a negative imprint of added metadynamics bias potential (Eq.2):

$$G(s) = -kT \log(P(s)) = -V(s) \qquad \text{(Eq.2)}$$

The vast majority of metadynamics applications use the well-tempered metadynamics algorithm for better convergence towards an accurate free energy surface prediction.
The packages metadynminer and metadynminer3d uses the Hills file generated by Plumed packages (filename HILLS) by loading it to RStudio by using the function “read.hills”:

```
hillsfile <- read.hills("HILLS.txt", per=c(FALSE, FALSE))
```

The parameter per indicates periodicity of the collective variable, which is not the case in this study.
Once HILLS file is loaded the sampling of the simulation is checked by plotting the hills with the function “plotheights”:

```
plotheights(hillsfile)
```

The estimation of the free energy is performed by the sum of negative values of all hills by function “fes”:

```
fesurface <- fes(hillsfile)
```

In well-tempered metadynamics, PLUMED automatically prescales the hills files by (ΔT+T)/ΔT when they are printed, eliminating the need for additional scaling in metadynminer. The "`fes`" function in metadynminer reconstructs the free energy surface using the Bias Sum algorithm from Hošek and Spiwok[14]. This method is highly efficient, as it avoids recalculating the Gaussian function for each individual hill. Instead, it utilizes a precomputed Gaussian hill that is dynamically repositioned at each hill center, significantly speeding up the process.

1.2. Entropy evaluation

Entropy was derived from the Helmoth Free energy equation (Eq.3):

$$\Delta F = \Delta U - T\,\Delta S \qquad \text{(Eq.3)}$$

Where,

ΔF = Helmholtz free energy, measured in joules, J.

ΔU = System's internal energy, measured in Joules.

T= Absolute temperature in kelvin

ΔS= System's entropy in joules per Kelvin.

The system internal energy was computed in each system using the PLUMED plugin.

2. Experimental section

2.1. Reagents and equipment's

All the reagents used were of analytical grade. 18-crown-6 was supplied by Fluorochem LTD (Glossop SK13 1QH, UK). Amberlite XAD-4 was supplied from thermo scientific (Waltham, Massachusetts, USA). Nitric acid 69%, hydrochloric acid 37%, formic acid, acetic acid, perchloric acid, methanol and potassium thiocyanate were supplied by Merck (Darmstadt, Germany). 10000 $mg \cdot L^{-1}$ strontium and lead standards were supplied by inorganic ventures (Christiansburg, USA). All solutions have been prepared using double deionized water.

The analysis of stable isotopes was performed using an OPTIMA 8300 ICP-OES detector (PerkinElmer, Waltham, USA) and an ELAN-6000 ICP-MS detector (PerkinElmer, Waltham, USA) from the Scientific and Technological Centres of the University of Barcelona (CCiTUB).

2.2. Crown ether immobilization

Amberlite XAD-4 was used as inert support. Firstly, the polymer was treated to eliminate stabilizers used for its storage. This treatment involves washing the polymer several times with large volumes of water until pH 7 in the rinsing solutions is reached. Subsequently, the polymer is dried overnight at 40°C and then subjected to a few additional rinses with methanol, until the organic solution becomes colourless. Finally, the polymer is dried overnight at 40°C.

The resin was prepared in a ratio of 60:40 (inert support: crown ether). The crown ether was dissolved in a predetermined quantity of methanol with moderate heating. Once fully dissolved, it was mixed with the pre-treated polymer in a round-bottom flask containing 200 ml of methanol. The mixture was left stirring for 45 minutes without applying heat. Following this, methanol was slowly evaporated over one hour at 20 inHg and 40°C using a rotary evaporator. After the evaporation period, 10 to 20 ml of methanol were added and stirred for 5 minutes. Subsequently, the organic solvent was evaporated in the rotary evaporator until complete dryness under the same conditions. Once dryness was achieved, the pressure was increased to 30 inHg.

2.3. Batch studies

The affinity of each metal (Sr^{2+} or Pb^{2+}) with the crown ether was assessed through batch experiments. All experiments were conducted using enough resin to ensure 0.15 mmol of crown ether and 0.045 mmol of metal in 5 ml of nitric acid, hydrochloric acid, perchloric acid, acetic acid, formic acid or potassium thiocyanate at concentrations of 6 M. The mixture was then stirred in an end-over-end shaker for 24 hours. This process ensures sufficient contact time between the resin and the target element in the working medium to facilitate interaction. After the allotted time, the solution was filtered using a 10 ml syringe and a 0.45 µm disk filter. The filtered solution was measured by ICP-OES.

Non-specific retention studies were performed in order to ensure that the retention observed was due to the resin and not due to the plastic of the tubes. In these studies, the procedure followed was the same but without addition of resin.

2.4. Data treatment

The weight distribution ratio, D_W was calculated from the batch experiment (Eq.4).

$$D_w = \frac{A_0 - A_S}{A_S} \cdot \frac{mL}{g} \quad \text{(Eq.4)}$$

Where A_0-A_s is the amount of cation sorbed on a known weight of resin (mg/g), and A_s is the amount of cation remaining in the solution (mg/ml).

2.5. References

[1] A.K. Malde, L. Zuo, M. Breeze, M. Stroet, D. Poger, P.C. Nair, C. Oostenbrink, A.E. Mark, An Automated force field Topology Builder (ATB) and repository: Version 1.0, J Chem Theory Comput 7 (2011) 4026–4037. https://doi.org/10.1021/ct200196m.

[2] J. Wang, R.M. Wolf, J.W. Caldwell, P.A. Kollman, D.A. Case, Development and testing of a general Amber force field, J Comput Chem 25 (2004) 1157–1174. https://doi.org/10.1002/jcc.20035.

[3] J. Wang, W. Wang, P.A. Kollman, D.A. Case, Automatic atom type and bond type perception in molecular mechanical calculations, J Mol Graph Model 25 (2006) 247–260. https://doi.org/10.1016/j.jmgm.2005.12.005.

[4] A. Jakalian, D.B. Jack, C.I. Bayly, Fast, efficient generation of high-quality atomic charges. AM1-BCC model: II. Parameterization and validation, J Comput Chem 23 (2002) 1623–1641. https://doi.org/10.1002/jcc.10128.

[5] P. Li, L.F. Song, K.M. Merz, Parameterization of highly charged metal ions using the 12-6-4 LJ-type nonbonded model in explicit water, Journal of Physical Chemistry B 119 (2015) 883–895. https://doi.org/10.1021/jp505875v.

[6] C.D. Berweger, W.F. Van Gunsteren, F. Mijller-Plathe, Force field parametrization by weak coupling. Re-engineering SPC water, 1995.

[7] B. Widrow, J. McCool, A comparison of adaptive algorithms based on the methods of steepest descent and random search, IEEE Trans Antennas Propag 24 (1976) 615–637.

[8] H.J.C. Berendsen, J.P.M. van Postma, W.F. Van Gunsteren, A. DiNola, J.R. Haak, Molecular dynamics with coupling to an external bath, J Chem Phys 81 (1984) 3684–3690.

[9] G. Bussi, D. Donadio, M. Parrinello, Canonical sampling through velocity rescaling, J Chem Phys 126 (2007).

[10] T. Darden, D. York, L. Pedersen, Particle mesh Ewald: An N· log (N) method for Ewald sums in large systems, J Chem Phys 98 (1993) 10089–10092.

[11] D. Ray, M. Parrinello, Kinetics from Metadynamics: Principles, Applications, and Outlook, J Chem Theory Comput 19 (2023) 5649–5670. https://doi.org/10.1021/acs.jctc.3c00660.

[12] Promoting transparency and reproducibility in enhanced molecular simulations, Nat Methods 16 (2019) 670–673.

[13] D. Trapl, V. Spiwok, Analysis of the Results of Metadynamics Simulations by metadynminer and metadynminer3d, ArXiv Preprint ArXiv:2009.02241 (2020).

[14] P. Hošek, V. Spiwok, Metadyn View: Fast web-based viewer of free energy surfaces calculated by metadynamics, Comput Phys Commun 198 (2016) 222–229. https://doi.org/10.1016/j.cpc.2015.08.037.

Section 3: Force field parameters

Li/Merz ion parameters of divalent to tetravalent ions for SPC/E water model (12-6-4 set)

MASS

Be2+ 9.01

Cu2+ 63.55

Ni2+ 58.69

Zn2+ 65.4

Co2+ 58.93

Cr2+ 52.00

Fe2+ 55.85

Mg2+ 24.305

V2+ 50.94

Mn2+ 54.94

Hg2+ 200.59

Cd2+ 112.41

Ca2+ 40.08

Sn2+ 118.71

Sr2+ 87.62

Ba2+ 137.33

Al3+ 26.98

Fe3+ 55.85

Cr3+ 52.00

In3+ 114.82

Tl3+ 204.38

Y3+ 88.91

La3+ 138.91

Ce3+ 140.12

Pr3+ 140.91

Nd3+ 144.24

Sm3+ 150.36

Eu3+ 151.96

Gd3+ 157.25

Tb3+ 158.93

Dy3+ 162.5

Er3+ 167.26

Tm3+ 168.93

Lu3+ 174.97

Hf4+ 178.49

Zr4+ 91.22

Ce4+ 140.12

U4+ 238.03

Pu4+ 244.06

Th4+ 232.04

NONBON

Be2+ 1.205 0.00120058   12-6-4 set for SPC\E water from Li and Merz, JCTC, 2014, 10, 289

Cu2+ 1.482 0.03364841   12-6-4 set for SPC\E water from Li and Merz, JCTC, 2014, 10, 289

Ni2+ 1.424 0.01995146   12-6-4 set for SPC\E water from Li and Merz, JCTC, 2014, 10, 289

Zn2+ 1.454 0.02639002 12-6-4 set for SPC\E water from Li and Merz, JCTC, 2014, 10, 289

Co2+ 1.457 0.02710805 12-6-4 set for SPC\E water from Li and Merz, JCTC, 2014, 10, 289

Cr2+ 1.424 0.01995146 12-6-4 set for SPC\E water from Li and Merz, JCTC, 2014, 10, 289

Fe2+ 1.450 0.02545423 12-6-4 set for SPC\E water from Li and Merz, JCTC, 2014, 10, 289

Mg2+ 1.429 0.02093385 12-6-4 set for SPC\E water from Li and Merz, JCTC, 2014, 10, 289

V2+ 1.502 0.03962711 12-6-4 set for SPC\E water from Li and Merz, JCTC, 2014, 10, 289

Mn2+ 1.495 0.03745682 12-6-4 set for SPC\E water from Li and Merz, JCTC, 2014, 10, 289

Hg2+ 1.641 0.10128575 12-6-4 set for SPC\E water from Li and Merz, JCTC, 2014, 10, 289

Cd2+ 1.541 0.05330850 12-6-4 set for SPC\E water from Li and Merz, JCTC, 2014, 10, 289

Ca2+ 1.634 0.09731901 12-6-4 set for SPC\E water from Li and Merz, JCTC, 2014, 10, 289

Sn2+ 1.778 0.19549490 12-6-4 set for SPC\E water from Li and Merz, JCTC, 2014, 10, 289

Sr2+ 1.778 0.19549490 12-6-4 set for SPC\E water from Li and Merz, JCTC, 2014, 10, 289

Ba2+ 1.937 0.33223312 12-6-4 set for SPC\E water from Li and Merz, JCTC, 2014, 10, 289

Al3+ 1.375 0.01205473 12-6-4 set for SPC\E water from Li et al., JPCB, 2015, 119, 883

Fe3+ 1.450 0.02545423 12-6-4 set for SPC\E water from Li et al., JPCB, 2015, 119, 883

Cr3+ 1.414 0.01809021 12-6-4 set for SPC\E water from Li et al., JPCB, 2015, 119, 883

In3+ 1.487 0.03507938 12-6-4 set for SPC\E water from Li et al., JPCB, 2015, 119, 883

Tl3+ 1.569 0.06484979 12-6-4 set for SPC\E water from Li et al., JPCB, 2015, 119, 883

Y3+ 1.624 0.09180886 12-6-4 set for SPC\E water from Li et al., JPCB, 2015, 119, 883

La3+ 1.763 0.18380968 12-6-4 set for SPC\E water from Li et al., JPCB, 2015, 119, 883

Ce3+ 1.786 0.20184160 12-6-4 set for SPC\E water from Li et al., JPCB, 2015, 119, 883

Pr3+ 1.782 0.19865859 12-6-4 set for SPC\E water from Li et al., JPCB, 2015, 119, 883

Nd3+ 1.735 0.16280564 12-6-4 set for SPC\E water from Li et al., JPCB, 2015, 119, 883

Sm3+ 1.703 0.14021803 12-6-4 set for SPC\E water from Li et al., JPCB, 2015, 119, 883

Eu3+ 1.721 0.15272873 12-6-4 set for SPC\E water from Li et al., JPCB, 2015, 119, 883

Gd3+ 1.646 0.10417397 12-6-4 set for SPC\E water from Li et al., JPCB, 2015, 119, 883

Tb3+ 1.666 0.11617738 12-6-4 set for SPC\E water from Li et al., JPCB, 2015, 119, 883

Dy3+ 1.637 0.09900804 12-6-4 set for SPC\E water from Li et al., JPCB, 2015, 119, 883

Er3+ 1.629 0.09454081 12-6-4 set for SPC\E water from Li et al., JPCB, 2015, 119, 883

Tm3+ 1.633 0.09675968 12-6-4 set for SPC\E water from Li et al., JPCB, 2015, 119, 883

Lu3+ 1.620 0.08965674 12-6-4 set for SPC\E water from Li et al., JPCB, 2015, 119, 883

Hf4+ 1.592 0.07543075 12-6-4 set for SPC\E water from Li et al., JPCB, 2015, 119, 883

Zr4+ 1.609 0.08389240 12-6-4 set for SPC\E water from Li et al., JPCB, 2015, 119, 883

Ce4+ 1.761 0.18227365 12-6-4 set for SPC\E water from Li et al., JPCB, 2015, 119, 883

U4+ 1.791 0.20584696 12-6-4 set for SPC\E water from Li et al., JPCB, 2015, 119, 883

Pu4+ 1.750 0.17392181 12-6-4 set for SPC\E water from Li et al., JPCB, 2015, 119, 883

Th4+ 1.773 0.19156806 12-6-4 set for SPC\E water from Li et al., JPCB, 2015, 119, 883

Li/Merz ion parameters of divalent to tetravalent ions for SPC/E water model (12-6 HFE set)

MASS

Be2+ 9.01

Cu2+ 63.55

Ni2+ 58.69

Pt2+ 195.08

Zn2+ 65.4

Co2+ 58.93

Pd2+ 106.42

Ag2+ 107.87

Cr2+ 52.00

Fe2+ 55.85

Mg2+ 24.305

V2+ 50.94

Mn2+ 54.94

Hg2+ 200.59

Cd2+ 112.41

Yb2+ 173.05

Ca2+ 40.08

Sn2+ 118.71

Pb2+ 207.2

Eu2+ 151.96

Sr2+ 87.62

Sm2+ 150.36

Ba2+ 137.33

Ra2+ 226.03

Al3+ 26.98

Fe3+ 55.85

Cr3+ 52.00

In3+ 114.82

Tl3+ 204.38

Y3+ 88.91

La3+ 138.91

Ce3+ 140.12

Pr3+ 140.91

Nd3+ 144.24

Sm3+ 150.36

Eu3+ 151.96

Gd3+ 157.25

Tb3+ 158.93

Dy3+ 162.5

Er3+ 167.26

Tm3+ 168.93

Lu3+ 174.97

Hf4+ 178.49

Zr4+ 91.22

Ce4+ 140.12

U4+ 238.03

Pu4+ 244.06

Th4+ 232.04

NONBON

Be2+ 0.915 0.00000105 HFE set for SPC\E water from Li et al., JCTC, 2013, 9, 2733

Cu2+ 1.149 0.00044254 HFE set for SPC\E water from Li et al., JCTC, 2013, 9, 2733

Ni2+ 1.166 0.00060803 HFE set for SPC\E water from Li et al., JCTC, 2013, 9, 2733

Pt2+ 1.176 0.00072849 HFE set for SPC\E water from Li et al., JCTC, 2013, 9, 2733

Zn2+ 1.178 0.00075490 HFE set for SPC\E water from Li et al., JCTC, 2013, 9, 2733

Co2+ 1.217 0.00146124 HFE set for SPC\E water from Li et al., JCTC, 2013, 9, 2733

Pd2+ 1.217 0.00146124 HFE set for SPC\E water from Li et al., JCTC, 2013, 9, 2733

Ag2+ 1.265 0.00303271 HFE set for SPC\E water from Li et al., JCTC, 2013, 9, 2733

Cr2+ 1.276 0.00354287 HFE set for SPC\E water from Li et al., JCTC, 2013, 9, 2733

Fe2+ 1.284 0.00395662 HFE set for SPC\E water from Li et al., JCTC, 2013, 9, 2733

Mg2+ 1.288 0.00417787 HFE set for SPC\E water from Li et al., JCTC, 2013, 9, 2733

V2+ 1.293 0.00446856 HFE set for SPC\E water from Li et al., JCTC, 2013, 9, 2733

Mn2+ 1.338 0.00789684 HFE set for SPC\E water from Li et al., JCTC, 2013, 9, 2733

Hg2+ 1.338 0.00789684 HFE set for SPC\E water from Li et al., JCTC, 2013, 9, 2733

Cd2+ 1.344 0.00848000 HFE set for SPC\E water from Li et al., JCTC, 2013, 9, 2733

Yb2+ 1.518 0.04490976 HFE set for SPC\E water from Li et al., JCTC, 2013, 9, 2733

Ca2+ 1.520 0.04560206 HFE set for SPC\E water from Li et al., JCTC, 2013, 9, 2733

Sn2+ 1.532 0.04990735 HFE set for SPC\E water from Li et al., JCTC, 2013, 9, 2733

Pb2+ 1.609 0.08389240 HFE set for SPC\E water from Li et al., JCTC, 2013, 9, 2733

Eu2+ 1.656 0.11008622 HFE set for SPC\E water from Li et al., JCTC, 2013, 9, 2733

Sr2+ 1.659 0.11189491 HFE set for SPC\E water from Li et al., JCTC, 2013, 9, 2733

Sm2+ 1.667 0.11679623 HFE set for SPC\E water from Li et al., JCTC, 2013, 9, 2733

Ba2+ 1.825 0.23380842 HFE set for SPC\E water from Li et al., JCTC, 2013, 9, 2733

Ra2+ 1.825 0.23380842 HFE set for SPC\E water from Li et al., JCTC, 2013, 9, 2733

Al3+ 0.991 0.00001107 HFE set for SPC\E water from Li et al., JPCB, 2015, 119, 883

Fe3+ 1.091 0.00013462 HFE set for SPC\E water from Li et al., JPCB, 2015, 119, 883

Cr3+ 1.196 0.00103208 HFE set for SPC\E water from Li et al., JPCB, 2015, 119, 883

In3+ 1.209 0.00128267 HFE set for SPC\E water from Li et al., JPCB, 2015, 119, 883

Tl3+ 1.213 0.00136949 HFE set for SPC\E water from Li et al., JPCB, 2015, 119, 883

Y3+ 1.459 0.02759452 HFE set for SPC\E water from Li et al., JPCB, 2015, 119, 883

La3+ 1.629 0.09454081 HFE set for SPC\E water from Li et al., JPCB, 2015, 119, 883

Ce3+ 1.597 0.07786298 HFE set for SPC\E water from Li et al., JPCB, 2015, 119, 883

Pr3+ 1.571 0.06573030 HFE set for SPC\E water from Li et al., JPCB, 2015, 119, 883

Nd3+ 1.551 0.05726270 HFE set for SPC\E water from Li et al., JPCB, 2015, 119, 883

Sm3+ 1.526 0.04772212 HFE set for SPC\E water from Li et al., JPCB, 2015, 119, 883

Eu3+ 1.507 0.04122946 HFE set for SPC\E water from Li et al., JPCB, 2015, 119, 883

Gd3+ 1.499 0.03868661 HFE set for SPC\E water from Li et al., JPCB, 2015, 119, 883

Tb3+ 1.485 0.03450196 HFE set for SPC\E water from Li et al., JPCB, 2015, 119, 883

Dy3+ 1.472 0.03091095 HFE set for SPC\E water from Li et al., JPCB, 2015, 119, 883

Er3+ 1.436 0.02236885 HFE set for SPC\E water from Li et al., JPCB, 2015, 119, 883

Tm3+ 1.426 0.02034021 HFE set for SPC\E water from Li et al., JPCB, 2015, 119, 883

Lu3+ 1.426 0.02034021 HFE set for SPC\E water from Li et al., JPCB, 2015, 119, 883

Hf4+ 1.098 0.00015685 HFE set for SPC\E water from Li et al., JPCB, 2015, 119, 883

Zr4+ 1.149 0.00044254 HFE set for SPC\E water from Li et al., JPCB, 2015, 119, 883

Ce4+ 1.360 0.01020237 HFE set for SPC\E water from Li et al., JPCB, 2015, 119, 883

U4+ 1.218 0.00148497 HFE set for SPC\E water from Li et al., JPCB, 2015, 119, 883

Pu4+ 1.281 0.00379705 HFE set for SPC\E water from Li et al., JPCB, 2015, 119, 883

Th4+ 1.468 0.02986171 HFE set for SPC\E water from Li et al., JPCB, 2015, 119, 883

SPC/E				
	***R*min/2 (Å)**	**ε (kcal/mol)**	**κ (Å–2)**	***C4***
Be2+	1.205	0.00120058	9.8	188.1
Cu2+	1.482	0.03364841	1.758	304.4
Ni2+	1.424	0.01995146	1.714	205.2
Zn2+	1.454	0.02639002	1.588	231.2
Co2+	1.457	0.02710805	1.41	209.2
Cr2+	1.424	0.01995146	1.096	131.2
Fe2+	1.45	0.02545423	1.095	155.4
Mg2+	1.429	0.02093385	0.987	122.2
V2+	1.502	0.03962711	1.06	206.6
Mn2+	1.495	0.03745682	0.828	154.9
Hg2+	1.641	0.10128575	0.751	300.2
Cd2+	1.541	0.0533085	0.819	198.8
Ca2+	1.634	0.09731901	0.23	89
Sn2+	1.778	0.1954949	0.286	201.1
Sr2+	1.778	0.1954949	0.137	96.3
Ba2+	1.937	0.33223312	0.072	85.8

P. Li and K.M. Merz, Jr. Taking into Account the Ion-Induced Dipole Interaction in the Nonbonded Model of Ions J. Chem. Theory Comput., 2014, 10, 289-297. Divalent cations for TIP3P, SPC/E, and TIP4PEW.

3.3. Discussion

3.3.1. Development of a new PSresin for alpha-emitting radionuclides

- Preliminary study

The development of a new PSresin for the analysis of alpha-emitting radionuclides started with the evaluation of three different extractants based on diphosphonic acid core structure (Fig 3.2). Among these extractants bis(2-ethylhexyl) methanediphosphonic acid is found, a compound utilized in actinide resin, which served as a reference for this work.

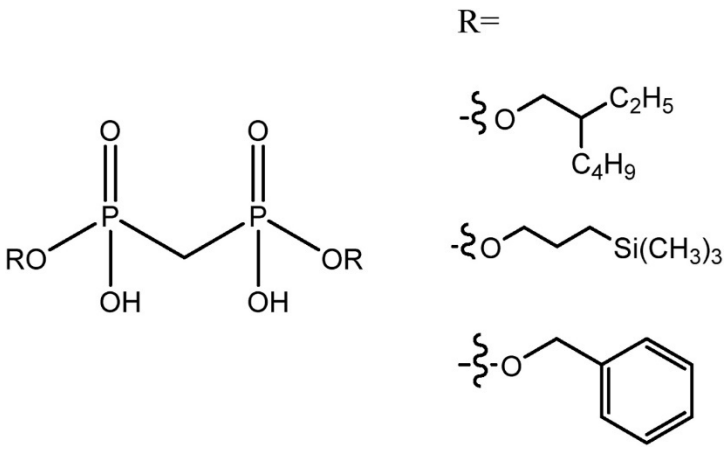

Fig 3.2 Core structure of the extractant studied and the different radicals

None of the selected extractants was commercially available, therefore, all three were synthesized in-house. The synthesis involved a standardized route: combining one equivalent of methanediphosphonic acid (MDPA) with two equivalents of the corresponding alcohol (benzylic alcohol, 3-(trimethylsilyl)-1-propanol, or 2-ethylhexanol). A coupling agent, dicyclohexyl carbodiimide (DCC), was then added dropwise to promote selective substitution. DCC was chosen for its steric effects, which favor the formation of the di-substituted product over the tetra-substituted one. Tetrahydrofuran (THF) served as the solvent in these reactions [20].

For PSresin development, each extractant was immobilized on PSms surface, in particular DIN-PSm, which integrates DIN within its structure to enhance alpha-beta discrimination by promoting triplet state population. The immobilization yielded three PSresin prototypes for alpha-emitters detection: EH-PSresin (R = 2-ethylhexyl),

BZ-PSresin (R = benzyl), and SI-PSresin (R = 3-(trimethylsilyl)-1-propyl), with a PSm-to-extractant ratio of 1:1/6, which is a common ratio optimized for PSm. Each prototype was then checked using scanning electron microscopy (SEM) to confirm proper and uniform extractant immobilization on the PSm surface (Fig 3.3).

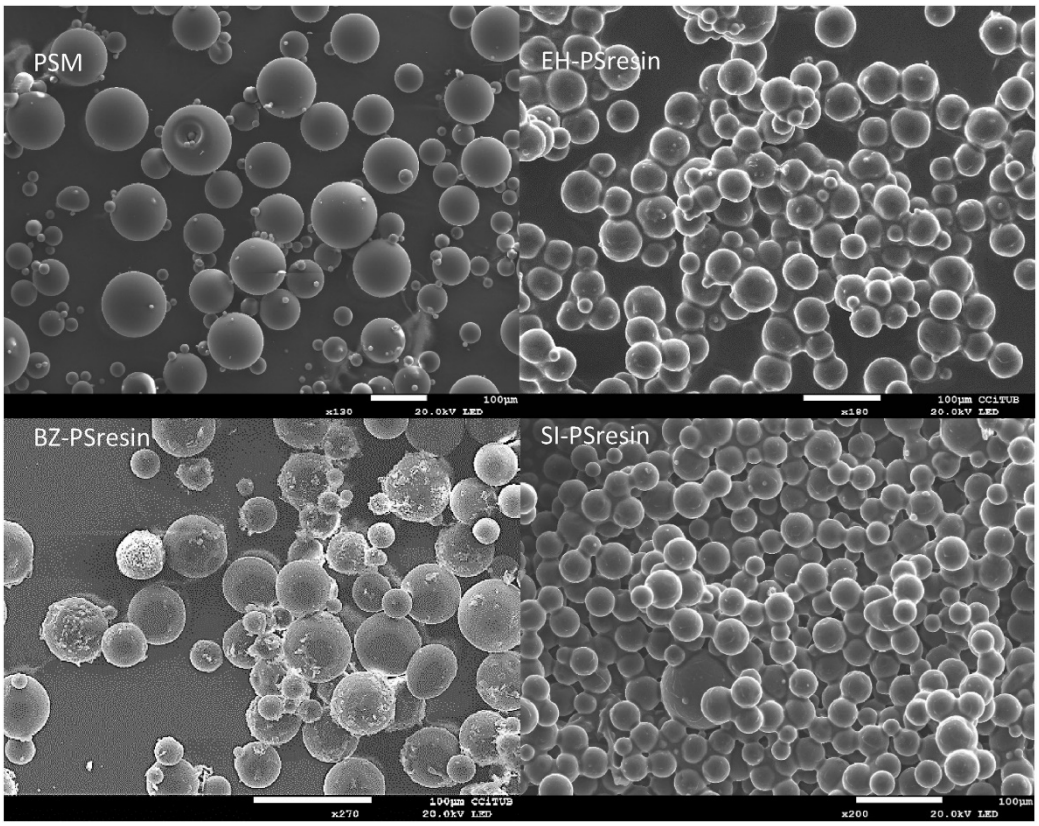

Fig 3.3 Secondary electron images for the different PSresins obtained using a scanning electron microscope. EH-PSresin (R = 2-ethylhexyl); BZ-PSresin (R = benzyl); SI-PSresin (R = 3-(trimethylsilyl)-1-propyl).

SEM images revealed that all three PSresin prototypes kept their spherical morphology with minimal agglomeration. Compared to the unmodified PSm surface, which appeared smooth, the PSresins exhibited distinct surface characteristics: EH-PSresin showed small folds, BZ-PSresin displayed scales, and SI-PSresin showed small crystals. These variations confirmed the presence of a surface layer of extractant.

Each PSresin was subsequently packed in an SPE cartridge for radiometric testing. The first analysis was conducted with ^{241}Am in a 0.5 M HCl medium. Americium was selected due to its stable trivalent state, which has a high affinity for diphosphonic acids, suggesting that retention and detection efficiencies for other alpha-emitting radionuclides would be comparable or lower. All three PSresin demonstrated high

detection efficiencies (~100 %). However, only EH-PSresin and SI-PSresin showed quantitative retention. BZ-PSresin achieved only a 50 % retention yield. This reduced retention is likely due to the steric hindrance imposed by the benzyl group, leading to the exclusion of BZ-PSresin as a viable candidate.

Further tests assessed the leaching stability and iron capacity of EH-PSresin and SI-PSresin. Given that both extractants are immobilized on DIN-PSm, high sample volumes may strip the extractant from the resin surface. However, neither PSresin had extractant leaching after passing 400 mL of 0.5 M HCl solution through the cartridges, confirming their stability for large-volume applications. Capacity tests showed comparable results for both resins, with iron capacities of 2 $mg \cdot g^{-1}$ and 1.9 $mg \cdot g^{-1}$ for EH-PSresin and SI-PSresin, respectively.

In additional tests the detection efficiency and retention for other alpha-emitting radionuclides, including ^{238}Pu, ^{nat}U, and ^{230Th} was measured. Detection efficiencies around 100% and quantitative retention for all confirmed consistent behaviour across both resins, regardless of the extractant radical. However, retention yields for ^{226}Ra and ^{210}Po, did not exceed 20 %, likely due to limitations in affinity within the chosen working medium.

The influence of the extractant radical on α/β discrimination was subsequently studied. ^{90}Y served as a pure beta-emitter as it was retained on the resin, while, ^{241}Am and ^{238}Pu were tested as alpha-emitters. Fig. 3.4 shows the α/β misclassification errors across different PSA values on the Quantulus detector. Both EH-PSresin and SI-PSresin had similar behaviour for beta discrimination. However, in alpha discrimination, while americium results were consistent between the two, misclassification for plutonium was slightly higher in EH-PSresin than SI-PSresin.

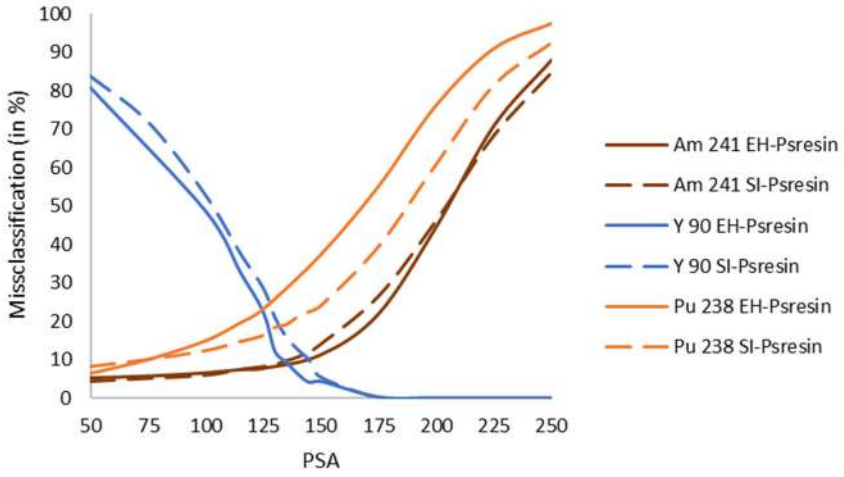

Fig 3.4 α/β missclassification at different PSA values with EH-PSresin (continuous line) and SI-PSresin (dashed line) for ^{241}Am and ^{238}Pu as the alpha emitters and $^{90}Sr/^{90}Y$ as the beta emitter.

These differences are attributed to two main factors. First, the radionuclide retention pattern within the PSresin cartridge can affects the scintillation mechanism; whether retained in specific cartridge regions or evenly distributed, the radionuclide's polarity and interaction with the extractant radical can impact performance. Second, the presence of silicon in SI-PSresin's extractant contributes unique properties, such as increased bond length, reduced steric hindrance, and higher nuclear charge relative to carbon. Silicon's low electronegativity and availability of five vacant 3d orbitals allow it to form dπ-pπ conjugates, potentially enhancing fluorescence yield, and in this specific situation enhancing the alpha classification. Organosilicon molecules are known to improve fluorescence properties, though the exact mechanisms remain under study [21].

Based on the findings, the SI-PSresin prototype, which uses bis(trimethylsilylpropanyl) methanediphosphonic acid as an extractant was selected as the starting point, for further development of an advanced α-PSresin

- Optimization α-PSresin

The primary goal of this project was to develop a PSresin that can be made commercially available. Achieving this requires a robust synthetic route of the extractant

capable of producing high yields and purity in the final product. Although the synthetic route initially used for the extractant and PSresin preparation was suitable at a laboratory scale, variability in product purity across syntheses and low yields when aiming for consistent purity presented challenges. Tetra-substitution was sometimes favored over the desired di-substitution, necessitating multiple purification steps and leading to product loses during each extraction.

To address these issues, four major modifications were implemented. The first, and most critical change was in the choice of coupling agent. Previously, DCC was employed; however, a significant drawback of DCC is the generation of an urea by-product, which is partially soluble in both organic and aqueous phases, complicating the isolation of the desired compound during workup. To improve this, two alternative coupling agents were explored: N, N'-diisopropyl carbodiimide (DIC), and 3-dimethylaminopropyl ethyl carbodiimide (EDC). Both agents produced urea derivatives that were more easily removed due to their low solubility in organic solvents. Between DIC and EDC, DIC emerged as the optimal choice, as it preferentially formed the desired di-substituted compound with a higher yield. In contrast, EDC's smaller molecular size provided insufficient steric hindrance, promoting the formation of the tetra-substituted compound.

The second modification involved changing the solvent. With DIC as the coupling agent, dichloromethane was selected over THF to ensure complete solubility and homogenization of all reagents. The third adjustment was an increase in solvent volume, which facilitated a greater dilution of reactants. This change further promoted di-substitution over tetra-substitution, although its impact was relatively minor given the steric hindrance provided by DIC. The fourth and final modification involved introducing the coupling agent dropwise over three hours promoted the selective formation of the di-substituted compound. Together, these adjustments increased the synthetic yield to over 70 %, with high purity confirmed by NMR analysis (Fig. 3.5), making the synthesis scalable for commercial PSresin production.

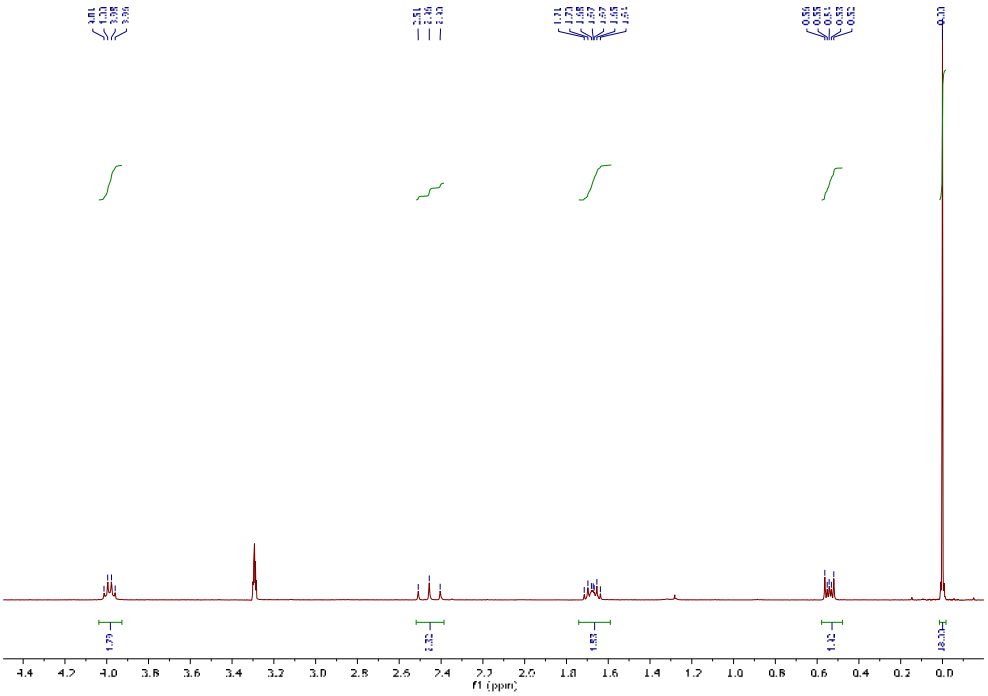

Fig 3.5 NMR spectrum for bis(trimethylsilylpropanyl)methanediphosphonic acid

The optimized extractant was then immobilized on DIN-PSm. Initially, the PSm-to-extractant ratio was set at 1:1/6, but two additional ratios—1:1/4 and 1:1/2.5—were tested to investigate potential improvements in capacity. All three PSresin ratios were successfully prepared, but during characterization, the 1:1/2.5 ratio had an excessive amount of immobilized extractant, impeding solution flow through the material. Consequently, this ratio was excluded from further testing. The remaining two ratios (1:1/4 and 1:1/6) showed 100 % detection efficiency and quantitative retention for ^{241}Am.

To further evaluate the resins, iron capacity tests were conducted (Table 3.1). The 1:1/4 ratio demonstrated 1.5 times the metal capacity of the 1:1/6 ratio, indicating enhanced performance with higher extractant ratio. Moreover, the optimized extractant notably doubled the iron capacity for the 1:1/6 ratio compared to the non-optimized version (SI-PSresin).

Table 3.1 Iron capacity in α-PSresin at two immobilization proportions compared with pre-optimized extractant.

	Pre-optimization	Post-optimization	
Psm to extractant ratio	**1:1/6**	**1:1/6**	**1:1/4**
Fe retained mg/g PSresin	1.88	4.01	5.81

Based on these results, the final PSm-to-extractant ratio selected for the α-PSresin development was 1:1/4. This ratio was then used to establish a method for gross alpha measurement in water samples, achieving both high detection efficiency and retention capacity suitable for a commercial application.

- Method development for gross alpha in water samples

One of the main characteristics of α-PSresin is its high affinity for alpha-emitting radionuclides; in fact, the retention is so strong that the consequent elution of them is almost only possible by leaching the extractant from the polymeric support using organic solvents. This characteristic makes α-PSresin a promising candidate for the development of a new method for gross alpha parameter determination.

The optimized α-PSresin demonstrated quantitative retention of all actinides with high detection efficiencies in a 0.5 M HCl working medium. However, this medium showed limited affinity for polonium and radium. Therefore, the working medium (both acid type and molar concentration) was optimized to selectively retain all alpha-emitting radionuclides relevant to gross alpha determination. This optimization study included actinides, ^{210}Po, and ^{226}Ra, and three acids (nitric, hydrochloric, and phosphoric acid) over a range of concentrations from pH 7 to 8 M. Common potential beta emitters interferents, such as ^{90}Sr, ^{210}Pb, and ^{210}Bi, were also included. Among the acids studied, nitric acid was selected as optimum for its similar affinity profile to actinides, radium, and polonium. Fig 3.6 shows the retention yield at each nitric acid concentration for each radionuclide.

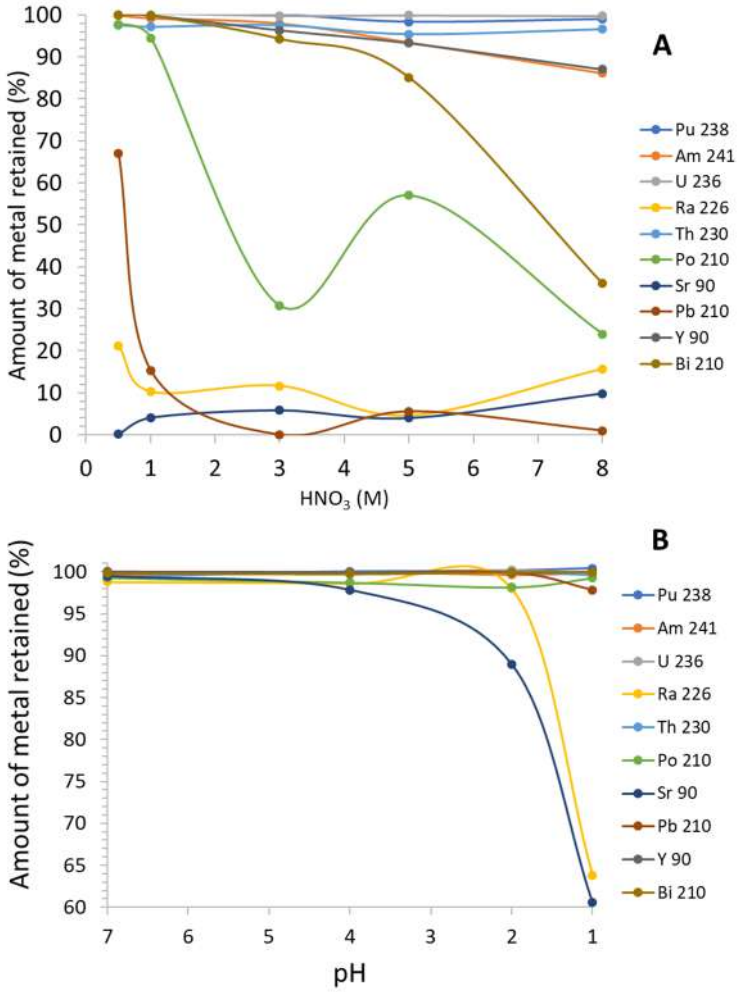

Fig 3.6 Results from the batch study. Proportion of metal retention (%) at nitric acid concentrations between 0.5 M and 8 M (A) and at pH values from 1 to 7 (B).

Actinides had consistent, quantitative retention across all concentrations, aligning with the strong affinity of diphosphonic extractants for actinides. Importantly, polonium and radium were quantitatively retained at low acid concentrations but not at high ones (> 1 M). This finding indicates that lower nitric acid concentrations are optimal for gross alpha determination. In contrast, beta emitters showed low retention at high acid concentrations, with only minor retention of ^{210}Bi and quantitative retention of ^{90}Y at 8 M HNO_3 and some retention at low acid concentrations. Nevertheless, α/β discrimination analysis can correct these beta emitter contributions to the scintillation signal.

A pH 2 working medium was selected for environmental monitoring purposes. This concentration achieves quantitative retention of radium and polonium and has the

added advantage of matching the acidified pH at which water samples typically arrive, thus simplifying the analytical process. For decommissioning waste samples, where actinides are the primary concern, the nitric acid concentration could be increased as radium and polonium can be neglected.

The working medium selection was based on batch studies using 24 hour contact time. In a cartridge configuration, however, contact time is reduced. Therefore, standards for each alpha emitter were prepared and passed through the α-PSresin cartridge. Retention results were as expected, except for polonium, which showed only 75 % retention. To improve this, polonium valence was previously adjusted to Po(IV) by adding 1 % H_2O_2 and heating at 50°C for 30 minutes, which increased retention to 97 %. These conditions were validated for each alpha emitter, resulting in quantitative retention and 100 % detection efficiency for all (Table 3.2).

Table 3.2 Quality parameters for each radionuclide (N=3).

Radionuclide	Retention (%)	Detection efficiency (%)
^{241}Am	>99.5[a]	100 (2)
^{238}Pu	>99.5[a]	100.5 (0.8)
^{236}U	>99.5[a]	101 (1)
^{230}Th	>99.5[a]	97.3 (0.2)
^{226}Ra	>99.5[a]	–
^{210}Po	97 (1)	88 (1)

[a] Activity on the effluent solution below LoD.

When working with PSresins, a tracer is recommended, as described in the general introduction. Selecting an effective tracer was challenging, as it needed to mimic the behaviour of all alpha emitters as closely as possible. Europium was chosen as the tracer, allowing for alpha emitter quantification on α-PSresin not only by ICP-OES but also via UV-VIS measurements (quantitative) or by simple visual colorimetric check (qualitative). A visual check will allow for fast detection of anomalies during the procedure, such as interference from high calcium or iron levels or high organic matter content.

Europium forms coloured complexes with Arsenazo (III) at pH 2.6–2.8. In the presence of europium at concentrations exceeding 0.5 $mg \cdot L^{-1}$, the complex turns purple, whereas the unbound form of Arsenazo (III) appears pink (Fig. 3.7). This allows for a qualitative retention check, which involves taking 10 mL of effluent post-sample passage through the PSresin cartridge, adjusting to the target pH, and adding Arsenazo (III).

Additionally, in case of need the retention yield can be measured by UV-VIS spectrometry at 654 nm within a 0.1 to 10 mg·L^{-1} concentration range.

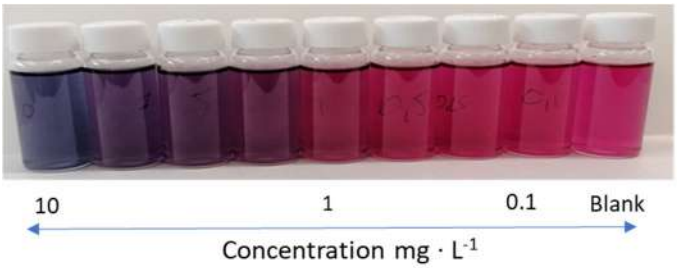

Fig 3.7 Colour obtained depending on the europium concentration when complexed with Arsenzao(III)

For calibration, two alpha emitters of different energies—^{238}Pu and ^{236}U—alongside ^{90}Sr/^{90}Y as beta emitters, were used. In PSresin, energy differences are more pronounced than in LSC, due to the inherent properties of PSresin. A dual alpha-emitter calibration helps reduce this variance, facilitating a standard calibration applicable to diverse alpha emitters.

The method was validated on interlaboratory water samples, yielding quantification errors below 8 % with either the qualitative or quantitative retention approach. Additionally, α-PSresin was tested on five samples from the Catalonia area, producing results comparable to those obtained by the Laboratori de Radiologia Ambiental (LRA) at the Universitat de Barcelona using the conventional LSC method, but with reduced analysis time and reagent use.

These findings confirm that α-PSresin can accurately measure gross alpha parameters with low quantification errors, using either the qualitative or quantitative UV-VIS colorimetric determination. For rapid analysis of multiple samples, the visual colorimetric check is a straightforward option. Additionally, the PSresin method provides lower background levels compared to conventional LSC, enabling faster detection of minimal activity levels for water monitoring. With a minimum detectable activity of 0.025 Bq·L^{-1}, results are delivered within 5–6 hours from sample reception, significantly faster than conventional methods, which require 24–48 hours. This method

also minimizes polonium losses, reduces sample salt content interference, prevents colour quenching, and allows simultaneous analysis of multiple samples without liquid scintillation cocktails, thus reducing waste.

- Method modifications for gross alpha determination in soil samples

The development of α-PSresin and its analytical methodology was initially focused on water samples. However, efforts have been made to adapt this method for soil samples, as conventional method faces several challenges due to quenching phenomena. To test the viability of α-PSresin for gross alpha determination in soils, real soil samples spiked with americium were analysed.

Soil samples were first calcinated and then digested in an acid solution (HNO_3 + HCl). In some cases, the α-PSresin got a brown-yellow coloration, likely due to by-products from the digestion process, calcination, or elevated iron content, which led to quenching effects. This color change lowered detection efficiency and impacted alpha recovery.

To minimize these influences, additional rinsing steps were tested to remove by-products from sample digestion. Different rinsing solutions—0.1 M EDTA, 0.1 M sodium thiosulfate, and 1 M phosphoric acid—were evaluated for their effectiveness in eluting or masking interfering elements that could be retained by α-PSresin. Additionally, since calcination and digestion could lead to polonium loss, the removal of the addition of hydrogen peroxide (previously used for ^{210}Po valence adjustment) was also considered.

Fig 3.8 shows the spectra obtained for each test compared with the developed water sample method (indicated in dark blue). Removing hydrogen peroxide improved quantification by narrowing the peak, suggesting that hydrogen peroxide was reacting with by-products from soil decomposition. Among the rinses, sodium thiosulfate (shown in yellow) provided the best spectral results, producing the narrowest peak. With sodium thiosulfate, the yellow colour observed when soil samples passed through the

α-PSresin disappeared, likely due to the elution of iron compounds from the soil as result of a redox reactions, effectively eliminating quenching.

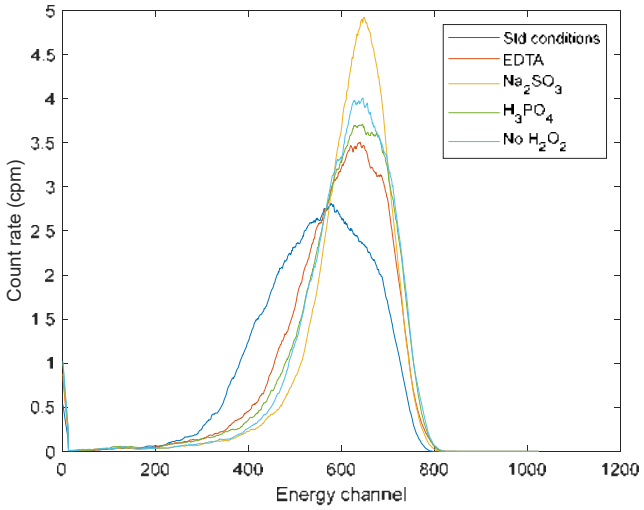

Fig 3.8 Spectra obtained for each respective new condition studied

Based on these results, the soil analysis method was modified by removing hydrogen peroxide (since polonium valence adjustment is unnecessary) and adding a final rinse with 5 mL of sodium thiosulfate.

To evaluate the matrix effect, various soil sample masses (0.05 to 1 g of calcinated soil) were tested to assess the impact on detection efficiency and the SQP(E) parameter. Table 3.3 presents these results.

Table 3.3 Detection efficiency and SQP(E) parameter correlated with the amount of sample taken.

mass (g)	SQP(E)	Detection efficiency %
0.05	755	101
0.1	769	100
0.5	764	102
1	771	101

The variation in soil sample quantity did not impact either the SQP(E) parameter or detection efficiency, indicating that the established conditions are suitable for sample masses up to 1 g. Fig 3.9 shows a comparison of spectra for each mass tested.

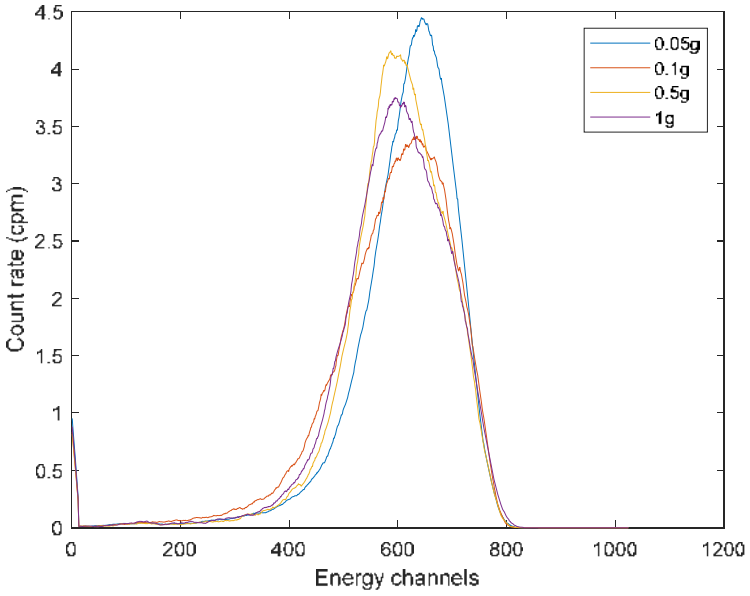

Fig 3.9 ^{241}Am spectrum of each mass sample

These findings confirm that the α-PSresin method is effectively applicable to soil samples for gross alpha determination. Furthermore, the methodological adjustments do not affect europium-arsenazo complex formation, maintaining both qualitative and quantitative retention yield assessments. This approach is being tested and implemented in the UPV/EHU, as a part of collaboration with Dra. Saroa Rozas.

3.3.2. Development of a scintillating iron imprinted polymer for ^{55}Fe

- Sc-Fe-IIP composition evaluation

The development of a new scintillating material for the determination of ^{55}Fe was based on imprinted polymers due to the lack of selective extractants for iron isolation [22]. The development of a scintillating ion-imprinted polymer for ^{55}Fe started by the evaluation of various combinations of monomers, crosslinkers, and chelating agents to determine the most effective configuration based on previous studies conducted by bulk polymerization. Styrene (St) and methyl methacrylate (MMA) were tested as monomers, ethylene glycol dimethacrylate (EGDMA) and divinylbenzene (DVB) as crosslinkers, and acrylic acid (AAC) and Methacrylic acid (MAA) as polymerizable chelating agents.

Additionally, 3-aminopropyl trimethoxy silane (APS) was explored as a non-polymerizable chelating agent [36]. Eleven polymers in total were prepared.

In this initial stage and based on IIP for iron described in literature [18] [31], the Sc-Fe-IIP's were prepared by suspension polymerisation containing the monomer and crosslinker in a 30:70 ratio and 1 g of iron complex (with a 1:14 iron-to-chelating agent ratio), along with 12 mL of toluene and 2 mL of methanol as porogens to stabilize the solution for the obtention of 14 g of polymer. Each polymer included PPO and POPOP as fluorescent solutes.

For each polymer, ^{14}C detection efficiency was measured, as ^{14}C provides a more sensitive assessment of slight improvements in scintillation due to composition modifications compared to ^{55}Fe, which has an exceptionally low energy and low detection efficiency. Iron capacity was tested at pH 4 and pH 6 in acetic acid solution. Results are presented in Table 3.4.

Table 3.4 Detection efficiency, quenching parameter, and iron capacity, at two media, for the different iron imprinted polymers obtained by suspension polymerization.

Chelating agent	Monomer composition	*^{14}C detection efficiency (%)*	SQP (E)	iron capacity (mg Fe · g Sc-Fe-IIP^{-1})	
				pH 4	pH 6
AAC	St:DVB	2.16(0.04)	490	>0.1	>0.1
	St:EGDMA	5.31(0.07)	586	3.58	7.24
	MMA:DVB	9.36(0.09)	470	5.36	23.05
	MMA:EGDMA	5.05(0.07)	475	3.34	16.00
APS	St:DVB	3.04(0.05)	473	>0.1	1.09
	St:EGDMA	9.65(0.08)	588	0.68	0.62
	MMA:DVB	4.09(0.06)	508	0.52	3.16
MAA	St:DVB	<0.05	510	0.62	0.78
	St:EGDMA	<0.05	532	1.21	3.36
	MMA:DVB	<0.05	504	1.66	3.09
	MMA:EGDMA	<0.05	489	1.34	13.84

The particle size of all polymers was approximately 1–2 mm in diameter. The optimal composition, yielding the highest detection efficiency, were the mixtures containing styrene and/or divinylbenzene, which provided a sufficient number of aromatic rings to enable effective energy transfer, particularly when using acrylic acid as the chelating agent. However, the detection efficiency achieved was lower than expected, as typical ^{14}C detection efficiency for plastic scintillators ranges from 50 % to 60 %. This reduced efficiency is primarily attributed to the particle size, which was larger than the ideal range for plastic scintillation microspheres (30–70 μm), where particle and optical

quenching are balanced. Additionally, MAA and AAC demonstrated higher iron capacities compared to APS, likely due to the inadequate integration of the APS complex into the polymer. Iron capacity for both AAC and MAA was higher at pH 6 than at pH 4, due to the deprotonation of acrylate groups at pH 6. Given the pKa values of AAC (4.25) and MAA (4.65), a working medium with pH ≥ 6 ensures complete deprotonation of the acrylate groups. These findings indicate that AAC is the most effective chelating agent for this application. Moreover, these prepared polymers were affected by chemical and colour quenching from the iron encapsulated within the polymer affected scintillation performance.

To address these issues, further studies focused on reducing particle size and incorporating bleaching agents—polymerizable phosphate compounds—to mitigate the reddish coloration associated with iron.

- Bleaching agent and particle size reduction

To achieve optimal particle size reduction, the PVA concentration was increased from 0.5 % to 10 %, and 1 % NaCl was added to raise the ionic strength. Additionally, the organic phase volume was reduced by half, from 26 mL to 13 mL. This modification yielded particle sizes of approximately 200–400 µm. Finally, increasing the total aqueous phase volume from 100 mL to 150 mL further reduced particle size to 30–60 µm, while keeping 13 ml organic phase volume. The increased PVA concentration allowed for better control over droplet formation, resulting in smaller, more uniform particles upon solidification. Reducing the organic phase volume improved droplet dispersion in the aqueous phase, and the increased aqueous volume provided additional space for stabilized droplet dispersion.

With an optimized particle size method established, two polymerizable bleaching agents were tested to counteract the red coloration caused by iron binding in the polymer. The agents tested were vinyl phosphonic acid (VPA), which serves as both a chelating and bleaching agent, with St and DVB as monomer and crosslinker respectively, and bis[2-(methacryloyloxy)ethyl] phosphate ($EGPO_4$), which functions as both a chelating agent and a crosslinker, with St as monomer. Both compounds contain phosphate groups capable of forming colourless complexes with iron. Both bleaching

agents successfully suppressed the reddish colour of the Sc-Fe-IIP polymer upon iron binding. However, VPA outperformed $EGPO_4$, as the latter increased polymer fragility, compromising microsphere formation. Fig 3.10 shows SEM images of the polymers synthesized with VPA and $EGPO_4$, where the $EGPO_4$-based polymer no longer had a spherical structure.

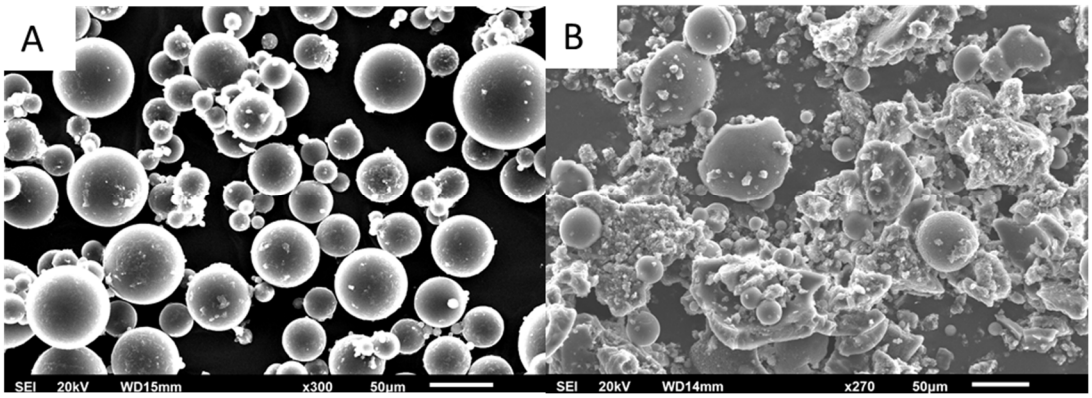

Fig 3.10 SEM images for each Sc_Fe_IIP prepared with bleaching agents.A St:DVB:VPA. B St:EGPO4

Therefore, the VPA incorporation was studied in Sc-Fe-IIP with St:DVB and MMA:DVB compositions, with AAC as chelating agent. In both cases, the modifications improved ^{14}C detection efficiency, reaching up to 18 %. The iron capacity remained consistent with values from Table 3.4 for the MMA matrix, but increased significantly for the St matrix, from 0 to 7 mg $Fe \cdot g^{-1}$ Sc-Fe-IIP.

Additionally, selectivity was tested against potential interfering elements (nickel, cobalt, and copper) and was observed that the polymer did not have any selectivity for iron over these other elements. Furthermore, when compared to the non-ion-imprinted polymer, the imprinting process appeared ineffective, as shown in Fig 3.11. This was attributed to an excess of chelating agents that failed to form the necessary iron-chelate complex before polymerization, leading to chelating agent polymerization on the surface losing its specificity as no cavity is formed.

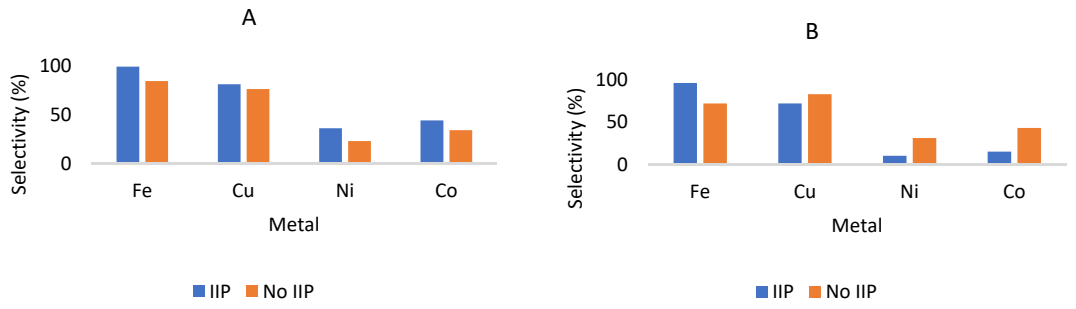

Fig 3.11 Selectivity of the optimised iron polymers (imprinted (IIP) and non-imprinted (NO IIP), obtained after size reduction and VPA inclusion. A St:DVB:VPA, B MMA:DVB:VPA.

To address the selectivity problem, 1.5 equivalents of triethylamine were added to the organic phase relative to the chelating agent quantity, and the iron-to-chelating agent ratio was increased from 1:14 to 1:1. Triethylamine deprotonates acrylic acid, facilitating the proper formation of the acrylic acid-iron binary complex, while the increased iron ratio ensures minimal free chelating agent of remaining unbound. This adjustment was tested in both the St and the MMA with DVB as backbones matrices. Table 3.5 compares results for both imprinted polymers against their non-imprinted counterparts.

Table 3.5 comparison between both imprinted polymers and with the respective non-imprinted

		Capacity (mg metal · g Sc-Fe-IIP^{-1})				Selectivity (%)			
	Composition	**Fe**	**Cu**	**Ni**	**Co**	**Fe**	**Cu**	**Ni**	**Co**
Imprinted	St:DVB:VPA	18(2)	0.9(0.7)	<0.10	0.5(0.2)	98(2)	7.8(0.1)	4.0(5)	<1
	MMA:DVB:VPA	19(2)	3.0(0.8)	<0.1	5(5)	95(1)	75(3)	26(4)	9(7)
Non imprinted	St:DVB:VPA	10(2)	9(1)	1(1)	2.6(0.4)	84.3(0.8)	76(8)	23(4)	34(8)
	MMA:DVB:VPA	16.9(0.3)	16(2)	3.7(0.9)	6(1)	72(3)	83(5)	31(4)	43(16)

In both cases, the iron capacity increased, but the styrene-based matrix had higher iron selectivity over potential interferents and the non-imprinted version. In contrast, the MMA matrix showed minimal improvement in selectivity relative to the non-imprinted version. These findings confirmed that the implemented adjustments successfully addressed the initial selectivity issues, leading to the final optimized composition for Sc-Fe-IIP with an iron capacity of 18 mg·g^{-1} and high selectivity for iron (98 % selectivity for iron with only 8 % and 4 % selectivity for copper and nickel, respectively, and no affinity for cobalt). Therefore, the final optimum composition for a

Sc-Fe-IIP includes styrene as the monomer, DVB as the crosslinker, AAC as the chelating agent, VPA as the bleaching agent, 1 g of binary complex compound and triethylamine for effective binary complex formation.

- Scintillation performance

The scintillation performance of this optimum polymeric composition was tested for ^{55}Fe, achieving a detection efficiency of 2.2 % using a Hidex detector and 47 % for ^{14}C. These values were deemed acceptable, as the detection efficiency for ^{3}H—similar in energy to ^{55}Fe—rarely exceeds 1.5 % in PSm. Nonetheless, to further enhance scintillation performance, several modifications to the polymer composition were explored, including reducing the iron binary complex compound to half (from 1 g to 0.5 g), incorporating polymerizable fluorescent solutes, and substituting styrene with vinyl toluene, which has been reported to improve quantum yield [23]. This final set of modifications yielded the following results: reducing the iron complex content enhanced scintillation capacity, doubling the detection efficiency for ^{55}Fe to 5 %. However, as could be anticipated, this reduction also led to a decrease in iron capacity. The addition of polymerizable fluorescent solutes and the replacement of styrene with vinyl toluene did not yield significant scintillation improvements, as the performance remained similar to that of the previous polymer composition. These modifications also adversely affected iron capacity and selectivity due to changes in the polymer matrix. Therefore, the most promising composition included styrene, divinylbenzene, acrylic acid, vinyl phosphonic acid, PPO, POPOP, and triethylamine with a 1g of iron complex content.

This optimized polymer prototype was then packed into a solid-phase extraction (SPE) cartridge. A spiked sample containing stable iron and ^{55}Fe was passed through the cartridge and measured with a Hidex detector. Initial tests demonstrated a 30 % to 40 % retention yield and a 5 % detection efficiency.

This initial prototype shows promise as an alternative to conventional methods, although further studies are necessary to increase efficiency and refine the methodology for reliable application.

- Sc-IIP versus PSresin

This chapter presents the development of two distinct scintillating materials: one for alpha-emitting radionuclides (α-PSresin) and another for ^{55}Fe (Sc-Fe-IIP), fulfilling the first and fourth objectives of this thesis.

The design strategies for these materials diverged significantly. The α-PSresin was developed using a scintillating support, PSm, onto which a selective extractant was immobilized, conferring a specific affinity for alpha-emitters. In contrast, the ^{55}Fe-selective Sc-IIP achieved selectivity through ion-imprinted polymerization, creating iron-specific cavities without the need for additional extractants. A comparative evaluation of these materials reveals the following differences in their preparation and properties:

- Material versatility and selectivity: PSresins offer greater versatility, as their affinity for different elements can be adjusted by changing the working medium, as observed with the α-PSresin. Conversely, Sc-IIP selectivity is fixed by the template used in synthesis, limiting flexibility but enhancing selectivity for the imprinted ion.
- Stability: The PSresins, composed of linear polystyrene, are less stable in aggressive or organic media compared to Sc-IIP. Crosslinkers in Sc-IIP polymers enhance structural stability, allowing them to withstand harsher conditions more effectively.
- Leaching and reusability: Sc-IIPs, with selectivity embedded in the polymer matrix, do not require an extractant and thus are not prone to leaching. PSresins, however, rely on surface-bound extractants held by weaker forces, making them susceptible to leaching, especially in high-volume samples. Consequently, Sc-IIPs generally offer better reusability than PSresins.
- Scintillation capacity: PSresins typically have stronger scintillating capacities, as they do not incorporate crosslinkers or other additives (e.g., chelating agents) that can hinder the scintillation mechanism as happens in Sc-IIPs.
- Preparation and reproducibility: PSresins are relatively straightforward to produce, especially if a commercial extractant is available. In cases requiring synthesized extractants, development may be slightly more complex but remains reproducible once optimized. Sc-IIP preparation is generally more challenging,

often complicated by solubility issues with ionic and organic compounds, and may produce inconsistent properties across batches due to slight variations in polymerization conditions. As observed with α-PSresin and Sc-Fe-IIP preparation.

In summary, Sc-IIPs are preferable when a highly selective material for a specific element is needed and no selective extractant is available. However, if suitable extractants are accessible, PSresins are typically simpler to optimize, produce, and scale. The choice between these materials largely depends on the availability of selective extractants.

3.3.3. Computational strategies for resins development

This project was a collaboration with Prof. Ali Hassanali, Dr. Alex Rodriguez, and Dra. Giulia Sormani from the Abdus Salam International Centre for Theoretical Physics (ICTP) in Trieste, Italy, where I performed my PhD stay. It was motivated by the challenges encountered during the development of the α-PSresin, where significant time and financial resources were invested to establish optimal conditions and identify a suitable extractant for gross alpha determination. The extractant evaluation process involved extensive batch studies with various radionuclides and stable elements to determine the ideal working medium. However, numerous trials resulted in unsatisfactory outcomes after several months of effort. For example, the BZ-PSresin, discussed in Section 3.3.1, achieved only a 50% retention yield due to insufficient affinity with americium. In hindsight, the application of computational tools could have provided early insights, potentially reduced the number of unsuccessful trials, and expedited the PSresin development process.

The computational method introduced in this thesis offers a streamlined approach using molecular dynamics and enhanced sampling techniques to evaluate affinity between target elements and extractants. Designed as a screening tool, this strategy can help identify promising working media by examining the system's free energy landscape, thus providing preliminary knowledge of extractant-element affinity and medium influence. The method was made to be both efficient and accessible, aiming to minimize computational demands while delivering essential insights, making it suitable for users with varied expertise.

The strategy was tested with 18-crown-6 as the extractant and strontium and lead as target metals with six working media (nitric acid, hydrochloric acid, formic acid, acetic acid, perchloric acid, and potassium thiocyanate) to assess the effect of the media in the binding affinity. Results from these simulations were validated by comparing them with experimental distribution coefficients batch studies.

- Studied system

The decision to use 18-crown-6 with strontium and lead stemmed from previous research on CE-PSresin, which utilized 4,4'(5')-di-t-butylcyclohexano-18-crown-6 along with 1-octanol and encountered affinity for both strontium and lead in strong nitric acid medium. The 18-crown-6 section constitutes the essential binding component (Fig.3.12), therefore, it will be used to evaluate the viability of the computational strategy in assessing the effect of the working medium in the affinity of the complex, looking for conditions in which the binding is selective for Sr^{2+} and not for Pb^{2+}.

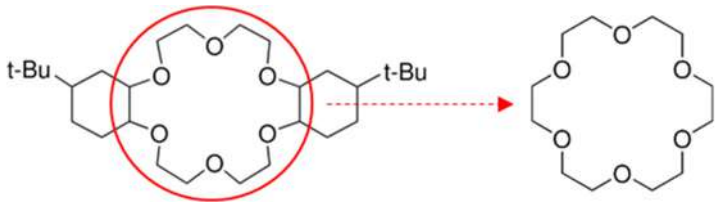

Fig 3.12 The crown ether used in CE-PSresin with the bounding core in red and the crown ether used for the proof of concept.

- Energy barrier and binding affinity

Initially, a 400 ns production run was conducted with a single crown ether molecule, two anion molecules, and one metal atom in a box of water molecules. However, the system struggled to explore all possible conformations, as evidenced by the distance between the centre of mass of the crown ether and the metal, which failed to close below 0.5 nm (Fig 3.13). This indicated that the system either required more simulation time or the inclusion of more atoms to facilitate interaction between the components. However, both options were computationally expensive.

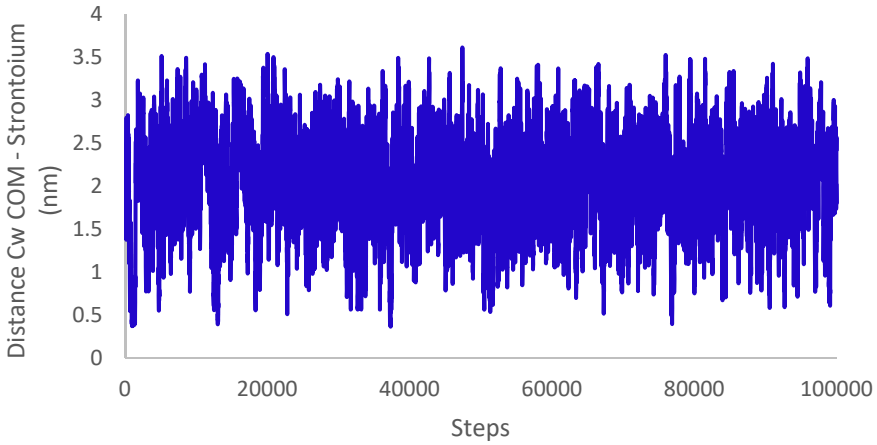

Fig 3.13 Temporal evolution of the distance between the COM of the crown ether and Sr^{2+} along the 400ns

To address the lack of sampling, enhanced sampling techniques were used. Initially, umbrella sampling simulation was performed in a system containing Sr^{2+}, the crown ether, and two chloride ions. A harmonic potential bias was introduced based on the distance between the metal and the centre of mass of the crown ether, divided into twelve windows. This analysis revealed the presence of a significant energy barrier preventing the system from overcoming the 0.5 nm distance while also identifying the global minimum at the binding conformation, located 0.05 nm from the centre of mass of the crown ether (Fig 3.14).

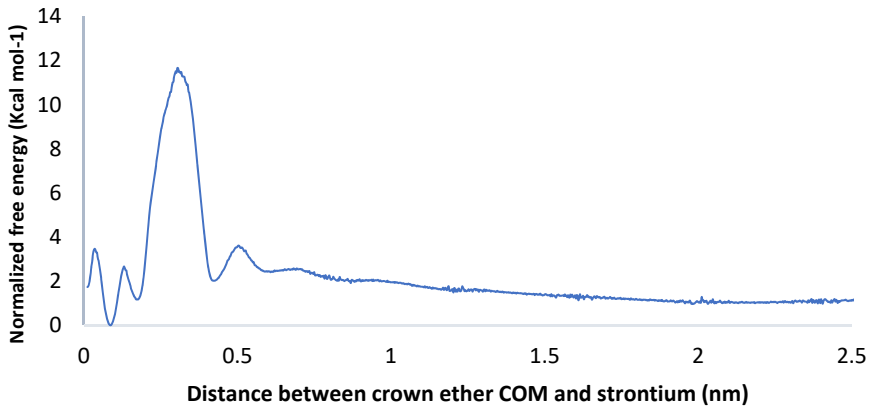

Fig 3.14 Normalized free energy for the crown ether Sr^{2+} system

Umbrella sampling simulations were valuable in determining the affinity between the crown ether and the metal ion; however, the role of anions in complex formation remained unclear, as its study through umbrella sampling simulations can be very time demanding.

- Metadynamics simulations and experimental validation

To examine the affinity between the crown ether and the metal ion and the anions role, metadynamics simulations were selected, as this technique allows for the exploration of all system possibilities through the addition of Gaussian functions. The initial focus was on studying the nitrate system for both metals with the crown ether to validate the simulation results against expected behaviours described in laboratory separations. This system is well-documented in the context of the 4,4'(5')-di-t-butylcyclohexano-18-crown-6 and 1-octanol resins and similar behaviour was expected with the crown ether used in this study.

Metadynamics simulations were performed using the PLUMED plugin, with configurations derived from the initial MD production run. To assess metal affinity and anion influence, two collective variables were analysed: the distance between the COM of the crown ether and the metal ion, and the coordination number between the metal ion and two nitrate anions. This approach enabled the reconstruction of the free energy landscape, revealing that both Sr^{2+} and Pb^{2+} exhibit comparable affinities for 18-crown-6, consistent with their known strong retention in crown ether-based resins. Furthermore, the presence of nitrate anions was shown to enhance the metal-crown ether affinity.

Both systems displayed similar complex conformations, with the metal ion centrally positioned within the crown ether and the nitrates axially coordinated to the metal, as illustrated by the structures extracted from the simulation (Fig. 3.15).

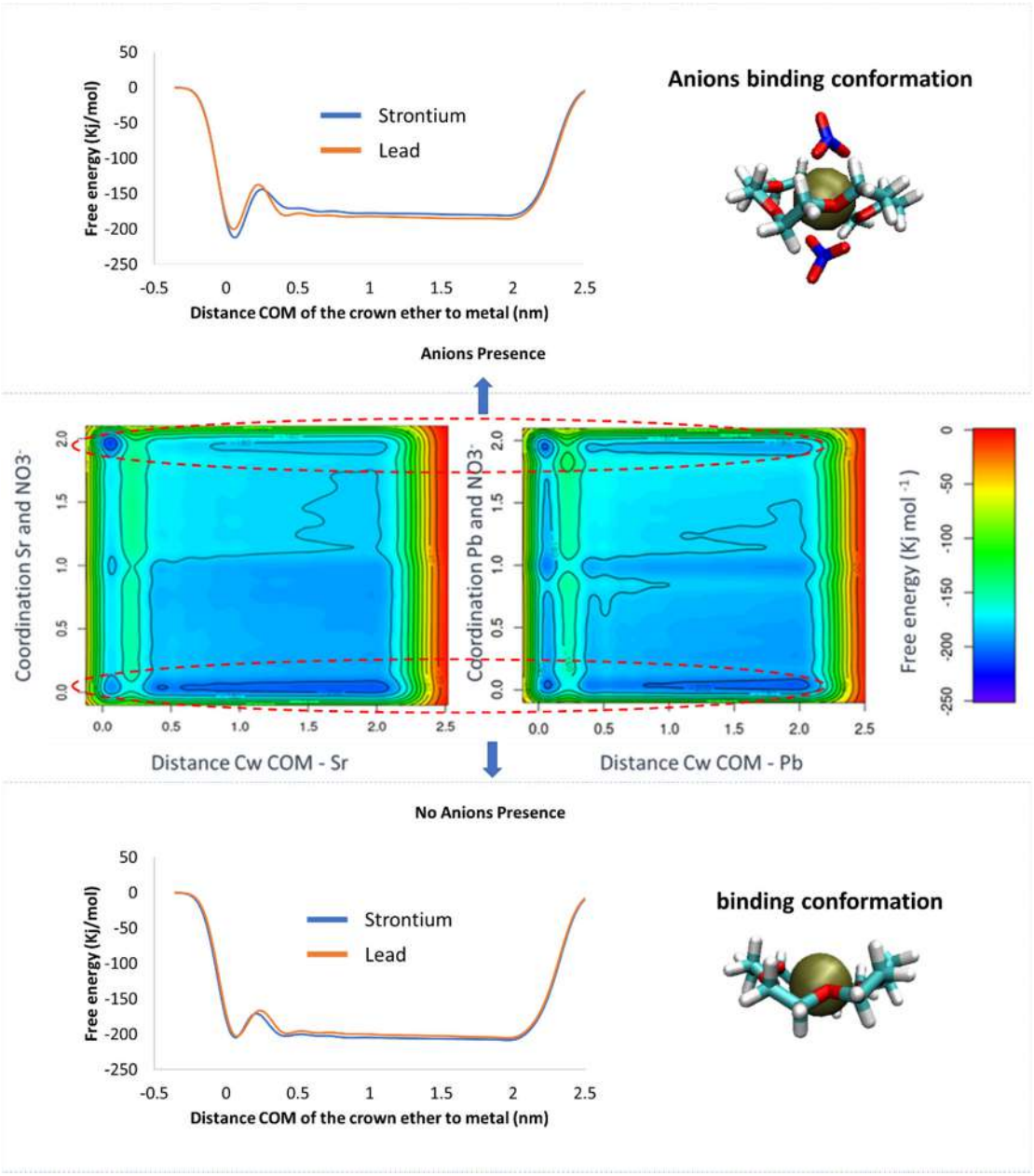

Fig 3.15 Top panel, evolution of the free energy at presence of nitrates, in the bonding of the metal with the 18-crown-6, along with the snapshot of the conformation of the complex in the bounding situation. Middle panel, free energy landscape for strontium and lead considering the coordination of the metal and the nitrates and the distance between the centre of masses of the 18-crown-6 and the metal. Bottom panel, evolution of the free energy without the presence of nitrates in the bonding of the metal with the 18-crown-6.

Anions played a critical role in stabilizing metal ion-crown ether complexes by neutralizing the complex's overall charge. This charge neutralization minimizes electrostatic repulsion, enhancing the stability of the complex. Additionally, anions contribute to the solvation shell surrounding the complex. In polar solvents like water, anions stabilize the metal ion-crown ether complex through interactions with solvent molecules, effectively lowering the system's total energy.

Given the challenges in separating Sr^{2+} and Pb^{2+} under nitrate conditions and with the goal of studying the simulation prediction level, the strategy was extended to five additional media (chloride, perchlorate, acetate, formate, and thiocyanate anions) for both Sr^{2+} and Pb^{2+}. For each medium, including the two nitrate systems, we calculated the free energy difference and compared it to the experimental D_w ratio obtained from batch experiments. This D_w parameter provides crucial information on the affinity between the target metal (Sr^{2+} or Pb^{2+}) and the crown ether in the respective medium, where a higher D_w indicates stronger metal-extractant affinity under those conditions. Fig 3.16 compares the calculated free energy differences with the experimentally determined D_w values. A strong correlation was observed for both metals, indicating that a negative ΔF (reflecting a more favourable binding interaction) corresponds with a higher D_w. This correlation demonstrates that the simulations reliably predict experimental outcomes. Moreover, the general trends in the simulations were consistently mirrored in the experimental data, validating the predictive accuracy of the computational model.

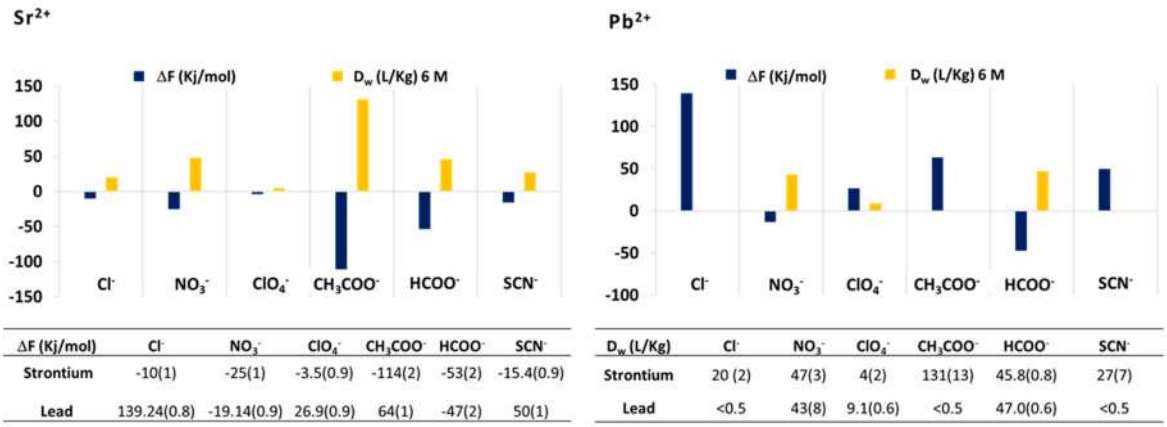

ΔF (Kj/mol)	Cl^-	NO_3^-	ClO_4^-	CH_3COO^-	$HCOO^-$	SCN^-
Strontium	-10(1)	-25(1)	-3.5(0.9)	-114(2)	-53(2)	-15.4(0.9)
Lead	139.24(0.8)	-19.14(0.9)	26.9(0.9)	64(1)	-47(2)	50(1)

D_w (L/Kg)	Cl^-	NO_3^-	ClO_4^-	CH_3COO^-	$HCOO^-$	SCN^-
Strontium	20 (2)	47(3)	4(2)	131(13)	45.8(0.8)	27(7)
Lead	<0.5	43(8)	9.1(0.6)	<0.5	47.0(0.6)	<0.5

Fig 3.16 Correlation between the differences in free energy and the experimental D_w for Sr^{2+} (left panel) and Pb^{2+} (Right panel). Left table differences in free energy for strontium and lead. Right table Dw for Strontium and lead.

Although a clear correlation was observed between the experimental and simulation results, the D_w values obtained in this study are relatively low compared to those of fully optimized resins, where a D_w value greater than 10^2 is indicative of high affinity.

Another important observation is that it is proved that the crown ether has the highest affinity for Sr^{2+} when acetate is used as counterion, while there are not either evidences of experimental binding between the Pb^{2+} and the crown-ether confirming

the lack of affinity. Acetate could thus be the optimal medium in which Sr-selective retention can be obtained using a PSresins.

- Thermodynamic explanation

To understand why strong binding is observed with Sr^{2+} when using acetate as the anion, but not with Pb^{2+}, we analysed the free energy, enthalpy and entropy of the systems. The thermodynamic parameters have been calculated for each system, taking as a reference point the non-bounding non-acetate situations, moving to the metal-crown ether binding in absence of acetate, and finally studying the effect of the acetate in the complex formation.

Fig 3.17 illustrates the differences in thermodynamic parameters due to the presence or not of acetate anions. In both cases, the binding of the metal ion to the crown ether alone (situation B) resulted in an unfavourable condition, characterized by a positive free energy difference. However, when acetate anions are introduced into the system (situation C), there is a noticeable internal energy penalty in both cases, accompanied by an increase in entropy.

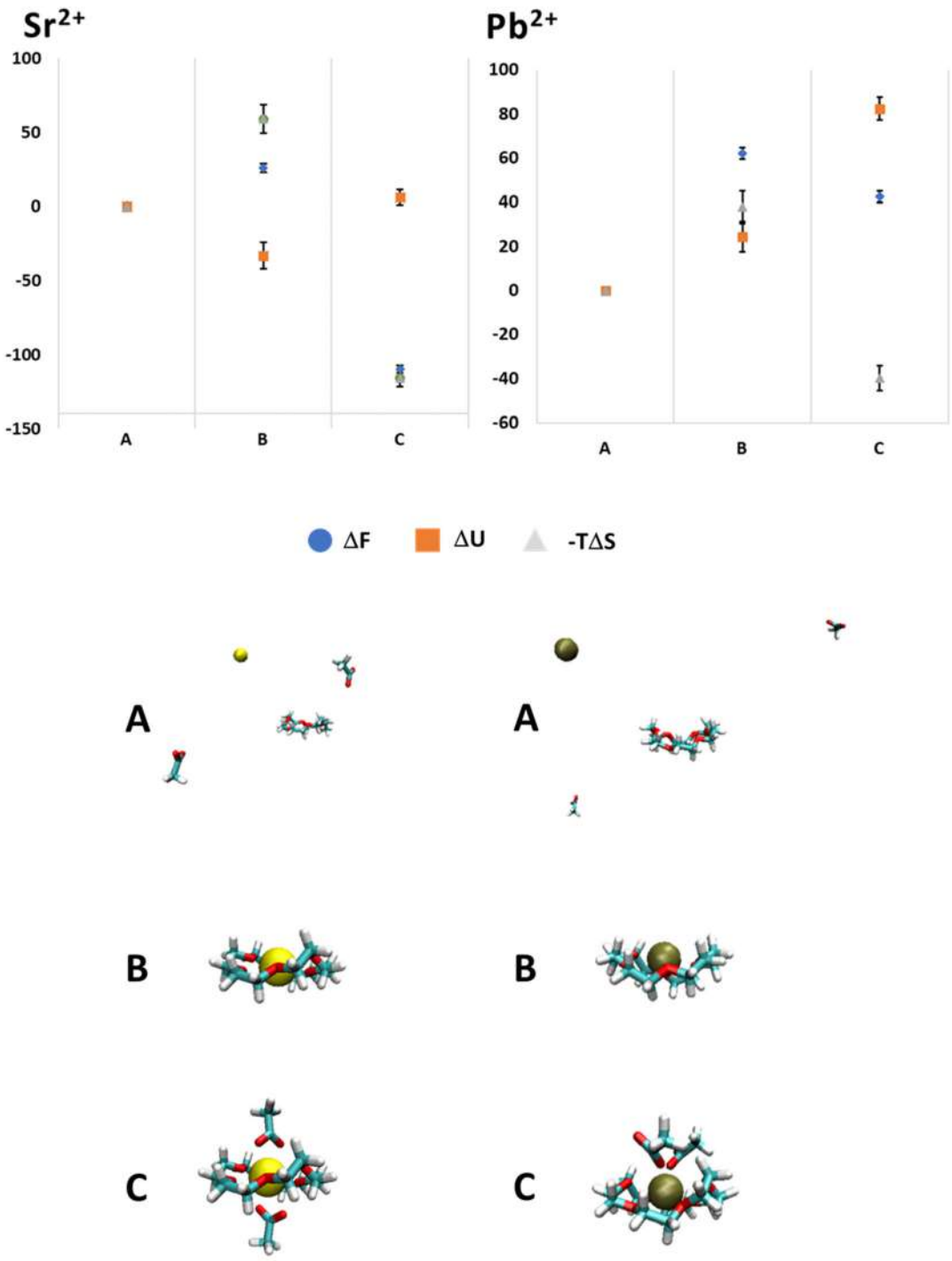

Fig 3.17 Thermodynamic study for Sr^{2+} left panels and for Pb^{2+} right panel.

In the Sr^{2+} system, entropy gain compensates for the internal energy penalty, leading to a favorable free energy change. In contrast, Pb^{2+} experiences insufficient entropy gain, making complex formation unfavorable. This explains why Pb^{2+} does not bind to the resin in an acetate medium, while Sr^{2+} does.

The addition of acetate anions to the Sr^{2+}-crown ether complex increases entropy by releasing water molecules, offsetting the enthalpic penalty and stabilizing the complex. For Pb^{2+}, however, strong initial binding to the crown ether and the structural rearrangements needed to accommodate acetates create a large internal energy penalty. The entropy gain from desolvation is insufficient to counterbalance this, making Pb^{2+} complexation thermodynamically unfavorable [34,35]. As temperature increases, Sr^{2+} stability improves due to amplified entropic contributions, whereas Pb^{2+} remains unstable because the internal energy penalty dominates.

Structural analysis (Fig. 3.18) shows that Sr^{2+} forms a stable axial acetate coordination, while Pb^{2+} adopts only a cis conformation. The expected axial structure does not form for Pb^{2+} due to steric hindrance and water molecules blocking acetate approach. This results in a less stable Pb^{2+}-crown ether-acetate complex

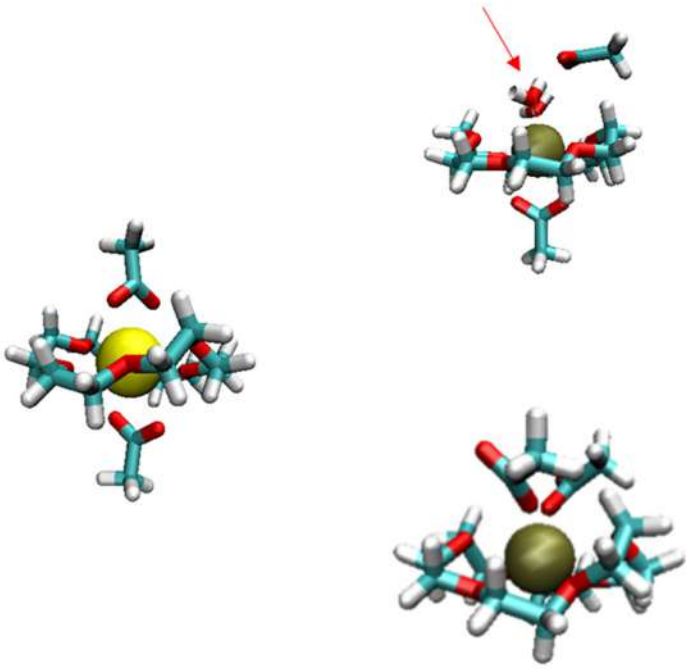

Fig 3.18 Snapshots in binding situation in presence of acetate. Left-panel for Sr^{2+} and right panel for Pb^{2+}.

The resulting binding conformation for Pb^{2+}-crown ether-acetate is thermodynamically less stable as it has been seen and this could be explained due to repulsion and steric hindrance effects between both acetates not leading to a very stable compound.

From the coordination point of view, Sr^{2+} ions typically prefer higher coordination numbers, allowing for more flexible coordination environments [36]. Thus, an interaction without significant disruption of the overall complex. Additionally, the Sr^{2+} and acetate-anions interactions are mainly ionic; reason for which they can integrate into the coordination sphere without causing major distortions or coordination competition [37,38]. In contrast, Pb^{2+} ions generally prefer lower coordination numbers, [39–41], and can have a more covalent interactions than Sr^{2+} due to the inert pair effect. This preference might result into a less flexible coordination sphere. Thus, when acetate anions attempt to coordinate with Pb^{2+}, they disrupt the Pb^{2+}-crown ether interactions, introducing significant steric and electronic strain. In addition, Pb^{2+} ions can have a stronger interaction with acetates, which can thus compete directly with the interactions between Pb^{2+} and the crown ether [42–45], not leading to a stable conformation.

These results confirmed the suitability of the computational strategy (Objective 5) to enhance the development of new resins. The use of metadynamics proved to be an effective approach, offering a high correlation between simulation outcomes and experimental data. This strategy can now be applied as a screening tool in the development of new selective materials, providing fast and cost-effective results, thereby streamlining the material development process.

3.4. References

[1] M. Ješkovský, J. Kaizer, I. Kontuí, G. Lujanienė, M. Müllerová, P.P. Povinec, Analysis of environmental radionuclides, in: Handbook of Radioactivity Analysis: Volume 2: Radioanalytical Applications, Elsevier, 2020: pp. 137–261. https://doi.org/10.1016/B978-0-12-814395-7.00003-9.

[2] V. Jobbágy, E. Dupuis, H. Emteborg, M. Hult, Performance evaluation of a European wide proficiency test on gross alpha/beta activity determination in drinking water, Applied Radiation and Isotopes 186 (2022) 110304. https://doi.org/10.1016/J.APRADISO.2022.110304.

[3] Triskem International, Product sheet, UTEVA resin, 33 (2015) 3–6.

[4] Triskem International, Product sheet, DGA Resin (Normal and Branched), 33 (2015) 5–9.

[5] Triskem International, Product sheet Actinide Resin TM.

[6] ISO 24390, 2023. Nuclear energy — Nuclear fuel technology — Methodologies for radioactivity characterization of very low-level waste (VLLW) generated by nuclear facilities.

[7] I.W. Croudace, B.C. Russell, P.W. Warwick, Plasma source mass spectrometry for radioactive waste characterisation in support of nuclear decommissioning: A review, J Anal At Spectrom 32 (2017) 494–526. https://doi.org/10.1039/c6ja00334f.

[8] T. Ruskov, R. Ruskov, I. Dobrevski, P. Menut, S. Konnova, N. Zaharieva, Radioactive ^{55}Fe contamination in the Primary Circuit of WWER-440, (2001) 364–368.

[9] X. Hou, L.F. Østergaard, S.P. Nielsen, Determination of ^{63}Ni and ^{55}Fe in nuclear waste samples using radiochemical separation and liquid scintillation counting, Anal Chim Acta 535 (2005) 297–307. https://doi.org/10.1016/j.aca.2004.12.022.

[10] I.A. Bagatur, Ay. Freidzon, M. Al, E. Baerends, J. Howard, L. Kuz, DFT calculations on the electronic and geometrical structure of 18-crown-6 complexes with Ag^{+}, Hg^{2+}, Ag^{0}, Hg^{+}, Hg^{0}, $AgNO_3$, and HgX_2 (X= Cl, Br, and I)." J of Mol Strc: THEOCHEM 588.1-3 (2002): 55-69. https://doi.org/10.1016/S0166-1280(02)00119-7.

[11] S. Hadisaputra, H. Dwi Pranowo, R. Armunanto, Extraction of strontium (II) by crown ether: insights from density functional calculation. Indonesian Journal of Chemistry 12.3 (2012): 207-216. https://doi.org/10.22146/ijc.21332.

[12] E.D. Glendening, D. Feller, An Ab Initio Investigation of the Structure and Alkaline Earth Divalent Cation Selectivity of 18-Crown-6, 1996. https://pubs.acs.org/sharingguidelines.

[13] F. Gámez, B. Martínez-Haya, S. Blanco, J.C. López, J.L. Alonso, Microwave spectroscopy and quantum chemical investigation of nine low energy conformers of the 15-crown-5 ether, Physical Chemistry Chemical Physics 14 (2012) 12912–12918. https://doi.org/10.1039/c2cp41635b.

[14] B. Martínez-Haya, P. Hurtado, A.R. Hortal, S. Hamad, J.D. Steill, J. Oomens, Emergence of symmetry and chirality in crown ether complexes with alkali metal cations, Journal of Physical Chemistry A 114 (2010) 7048–7054. https://doi.org/10.1021/jp103389g.

[15] W. You, Z. Tang, C.E.A. Chang, Potential Mean Force from Umbrella Sampling Simulations: What Can We Learn and What Is Missed?, J Chem Theory Comput 15 (2019) 2433–2443. https://doi.org/10.1021/acs.jctc.8b01142.

[16] A. Laio, M. Parrinello, Escaping free-energy minima. Proceedings of the national academy of sciences 99.20 (2002) 12562-12566. https://doi.org/10.1073/pnas.202427399.

[17] I. Abdulazeez, B. Salhi, N. Baig, A. Al-Saadi, Molecular dynamics simulation of the fractionation of lithium and magnesium-ions on crown ether-grafted cellulose acetate polyelectrolyte membranes, J Mol Liq 376 (2023) 121475 . https://doi.org/10.1016/j.molliq.2023.121475.

[18] P.D. J Grootenhuis, P.A. Kollman, van Eerden, D.J. Chem Soc, I.D. J Am Chem, Molecular Mechanics and Dynamics Studies of Crown Ether-Cation Interactions: Free Energy Calculations on the Cation Selectivity of Dibenzo-18-crown-6 and Dibenzo-30-crown-10, J. Am. Chem. Soc. 111 (1989) 2152-2158. https://doi.org/10.1021/ja00188a032

[19] P. Sappidi, A. Boda, S.M. Ali, J.K. Singh, Adsorption of Gadolinium (Gd3+) Ions on the Dibenzo Crown Ether (DBCE) and Dicyclo Hexano Crown Ether (DCHCE) Grafted on the Polystyrene Surface: Insights from All Atom Molecular Dynamics Simulations and Experiments, Journal of Physical Chemistry C 123 (2019) 12276–12285. https://doi.org/10.1021/acs.jpcc.9b01722.

[20] D.R. McAlister, M.L. Dietz, R. Chiarizia, A.W. Herlinger, Metal ion extraction by silyl-substituted diphosphonic acids. I. P,P'-di[3-(trimethylsilyl)-1-propylene] methylene- and ethylenediphosphonic acids, Sep Sci Technol 36 (2001) 3541–3562. https://doi.org/10.1081/SS-100108348.

[21] Z. Chen, S. Feng, D. Wang, Organosilicon Fluorescent Materials, Polymers (Basel) 15 (2023). https://doi.org/10.3390/polym15020332.

[22] M. Budnicka, M. Sobiech, J. Kolmas, P. Luliński, Frontiers in ion imprinting of alkali- and alkaline-earth metal ions – Recent advancements and application to environmental, food and biomedical analysis, TrAC - Trends in Analytical Chemistry 156 (2022) 116711. https://doi.org/10.1016/j.trac.2022.116711.

[23] N. Nijegorodov, V. Vasilenko, P. Monowe, M. Masale, Systematic investigation of the influence of methyl groups upon fluorescence parameters and the intersystem crossing rate constant of aromatic molecules, Spectrochim Acta A Mol Biomol Spectrosc 74 (2009) 188–194. https://doi.org/10.1016/j.saa.2009.06.003.

CHAPTER 4 - Development of greener and faster alternatives for radiostrontium and plutonium isotope measurement

4.1. Introduction

During radioactivity monitoring, two distinct scenarios can be identified: incident-driven monitoring, in response to incidents such as accidents, acts of terrorism, or nuclear tests, and routine environmental monitoring. In both cases, it is essential to quantify several radionuclides, including radiostrontium and plutonium isotopes.

4.1.1. Radiostrontium

Radiostrontium refers to radioactive isotopes of strontium, particularly ^{90}Sr and ^{89}Sr. ^{90}Sr is generated during the fission of heavy nuclei like ^{235}U or ^{239}Pu, which are commonly used in nuclear reactors and atomic weapons. ^{89}Sr is generated as well during the fission of heavy nuclei in significant quantities within nuclear power plants. Both isotopes are high-energy beta-emitting radionuclides: ^{89}Sr has a E_{max} of 1.50 MeV and a half-life of 50.56 days, while ^{90}Sr has an E_{max} of 0.55 MeV and a longer half-life of 28.79 years.

Radiostrontium can be released into the environment through nuclear weapons testing, accidental or authorized discharges from nuclear power plants, and nuclear accidents. Its environmental presence is of significant concern due to its high mobility, readily transferring from water to soil and subsequently to biota. For example, plants absorb radiostrontium from contaminated soil, which is then ingested by livestock, leading to accumulation in milk. The primary human exposure pathways are ingestion of contaminated food and inhalation of airborne dust particles. Once ingested, approximately 30% of radiostrontium is absorbed into the human body, where it predominantly accumulates in bones and teeth by substituting for calcium due to their chemical similarity. Once integrated into bone tissue, radiostrontium serves as a persistent source of ionizing radiation, leading to cellular damage and substantially increasing cancer risk [1]. This poses a significant challenge for public health, particularly following nuclear incidents or accidents [2].

Radiostrontium determination is crucial for both emergency response and routine environmental monitoring. During nuclear emergencies, quantifying ^{89}Sr and ^{90}Sr provides a rapid indicator of recent fission activity, allowing responders to assess the extent and timing of contamination. Notably, ^{89}Sr activity may be one or two orders of

magnitude higher than that of ^{90}Sr in such events, underscoring the importance of its measurement.

In long-term environmental monitoring, ^{90}Sr is the primary radiostrontium isotope of interest due to its long half-life, leading to persistent contamination over years. Regulatory agencies routinely monitor ^{90}Sr in soil, water, and food to comply with environmental protection standards. Its sustained presence serves as a reliable marker of radioactive contamination in regions affected by nuclear activities or accidents. Additionally, ^{89}Sr requires environmental monitoring for several months post-emergency to confirm its complete decay. This step is crucial to ensure accurate assessment of residual contamination levels and to verify that ongoing exposure risks from ^{89}Sr have been eliminated.

Conventional methods for radiostrontium determination typically involve chemical separation using extraction resins or successive coprecipitation. Among the common approaches, the successive precipitation method and solid-phase extraction, followed by the measurement with LSC are the most widely used.

- Successive precipitation: This process begins with an initial precipitation with ammonium carbonate to concentrate strontium, particularly in high-volume samples, while eliminating alkali metals. The precipitate is then dissolved in fuming nitric acid, filtered, and adjusted to a pH of 5-5.2 using an ammonium acetate buffer and ammonia. Following the sample is boiled and a chromate solution is added to precipitate lead, barium, and radium interferences while still hot. Finally, yttrium is coprecipitated using iron in a basic medium with ammonia. The strontium-containing solution undergoes a final carbonate precipitation and is dissolved in 0.2 M nitric acid. This final solution is then mixed with LSC cocktail and measured.
- Solid-phase extraction: This method uses a selective resin, Sr-resin, to isolate strontium from interferences in the sample, employing a 3 M nitric acid medium to ensure quantitative strontium retention. Following retention, a two-step elution is performed: the first with a 3 M nitric acid/0.05 M oxalic acid solution to remove Pu(IV), Np(IV), Zr(IV), or Ce(IV); the second with 8 M nitric acid to eliminate residual oxalic acid and any K^+ or Ba^{2+}. Finally, a 0.05 M nitric acid

solution elutes the strontium, which is then mixed with an LSC cocktail and measured. Although the Sr-resin is effective for strontium isolation, pretreatment steps to remove organic matter or concentrate strontium are often required.

Both methods are well-established for isolating radiostrontium from complex sample matrices and interferences. However, they are labour-intensive and time-consuming, especially the successive precipitation method, which also uses high-risk reagents like chromates and fuming nitric acid. Furthermore, LSC measurement produces substantial mixed liquid waste, requiring specialized waste management procedures. For separate quantification of ^{89}Sr and ^{90}Sr, delayed counting of ^{90}Y in-growth is required [3,4]. Typically, an initial measurement of radiostrontium (^{89}Sr+^{90}Sr) is performed immediately after separation from the matrix interferences, followed by a second measurement after reaching secular equilibrium, allowing the indirect determination of ^{90}Sr through the in-growth of ^{90}Y. However, this delayed counting strategy is unsuitable for radiological emergencies or environmental monitoring, where fast and reliable results are required. To address this limitation, several methods have been developed to measure both radioisotopes simultaneously in a single measurement. These methods involve LSC using two or three energy windows or performing sequential measurements through Cherenkov and LSC. Both strategies typically result in high relative biases around 20 % [4–7].

To address these limitations and reduce mixed waste generation, a PSresin using a crown-ether extractant, CE-PSresin, was developed, showing high performance in radiostrontium determination [5,6], as explained in section 1.3.3. While CE-PSresin effectively isolates radiostrontium, it also has a strong affinity for ^{210}Pb, a naturally occurring radionuclide. Although this does not pose a problem in emergency situations (where natural radionuclide activity is negligible), it complicates environmental monitoring, where high levels of ^{210}Pb may interfere with results as it cannot be selectively eluted from the CE-PSresin.

To overcome these challenges, this thesis introduces a novel and environmentally friendly method using CE-PSresin for ^{90}Sr determination in high ^{210}Pb content samples. Additionally, a combination of CE-PSresin and α-Psresin (developed in this thesis,

Chapter 3) was evaluated for simultaneous ^{89}Sr and ^{90}Sr determination in a single measurement addressing the need for rapid, accurate, and environmentally friendly methods.

4.1.2. Plutonium

Plutonium isotopes are generally by-products of nuclear reactions, commonly associated with the nuclear industry, including nuclear reactors for energy production, the military industry, and nuclear reprocessing. All plutonium isotopes are artificial. The most commonly found and relevant isotopes, due to their long half-lives and energetic alpha decay are: ^{238}Pu, with a half-life time of 87.7 years and an alpha emission of 5.59 MeV, produced by neutron capture of ^{237}Np in reactors, producing the unstable ^{238}Np that decay into ^{238}Pu in few days; ^{239}Pu is produced by neutron capture of ^{238}U and has a half-life of 24100 years and a alpha emission of 5.15 MeV; and ^{240}Pu, produced when ^{239}Pu captures an additional neutron and with a half-life of 6560 years and an alpha emission of 5.25 MeV.

Plutonium isotopes can be found in environment at very low activities, primarily as a result of nuclear weapon testing conducted during the 1950s and 1960s. Additional contributions comes from nuclear accidents (i.e., Chernobyl (1986) or Thule (1968)) and isolated releases from reprocessing plants [8]. Consequently, plutonium determination is not only limited to nuclear emergencies but also for environmental monitoring.

Plutonium isotopes pose long-term environmental concerns due to their persistence and low mobility. Unlike radiostrontium, plutonium isotopes tend to adhere strongly to soil particles, limiting their movement through ecosystems. However, when introduced to water bodies, plutonium can bind to sediments. Since plutonium isotopes are not readily absorbed by plants, their primary route into the human body is through inhalation of contaminated dust or ingestion of particles, typically from soil resuspension in contaminated areas. Once inhaled or ingested, plutonium has a strong affinity for bone and liver tissue, where it deposits and continues emitting radiation, increasing risk of cancer in different tissues over time.

Plutonium chemistry is complex, characterized by the multiple oxidation's states in aqueous solution. Plutonium mainly exists in four oxidation states—Pu(III), Pu(IV), Pu(V),

and Pu(VI) being Pu(III) and Pu(IV) the most stable under acidic conditions and Pu(V) and Pu(VI) on alkaline conditions. This rich chemical behaviour complicates plutonium isolation, as the coexistence of multiple oxidation states in solution complicates chemical separation because each form requires different reagents and conditions for the effective extraction increasing the complexity and cost of its determination.

For plutonium isolation, several chemical separation techniques are used for plutonium isolation, yet the most common are solvent extraction, ion exchange chromatography, and extraction chromatography [8].

- Solvent extraction: Organic solvents for this goal include TTA (thenoyltrifluoroacetone)-benzene [9] with a quantitative chemical yield recovery or TOA-Xylene solution with a chemical yield recovery ranging between 50 to 70 % [10]. For example, TTA-bencene extraction requires an initial valence adjustment of plutonium via oxidation with $NaNO_2$, followed by back-extraction with 10 M nitric acid. Solvent extraction allows for fine-tuning of selectivity and high recoveries; however, it is generally impractical for routine analyses because achieving complete separation requires multiple sequential extraction steps, making it time-intensive. Additionally, challenges such as phase separation issues and partial solubility of the phases can lead to notable plutonium losses. The process also generates a significant volume of hazardous organic waste, adding environmental concerns.
- Ion exchange chromatography: The separation of plutonium using anion-exchange techniques is based on the strong affinity of Pu(IV) anion complexes for the resin in a nitric acid medium, where Pu(IV) forms stable nitrate complexes with NO_3^-. Most elements do not form anion complexes in this acidic medium, meaning they are not retained on the anion-exchange column. Additionally, Pu in its III, V, and VI oxidation states, along with other transuranic elements, do not form anionic complexes, further facilitating selective retention of Pu(IV). Thorium behaves similarly to Pu(IV) by forming a strong nitrate complex, while uranium forms only a weak nitrate complex, allowing for efficient separation of uranium from plutonium within the nitric acid medium. Generally, plutonium isolation is accomplished by valence

adjustment of the target analyte. The sample is loaded onto anion-exchange column in high nitric acid concentrations (8 M), few rinses with the same solution are performed to remove Am and U, and rises with 9–12 M HCl to remove Th. Finally, elution of Pu is achieved by reducing plutonium to plutonium (III). Some examples of anion-exchange resins are Dowex 1 × 8 for which a 60 % plutonium recovery yield is achieved or Bio Rad AG 1 × 8 for which a 80 % plutonium recovery yield is achieved[11,12]. Anion exchange chromatography allows a good isolation of plutonium, however, the process in some case is very slow as the oxidation or reduction reaction for the striping can take more than hours given.

- Extraction chromatography: A notable example for plutonium isolation is with the use of TEVA-resin. Teva-resin is composed of a quaternary amine immobilized on a polymeric support. It presents a high affinity for actinides in 2-4 M nitric acid or HCl. The loaded sample is firstly adjusted to Pu(IV) and loaded in the TEVA-resin under 3 M nitric acid, afterwards, rinses with HCl solution are performed to eliminate interferences and finally plutonium is eluted by 0.1 M nitric acid-0.1 M HF, achieving a plutonium chemical recovery in soils, seaweed and sediments ranging between 70 to 92 % with decontamination factors of 10^5 for U, Th and Am [13]. Extraction chromatography is the chemical separation method which ensure higher plutonium recoveries in less time and reagent consumption compared to the other two chemical separation methods discussed.

Post chemical separation, plutonium quantification can be performed using alpha spectrometry or LSC, being alpha spectrometry the technique most used to quantify plutonium isotopes thanks to its lowest detection limit due to an extremely low background. Nevertheless, the preparation of alpha sources is time consuming and not suitable for fast or emergency uses. Liquid scintillation can also be used for plutonium analysis since it has acceptable detection limits and sample preparation for measurement is easy. However, mixed wastes are produced posing environmental concern.

Regardless of the separation strategy and the detection technique used, plutonium analysis is a lengthy task and involves a large use of reagents and the generation of mixed wastes (particularly in LSC). For that reason, in this chapter a green method using a PSresin based on aliquat·336, AL-PSresin [14] has been developed, for the determination of plutonium intended for emergency situations where fast, and high plutonium recoveries are required. Additionally, given the common source generation of radiostrontium and plutonium a common analytical method has been developed for their sequential quantification using AL-PSresin and CE-PSresin.

4.2. Results

The results of this chapter are classified into three scientific publications. Article #5, focused on the development of a new strategy using CE-PSresin for radiostrontium analysis in environmental samples with ^{210}Pb. Article #6 is based on the use of PSresin for plutonium isotopes determination in river and seawater samples and article #7 for sequential determination of a mixture of radionuclides (^{90}Sr+^{89}Sr and ^{90}Sr + plutonium isotopes) in river water samples using sequential PSresin's. Finally, the chapter finish with a global discussion where all works are further discussed.

These scientific publications are:

Article #5: I. Giménez, J. Rotger, E. Apellániz, H. Bagán, J. Tent, A. Rigol, A. Tarancón, A new method based on selective fluorescent polymers (PSresin) for the analysis of ^{90}Sr in the presence of ^{210}Pb in environmental samples, Applied Radiation and Isotopes 199 (2023). https://doi.org/10.1016/j.apradiso.2023.110879.

Article #6: A. Torres, **I. Giménez**, H. Bagán, A. Tarancón, Analysis of isotopes of plutonium in water samples with a PSresin based on aliquat·336, Applied Radiation and Isotopes 187 (2022) 110333. https://doi.org/10.1016/j.apradiso.2022.110333.

Article #7: I. Giménez, H. Bagán, A. Tarancón, Simultaneous radionuclide determination using PSresin: 2in2 and 2in1 tandem configuration, Anal Chim Acta 1337 (2025) 343573. https://doi.org/10.1016/j.aca.2024.343573

Article #5

A new method based on selective fluorescent polymers (PSresin) for the analysis of ^{90}Sr in the presence of ^{210}Pb in environmental samples

Applied Radiation and Isotopes 199 (2023) 110879

Contents lists available at ScienceDirect

Applied Radiation and Isotopes

journal homepage: www.elsevier.com/locate/apradiso

A new method based on selective fluorescent polymers (PSresin) for the analysis of ^{90}Sr in presence of ^{210}Pb in environmental samples

I. Giménez [a,1], J. Rotger [a,1], E. Apellániz [a], H. Bagán [a], J. Tent [a], A. Rigol [a,c], A. Tarancón [a,b,c,*]

[a] Departament d'Enginyeria Química i Química Analítica, Universitat de Barcelona, Marti i Franqués, 1-11, ES, 08028, Barcelona, Spain
[b] Serra-Húnter Programme, Generalitat de Catalunya, Barcelona, Spain
[c] Institut de Recerca de l'Aigua, Universitat de Barcelona, Spain

A B S T R A C T

^{90}Sr is of major concern in emergency and environmental control plans. It is one of the main fission products in nuclear facilities and is a high-energy beta emitter that presents chemical properties similar to those of calcium. ^{90}Sr is commonly detected using methods based on liquid scintillation counting (LSC) following a chemical separation to remove potential interferences. However, these methods generate mixed wastes (hazardous and radioactive). In recent years, an alternative strategy using PSresins has been developed. For ^{90}Sr analysis with PSresins, ^{210}Pb is the main interferent that should be considered, as it is also strongly retained in the PSresin. In this study, a procedure was developed involving a precipitation with iodates to separate lead from strontium before the PSresin separation. Moreover, the method developed was compared with well-established and routinely used methods based on LSC, revealing that the new method produced equivalent results in less time and with less waste generation.

1. Introduction

Nuclear energy currently accounts for up to 11.5% of global electricity production (Schneider et al., 2022). This energy source offers the advantage of being carbon dioxide (CO_2) emission-free, making it a valuable tool in the strategy against climate change. Additionally, it is a cost-effective source of energy. However, it carries the risk of environmental contamination, particularly in the event of accidents or uncontrolled spills during nuclear power plant (NPP) operations and decommissioning, which can result in the release of radionuclides into the environment. To mitigate the potential damage caused by such incidents, efficient environmental monitoring is crucial. Among the pure beta-emitting radionuclides that could contaminate the environment, ^{90}Sr (E_{max}: 545.9 keV) is of particular interest in environmental measurements because it is one of the main ^{235}U fission products and may remain in the environment for a longer time due to its long half-life ($T_{1/2}$: 28.80 years) (Bé et al., 2016). The danger of ^{90}Sr stems from its high mobility, migrating from rivers and soils into food chains. It can contaminate products like milk, as it shares physicochemical properties with calcium and can be absorbed into the body. Once ingested, it becomes a source of radiation in the bones. The Spanish normative, following European directives and international recommendations, has set the limit of ^{90}Sr in drinking water at 4.9 Bq/L (REAL DECRETO 3, 2023).

Historically, ^{90}Sr analysis has been a matter of concern due to the need to separate out interferences prior to beta counting. Various methods have been described in the literature for ^{90}Sr analysis, with the main difference being the strategy followed to separate out the most common interferents (Vajda and Kim, 2010). One of the most used methods is the one recommended by the International Atomic Energy Agency (IAEA). It involves the separation of strontium from interferents, mainly calcium but also lead, yttrium or actinides, by exploiting the different solubility of the respective nitrates, chromates and hydroxides using fuming nitric acid and chromate as the precipitating agents (IAEA et al., 1989; Tayeb et al., 2015; Johnson et al., Pecora). This method is laborious, and to achieve good separation, the precipitations need to be repeated several times. The methods in the literature often include a preliminary precipitation step (for separation or sample concentration) followed by other separation strategies. Chobola et al. (2006) recommended first preconcentrating the strontium in an alkaline medium by precipitating with carbonates, whereas Maxwell and Culligan (2009) suggested coprecipitation of strontium along with calcium using phosphate. Several methods suggest the use of extraction chromatography for ^{90}Sr isolation. Extraction chromatography or solid-phase extraction follows the same principles as solvent extraction, but the compounds that interact selectively with the target element are impregnated in a

* Corresponding author. Departament d'Enginyeria Química i Química Analítica, Universitat de Barcelona, Marti i Franqués, 1-11, ES, 08028, Barcelona, Spain.
E-mail address: alex.tarancon@ub.edu (A. Tarancón).
[1] Both authors contributed equally to the development of this work.

https://doi.org/10.1016/j.apradiso.2023.110879
Received 22 December 2022; Received in revised form 22 May 2023; Accepted 25 May 2023
Available online 26 May 2023

solid support (i.e, resin) and placed in a chromatographic column. As an example, is the case of the Sr-Resin developed by Eichrom Technologies (Eichrom Technologies, 2014) and based on the work of Horwitz et al. (1991). This extraction chromatography resin contains a crown ether, 4, 4′(5')-di-t-butylcyclohexano-18-crown-6 (DtBuCH18C6), that specifically retains strontium through a complexation in a strong nitric media solution, effectively removing interfering cations. After elution, the strontium can be measured using a liquid scintillation counter or a proportional counter (Triskem International, 2015).

Although the pretreatment methods for Sr analysis are robust and several applications have been established, they do have certain weaknesses. For example, lengthy procedures can be a problem in emergency situations. Furthermore, measuring ^{90}Sr by liquid scintillation generates a significant amount of mixed liquid waste (hazardous and radioactive). Proper management of this kind of waste requires specific treatment procedures. Moreover, the use of hazardous reagents such as fuming nitric acid and chromates poses risks for the analyst. In this context, new methods are being developed to reduce procedure length, waste generated and the use of dangerous reagents. One promising approach involves the use of plastic scintillation resins (PSresins).

PSresins are produced by immobilizing a selective extractant, which is specific for a certain radionuclide, onto the surface of plastic scintillation microspheres (Coma et al., 2019; Torres et al., 2022; Giménez et al., 2021). These PSresins, when packaged in a solid-phase extraction (SPE) cartridge, offer several advantages. Firstly, they integrate the separation and measurement process into a single step, eliminating the need for liquid scintillators and thus reducing the generation of mixed wastes. Furthermore, it reduces the number of procedure steps by eliminating the requirement for elution or processing of the measuring sample. Moreover, the use of fuming nitric acid to remove interferents is avoided.

This approach has been already applied for radiostrontium (Bagán et al., 2011) using 4′,4''(5″)-di-tert-butyldicyclohexane-18-crown-6 in 1-octanol (Sr-PSresin) as the extractant (Sáez-Muñoz et al., 2018). However, it has been observed that there are other elements, such as lead, that are also retained in the column and cannot be eluted. In fact, that same PSresin can be used to measure ^{210}Pb (Lluch et al., 2016), a naturally occurring low beta-emitting radionuclide that could be present in environmental samples. When both ^{210}Pb and ^{90}Sr are measured with the PSresin, the ^{210}Pb spectrum overlaps with part of the ^{90}Sr spectrum when the measured immediately after separation (Fig. 1). This overlap persists throughout the whole spectrum when secular equilibrium was achieved after 21 days due to the ingrowth of ^{210}Bi. Therefore, quantification of ^{90}Sr can only be performed at t = 0 in the region above channel 450, where the influence of ^{210}Pb is minimal, or at 21 days if all the Pb has been completely removed from the loading sample. Removal of Pb is crucial to avoid quantification errors and false positive results. Precipitation methods can be effective in achieving separation if one of the elements (target or interferent) precipitates quantitatively. In the case of extraction chromatography, successful separation can be achieved if the target or the interferent is retained or eluted quantitatively during loading, cleaning or elution. With the PSresin, as the target radionuclide must remain in the column for later measurement, the interferent (Pb) cannot be retained during loading or cleaning stages. Since Pb has a higher affinity for the crown ether than Sr, a selective precipitation is necessary before column separation to prevent the loading and retention of ^{210}Pb in the PSresin.

This study presents a novel analytical method for the measurement of ^{90}Sr in environmental samples, even in the presence of ^{210}Pb, utilizing PSresins. The proposed method demonstrates successful quantification through the utilization of optimal windows and a selective pretreatment procedure involving the precipitation of strontium before passing it through the PSresin. A comprehensive comparison of this new method with various standard methods currently in use has been conducted.

2. Experimental

2.1. Reagents and solutions

All the reagents used were of analytical grade and double deionized water was used. Lead and strontium standards (10000 mg/L) were from Inorganic Ventures (Christiansburg, USA). Iron solution of 5 mg/L was prepared with iron nitrate (III) supplied by Sigma Aldrich (Burlington, MA, USA). Nitric acid (69%), ammonia (25%) and oxalic acid were supplied by PanReac (Castellar del Vallés, Spain). Crown ether, 4′,4''(5″)-di-tert-butyldicyclohexane-18-crown-6, 1-octanol, sodium iodate, di-ammonium hydrogen phosphate, potassium iodate and calcium nitrate were supplied by Sigma Aldrich (Burlington, MA, USA). A ^{210}Pb active stock solution of 160 Bq/g (4.8) was prepared from a standard of 35.5 kBq/g (1.1) (CEA/DAMRI, Gif-Sur-Yvette CEDEX, France) with 22 years of ingrowth, while a ^{90}Sr/^{90}Y active stock solution of 38.45 Bq/g (0.29) was prepared from a standard of 4071 Bq/g (31) in a solution of strontium (100 μg/g) and yttrium (100 μg/g) in 0.1 M HCl (Amersham International, Buckinghamshire, England).

Sr-PSresin was prepared following a procedure developed in (Bagán et al., 2011) using plastic scintillation microspheres of 60 μm (Santiago et al., 2013) and the crown ether. Sr-Resin in 2 mL cartridges were supplied by TrisKem International (Rennes, France).

Empty SPE cartridges (2 mL) and frits were supplied by TrisKem International (Rennes, France). 20 mL polyethylene vials and the Gold XR liquid scintillation cocktail were purchased from PerkinElmer (Waltham, USA).

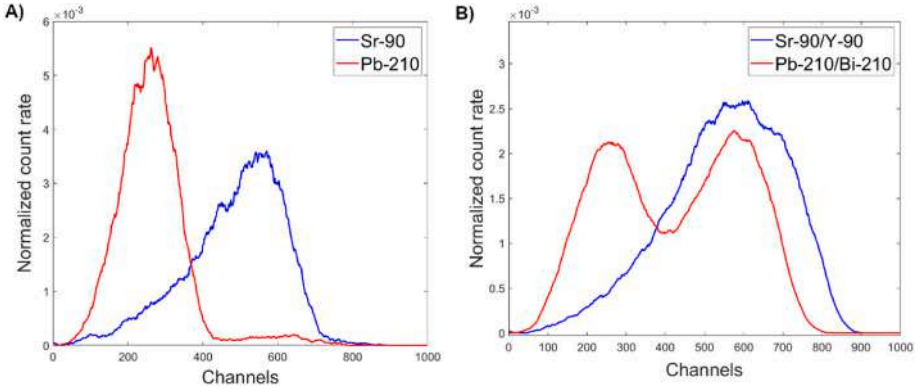

Fig. 1. ^{210}Pb (red) and ^{90}Sr (blue) normalized spectra in the PSresin at time 0 (A) and with ingrowth daughters at time >21 days (B). (For interpretation of the references to colour in this figure legend, the reader is referred to the web version of this article.)

2.2. Samples

The samples analyzed for method comparison were:

- River water sample

Spiked river water samples were prepared by adding known amounts of ^{210}Pb and ^{90}Sr/^{90}Y standards to river water obtained from the Ebro River in Ascó (Tarragona, Spain). The samples were filtered through a 0.45-μm filter before being spiked. Two activity levels were prepared: 4.9 Bq/L and 0.49 Bq/L.

- MAPEP water samples

Two interlaboratory samples from the MAPEP program were used: MAPEP-16-MaW34, with a ^{90}Sr activity range of 5.65–10.48 Bq/L, and MAPEP-10-MaW22 without strontium. The samples were diluted 1:10.

- CSN Interlaboratory water sample (CSN sample)

An interlaboratory sample from the Consejo Seguridad Nuclear (CSN) with a ^{90}Sr activity of 4.1 Bq/L (0.2) was used. This sample contains other radionuclides, with ^{57}Co (4.7 Bq/L), ^{60}Co (3.1 Bq/L), ^{134}Cs (3.8 Bq/L), ^{238}Pu (0.41 Bq/L), ^{226}Ra (0.62 Bq/L), ^{210}Pb (0.62 Bq/L) and ^{228}Ra (1.12 Bq/L) being the most relevant.

2.3. Apparatus

A Quantulus 1220 liquid scintillation spectrometer (PerkinElmer, Waltham, USA) with logarithmic amplification, a multichannel analyzer (MCA) (4096 channels distributed in four segments of 1024), alpha/beta discrimination and background reduction via an active guard were used for the scintillation measurements.

The analysis of stable strontium and lead for yield determination was undertaken using an OPTIMA 8300 ICP-OES detector (PerkinElmer, Waltham, USA) or an ELAN-6000 ICP-MS detector (PerkinElmer, Waltham, USA) from the Technological and Scientific Centres of the University of Barcelona (CCiT-UB).

2.4. Procedures

2.4.1. Preparation of the Sr-PSresin cartridges

Sr-PSresin cartridges (Coma et al., 2019) were prepared by filling a 2 mL SPE cartridge with 1.4 g of Sr-PSresin into. The cartridges were sealed with a filter and a stopper. To ensure PSresin homogenization, the cartridges were placed in a vacuum chamber, and 10 mL of water were passed through each one at a flow rate of 1 mL/min. Prior to loading the sample onto the cartridge, each column was vortexed for 3 min at 3000 rpm.

2.4.2. Study of preliminary precipitation methods previous to PSresin separation

A preliminary study was conducted to investigate the necessary pretreatment for separating Pb and Sr before passing through the PSresin was performed. The aim was to identify the precipitation method that yielded optimal results for the purpose of the paper. For this study, four samples were prepared in 25 mL conical tubes, each containing 5 mg of lead and 5 mg of strontium. Later, both metals were measured in the different solutions obtained using ICP-OES to confirm if the separation was achieved and to determine the separation yield.

- Separation of lead and strontium by oxalate precipitation

3 g of oxalic acid and 2 g of calcium nitrate were added to the samples. The mixture was placed in a water bath at 45 °*C* for 15 min. NH_3 was added until the pH ranged between 4 and 6.5, leading to the precipitation of strontium. The tubes were centrifuged at 5000 rpm for 5 min to separate the precipitate from the supernatant where lead should remain. The precipitate was further xtreated with 8 M nitric acid and placed in a water bath for 45 min at 45 °*C* for solubilization.

- Separation of lead and strontium by chromate precipitation

4.85 g of potassium chromate and 0.4 g of barium nitrate were added to the samples. The mixture was placed in a water bath for 1 h at 45 °*C* to maximize the solubilization of strontium chromate. Nitric acid was then added to the samples until the pH reached a range between 3 and 5.5, measured with a pH-meter. Within this pH interval, lead precipitates while strontium remains in solution. The samples were centrifuged for 5 min at 5000 rpm. The supernatant was separated and adjusted with ammonia until the pH ranged between 8 and 10, causing strontium to precipitate. To facilitate coprecipitation of strontium, 0.2 g of barium, in the form of barium nitrate, was added during this step. The tubes were centrifuged once again and the strontium precipitate was separated from the supernatant. The precipitate was treated with nitric acid and placed in a water bath at 45 °*C* for solubilization.

- Separation of lead and strontium by iodate precipitation

1 g of sodium iodate and 0.41 g of calcium nitrate were added to the samples. The mixture was then placed in a water bath for 15–20 min at 45 °*C*. The solution was adjusted, if necessary, to a pH range of 1 and 8 using nitric acid to facilitate the precipitation of lead. Afterward, the samples were centrifuged for 5 min at 5000 rpm. The supernatant, where strontium should remain, was separated from the solid. The solid, containing only lead, was dissolved with nitric acid and put in a water bath for 10 min.

- Separation of lead and strontium by hydrogen phosphate and citrate precipitation

0.125 g of di-ammonium hydrogen citrate and 0.25 g of di-ammonium hydrogen phosphate were added to the samples. The mixture was then neutralized to pH 7. As a result, the solution became cloudy, indicating the formation the formation of to lead phosphate, and was left to stir for 10 min. Subsequently, the solution was filtered, and the resulting solution was adjusted to a pH of 10, causing the formation of a suspended strontium precipitate. The mixture was allowed to sit for 30 min without stirring before the tubes were centrifuged. The supernatant was separated from the precipitate. The solid precipitate, containing only strontium, was dissolved with nitric acid.

2.4.3. Methods for ^{90}Sr analysis

The performance of the PSresin method was compared with two methods already employed in our laboratory for the analysis of ^{90}Sr. The detailed procedures for each method are described next.

- Extraction chromatography-LSC (EC-LSC)

A 100 mL aliquot of the interlaboratory water sample from the CSN was spiked with 5 mg of a strontium solution and evaporated to dryness. The resulting solid was reconstituted with 10 mL of 3 M nitric acid. Sr-Resin TrisKem cartridges were then placed in a vacuum chamber and conditioned with 20 mL of 3 M nitric acid at a flow rate of 1 mL/min. Subsequently, 10 mL of the sample were passed through the cartridges at a flow rate of 2 mL/min, followed by two elutions. The first involved 10 mL of a 3 M nitric acid/0.05 M oxalic acid solution (1 mL/min) ro remove Pu(IV), Np(IV), Zr(IV) or Ce(IV), which could be retained by Sr-Resin. The second elution utilized 10 mL of 8 M nitric acid to remove any remaining oxalic acid and ensure complete removal of K^+ and Ba^{2+}. Finally, the strontium retained in the cartridges was eluted with 30 mL of 0.05 M nitric acid. The resulting solution was evaporated to dryness

and reconstituted with 20 mL of 0.2 M nitric acid. 8 mL of this final sample were mixed with 12 mL of scintillation cocktail (Ultima Gold XR) and measured in a Quantulus detector. The final sample was also analyzed by ICP-OES to determine the amount of stable strontium present. The ICP-OES results were used to calculate the strontium recovery by comparing the amount of stable strontium initially added to each sample. Three replicate samples were analyzed.

- Successive precipitations-LSC (SUC-LSC)

1 L of the river water sample spiked with ^{90}Sr was analyzed. The sample was filtered through a fiberglass filter (1.6 μm porous size). To the filtered solution, 56 mg of stable strontium was added, followed by heating and stirring. Subsequently, 1 mL of 25% ammonia and 20 g of ammonium carbonate were added. After the solution reached room temperature, it was filtered through a fiberglass filter (1.6 μm porous size). The resulting precipitate was redissolved with 8 M nitric acid (10 mL) and double deionized water (10 mL). To this solution, 50 mL of fuming nitric acid were added, and another filtration step was performed using fiberglass filter with a porous size of 1.6 μm. The precipitate was redissolved in 20 mL of double deionized water. The process of isolating the precipitate and redissolving it was repeated after the addition of 60 mL of fuming nitric acid. Following this, 0.5 mL of a stable barium solution (10 mg/L) were added, followed by 4 M ammonia to achieve a pH of 5–5.2 and 1.5 mL of an ammonium acetate buffer solution (pH 5.2). The solution was heated to boiling and 0.5 mL of a 1.5 M sodium chromate solution were added. After cooling the solution, it was filtered once again using a fiberglass filter (1.6 μm porous size). Subsequently, 1 mL of 25% ammonia and 20 g/L ammonium carbonate were added to the filtered solution. The mixture was heated and filtered again using a fiberglass filter (1.6 μm porous size) once it reached room temperature. The solid obtained was redissolved in 10 mL of 4 M nitric acid and 20 mL of water. To this solution, 1 mL of a 6% hydrogen peroxide solution and 0.5 mL of a 5 mg/L iron (III) solution were added. The solution was boiled for 10 min, followed by 15 mL of 25% ammonia to achieve a pH of between 9 and 10. After cooling to room temperature, another filtration step was carried out using a fiberglass filter (1.6 μm porous size), with the solid washed with diluted ammonia before the addition of ammonium carbonate to the filtered solution. The solution was heated, before cooling it down and filtering it through a fiberglass filter (1.6 μm porous size). The resulting precipitate was redissolved with 40 mL of 0.2 M nitric acid. The solution was then evaporated to dryness and reconstituted with 20 mL of 0.2 M nitric acid. For measurements, 8 mL of the final sample solution were mixed with 12 mL of the Ultima Gold XR liquid scintillation cocktail and analyzed using a Quantulus detector. In addition, the final sample was analyzed using ICP-OES to determine the concentration of stable strontium present, enabling the calculation of recovery. Only one replicate was analyzed.

- PSresin method

This method consisted of two steps: the precipitation of strontium using phosphate and iodate, followed by final separation with the PSresin. The selection of the pretreatment was based on the results obtained from the preliminary study (sections 3.4.2 and 4.1).

Samples containing known activity of ^{90}Sr and ^{210}Pb were prepared in beakers. 1 g of sodium iodate as the precipitating agent and 0.41 g of calcium nitrate were added to the samples. The beakers were boiled for 15 min and then centrifuged for 5 min at 5000 rpm. The supernatant was decanted, and 0.5 g of di-ammonium hydrogen phosphate was added. Ammonia was added until a pH of 10 was reached, resulting in the formation of a strontium precipitate. This step is crucial to remove other matrix interferences that are not separated during the iodate precipitation. The mixture was centrifuged again, and the supernatant was decanted. The remaining solid was dissolved in 11.5 mL of 8 M nitric acid. Subsequently, 10 mL of this solution were passed through the PSresin cartridge. Fig. 2 illustrates the procedure diagram.

PSresin cartridges were connected to a vacuum box, and the pressure was adjusted to 5 inHg. They were then conditioned with 2 mL of 8 M nitric acid. Next, 10 mL of the sample were passed. Afterward, two rinses with 2 mL of 8 M nitric acid and two rinses with 2 mL of 6 M lithium nitrate were performed. Finally, the cartridges were left for 5 min at 20 inHg to remove any remaining solution between the PSresin particles. The PSresin cartridges were placed in a 20 mL polyethylene scintillation vial for measurement. The solution that passed through the PSresin was collected in a 50 mL conical tube to determine the yield.

2.5. Measurements

All the measurements with the Quantulus detector were performed in the low coincident bias and "^{14}C" configuration.

The samples were measured immediately after separation to prevent ^{90}Y ingrowth, using 3 cycles of 20 min with 10 min for the SQP(E) parameter. The river water samples, having an activity of 0.49 Bq/L, and the MAPEP samples were measured in 15 cycles of 20 min, with 10 min for the SQP(E). Blank samples were measured using the same time durations.

The samples were measured after 21 days for 12 h, with 10 min for the SQP(E).

The ICP-OES samples were prepared by diluting a certain amount of solution with 1% nitric acid to achieve a maximum concentration of 5 mg/L of Sr or Pb. The fractions measured included solutions from the preliminary study that might contain lead or strontium, samples from the different steps of the separation procedure, eluted solutions from the PSresin cartridge and the Sr-Resin as well as he initial samples and standards.

2.6. Data treatment

The spectra obtained from the scintillation measurements were smoothed using the Savitzky–Golay algorithm, with an average window of 21 points and a first-degree polynomial. The smoothing process was applied within the range channels 1 to 1024. The net spectrum was obtained by subtracting the spectrum of the corresponding blank solution. The detection efficiency spectrum was obtained as the ratio between the net counts in each channel and the activity in the PSresin cartridge.

The uncertainty values quoted correspond in all cases to the standard deviation of replicate measurements.

The optimal windows were determined using in-house program built in Matlab 2019 (Mathworks, Natick, Massachusetts, USA). The program calculated the figure of merit (Eff^2/Bkg) for several channel windows and identifies the region with the highest FM value.

The Medusa/Hydra free software (Royal Institute of Technology, Stockholm, Sweden) was used to simulate the chemical equilibrium and plot the logarithm of the concentration against pH variation (1–14) for the different precipitating agents investigated. The simulations were conducted using a 100 mL volume containing 5 mg of Sr and 5 mg of Pb, with the precipitating agents present at a concentration of 1 M.

3. Results and discussion

The work was divided into two sections. The first section aimed to investigate various precipitation pre-treatments to selectively remove Pb from Sr prior to passing the sample to the PSresin. In the second section, the final procedure, including precipitation, separation, and measurement of Sr using the PSresin, was validated by comparing it with established reference methods.

3.1. Preliminary lead separation studies

The initial phase involved investigating different precipitation pre-

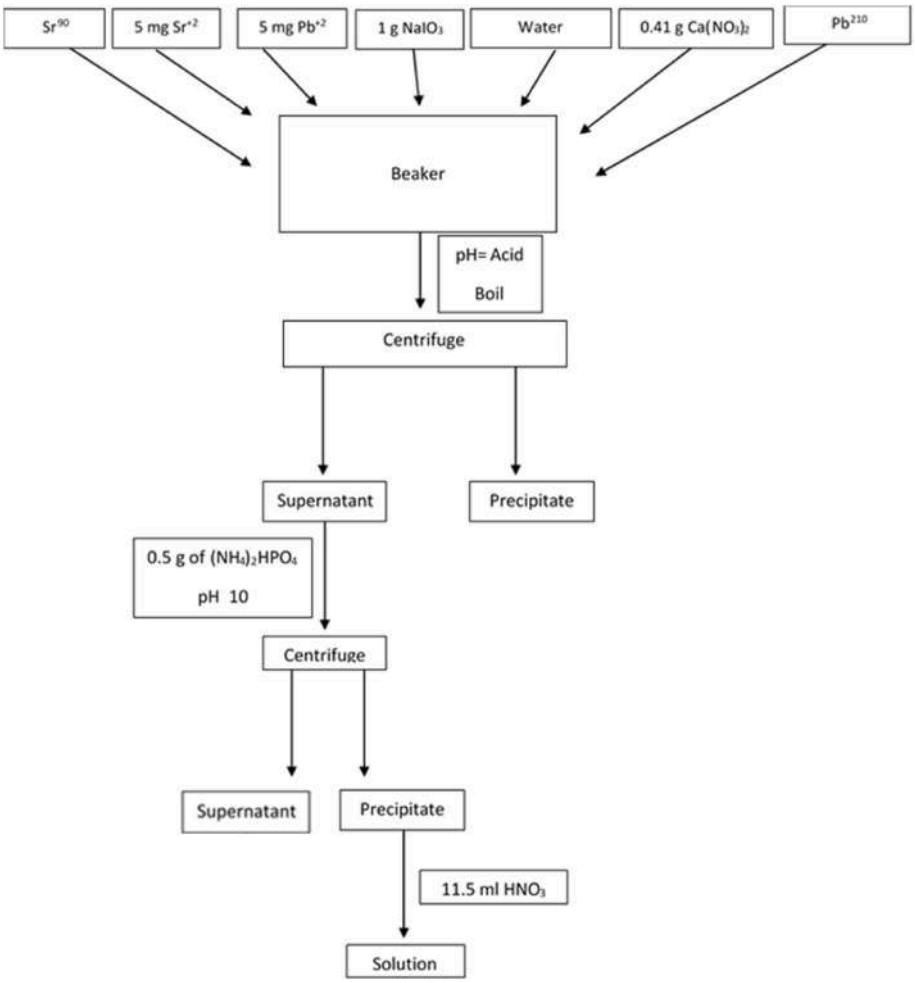

Fig. 2. Pre-treatment involving the use of iodate and phosphate to precipitate strontium.

treatments in which Pb could be removed selectively from Sr. The selection of methods was based on their descriptions in the literature and the results obtained from the software Medusa. Four different precipitation methods were evaluated, namely oxalate, hydrogen phosphate plus citrate, chromate or iodate. Table 1 shows the recovery of Sr and Pb in the solution after the application of each procedure to four replicate samples.

The hydrogen phosphate plus citrate method demonstrated a separation efficiency of 59% (11) of Sr, carrying with only 6% (8) of Pb being carried along. However, this method was quite irreproducible, as indicated by the standard deviations and the RSD values associated with it. This is not, in fact, a problem for Sr, but it poses a concern for Pb, as there is a probability that Pb may reach the PSresin cartridge. In one of the replicates, 18% of Pb remained in the solution. Due to the lack of reproducibility, this method was not selected for further use.

The chromate proved effective in separating Sr, with almost no Pb remaining in the solution. It resulted in the lowest concentration of Pb in the strontium fraction compared to other methods. However, the yield of Sr was too low and the method displayed low reproducibility. Moreover, the use of chromate is not recommended due to its toxicity. However, the main reason for discarding this method was the yellow solution, which would produce color quenching when loaded into the PSresin cartridge, thereby decreasing the detection efficiency.

In the iodate method, a recovery of 72% (2) for Sr and only 5% (1) of Pb was achieved. On first sight, this method was more reproducible than the phosphate method, with better recovery rates. However, it was observed that in the initial acidic medium, both metals precipitated upon the addition of iodate, contradicting the indications from the Medusa diagrams which suggested only Pb would precipitate. By adding 8 M nitric acid, only strontium iodate dissolved, effectively separating Sr from Pb. Despite this discrepancy, this iodate method could be optimal for the separation of Sr from Pb.

Finally, precipitation with oxalate did not result in a satisfactory separation as both metals were precipitated and dissolved together, without achieving the desired selectivity.

Among the four methods, precipitation with iodates was selected. Even with that, the precipitation of Pb and Sr was temperature-dependent, as strontium iodate could be redissolved in boiling water (Sunderman and Townley, 1960). Therefore, separation using this method was not consistently satisfactory.

Bearing in mind the results from the preliminary study and the available literature, a final procedure was developed (experimental section 3.4.3) that was suitable for use with the Sr-PSresin. In this procedure, the precipitation of Sr from the sample was carried out using iodate and calcium as a coprecipitating agent, along with the boiling of

Table 1
Recovery of strontium and lead from the sample after applying the precipitation procedure, expressed as the mean plus standard deviation in brackets. 4 replicates were done for each method.

Method	Sr %	Pb %
Oxalate	83 (2)	103 (4)
Hydrogen phosphate + citrate	59 (11)	6 (8)
Chromate	31 (15)	0.65 (0.03)
Iodate	72 (2)	5 (1)

the sample. Increasing the temperature resulted in an increase in the solubility of Sr, allowing it to remain in solution while lead iodate precipitated. After removing the lead iodate precipitate, Sr was precipitated using hydrogen phosphate in a basic medium and subsequently dissolved in 8 M nitric acid for passage through the PSresin. This method was proven successful in achieving a nearly complete recovery of Sr, with only 3% of Pb remaining (Table 2), effectively eliminating any potential matrix interference. Furthermore, the method demonstrated good reproducibility.

The absence of ^{210}Pb in the PSresin was verified by examining the spectra obtained from cartridge measurements (Fig. 3). It was observed the absence of any peak within the energy channel range of 100–400. This confirmed that there was no presence of ^{210}Pb in the PSresin.

Once the method development was complete, the detection efficiency for ^{90}Sr in the PSresin was determined by analyzing three replicate standard samples of 10 mL. The integration window was selected following the study of the figure of merit, which involved choosing the window with the highest difference between the ^{210}Pb and ^{90}Sr spectra. To achieve this, the spectrum of a standard sample of ^{210}Pb was utilized as reference for the blank, while the spectrum of the ^{90}Sr standard served as the sample. This approach generated a channel range where the influence of ^{210}Pb on ^{90}Sr was minimal. Table 3 presents the detection efficiency values immediately after separation and after a 21-day period in the optimal window.

Concerning the selected optimal windows, it is important to note that immediately after separation, the contribution of Pb to the counting rate was minimal, as indicated by the absence of any signal from ^{210}Pb above 450 (Fig. 1). However, at equilibrium, there was a noticeable overlap with ^{210}Bi, highlighting the need for effective separation of ^{210}Pb from ^{90}Sr.

The complete method was initially validated by applying it to two different interlaboratory samples (MAPEP-16-MaW34 and MAPEP-10-MaW22). Table 4 shows the results obtained for both samples. For the MAPEP-16-MaW34 sample, the results obtained fell within the acceptable range for both time zero and secular equilibrium. Regarding the MAPEP-10-MaW22 sample, the results obtained were satisfactory because the sample did not contain ^{90}Sr and the count rate registered was below the limit of detection.

3.2. Validation through method's comparation

The method validation was performed by comparing the PSresin method with the two most common methods for ^{90}Sr analysis:

- EC-LSC method was compared with the PSresin method using a water sample with medium ^{90}Sr activity that also contained other radionuclides.
- The SUC-LSC method was compared with the PSresin method using a river water sample spiked with a very low activity of ^{90}Sr.

3.2.1. EC-LSC vs the PSresin method

100 mL of an interlaboratory water sample from the CSN with a theoretical ^{90}Sr activity of 4.1 Bq/L (0.2) (CSN sample) and containing several interferents was analyzed following two different procedures: (1) The EC-LSC method (Triskem International, 2015) (Triskem International, 2023) and (2) The PSresin method with Pb separation (PSresin). Three replicate samples were analyzed by each method. The results obtained are summarized in Table 5.

The Sr recoveries varied for each method, but they were all acceptable as they were higher than 50%, which can be considered the minimum value acceptable to keep the variability associated to the yield determination in an acceptable range. The PSresin method achieved a high recovery, indicating that the precipitation with iodate and phosphate was nearly quantitative. In addition, the PSresin method efficiently removed almost all the Pb, with only 6% (2) remaining in the sample. In contrast, The EC-LSC method yielded lower recoveries, possibly due to the step of Sr elution, where some Sr might have remained retained in the Sr-Resin cartridge.

Regarding the determination of ^{90}Sr activity, the EC-LSC method consistently yielded accurate and reproducible results. In contrast, the PSresin method for immediate measurements produced slightly higher values for ^{90}Sr activity, which were still within the acceptance range when taking into account the measurement variability. After 21 days, the bias in the PSresin method was corrected, resulting in values that closely approached both the theoretical activity and the values obtained

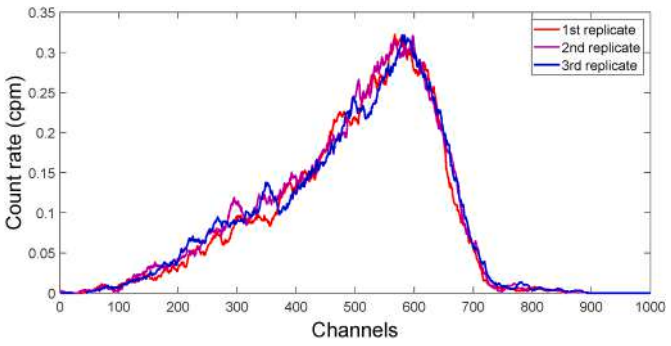

Fig. 3. Spectra obtained with the PSresin after the precipitation with iodates.

Table 3
Detection efficiency for ^{90}Sr at separation (t = 0) and after 21 days (t > 21 days) in the full and optimal windows. Three 100 mL replicate standard samples were analyzed.

t = 0		t > 21 days	
Full (1:1024)	Optimus (450:632)	Full (1:1024)	Optimus (517:875)
86 (4)	51 (3)	179 (8)	126 (6)

Table 4
Quantification of ^{90}Sr in MAPEP samples. Three replicates were performed.

	Activity (Bq/L)		
	t = 0	t > 21 days	Acceptance range 2019
MAPEP-16-MaW34	7.2 (0.7)	5.64 (0.5)	5.65–10.48
MAPEP-10-MaW22	<0.37 Bq/L	<0.20 Bq/L	Not present

Table 2
Recovery of Sr and Pb by precipitating with iodate before precipitating with hydrogen phosphate. Three replicates were performed.

Sr (%)	90 (4)
Pb (%)	3 (1)

Table 5
Results obtained in the analysis of CSN sample with medium activity containing interferents using the EC-LSC and PSresin methods. Three 100 mL replicate samples were analyzed.

	Recovery (%)		Activity of ^{90}Sr (Bq/kg)		Background signal (cpm) (optimal window)
	Sr	Pb	t = 0	t > 21 days	
EC-LSC	69 (2)	/	3.9 (0.2)	4.09 (0.08)	4.2 (0.2)
PSresin	87.6 (0.4)	6 (2)	4.6 (0.6)	4.1 (0.1)	0.18 (0.03)

through the EC-LSC method. The results demonstrated the viability of the method by using the PSresin, since none of the other radionuclides present in the sample, including ^{210}Pb, were detected. Finally, the results and variability of the EC-LSC and PSresin methods were equivalent at 21 days.

In view of this, measurements performed at each time point serve different purposes. Immediate measurements offer a quick and initial estimate of the ^{90}Sr activity level in a sample, while measurements after 21 days provide more accurate and precise values of ^{90}Sr activity, but with a longer waiting time.

3.2.2. SUC-LSC vs the PSresin method

For this comparison, a river sample of a large volume (1 L) fortified with a lower activity level (0.4 Bq/L of ^{90}Sr) was used. As the sample volume was quite large, an additional step of carbonate precipitation was introduced. Therefore, the matrix effect in the PSresin method was first studied by analysing 4 samples of increasing volume (100, 250, 500 and 1000 mL), all containing the same level of ^{90}Sr activity (0.4 Bq). The obtained results (Table 6) showed that the quantification was accurate and no matrix effect on the scintillation properties was observed.

After confirming the absence of a matrix effect, the analysis of 1 L river water samples spiked with 0.4 Bq of ^{90}Sr was conducted using two different methods: the PSresin method (three replicates) and the SUC-LSC method, which involved successive precipitations and LSC (one replicate). Both methods yielded optimal results, as it can be seen in Table 7. At t = 0, the SUC-LSC method had lower bias, although the bias for the PSresin method was still acceptable for a preliminary analysis. In this regard, the PSresin method was notably faster and less laborious with a total processing time of 5–6 h compared to the 20 h for the SUC-LSC method. Moreover, if we pay attention to the measurements conducted at secular equilibrium (t > 21 days), both methods showed the same bias, indicating that the PSresin method can provide the same results for an environmental sample as the reference procedure SUC-LSC, but with a shorter and less laborious method as well as the possibility of processing more than one sample at the same time.

3.2.3. Quality parameter comparison

As the final step in comparing the methods, the values of various quality parameters were assessed, including background, detection efficiency, limit of detection, and analysis time. These parameters were compared and summarized in Table 8.

In terms of the background signal, the LSC methods had higher values compared to the PSresin method. The LSC methods require mixing the sample (8 mL) with a scintillation cocktail (12 mL), resulting in a total volume of 20 mL in the counting vials. In contrast, the PSresin method only requires the presence of the PSresin cartridge (1.4 g of the PSresin) with the retained ^{90}Sr in the counting vial. This dissimilarity in the sample volume and scintillation material makes the LSC method more prone to generating extra background signals through interactions with external radiation. Moreover, the optimal window in the PSresin method is smaller compared to the LSC method, which also affects the registered background signals.

This, in fact, also explains the differences in the detection efficiencies. While both methods presented similar values in the total window, the PSresin method employed an optimal window designed to minimize the potential contribution of ^{210}Pb. As a result, a smaller window excluding the first 400 channels was using decreasing the value of detection efficiency.

The combination of these parameters, along with the yield, led to the LoD values calculated following the curie's expression (Currie, 1968). As shown in Table 8, the PSresin method presented a lower limit of detection compared to the other methods. Nevertheless, all methods have LoD values clearly below the values required by the Spanish regulation (0.4 Bq/L).

Finally, the PSresin method appeared to be as fast as the EC-LSC method for samples with high and medium activity levels. For samples with low activity, the PSresin method was significantly faster than the SUC-LSC method. In this sense, the addition of the Pb precipitation step introduces some time delay that is compensated by the simplification of the separation process in the column.

Table 6
Bias in the quantification of the river water samples with increasing volume (0.4 Bq/L).

	t = 0	t > 21 days
Volume	Bias (%)	Bias (%)
100 mL	8.9	6.6
250 mL	6.8	−5.2
500 mL	8.0	0.4
1000 mL	4.7	−1.1

Table 7
Results for the spiked river water samples at environmental levels. One replicate sample was analyzed by SUC-LSC and three with PSresin.

Method	Sr recovery (%)	Bias (%)	
		t = 0	t > 21 days
SUC-LSC (n = 1)	80.3	1.0	3.5
PSresin	63.3	4.7	−1.1
PSresin	81.3	12.8	−8.3
PSresin	75.5	12.7	−1.9

Table 8
Summary of the quality parameters of the methods applied.

	Efficiency		Background (cpm)	LoD (Bq/L)	Time of analysis (hours)
	t = 0	t > 21 days			
EC-LSC	96.5 (0.4)	193 (1)	4.1	0.081**	6-7
SUC-LSC				0.068**	20
PSresin	51* (3)	126* (6)	0.3	0.027**	5-6

* Optimum windows detection efficiency
** (1 L and 1 h counting time)

4. Conclusion

A new procedure for ^{90}Sr analysis involving the removal of ^{210}Pb interference has been developed. This procedure incorporates a selective precipitation step with iodates and subsequent redissolution in boiling water, resulting in a high recovery rate of 90% for while minimizing the presence of Pb to only 3%. This makes the quantification of ^{90}Sr possible in samples containing low amounts of ^{210}Pb. Moreover, the procedure has demonstrated its reliability by avoiding false positive results, since the interlaboratory sample MAPEP-10-MaW22, which does not contain ^{90}Sr, was analyzed correctly.

For samples with medium and high activity that contain interferents, the proposed method has demonstrated satisfactory performance when compared to the most commonly used method EC-LSC. The quantification is acceptable and the limit of detection is lower for the same time of analysis.

For samples with low activity and high volume, the PSresin method can reach lower detection limits than the SUC-LSC method with highly reproducible results. While the accuracy of the PSresin method is acceptable, the SUC-LSC method gives better results in this regard. The PSresin method has the advantage of shorter analysis time (5–6 h for the PSresin method vs 20 h for the SUC-LSC method) and uses fewer harmful reagents. Finally, the PSresin method generate less waste, avoiding the production of mixed waste associated with LSC analysis.

CRediT authorship contribution statement

I. Giménez: Writing – review & editing, Writing – original draft, Methodology, Investigation, Formal analysis, Data curation. **J. Rotger:** Validation, Investigation, Formal analysis, Data curation. **E. Apellániz:** Investigation, Formal analysis. **H. Bagán:** Writing – review & editing, Supervision, Methodology, Conceptualization. **J. Tent:** Visualization, Supervision, Methodology. **A. Rigol:** Writing – review & editing, Supervision, Methodology, Funding acquisition, Conceptualization. **A. Tarancón:** Writing – review & editing, Supervision, Project administration, Methodology, Funding acquisition, Conceptualization.

Declaration of competing interest

The authors declare that they have no known competing financial interests or personal relationships that could have appeared to influence the work reported in this paper.

Data availability

Data will be made available on request.

Acknowledgments

This work was carried out in a Generalitat de Catalunya Research Group (2021 SGR 01342) and has received funding from the Ministerio de Ciencia e Innovación de España (PID2020-114551RB-I00). I. Giménez thanks the University of Barcelona for the PREDOCS-UB grant.

References

Bagán, H., Tarancón, A., Rauret, G., García, J.F., 2011. Radiostrontium separation and measurement in a single step using plastic scintillators plus selective extractants. Application to aqueous sample analysis. Anal. Chim. Acta 686 (1–2), 50–56. https://doi.org/10.1016/j.aca.2010.11.048.

Bé, M.-M., Chisté, V., Dulieu, C., Kellett, M., Mougeot, X., Arinc, A., Chechev, V.P., Kummenko, N.K., Kinédi, T., Luca, A., Nichols, A.L., 2016. Table of radionuclides. In: 8 - A = 41 to 198)". Bureau International des Poids et Mesures, vol. 8, ISBN 978-92-822-2264-5.

Chobola, R., Mell, P., Daróczi, L., Vincze, A., 2006. Rapid determination of radiostrontium isotopes in samples of NPP origin. J. Radioanal. Nucl. Chem. 267 (2), 297–304. https://doi.org/10.1007/s10967-006-0044-6.

Coma, A., Tarancón, A., Bagán, H., García, J.F., 2019. Automated separation of 99Tc using plastic scintillation resin PSresin and openview automated modular separation system (OPENVIEW-AMSS). J. Radioanal. Nucl. Chem. 321 (3), 1057–1065. https://doi.org/10.1007/s10967-019-06659-7.

Currie, L.A., 1968. Limits for qualitative detection and quantitative determination. Application to radiochemistry Anal. Chem. 40 (3), 586–593, 110.1021/ac60259a007.

Eichrom Technologies. Strontium-89/90 in Water" Analytical Procedure, 2014. Available at: https://www.eichrom.com/wp-content/uploads/2018/02/srw01-15_sr-water-vbs.pdf.

Giménez, I., Bagán, H., Tarancón, A., García, J.F., 2021. PSresin for the analysis of alpha-emitting radionuclides: comparison of diphosphonic acid-based extractants. Appl. Radiat. Isot. 178 https://doi.org/10.1016/J.APRADISO.2021.109969, 109969.

Horwitz, E.P., Dietz, M.L., Fisher, D.E., 1991. SREX: a NEWPROCESS for the extraction and recovery of strontium from acidic nuclear waste streams. Solvent Extr. Ion Exch. 9 (1), 1–25. https://doi.org/10.1080/07366299108918039.

IAEA, "Measurements of Radionuclides in Food and Environment, Guidebook", A., 1989. Technical Report Series No.295. IAEA, Vienna, 70–91.

V. J. 0 Johnson, K. W. Edwards, S. L. Udall, and W. T. Pecora, "Determination of Strontium-90 in Water UNITED STATES DEPARTMENT of the INTERIOR.

Lluch, E., Barrera, J., Tarancón, A., Bagán, H., García, J.F., 2016. Analysis of 210Pb in water samples with plastic scintillation resins. Anal. Chim. Acta 940, 38–45. https://doi.org/10.1016/j.aca.2016.08.004.

Maxwell, S.L., Culligan, B.K., 2009. Rapid method for determination of radiostrontium in emergency milk samples. J. Radioanal. Nucl. Chem. 279 (3), 757–760. https://doi.org/10.1007/s10967-008-7368-3.

REAL DECRETO 3/2023, de 10 de enero, por el que se establecen los criterios técnico-sanitarios de la calidad del agua de consumo, su control y suministro. Boletín Oficial del Estado 9, 2023, 11 de Enero de 2023, 4253-4354.

Sáez-Muñoz, M., Bagán, H., Tarancón, A., García, J.F., Ortiz, J., Martorell, S., 2018. Rapid method for radiostrontium determination in milk in emergency situations using PS resin. J. Radioanal. Nucl. Chem. 315 (3), 543–555. https://doi.org/10.1007/s10967-017-5682-3.

Santiago, L.M., Bagán, H., Tarancón, A., Garcia, J.F., 2013. Synthesis of plastic scintillation microspheres: evaluation of scintillators. Nucl. Instrum. Methods Phys. Res. 698, 106–116. https://doi.org/10.1016/j.nima.2012.09.028.

Schneider, M., et al.. The world nuclear industry status report 2022 aviel verbruggen [Online]. Available: www.WorldNuclearReport.org.

Sunderman, D.N., Townley, C.W., 1960. The Radiochemistry of Barium, Calcium, and Strontium" NAS-NS 3010. In: Nuclear Science Series, vol. 125. U.S. Department of Commerce.

Tayeb, M., Dai, X., Corcoran, E.C., Kelly, D.G., 2015. Rapid determination of ^{90}Sr from ^{90}Y in seawater. J. Radioanal. Nucl. Chem. 304, 1043–1052. https://doi.org/10.1007/s10967-015-3935-6.

Torres, A., Giménez, I., Bagán, H., Tarancón, A., 2022. Analysis of isotopes of plutonium in water samples with a PSresin based on aliquat·336. Appl. Radiat. Isot. 187 https://doi.org/10.1016/j.apradiso.2022.110333, 110333.

Triskem International, 2015. SR resin product sheet. Available at: https://www.triskem-international.com/scripts/files/5f463447ad4026.94629022/PS_SR-Resin_EN_160927.pdf.

Triskem International, 2023. Extraction Chromatography. Technical Documentation All Resins " 10-1. Available at: https://www.triskem-international.com/scripts/files/5ee8cbaf847631.58650092/technical-doc-all-resins-en-online.pdf.

Vajda, N., Kim, C.K., 2010. Determination of radiostrontium isotopes: a review of analytical methodology. Appl. Radiat. Isot. 68 (12), 2306–2326. https://doi.org/10.1016/j.apradiso.2010.05.013.

Article #6

Analysis of isotopes of plutonium in water samples with a PSresin based on aliquat·336

Applied Radiation and Isotopes 187 (2022) 110333

Contents lists available at ScienceDirect

Applied Radiation and Isotopes

journal homepage: www.elsevier.com/locate/apradiso

Analysis of isotopes of plutonium in water samples with a PSresin based on aliquat·336

A. Torres [a], I. Giménez [a], H. Bagán [a], A. Tarancón [a,b,c,*]

[a] Department of Chemical Engineering and Analytical Chemistry, University of Barcelona, Marti i Franqués, 1-11, ES-08028, Barcelona, Spain
[b] Serra-Húnter Programme, Generalitat de Catalunya, Barcelona, Spain
[c] Institut de Recerca de l'Aigua, University of Barcelona, Spain

A B S T R A C T

There is a necessity to have techniques capable to perform rapid determinations of specific radionuclides with the aim to provide fast response in emergency situations where a large number of samples need to be measured in a short time. Plastic Scintillation Resins (PSresins) raises as an adequate tool to achieve this purpose and in the present study a methodology to determine plutonium using a PSresin based on Aliquat·336 was developed. Different sample treatments have been studied under acidic conditions with an emphasis on valence adjustment treatment to achieve an effective retention within the PSresin. Under 3 M nitric acid conditions and an iron sulphamate (II) + nitrite valence adjustment, quantitative retention and 100% detection efficiency were achieved. The retention of the different interferences evaluated (^{238}U, ^{230}Th, ^{241}Am, ^{210}Pb and ^{99}Tc) was low and therefore they do not interfere significantly in the determination of plutonium, except for ^{99}Tc. Finally, a stable tracer to calculate the PSresin separation yield was studied, revealing that gold is suitable for this purpose. This procedure was applied to the analysis of spiked sea and river water samples, obtaining errors lower than 10% in their quantification.

1. Introduction

Plutonium isotopes are used in the military industry, in nuclear reactors for energy production, and nuclear reprocessing industry. Plutonium isotopes are present in the environment at very low activities. The majority is the result of nuclear weapon testing performed mainly during 1950–1960. Nuclear accidents (i.e., Chernobyl (1986), Thule (1968) or the Systems for Nuclear Auxiliary Power generator (1964)) and isolated releases from reprocessing plants have made a small contribution (Qiao et al., 2009). Plutonium isotopes, as well as other transuranic isotopes, are considered among the most radiotoxic elements and as a consequence effective environmental monitoring is required to protect ecosystems from their potential release. Moreover, plutonium isotopes are considered one of the main threats in terrorist attacks and therefore we need methods of analysis, in terms of sample treatment and detection, that would be capable of providing a fast response in emergency situations (Dolique et al., 2019; Kim et al., 2015; Landstetter et al., 2015; Lemons et al.; Qiao et al., 2011).

All plutonium isotopes are artificial and the most commonly found are ^{238}Pu, ^{239}Pu, ^{240}Pu, and ^{241}Pu. All these radionuclides are alpha emitters except ^{241}Pu, which is a low beta energy emitter. They can only be measured using techniques capable of detecting low penetration particles, such as alpha spectrometry and scintillation. A chemical treatment is required to isolate plutonium from other radionuclides for scintillation detection, and to isolate plutonium from most of the other components of the sample (i.e., several stable cation, anion and organic compounds) in alpha spectrometry to avoid attenuation of the alpha particles (Vajda and Kim, 2010), (Hou and Roos, 2008). Plutonium presents a rich chemistry and depending on the complexity of environmental samples, its determination can be quite challenging, involving long and tricky sample treatments. Separation can be achieved using a variety of strategies including co-precipitation, solvent extraction, and ion-exchange or extraction chromatography with different extractants (Qiao et al., 2009), (Hou and Roos; Liu et al., 2016a; Vajda and Kim, 2010).

Alpha spectrometry is the technique most used to quantify plutonium isotopes. It has the lowest detection limit thanks to an extremely low background, although the preparation of alpha sources is time consuming and not suitable for fast or emergency uses. Liquid scintillation can also be used for plutonium analysis since it has acceptable detection limits and sample preparation for measurement is easy. However, no specific information about each specific isotope is obtained and mixed wastes (hazardous and radioactive) are produced. An alternative to these techniques, especially suited for fast analysis in

* Corresponding author. Department of Chemical Engineering and Analytical Chemistry, University of Barcelona, Marti i Franqués, 1-11, ES-08028, Barcelona, Spain.
E-mail address: alex.tarancon@ub.edu (A. Tarancón).

https://doi.org/10.1016/j.apradiso.2022.110333
Received 25 November 2021; Received in revised form 3 May 2022; Accepted 11 June 2022
Available online 17 June 2022

emergencies, is based on the use of Plastic Scintillators in the form of resins (PSresins). A PSresin is a plastic scintillation microsphere (PSm) coated with a selective extractant. When packed in a solid phase extraction cartridge it allows the combination of separation through extraction chromatography and measurement through scintillation within a single material (Bagán et al., 2011; Coma et al., 2019; Lluch et al., 2016; Sáez-Muñoz et al., 2018). This not only simplifies the analytical method, but also reduces the number of reagents required, since elution steps are no longer required, thus also avoiding the generation of mixed wastes derived from the use of liquid scintillation cocktails. The development of a method of analysis of plutonium isotopes with PSresin will therefore provide a new tool for the analysis of plutonium that will be of interest in emergency situations, where sample treatment has to be simplified and more than one sample needs to be treated simultaneously.

In this work, the PSresin proposed for the retention of plutonium isotopes is based on a quaternary aliphatic amine (known as aliquat-336). This PSresin has been studied in detail previously for the analysis of ^{99}Tc (Coma et al., 2019), (Barrera et al., 2016) but may also be used for plutonium since several methods using extraction chromatography with this extractant have been described (Horwitz et al., 1993; Kumar et al., 2013; Lemons et al., Liu et al., 2016a,b, Maxwell et al., 2014, 2015; Maxwell and Culligan, 2006; Varga et al., 2007). In these methods, the oxidation state is adjusted to Pu(IV) after a preconcentration process since this is the valence at which retention of plutonium is highest. The medium of the loading solution can be nitric acid (2–4 M) (Liu et al., 2016b), (Lemons et al., 2017b) or hydrochloric acid (9 M) (Varga et al., 2007), (TrisKem International, 2015). To adapt these procedures to include the use of a PSresin three issues need addressing. First, the valence adjustment treatment and loading and cleaning media for optimum scintillation measurement of plutonium with the PSresin in the column need to be established. Second, as plutonium is not eluted from the resin, the potential retention of interferents needs to be evaluated and minimized with cleaning steps. Finally, a non-radioactive element with analogous behaviour to plutonium under the treatment conditions is needed for tracing the yield of the separation, since if a plutonium radiotracer is used it would interfere with the scintillation signal coming from the plutonium isotopes in the sample.

2. Experimental

2.1. Reagents

All the reagents used were of analytical grade. Polystyrene (PS) (MW 250,000 g/mol) was supplied by Acros Organics (Geel, Belgium). Fully hydrolysed polyvinyl alcohol (PVA), 2,5-diphenyloxazole (PPO), nitric acid (69%), L(+)-ascorbic acid (≤99%) and hydrogen peroxide (30%) were from Panreac (Castellar del Valles (Barcelona), Spain); hydrochloric acid (37%), methanol (≤99.9% for HPLC), hydroxylammonium chloride (≤90%), amidosulphuric acid, aluminium nitrate nonahydrate, aliquat-336 and dichloromethane (99.9%) were supplied by Merck (Darmstadt, Germany). 1,4-bis(5-phenyl-2-oxazolyl) benzene (POPOP) was purchased from Carlo Erba Reagents (Chaussée du Vexin, France). Standards of tin (1000 ppm), cerium (1000 ppm), gold (1000 ppm) and samarium (1000 ppm) from Inorganic Ventures (Christiansburg, USA) were used. Europium (III) chloride hydrate and ammonium molybdate were provided by Alfa Aesar (Heysham, United Kingdom).

A ^{238}U active stock solution of 2.22 (0.03) Bq/g was prepared from a standard of 101.34 (1.18) Bq/g from Eckert and Ziegler (Berlin, Germany). A ^{241}Am active stock solution of 47.4 (1.2) Bq/g in 0.5 M HCl was prepared from a standard of 55.44 (1.3) kBq/g and a ^{238}Pu active stock solution of 46.3 (1.4) Bq/g was supplied by GE Healthcare-Amersham International (Buckinghamshire, England). A ^{230}Th active stock solution of 2.38 (0.03) Bq/g was prepared from a standard of 23.59 (0.27) Bq/g from the National Institute of Standards and Technology (NIST) (Gaithersburg, USA). A ^{226}Ra active stock solution of 4.0 (0.1) Bq/g in HNO_3 was prepared from a standard of 1986 (62) kBq/g supplied by Ciemat (Madrid, Spain). A ^{210}Pb active stock solution of 160 (5) Bq/g was prepared from a standard of 35.5 (1.1) kBq/g provided by CEA/DAMRI (GIF-SUR-YVETTE CEDEX, France).

OptiPhase Supermix liquid scintillation cocktail from PerkinElmer (Waltham, USA) was used for the liquid scintillation measurements.

Plastic scintillation microspheres were prepared as described previously (Santiago et al., 2013).

PSresin were prepared by coating PSm with aliquat·336 as described previously (Barrera et al., 2016).

2.2. Apparatus

A Quantulus liquid scintillation spectrometer (PerkinElmer, Waltham, USA) with logarithmic amplification, a multichannel analyser (MCA) (4096 channels distributed in four segments of 1024), alpha/beta discrimination and background reduction by an active guard was used for the scintillation measurements.

The analysis of stable isotopes was performed using an OPTIMA 8300 ICP-OES detector (PerkinElmer, Waltham, USA) or an ELAN-6000ICP-MS detector (PerkinElmer, Waltham, USA).

2.3. Procedures

2.3.1. Separation and measurement of plutonium solutions in the PSresin

One gram of the PSresin was packed in a 2-mL SPE cartridge from Triskem International (Rennes, France). The cartridge was placed in a vacuum chamber connected to a pump and 10 ml of deionized water were passed through it at a flow rate of 1 mL/min (around 3–5 inHg). Afterwards, the cartridges were shaken for 180 s at 50 Hz in an IKA MS3 digital vortex (Merck, Darmstadt, Germany) for homogenization.

Standard were prepared in polyethylene vials by adding 72 μL of ^{238}Pu standard and the corresponding medium up to 11 mL. The activity of the sample was around 3.33 Bq. Some samples were passed through the column without a valence adjustment treatment. Others were passed through after applying a valence adjustment treatment. Two different treatments were evaluated. One consisted of adjusting the valence with hydroxylamine and sodium nitrate and the other one was based on the adjustment with iron sulphamate (II), ascorbic acid and sodium nitrite (Liu et al., 2016b), (Lemons et al., 2017b), (Varga et al., 2007), (TrisKem International, 2015). Mediums evaluated were HCl 9 M, HNO_3 3 M and HNO_3 0.5 M. The addition of $Al(NO_3)_3$ 0.5 M to the HNO_3 3 M solutions was also evaluated (Maxwell et al., 2014).

To perform the sample analysis, the PSresin cartridge was placed in a vacuum box connected to a vacuum pump. The cartridge was first conditioned with 2 mL of the sample medium. Afterwards, 10 mL of the sample solution were passed through the cartridge. The flow was around 1 mL/min, which corresponds to a pressure of 3–5 inHg. Once the sample was loaded, two rinses with 2 mL of the loading sample medium were performed, followed by two rinses with 2 mL of 9 M HCl and two rinses with 2 mL of 0.5 M HNO_3. Finally, to ensure the dryness of the cartridge, the pressure was increased to 15–20 inHg for 10 min after removal of solution.

The solutions eluted after passing through the sample and rinsing the cartridge (referred to as “waste”) were collected in Corning (New York, USA) 50-mL conical tubes.

Once the separation process was complete, the PSresin cartridge was placed in a 20-mL polyethylene vial with no further operations (PerkinElmer, Massachusetts, USA) and measured in the scintillation counter.

The waste was also measured by liquid scintillation to determine the proportion of plutonium that was not retained. For this, 1 mL of the waste was mixed with 19 mL of liquid scintillator (Optiphase hifase 3) in a 20 mL polyethylene vial. The vials were shaken for 180 s in the vortex at 60 Hz to homogenize the mixture. Standard samples were prepared using this cocktail:sample proportion to determine the detection efficiency of Pu in the LSC measurements.

Blanks were prepared by adding deionized water instead of the plutonium standard.

2.3.2. Evaluation of the interferent's retention in the PSresin

To determine the retention of possible interferents within the PSresin, other radionuclides (^{nat}U and daughters,^{230}Th, ^{241}Am, ^{226}Ra and daughters, ^{99}Tc, ^{210}Pb and daughters) were tested under the optimum sample treatment conditions. The quantity of each radionuclide added to each sample is meant to achieve 3.33 Bq in a final volume of 11 mL of the sample. The rinsing media used were the same as mentioned above. Each interferent was analysed separately and the columns and wastes obtained after the loading and cleaning steps were measured as described earlier.

2.3.3. Search for stable elements chemically analogous to plutonium

The elements evaluated as potential chemical analogues of plutonium in the optimum conditions of separation were: europium; molybdenum; samarium; tin; cerium; and gold. Solutions of 1 mg of the different elements in 11 mL of final volume were passed through the PSresin in the optimum conditions of separation and the waste obtained after loading and each rinsing step was collected in different 50 mL conical tubes and analysed by ICP-MS to evaluate the retention of those elements within the PSresin. Dilutions from the sample and the collected wastes were diluted to a final concentration of HNO_3 1% or HCl 1% depending on the original medium of the waste.

2.3.4. Analysis of spiked water samples

Spiked river water and seawater samples with 10 Bq/L were analysed to determine the viability of applying the final method to the analysis of Pu isotopes in environmental samples. Seawater was collected from *Platja de Sant Miquel* in Barcelona on November 28, 2020 and river water was collected from the Ebro River where it passes through *Flix* on February 24, 2012. Samples were filtered using filter paper before analysis. Non-spiked (blank) and samples spiked with 10 Bq/L of ^{238}Pu were analysed.

Three sample treatments were applied to 100 ml of sample: evaporation to dryness and redissolution with 4 mL 8 M nitric acid and 1 mL 30% hydrogen peroxide plus evaporation until dryness; partial evaporation until 1 mL volume and redissolution in 8 M nitric acid with 4 mL and evaporation until less of 1 ml without arriving dryness; evaporation to dryness and redissolution with a 3:2 mixture of concentrated nitric acid and hydrochloric acid (aqua regia) and evaporation to dryness. In all procedures, the dried sample is redissolved in 3 M nitric acid plus 0.5 M aluminium nitrate. Afterwards, valence adjustment with iron sulphamate was performed.

2.4. Measurement conditions

A "low" coincident bias and a "high-energy" multichannel analyser configuration were used for the scintillation measurements. The counting time for the measurement of the PSresin cartridges was 1 h for standard samples and 5 h for spiked water samples. Liquid scintillation samples of the wastes were measured for 1 h. The external quenching parameter (SQP(E)) was measured for 10 min in each vial. The measurement vials were stored in the dark for 2 h before counting.

2.5. Data treatment

Data obtained from the Quantulus detector was treated using MATLAB (The mathwork, Natick, Massachusetts (USA)) computing software. Spectra were softened using the Savitzky Golay algorithm with an average window of 10 points for each side and a polynomial of 1st degree for improving graphical representation.

The detection efficiency was calculated as the ratio between the net count rate (as counts per minute) measured by the detector and the activity in the PSresin column as disintegrations per minute. The yield (proportion of radionuclide retained within the PSresin) was calculated as the proportion of activity in the column relative to the activity in the sample (in disintegrations per minute). Activity in the column was obtained from the difference between the activity of the sample and the activity in the wastes measured by LS. Activity in the wastes was calculated considering a detection efficiency value of 100% obtained in the measurement of standard solutions. In the case of stable metals, the same concept was applied, using the amount of stable metal measured by ICP-MS in the sample and in the waste.

3. Results

Aliquat·336 has been widely reported as capable of retaining Pu isotopes and therefore the aliquat·336-PSresin already developed by the authors for ^{99}Tc (Barrera et al., 2016) could be used for Pu isotope analysis since alpha emitters are also efficiently detected with plastic scintillators in the form of microspheres. Nevertheless, the most appropriate chemical pretreatment and separation conditions for direct measurement of the Pu retained on the PSresin needed to be determined, including the evaluation of the non-retention of potential interferents. Moreover, the efficiencies needed to be high and reproducible and the spectrum shape acceptable. However, the main challenge was developing a strategy to trace the separation process without the use of the classical plutonium tracer (i.e. ^{242}Pu) since it may interfere with the scintillation signal. Finally, the full procedure proposed was evaluated for the analysis of river and seawater samples.

3.1. Plutonium separation conditions

According to the retention of plutonium on aliquat-336 in acid medium described in the literature (TrisKem International, 2015), the media in which plutonium retention is highest are hydrochloric acid 9 M and nitric acid from 0.5 to 4 M, 3 M being the most commonly used (Maxwell et al., 2014), (Maxwell et al., 2015), (Liu et al., 2016b).

Plutonium retention on aliquat·336 not only depends on the loading medium, but also on the oxidation state, which needs to be adjusted before passing through the column (Maxwell and Culligan, 2006). To achieve the Pu (IV) oxidation state, which is the state with the highest retention, several redox reactions have been described in the literature (Qiao et al., 2009), (Vajda and Kim, 2010), (Maxwell et al., 2015), (Liu et al., 2016b). Nevertheless, the fastest and most effective way to achieve this state is to reduce Pu to Pu (III) and then oxidize it to Pu (IV) which is the most common procedure used in LSC. In order to achieve this objective in the analysis with PSresin, two different strategies were tested by analysing standard samples in order to found the procedure with less quenching effect on the PSresin. The first valence adjustment applied involved the use of hydroxylamine as a reducing agent and sodium nitrate as an oxidizing agent. This strategy was studied under loading conditions of 9 M hydrochloric acid, obtaining a brown coloured solution and effervescence. The percentage retention of plutonium in the PSresin cartridge was 96.2% and the detection efficiency was 96.7%. Even though these results were good, the spectrum (Fig. 1) was shifted to low energies channels. This was also consistent with the SQP(E) parameter, which was 616.

The low SQP(E) value means that a high quenching effect occurred due to the reaction of Cl^- with NO_2^- under a high concentration of HCl and the formation of brown coloured species that did not disappear, even after strong agitation (as happens with NO_2). Therefore, the spectrum was wider and shifted to lower energies.

The shape of the spectrum is not ideal for quantifying plutonium with PSresin since it can lead to deviations in the determination of the detection efficiency if quenching increases. The same valence adjustment method was performed in a 3 M nitric acid loading medium but did not work properly, leading to a plutonium retention of around 60%. This is because hydroxylamine reacted with the nitric acid instead of plutonium, not achieving the initial reduction of plutonium.

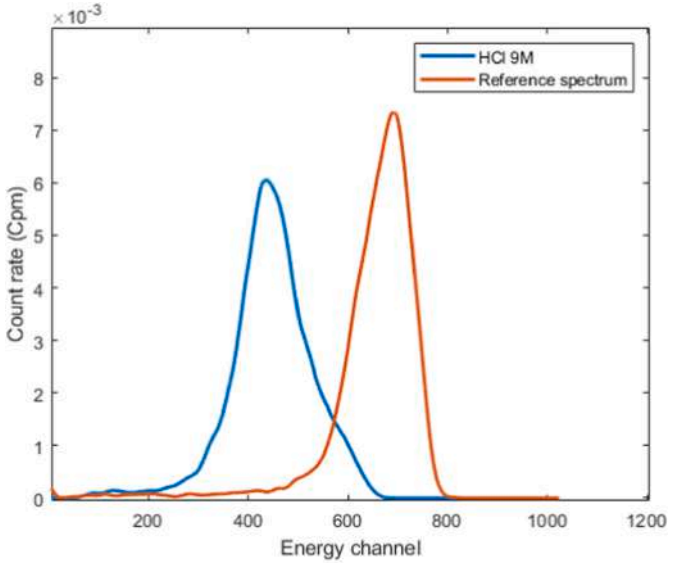

Fig. 1. Normalized spectra obtained in the analysis of ^{238}Pu with PSresin using hydroxylamine/sodium nitrite treatment in HCl 9 M and a plutonium reference spectrum measured with the PSresin.

The second adjustment was based on the use, in the following order, of: iron (II) sulphamate as a reducing agent; ascorbic acid to reduce the Fe (III) to Fe (II) and to ensure that all the plutonium species have been reduced to Pu(III); sodium nitrite (Liu et al., 2016b). This valence adjustment method was applied in two different media: HNO_3 3 M and HNO_3 3M with $Al(NO_3)_3$ 0.5 M. $Al(NO_3)_3$ 0.5 M is usually employed because it confers stability to the separation process and can be useful in future sample treatments based on phosphate precipitation (Maxwell et al., 2014).

The retention of plutonium in the PSresin cartridge was quantitative and detection efficiency was optimal under both media (Table 1). SQP (E) values were very similar for both media, with slightly low to normal values (i.e. around 780) due to blue colouration on the column caused by the presence of residues of iron (II) sulphamate. As the values were acceptable, successive cleaning steps with HCl 9 M and HNO_3 0.5 M media were performed. Slight colour changes were seen during cleaning. When HCl 9 M was passed through, the column took on a green colouration that was lost during the HNO_3 0.5 M cleaning step, leaving the column colourless, unlike in the treatment with hydroxylamine, which had a positive impact on scintillating measurement as colour quenching did not affect the resulting spectrum. This was reflected in the spectrum position, which was narrower and located at higher energies (Fig. 2). Treatment with or without the presence of $Al(NO_3)_3$ 0.5 M did not lead to significant differences. Thus, $Al(NO_3)_3$ was incorporated into the separation process.

Table 1
Yield, detection efficiency and SQE(E) obtained after in each step in the analysis of ^{238}Pu with PSresin using iron (II) sulphamate/sodium nitrite treatment in HNO_3 3M media without and including $Al(NO_3)_3$ 0.5 M

		Without $Al(NO_3)_3$ 0.5 M	With $Al(NO_3)_3$ 0.5 M
Yield (%)	Loading (3 M HNO_3)	100	100
	1st cleaning (9 M HCl)	98	97
	2nd cleaning (0.5 M HNO_3)	96	96
Efficiency (%)	Loading (3 M HNO_3)	96	98
	1st cleaning (9 M HCl)	94	97
	2nd cleaning (0.5 M HNO_3)	91	97
SQP(E)	Loading (3 M HNO_3)	680	684
	1st cleaning (9 M HCl)	676	676
	2nd cleaning (0.5 M HNO_3)	679	671

Five replicate standard samples were analysed under the optimum conditions to evaluate reproducibility of plutonium retention, detection efficiency and spectrum position in the PSresin cartridge. Values of yield, efficiency and SQP(E) obtained (Table 2) demonstrated that retention yield was almost quantitative, that all particles emitted were detected and that the columns still showed slight colouration, which slightly reduced the SPQ(E) values. The reproducibility was good since the relative standard deviation was around 5%.

However, as shown in Fig. 3 the spectra position of the five samples varied slightly. This could be because of colour quenching or changes in the retention pattern of Pu within the PSresin due to the influence of the components present in the solution or generated in the valence adjustment. Nevertheless, integration between channels 350 and 800 would cover all signals from Pu. Therefore, it can be concluded that this method leads to high and reproducible plutonium retentions and detection efficiencies.

3.2. *Study of interferent's retention*

Samples can contain other radionuclides apart from plutonium, the presence of which could interfere in its determination. For this reason, an estimation of the retention of those radionuclides with a high probability of being found in an environmental sample was needed. These radionuclides include natural radionuclides such as ^{238}U (in equilibrium with ^{234}Th, ^{234}Pa, ^{234}U), ^{230}Th and ^{210}Pb (in equilibrium with ^{210}Bi and ^{210}Po) and artificial radionuclides such as ^{99}Tc and ^{241}Am.

Samples were prepared individually for each radionuclide and analysed by applying the optimum sample treatment. Once the separation process was complete, the count rate obtained from the column and the wastes from each step was used to determine the amount of radionuclide retained in the PSresin cartridge. The results are shown in Tables 3 and 4.

The retention of each interferent, once the separation process was complete, was very low (below 4%), with the exception of ^{99}Tc, which was almost completely retained in HCl media, and is slightly retained in HNO_3 media. Nevertheless, the presence of ^{99}Tc cannot be considered usual in environmental samples and moreover the position of its spectrum (from the 0 to 650 channels) was sufficiently different to that of Pu to allow its identification in the spectrum and also Pu determination. The majority of the interferents were not retained in the 3 M HNO_3 and 0.5 M $Al(NO_3)_3$ media, with the exception of ^{230}Th, which was eluted in the 9 M HCl cleaning step. Therefore it can be concluded that the media selected can be used for column cleaning and decontamination from interferences, which could be improved further by performing cleaning steps with higher volumes of HNO_3 3 M and $Al(NO_3)_3$ 0.5 M and HCl 9 M. Thus, Pu can be quantified using aliquat-336 PSresin.

3.3. *Stable tracer for Pu*

Once we had demonstrated that the method developed allows Pu retention while separating it from other possible interferents, we had to find a tracer to allow accurate quantification of retention when measuring a real environmental sample. ^{242}Pu is usually employed for this purpose in alpha spectrometry analysis as it is not found in natural samples. However, a radioactive tracer cannot be added when scintillation techniques are used since its signal will overlap with the signal of the other Pu isotopes in the sample. For radionuclides like ^{90}Sr or ^{210}Pb, the stable element can be used to trace the progress of separation since its concentration is measured by ICP or other techniques before and after column separation. Nevertheless, there is no stable isotope for Pu and therefore, a stable element that may act as an analogue of Pu in the separation conditions is needed.

Stable elements that were taken into consideration were those with at least one of the following characteristics: a similar chemistry to Pu;

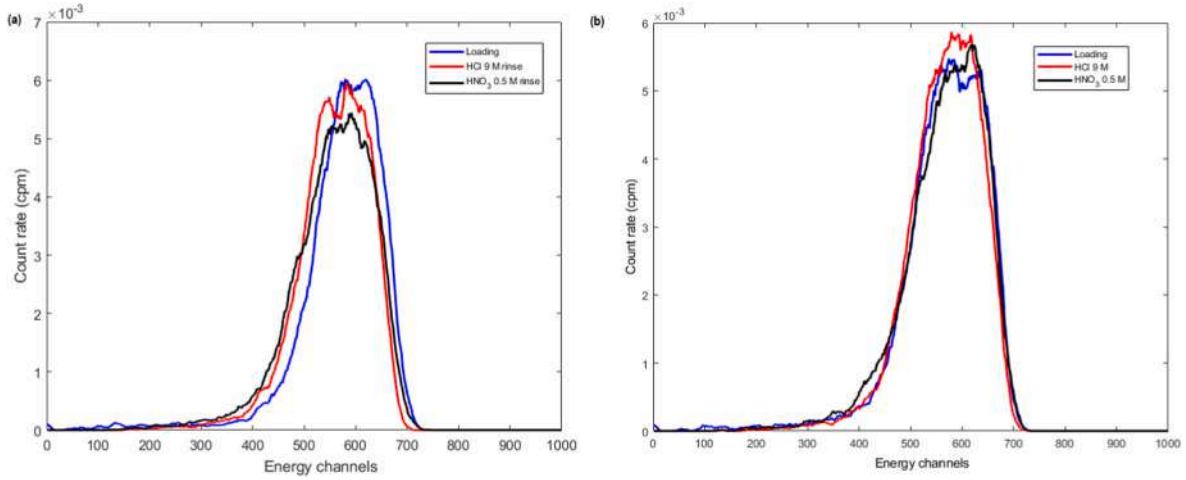

Fig. 2. Spectra obtained in the analysis of ^{238}Pu with PSresin using iron (II) sulphamate/sodium nitrite treatment in HNO_3 3M media (A) without and (B) with Al $(NO_3)_3$ 0.5 M.

Table 2
Yield, detection efficiency and SQE(E) in the analysis of five replicate standard samples of ^{238}Pu with PSresin. Mean values and standard deviation.

Yield (%)	98(5)
Efficiency (%)	100(6)
SQP(E)	722(9)

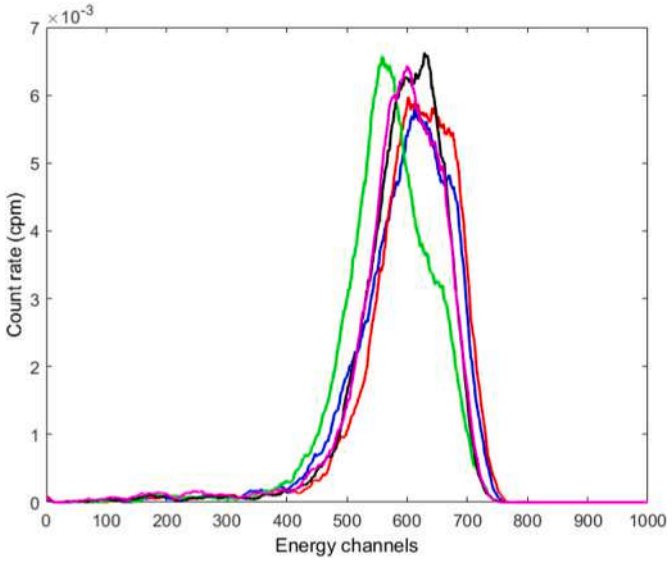

Fig. 3. Spectra obtained in the analysis of five replicate standard samples of ^{238}Pu with PSresin.

Table 3
Proportion of interferent radionuclides retained in the PSresin.

Radionuclide	Activity (Bq)	% Retained
^{238}U and daughters	3.33	2.0
^{230}Th	3.32	3.6
^{210}Pb and daughters	3.35	3.6
^{241}Am	4.48	1.0
^{99}Tc	3.32	11.2

Table 4
Proportion of the total activity eluted in each phase in relation to the 100% eluted.

Radionuclide	% not retained in loading step + eluted with HNO_3 and Al $(NO_3)_3$	% eluted with HCl 9 M	% eluted with HNO_3 0.5 M
^{238}U and daughters	78.4	16.1	5.4
^{230}Th	1.2	92.2	6.6
^{210}Pb and daughters	84.2	15.5	0.4
^{241}Am	100	0	0
^{99}Tc	93.8	4.8	1.6

similar oxidation states (i.e. III and IV); retention in strong anionic exchange resins (Bajo, 2007; Despotopulos, 2016; Faris and Buchanan, 1964; Xing and Lee, 2019); and close to Pu in the periodic table. The list of appropriate elements includes Eu, Mo, Sn, Ce, Sm and Au. Samples containing 1 mg of the corresponding element were treated following the same procedure used for standard samples. Solutions obtained after each cleaning step was collected as separate wastes so that it was easier to track in which cleaning step the metal was eluted. The proportion of stable element eluted in each step relative to the total content of each radionuclide in the loading solution is shown in Table 5.

It can be seen that none of the elements were retained within the column after the procedure with the exception of gold (III), which was retained quantitatively, like Pu, when the loading medium was nitric acid. In spite that gold and plutonium present different valence states and a different chemistry both presented quantitative retention on the column on the different media used showing some phenomenological similitudes between both regarding the aliquat·336 extraction. The fact that the chemistry may be different was put into evidence during valence adjustment, as the addition of the reagents reduced gold and part of it precipitated as metal gold.

Table 5
Proportion of stable element eluted in each step of the PSresin separation.

	Eu (%)	Mo (%)	Sn (%)	Ce (%)	Sm (%)	Au (%)
Effluent of the Loading (3 M HNO_3 + 0.5 M Al$(NO_3)_3$)	54	97.3	75.4	100	100	0
Effluent of the 1st cleaning (9 M HCl)	0	0.3	19.3	0	0	0
Effluent of the 2nd cleaning (0.5 M HNO_3)	46	2.4	5.3	0	0	0

The above results indicated that the presence of Cl^- in the solution might stabilize gold as $[AuCl_4]^-$. For this reason, the medium used when gold was added was a 5:4 mixture of 3 M HNO_3 and 0.5 M $Al(NO_3)_3$ with 1 M HCl. The use of this medium permitted gold stabilization, avoiding its precipitation during valence adjustment. It must be noted that during the valence adjustment when ascorbic acid was added, a pink-orange solution was obtained. That was due to the formation of gold nanoparticles, an amorphous formation of metallic gold that was further dissolved when sodium nitrite was added.

Results obtained in the analysis of standard samples containing plutonium and gold as the tracer (0.75 mg) (Table 6) showed that retention was quantitative (for Pu measured by LS and Au by ICP-MS) which demonstrates that the change in the medium did not changed the retention of plutonium in the PSresin cartridge and that Au can be used as a tracer.

Regarding the detection efficiency Table 6 shows that it was slightly lower when gold was retained in the PSresin cartridge, although values were highly reproducible. The SQP(E) values were similar to those obtained without using gold, however, the spectra obtained (Fig. 4) showed a shift to low energy channels due to the presence of gold.

This movement of the spectra was associated with the presence of a yellow ring on the top of the PSresin caused by the gold that was retained, leading to colour quenching. It is important to highlight the discrepancy between the SQP(E) values (indicative of low quenching) and the spectrum position (indicative of high quenching). This is because SQP(E) considers the end of the spectrum produced by the Compton electrons. Compton electrons are produced within the PSresin bed, which includes areas without colour quenching (almost all the PSresin) and areas with high colour quenching (the top of the cartridge). There are several scintillation emissions that do not suffer colour quenching and therefore the SQP(E) value is not affected by the yellow ring on the top of the vial. In contrast, if Pu is retained in a similar position to that of gold (at the top of the PSresin bed) scintillation emissions generated by Pu would be affected by colour quenching when measured and consequently the spectrum would to low energies. The fact that spectra is shifted to low energies but a small proportion is still place at high energies, suggest that most of the plutonium is place at the same position as gold and a small proportion is in a less quenched area (with fewer or without gold). These results, then, confirmed the similar behaviour of Pu and Au in the PSresin.

With the aim of reducing the effect of the Au ring on the scintillation measurements, the addition of lower amounts of gold (i.e. 0.1 mg, 0.25 mg and 0.5 mg) was studied. The resulting detection efficiencies (Table 7) and spectra positions (Fig. 5) confirmed that both depend on the amount of gold the sample is spiked with, since efficiency decreases and the spectrum moves to low energies and becomes broader when increasing amounts of gold are added.

Despite this behaviour, the results show that low amounts of gold (below 0.25 mg) do not causes a loss of detection efficiency and therefore this amount was selected and used as a stable tracer for plutonium measurement.

3.4. Analysis of spiked water samples

100 mL of two different spiked water samples (river water and seawater) were analysed with the aim of determining which pretreatment is needed and whether the full method could be applied to environmental samples of differing composition (i.e. mineral salts, organic matter, …).

The first sample pretreatment evaluated consisted of evaporation to dryness and the treatment of the residue with 8 M HNO_3 and H_2O_2 30% to ensure organic matter destruction. Following a second evaporation to dryness, the samples were reconstituted in HNO_3 3 M and $Al(NO_3)_3$ 0.5 M. The results obtained were satisfactory since retention of Pu within the PSresin in the column was quantitative and the quantification error was low: 1.3% for seawater and below 0.5% for river water. Moreover, SQP(E) values were high, at 714 and 717 for seawater and river water

Table 6
Yield, detection efficiency and SQP(E) obtained in the analysis of standard samples containing gold as the tracer.

	Yield Au (%)	Detection efficiency (%)	SQP
Blank with Au	98.8	–	696
Active without Au	–	94	724
Active with Au (1st replicate)	99.3	88	719
Active with Au (2nd replicate)	99.5	88	705
Active with Au (3rd replicate)	99.7	88	706

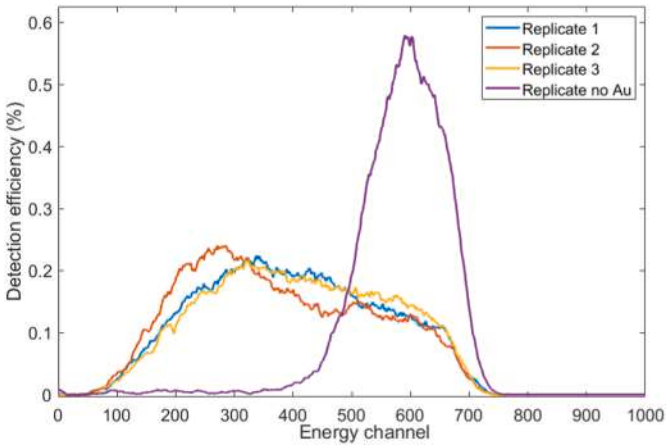

Fig. 4. Spectra obtained in the analysis of standard samples containing 0.75 mg of gold as the tracer. (For interpretation of the references to colour in this figure legend, the reader is referred to the Web version of this article.)

Table 7
Values of detection efficiency versus mg of gold

Amount of Au (mg)	Detection efficiency (%)
0.1	94.5
0.25	95.1
0.5	90.9
0.75	87.9

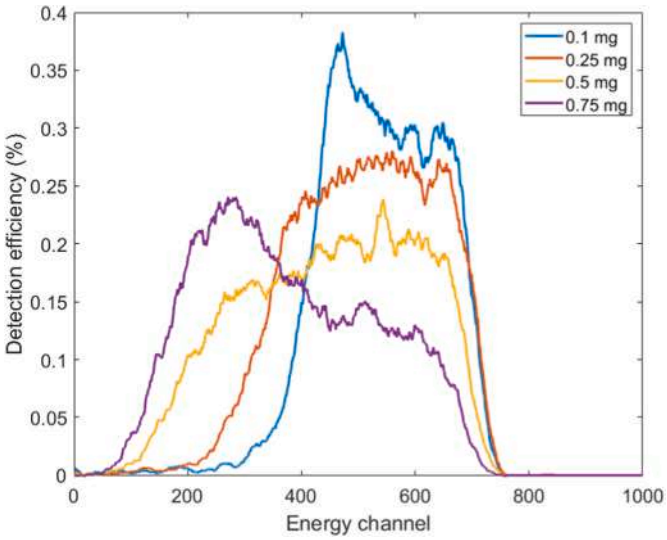

Fig. 5. Spectra obtained in the analysis of samples containing different amounts of Au.

respectively, and the spectrum appeared well positioned and defined (Fig. 6A and B).

Having shown that the method developed is not affected by the sample matrix, the same samples were analysed but with the addition of gold as a tracer (0.25 mg). In this case, the results were not satisfactory in terms of gold recovery since gold remained precipitated during the reconstitution of the sample after the last evaporation step. Therefore, this pretreatment was discarded since it was valid for Pu but not for Au.

In order to find a pretreatment condition compatible with the addition of gold, two different approaches were considered: preconcentration without evaporation to dryness to avoid gold precipitation and aqua regia treatment of the evaporation residue to allow gold redissolution.

For the blank and active samples of river and seawater treated without full evaporation, it was shown that the retention of gold was quantitative, as well as the retention of plutonium, the retention of which was confirmed by the measurement of the eluted solutions by liquid scintillation. However, the presence of incompletely digested organic matter affected the position of the spectra (Fig. 6C and D), which were partially located below channel 200. As a consequence, the quantification error was high (31% for river water and 14% for seawater) due to the fact that the presence of organic matter causes quenching that modifies the detection efficiency.

Pretreatment with aqua regia was more satisfactory, with the spectra obtained being in a similar position to the standard sample spectrum (Fig. 6E and F). Moreover, the recovery was high and quantification error was below 10% for both water matrices. To confirm the viability and reproducibility of the aqua regia treatment, two more replicates were performed under the same conditions (Table 8). The yield obtained was high in all cases and quantitative in most of them. Again, plutonium quantification had errors below 10%, which demonstrates that spectrum position was adequate and that the detection efficiency obtained in standard samples (95%) can be used for the quantification of samples. Moreover, the results confirmed that gold works well as a tracer of

Table 8
Yield and quantification deviation obtained in the analysis of spiked river water and seawater samples treated though evaporation to dryness and aqua regia redissolution.

Sample	Yield (%)	Quantification error (%)
River water (blank)	99.3	
River water (1st replicate)	92.2	9
River water (2nd replicate)	99.4	6
River water (3rd replicate)	99.9	8
Seawater (blank)	72.9	
Seawater (1st replicate)	76.6	−4
Seawater (2nd replicate)	99.9	−4
Seawater (3rd replicate)	99.9	10

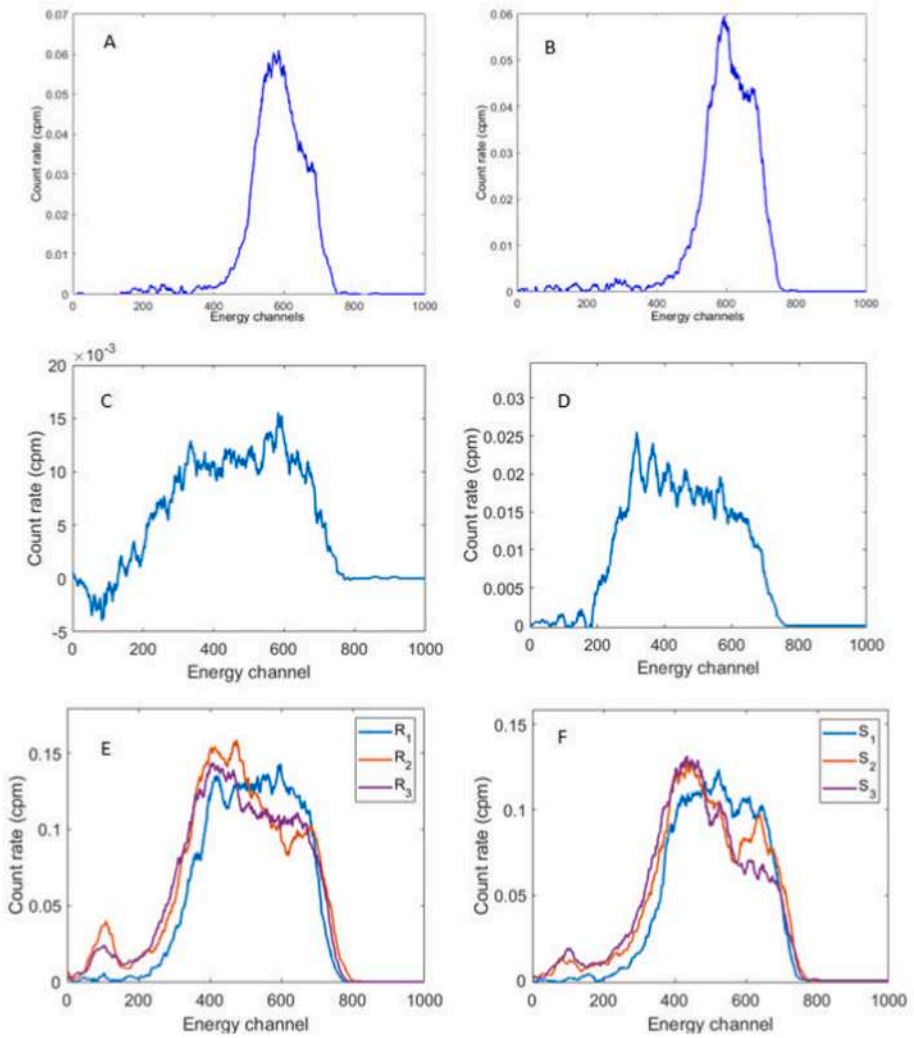

Fig. 6. Spectra obtained in the analysis of spiked river water and seawater samples treated though evaporation to dryness (A river; B sea). Spectra obtained in the analysis of spiked river water and seawater samples treated through incomplete evaporation to dryness (one replicate) (C river; D sea) and aqua regia redissolution (three replicates) (E river; F sea).

plutonium due to the fact that, in those cases where the retention of plutonium in the PSresin cartridge was not quantitative, this retention was correctly evaluated through the measurement of gold, as well as in those with quantitative retention of plutonium.

It should be pointed out that there was a small amount of luminescence between energy channels 0 to 200. However, the associated increase in counts had no effect on quantification since the integration window was between channels 200 and 1024.

Finally, the minimum detectable activity was calculated with Curie's expression being 0.073 Bq/L, taking into consideration a sample volume of 100 mL, a background value of 1.20 cpm and 3 h of measurement.

4. Conclusions

Pu determination using PSresin was found to be effective, with optimal separation from other interferents found in environmental samples. As a consequence, the rapid determination of Pu is possible while avoiding the generation of mixed wastes. The need to perform adequate valence adjustment under acidic conditions to achieve Pu (IV) as the overall oxidation state was demonstrated. Samples in HNO_3 3 M and $Al(NO_3)_3$ 0.5M with the addition of iron sulphamate(II), ascorbic acid and sodium nitrite gave the optimal results. A complete separation process was established, showing good reproducibility of results. The application of this method to real environmental samples showed good results when nitric acid and hydrogen peroxide pretreatment were performed and no gold was used.

For quantifying the retention of plutonium, it was shown that gold behaves in an analogous way to plutonium, enabling its use as a tracer. In this scenario, HCl 1 M is needed in the loading solution to stabilize gold and avoid its reduction to metallic gold and its precipitation. Under such conditions, the amount of Pu in seawater and river water samples was determined with quantification errors below 10%. The use of gold as a tracer was shown to be successful since even the samples with no quantitative retention of Pu were quantified correctly thanks to the gold correction. Nevertheless, it should be pointed out that gold and plutonium have different chemistry, and therefore this phenomenological similar behaviour observed in the treatment and separation conditions described should be contrasted with other quality control processes (e.g. periodic measurement of spiked samples). Moreover, this phenomenological similitude should be checked again when changes on the procedure or in the nature of the sample took place.

This study was therefore successful at developing a new methodology to achieve Pu isotope quantification without the use of alpha spectrometry as the detection technique, allowing its determination within 1.5 h of separation plus 3 h of measurement with a limit of detection low enough for emergency situations.

CRediT authorship contribution statement

A. Torres: Investigation, Formal analysis, Data curation. **I. Giménez:** Investigation, Formal analysis, Data curation. **H. Bagán:** Writing – review & editing, Validation, Supervision, Methodology. **A. Tarancón:** Writing – original draft, Supervision, Resources, Funding acquisition.

Declaration of competing interest

The authors declare that they have no known competing financial interests or personal relationships that could have appeared to influence the work reported in this paper.

Acknowledgment

We thank the Spanish Ministerio de Ciencia e Innovación (MCIN) for financial support of the project PID2020-114551RB-I00 under award MCIN/AEI/10.13039/501100011033, the Catalan Agència de Gestió d'Ajuts Universitaris i de Recerca (AGAUR) for financial support under award 2017-SGR-907 and the Consejo de Seguridad Nuclear (CSN) for financial support under award CSN/PIN/ACRA/1805/475. I. Giménez also thanks the University of Barcelona for the PREDOCS-UB grant.

References

Bagán, H., Tarancón, A., Rauret, G., García, J.F., 2011. Radiostrontium separation and measurement in a single step using plastic scintillators plus selective extractants. Application to aqueous sample analysis. Anal. Chim. Acta 686 (1–2), 50–56.
Bajo, S., et al., 2007, 07. Separation of Plutonium on the Anion Exchanger BIO-RAD 1-X2 and its Application to Radiochemical Analysis.
Barrera, J., Tarancón, A., Bagán, H., García, J.F., 2016. A new plastic scintillation resin for single-step separation, concentration and measurement of technetium-99. Anal. Chim. Acta 936, 259–266.
Coma, A., Tarancón, A., Bagán, H., García, J.F., 2019. Automated separation of 99Tc using plastic scintillation resin PSresin and openview automated modular separation system (OPENVIEW-AMSS). J. Radioanal. Nucl. Chem. 321 (3), 1057–1065.
Despotopulos, J.D., et al., 2016. Production and isolation of homologs of flerovium and element 115 at the lawrence livermore national laboratory center for accelerator mass spectrometry. J. Radioanal. Nucl. Chem. 308 (2), 567–572.
Dolique, I., Kabai, E., Schuster, M., 2019. Fast method for the determination of radiostrontium and plutonium isotopes in food samples. J. Radioanal. Nucl. Chem. 322 (3), 1423–1430.
Faris, J.P., Buchanan, R.F., 1964. Anion exchange characteristics of the elements in nitric acid medium, 1157-115 Anal. Chem. 36–6.
Horwitz, E.P., Chiarizia, R., Dietz, M.L., Diamond, H., Nelson, D.M., 1993. Separation and preconcentration of actinides from acidic media by extraction chromatography. Anal. Chim. Acta 281 (2), 361–372.
Hou, X., Roos, P., Nov. 2008. Critical comparison of radiometric and mass spectrometric methods for the determination of radionuclides in environmental, biological and nuclear waste samples. Anal. Chim. Acta 608 (2), 105–139.
Kim, H., Chung, K.H., Jung, Y., Jang, M., ja Kang, M., Choi, G.S., 2015. A rapid and efficient automated method for the sequential separation of plutonium and radiostrontium in seawater. J. Radioanal. Nucl. Chem. 304 (1), 321–327.
Kumar, R., Dubla, R., Yadav, J.R., Rao, D.D., 2013. A method for estimation of Pu-isotopes in urine samples using TEVA resin and alpha spectrometry. J. Radioanal. Nucl. Chem. 295 (3), 2147–2152.
Landstetter, C., Damberger, V., Zapletal, M., Katzlberger, C., 2015. Development of a rapid method to determine plutonium in foodstuffs. J. Radioanal. Nucl. Chem. 304 (1), 343–347.
Lemons, B., Khaing, H., Ward, A., Thakur, P., December 2017. A rapid method for the sequential separation of polonium, plutonium, americium and uranium in drinking water. Appl. Radiat. Isot. 136, 10–17, 2018.
Lemons, B., Khaing, H., Ward, A., Thakur, P., December 2017. A rapid method for the sequential separation of polonium, plutonium, americium and uranium in drinking water. Appl. Radiat. Isot. 136, 10–17, 2018.
Liu, B., Shi, K., Ye, G., Guo, Z., Wu, W., 2016a. Method development for plutonium analysis in environmental water samples using TEVA microextraction chromatography separation and low background liquid scintillation counter measurement. Microchem. J. 124, 824–830.
Liu, B., Shi, K., Ye, G., Guo, Z., Wu, W., 2016b. Method development for plutonium analysis in environmental water samples using TEVA microextraction chromatography separation and low background liquid scintillation counter measurement. Microchem. J. 124, 824–830.
Lluch, E., Barrera, J., Tarancón, A., Bagán, H., García, J.F., 2016. Analysis of 210Pb in water samples with plastic scintillation resins. Anal. Chim. Acta 940, 38–45.
Maxwell, S.L., Culligan, B.K., 2006. Rapid column extraction method for actinides in soil. J. Radioanal. Nucl. Chem. 270 (3), 699–704.
Maxwell, S.L., Culligan, B.K., Hutchison, J.B., Utsey, R.C., McAlister, D.R., 2014. Rapid determination of actinides in seawater samples. J. Radioanal. Nucl. Chem. 300 (3), 1175–1189.
Maxwell, S.L., Culligan, B., Hutchison, J.B., McAlister, D.R., 2015. Rapid fusion method for the determination of Pu, Np, and Am in large soil samples. J. Radioanal. Nucl. Chem. 305 (2), 599–608.
Qiao, J., Hou, X., Miró, M., Roos, P., 2009. Determination of plutonium isotopes in waters and environmental solids: a review. Anal. Chim. Acta 652 (1–2), 66–84.
Qiao, J., Hou, X., Roos, P., Miró, M., 2011. Rapid isolation of plutonium in environmental solid samples using sequential injection anion exchange chromatography followed by detection with inductively coupled plasma mass spectrometry. Anal. Chim. Acta 685 (2), 111–119.
Sáez-Muñoz, M., Bagán, H., Tarancón, A., García, J.F., Ortiz, J., Martorell, S., 2018. Rapid method for radiostrontium determination in milk in emergency situations using PS resin. J. Radioanal. Nucl. Chem. 315 (3), 543–555.
Santiago, L.M., Bagán, H., Tarancón, A., Garcia, J.F., 2013. Synthesis of plastic scintillation microspheres: evaluation of scintillators. Nucl. Instruments Methods Phys. Res. Sect. A Accel. Spectrometers, Detect. Assoc. Equip. 698, 106–116.
TrisKem International, 2015. TEVA Product Sheet 33 (September), 1–4.

Vajda, N., Kim, C.K., 2010. Determination of Pu isotopes by alpha spectrometry: a review of analytical methodology. J. Radioanal. Nucl. Chem. 283 (1), 203–223.
Varga, Z., Surányi, G., Vajda, N., Stefánka, Z., 2007. Improved sample preparation method for environmental plutonium analysis by ICP-SFMS and alpha-spectrometry. J. Radioanal. Nucl. Chem. 274 (1), 87–94.
Xing, W.D., Lee, M.S., 2019. Recovery of gold(III) from the stripping solution containing palladium(II) by ion exchange and synthesis of gold particles. J. Ind. Eng. Chem. 69, 255–262.

Article #7

Use of PSresin in tandem for a mixture of radionuclides (^{89}Sr plus ^{90}Sr and ^{90}Sr plus plutonium isotopes) determination

Analytica Chimica Acta 1337 (2025) 343573

Contents lists available at ScienceDirect

Analytica Chimica Acta

journal homepage: www.elsevier.com/locate/aca

Simultaneous radionuclide determination using PSresin: 2in2 and 2in1 tandem configuration

I. Giménez [a], H. Bagán [a], A. Tarancón [a,b,c,*]

[a] Departament d'Enginyeria Química i Química Analítica, Universitat de Barcelona, Marti i Franqués, 1-11, ES-08028, Barcelona, Spain
[b] Serra-Húnter Programme, Generalitat de Catalunya, Barcelona, Spain
[c] Institut de Recerca de l'Aigua, University of Barcelona, Spain

HIGHLIGHTS

- New methodology for simultaneous determination of radiostrontium and plutonium isotopes using a plastic scintillation resin.
- ^{89}Sr and ^{90}Sr quantification in a single measurement in less than 5 h.
- Determination of ^{90}Sr and ^{239}Pu in less than 8 h with a single measure.

GRAPHICAL ABSTRACT

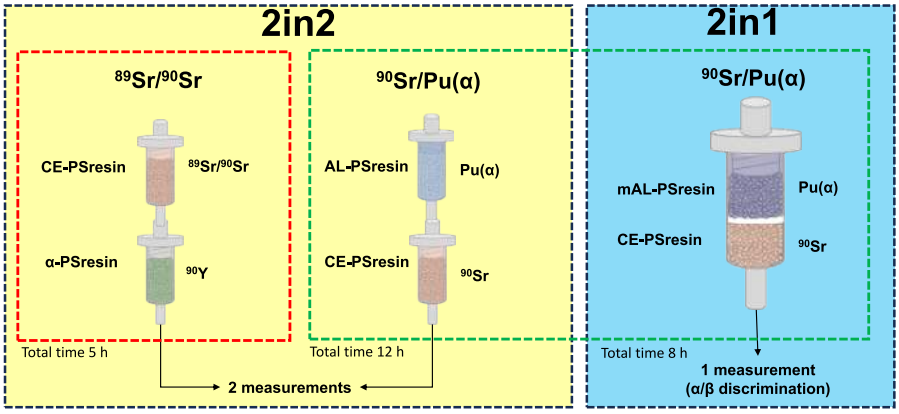

ABSTRACT

Background: Analyzing mixtures of radionuclides is a complex task. Two situations are the mixtures of ^{89}Sr with ^{90}Sr and ^{90}Sr with plutonium isotopes. The challenge arises in emergency scenarios resulting from accidents where the activity of ^{89}Sr is over 20 times higher than that of ^{90}Sr, complicating its quantification and requiring delayed measurements. In scenarios involving accidents, both ^{90}Sr and plutonium isotopes, may be present within various matrices. Given their distinct elemental properties, separation is typically achieved using different methods, followed by a measurement post-elution through alpha spectrometry and scintillation techniques. Therefore, methods which allow the fast and reliable determination of those mixtures are still required in routine laboratories.

Results: A novel method for the simultaneous determination of radionuclide mixtures using PSresin is introduced. This innovative approach utilizes PSresins in tandem and has been applied to the analysis of ^{89}Sr and ^{90}Sr, as well as mixtures of ^{90}Sr and plutonium isotopes. Two strategies were investigated: using two PSresin in two cartridges and two measurements (2in2); and using two PSresin in a single cartridge and one measurement employing α/β discrimination (2in1). The methods were validated with standard solutions and applied to river water samples, achieving quantification errors below 10 % for both strategies within 5 and 8 h, respectively, from sample reception.

Significance: This represents a great improvement for ^{89}Sr and ^{90}Sr quantification which is achieved in less than 5 h since sample reception reducing the 30 days required by conventional methods. Additionally, the simultaneous measurement of ^{90}Sr and plutonium isotopes reduce the number of required analysis to half, reducing the overall time and cost of the analysis.

* Corresponding author. Departament d'Enginyeria Química i Química Analítica, Universitat de Barcelona, Marti i Franqués, 1-11, ES-08028, Barcelona, Spain.
E-mail address: alex.tarancon@ub.edu (A. Tarancón).

https://doi.org/10.1016/j.aca.2024.343573
Received 23 October 2024; Received in revised form 17 December 2024; Accepted 18 December 2024
Available online 19 December 2024

1. Introduction

Human activities can introduce anthropogenic radionuclides into the environment, leading to their accumulation. Among these radionuclides, radiostrontium and plutonium isotopes are particularly significant, representing the most important artificial radionuclides among beta and alpha emitters, respectively.

Radiostrontium is considered one of the most biologically hazardous radionuclides due to its chemical similarity to calcium. When ingested or inhaled, it can replace calcium in bones, leading to its accumulation in bone tissue, where it irradiates bone marrow and surrounding tissues. Prolonged exposure can cause cellular damage, potentially resulting in bone cancer, leukemia, or other types of cancer. The primary route of radiostrontium incorporation into the human body is through diet, particularly via water and cow's milk. Radiostrontium is released from authorized discharges from nuclear power plants, although unexpected increases of its activity can happen in case of a nuclear power plant accidents, illegal discharges, acts of terrorism or nuclear weapon testing. Therefore, monitoring radiostrontium is crucial to ensure public safety [1,2].

The two primary radiostrontium isotopes are ^{90}Sr (E_{max}: 0.546 MeV; $T_{1/2}$: 28.75 years), and ^{89}Sr (E_{max}: 1.495 MeV; $T_{1/2}$:50.53 days). ^{90}Sr poses a greater concern as a contaminant compared to ^{89}Sr, due to its longer half-life and the high energy of its decay product ^{90}Y (E_{max}:2.280 MeV; $T_{1/2}$: 64 h). The International Atomic Energy Agency (IAEA) has classified ^{90}Sr as a high-risk radionuclide, resulting in stricter regulatory measures for its environmental monitoring compared to ^{89}Sr. However, in ^{235}U fission reactions, the activity of ^{89}Sr can be much higher than that of ^{90}Sr. Therefore, in the event of a release, its activity could be one or two orders of magnitude higher. Consequently, environmental after a release must account for the presence and impact of ^{89}Sr [3,4].

Conventional methods for radiostrontium analysis typically involve chemical separation using extraction resins or coprecipitation methods, combined with various measuring techniques [5–8]. However, these methods often require the use of high-risk reagents and lengthy chemical separations. Additionally, the separate measurement of ^{89}Sr and ^{90}Sr is dependent on the delayed counting of the ^{90}Y in-growth [4,9]. Typically, an initial measurement of radiostrontium is performed immediately after separation from the matrix interferences, followed by a second measurement after reaching secular equilibrium, allowing the indirect determination of ^{90}Sr through the in-growth of ^{90}Y. However, this delayed counting strategy is unsuitable for radiological emergencies, where fast results are needed, and for routine environmental monitoring. To address this limitation, several methods have been developed to measure both radioisotopes simultaneously in a single measurement. These methods involve liquid scintillation counting (LSC) using two or three energy windows or performing sequential measurements through Cherenkov and LSC. Both strategies typically result in relative biases around 20–30 % [4,10–12]. In addition, these strategies generate mixed wastes (hazardous and radioactive). Therefore, there is a need for new methods that can accurately quantify the activity of both radionuclides simultaneously in a single measurement with acceptable quantification errors.

Among alpha emitters, plutonium isotopes are considered some of the most important radionuclides due to their toxicity and their accumulation in the food chain [13]. The sources of plutonium included nuclear power plants, nuclear fuel reprocessing activities and the nuclear weapons industry. The plutonium contribution consists of different isotopes, with ^{239}Pu and ^{240}Pu being of particular interest due to their higher abundance and long half-lives.

Conventional methods for plutonium isotopes analysis aim for specific separation of plutonium to minimize self-absorption effects and peak overlapping. The separation of plutonium from other actinides present in a sample involves the use of extraction chromatographic resins like UTEVA, TEVA or DGA resins followed by measurement through LSC, which generates a considerable amount of mixed wastes [14–22]. The determination can also be performed by α-spectrometry, which offers a very good detection limit and the ability to discriminate the different plutonium isotopes, although source preparation by microprecipitation is a lengthy procedure [23–27]. Both strategies rely on laborious procedures, highlighting the need for faster methods to provide rapid responses, especially in emergency situations. Additionally, due to the common origin of plutonium isotopes and radiostrontium, there is a high probability that both radionuclides will be present in the same sample, particularly in emergencies, doubling the number of analyses required. This underscores the importance of developing procedures that allow the simultaneous determination of both radionuclides [28].

PSresins have been developed over the past decade to reduce the generation of mixed wastes and create quicker methods for radionuclide determination. PSresin are plastic scintillation resins consisting of plastic scintillation microspheres (PSm) coated with a selective extractant, combining separation and measurement into a single step. This strategy has already been applied for radiostrontium determination using the PSm coated with a crown-ether (CE-PSresin) in river water and milk samples, achieving quantification errors below 4 % [29,30]. However, the determination of ^{89}Sr and ^{90}Sr was performed by deconvolution methods, resulting in quantification errors around 30 % [30]. For plutonium analysis, PSm coated with aliquat·336 (AL-PSresin) has been used for quantification, with errors below 10 % [31]. Despite these advances, there are no existing methods based on PSresin for determination of ^{89}Sr and ^{90}Sr with low quantification errors, nor methods that unify the determination of radiostrontium and plutonium.

The aim of this work has been to develop innovative strategies for the simultaneous measurement of challenging radionuclide mixtures, specifically ^{89}Sr and ^{90}Sr, as well as ^{90}Sr and plutonium isotopes, using PSresins. For ^{89}Sr and ^{90}Sr determination, the goal is the development of a method for the quantification of both isotopes with quantification errors lower than 20 % and without the need of a delayed measurement. For ^{90}Sr and plutonium isotopes, the focus is on developing a method for simultaneous determination (in one or two measurements) that significantly reduces the costs, time, and manpower in half compared with conventional methods. Moreover, these methods are designed to be environmentally friendly by avoiding the use of hazardous and toxic reagents and preventing the generation of mixed wastes thanks to the use of PSresins, which enables a cleaner, safer, and more sustainable alternative to conventional methods, making these strategies not only efficient but also aligned with environmental sustainability.

To achieve these goals, two different strategies were studied:

- 2in2: two different PSresin packed in separate SPE cartridge and used in tandem.
- 2in1: two different PSresin packaged in a single SPE cartridge, separated by a frit.

The 2in2 strategy allows for the separation of the cartridges after sample loading, enabling application of cleaning steps to remove interferences. However, this approach requires two measurements. In contrast, the 2in1 strategy involves only one measurement, making the detection process is faster. In this case, some form of discrimination is needed to differentiate the scintillation signal from each PSresin.

The 2in2 strategy has been applied for the simultaneous quantification of ^{89}Sr and ^{90}Sr, using α-PSresin [32,33] for the measurement of ^{90}Y and CE-PSresin [29] for the measurement of total radiostrontium. This strategy has also been used for simultaneous determination of ^{90}Sr and ^{239}Pu using CE-PSresin and AL-PSresin, respectively.

The 2in1 strategy has been applied for the simultaneous determination of ^{90}Sr and ^{239}Pu using CE-PSresin and a modified version of AL-PSresin [34], named mAL-PSresin. This modified PSresin incorporates a pulse delayer into the polymer matrix, allowing the determination of ^{90}Sr retained on the CE-PSresin and the ^{239}Pu retained on the mAL-PSresin through α/β discrimination in a single measurement.

2. Experimental section

2.1. Reagents

All the reagents used were of analytical grade. Polystyrene (PS) (MW 250,000 g mol^{-1}) was supplied by Acros Organics (Geel, Belgium). Fully hydrolysed polyvinyl alcohol (PVA), 2,5-diphenyloxazole (PPO), nitric acid (69 %), L (+)-ascorbic acid (≤99 %) and hydrogen peroxide (30 %) were obtained from Panreac (Castellar del Valles, Spain). Hydrochloric acid (37 %), methanol (≤99.9 % for HPLC), amidosulfonic acid, aluminium nitrate nonahydrate, aliquat-336, 1,4-bis(5-phenyl-2-oxazolyl) benzene (POPOP), yttrium nitrate hexahydrate (99.8 % trace metals basis), biphenyl and dichloromethane (99.9 %) were supplied by Merck (Darmstadt, Germany). Strontium standard (10,000 ppm) was supplied from Inorganic Ventures (Christiansburg, USA). *p*-Terphenyl was supplied by Honeywell Fluka (Charlotte, US).

^{239}Pu active stock solution of 32 (1) Bq·g^{-1} was supplied by GE Healthcare-Amersham International (Buckinghamshire, England) and ^{90}Sr/^{90}Y active stock solution of 4071 (31) Bq·g^{-1} was supplied by GE Healthcare-Amersham International (Buckinghamshire, England). ^{89}Sr active stock solution of 13.02 (0.09) KBq·g^{-1} in a solution of strontium (50 μg g^{-1}) and 0.1 M HCl was supplied by Eckert and Ziegler (Berlin, Germany).

2.2. Apparatus

Scintillation measurements were performed using a Quantulus liquid scintillation spectrometer (PerkinElmer, Waltham, USA) and a HIDEX 300 SL super low-level detector (Hidex, Turku, Finland).

The analysis of stable isotopes was performed using an OPTIMA 8300 ICP-OES detector (PerkinElmer, Waltham, USA) or an ELAN-6000 ICP-MS detector (PerkinElmer, Waltham, USA) from the scientific and technological centres of the University of Barcelona (CCiTUB).

2.3. PSresin cartridge preparation

CE-PSresin, mAL-PSresin and α-PSresin were prepared following established literature methods [29,33,34]. The mAL-PSresin was prepared using a new PSm support that incorporates biphenyl and *p*-Terphenyl trapped in the polymeric matrix, modifying the existing procedure [35]. Cartridges for CE-PSresin and α-PSresin were prepared by packaging 1.4 g of the respective PSresin into a 2-mL SPE cartridge (length: 3.2 cm; internal diameter: 1 cm; external diameter: 1.2 cm) from Triskem International (Rennes, France). MSP-PSresin cartridges were prepared by packing 0.5 g of mAL-PSresin and 0.5 g of CE-PSresin, in that order, into a 2-mL SPE cartridge with a frit separating the two PSresins. The cartridges were closed with a filter and a stopper, placed in a vacuum chamber, and 10 mL of water were passed through each one at a flux of 1 mL min^{-1}. Before loading, each column was shaken for 3 min in a vortex at 3000 rpm to ensure homogenization of the PSresin.

2.4. Procedures

2.4.1. 2in2 tandem separations

2.4.1.1. Standards sample analysis. For the analysis of ^{89}Sr and ^{90}Sr, standard samples containing 5 mg of stable strontium, 1 mg of stable yttrium and 200 dpm of ^{90}Sr (and ^{90}Y) or ^{89}Sr in 11 mL of the corresponding working media (3 M, 6 M and 8 M nitric acid) were prepared. The solution was loaded into the CE-PSresin or the α-PSresin at a flow rate of approximately 1 mL min^{-1}, corresponding to a pressure of 3–5 inHg. Once the sample was loaded, it was rinsed twice with 2 mL of the loading sample medium, followed by two rinses with 2 mL of 6 M lithium nitrate for each PSresin.

For the analysis of ^{90}Sr and plutonium, standard samples were prepared by adding ^{239}Pu (200 dpm) and/or ^{90}Sr (200 dpm) standard, 1 mg of stable strontium and 3 M HNO_3/0.5 M $Al(NO_3)_3$ medium up to 11 mL. Samples were then subjected to valence adjustment treatment by sequentially adding first 20 μL of 0.6 M iron sulphamate (II), 1 mL of 1.5 M ascorbic acid and 1 mL of 3.5 M sodium nitrite. Once Pu was in +IV valence state, the sample was passed through the mAL-PSresin and CE-PSresin and rinsed twice with 2 mL of the 3 M HNO_3/0.5 M $Al(NO_3)_3$ solution. Both cartridges were then rinsed separately with 6 M HNO_3 (2 mL, twice) and 6 M $LiNO_3$ (2 mL, twice) for the CE-PSresin and 9 M HCl (2 mL, twice) and 0.5 M HNO_3 (2 mL, twice) for mAL-PSresin.

Finally, in both cases, the pressure was increased to 15–20 inHg for 10 min to ensure the cartridges were thoroughly dried. The eluates were collected in 25 mL conical tubes for the analysis of the stable isotopes by ICP-OES to determine the yield for strontium and yttrium. Concentration of Sr^{2+} and Y^{3+} in the ICP tubes for the standards after dilution (1:100) with HNO_3 1 % were of 5 and 1 mg/L, respectively. Sr^{2+} and Y^{3+} concentrations in the eluates ICP tubes after dilution (1:10) were just above or in the limit of detection (0.02 mg/L and 0.05 mg/L, respectively) if a 99 % retention is assumed. For Y^{3+}, samples below the LD were also measured by ICP-MS.

2.4.1.2. River water sample analysis. River water from Ebro River was spiked with four different ratios of ^{90}Sr to ^{89}Sr (1:1, 3:1, 1:3 and 1:4) with a reference activity of 20 Bq·L^{-1}. Additionally, 1 mg of yttrium and 5 mg of stable strontium were added. Fig. S1 in supplementary material shows the whole separation diagram.

For ^{90}Sr:^{239}Pu mixtures, the sample was spiked to achieve an activity of 5 Bq·L^{-1} for each radionuclide, along with 1 mg of Sr^{2+}. Fig. S2 in supplementary material shows the whole separation diagram.

In all cases, 100 mL of sample was analyzed. The sample was evaporated to dryness, then redissolved in 4 mL of 8 M nitric acid and 1 mL of 30 % hydrogen peroxide. This was followed by further evaporation to dryness and redissolution in 10 mL of the working medium. The separation procedure using PSresin was conducted as described in section 2.4.1.1.

2.4.2. 2in1 tandem separation

2.4.2.1. Standards sample analysis. Standard solutions for strontium and plutonium were prepared by adding 100 dpm of ^{90}Sr or/and ^{239}Pu, 1 mg of stable strontium and 3 M HNO_3/0.5 M $Al(NO_3)_3$ solution to a final volume of 11 mL in a 20 mL polyethylene vial. Valance adjustment was performed as described previously. 10 mL of the solution were passed through the MSP-PSresin cartridge (including mAL-PSresin and CE-PSresin), which had been preconditioned with 2 mL of the working medium. The cartridge was then rinsed four times with 2 mL of the loading medium. To ensure the dryness of the cartridge, the pressure was increased to 15–20 inHg for 10 min. The cartridge effluents were collected in a 25 mL conical tube and measured by ICP-OES together with an aliquot of the sample to determine the retention yield for strontium.

2.4.2.2. River water sample analysis. Two 100 mL river water samples, each spiked with 5 Bq·L^{-1} of ^{90}Sr and ^{239}Pu and 1 mg of stable strontium, were analyzed. Organic matter was removed by evaporation to dryness, followed by redissolution in 4 mL of 8 M nitric acid and 1 mL of 30 % hydrogen peroxide. Sample was then evaporated to dryness again and redissolved in 10 mL of the working medium. Valence adjustment subsequently applied. The separation procedure followed the method described in section 2.4.2.1. Fig. S3 in supplementary material shows the whole separation diagram.

2.5. Measurements

CE-PSresin and α-PSresin cartridges for ^{89}Sr/^{90}Sr determination were

measured for 1 h immediately after separation using a Quantalus Wallac 1220 with the low coincident bias and "14C" configuration. The external quenching parameter (SQP(E)) was measured for 10 min for each vial.

CE-PSresin, AL-PSresin and MSP-PSresin for ^{90}Sr/Pu determination were measured using a HIDEX 300 SL super low-level detector for 1 h for the standard solutions and 3 h for the river water samples. The pulse length index (PLI) level was set at 19 after optimization. The external quenching parameter QPE was measured for 1 min for each vial.

2.6. Data treatment

Scintillation spectra were smoothed with the Savitzky–Golay filter (21 points and a first-degree polynomial). Detection efficiency corresponds to the net count rate divided by the activity retained in the α-PSresin, Sr-PSresin or MSP-PSresin.

^{89}Sr and ^{90}Sr activities were obtained following Eq. (1) and Eq. (2), respectively.

$$Act^{90}Sr = Act^{90}Y = \frac{r_{\alpha-ps}}{\varepsilon^{90}Y \cdot RY^{3+} \cdot V \cdot 60} \quad \text{(Eq.1)}$$

$$Act^{89}Sr = \frac{\frac{r_{CE}}{RSr^{2+} \cdot 60} - Act^{90}Sr \cdot V \cdot \varepsilon^{90}Sr}{\varepsilon^{89}Sr \cdot V} \quad \text{(Eq.2)}$$

Where Act^{90}Sr and Act^{89}Sr, refer to the activity of ^{90}Sr and ^{89}Sr in Bq·L^{-1}; $\varepsilon^{90}Y$, $\varepsilon^{90}Sr$ and $\varepsilon^{89}Sr$ refer to the detection efficiency for ^{90}Y, ^{90}Sr and ^{89}Sr, respectively; RY^{3+} and RSr^{2+} refer to the separation yield for yttrium and strontium, respectively; V to the volume of sample (in L); and $r_{\alpha\text{-ps}}$ and r_{CE} to the count rate (in cpm) obtained in the α-PSresin and CE-PSresin, respectively.

^{239}Pu and ^{90}Sr activities in MSP-PSresin were obtained following Eq. (3) and Eq. (4), respectively:

$$ACT_{Pu} = \frac{r_\alpha \cdot E_\beta - r_\beta \cdot I_\beta}{(E_\alpha \cdot E_\beta - I_\alpha \cdot I_\beta) \cdot 60 \cdot V} \quad \text{(Eq.3)}$$

$$ACT_{Sr} = \frac{r_\beta \cdot E_\alpha - r_\alpha \cdot I_\alpha}{(E_\alpha \cdot E_\beta - I_\alpha \cdot I_\beta) \cdot 60 \cdot V \cdot RSr^{2+}} \quad \text{(Eq.4)}$$

Where Act_{Pu} and Act_{Sr}, refer to the activity of ^{239}Pu and ^{90}Sr in Bq·L^{-1}; E_α, and E_β refer to the detection efficiency of plutonium in the alpha spectrum and ^{90}Sr in the beta spectrum; I_α, and I_β refer to the alpha and beta misclassification error, respectively; RSr^{2+} refers to the strontium retention in the MSP-PSresin cartridge; V to the volume of sample (in L); and r_α and r_β to the triple coincidence count rate (in cpm) in the alpha region and the beta region, respectively.

^{239}Pu and ^{90}Sr activities in 2in2 tandem were obtained directly from the sample volume (in L); the triple coincidence count rate (in cpm); the detection efficiencies in the AL-PSresin and CE-PSresin; and the yield of strontium.

3. Results and discussion

The results presented in this work are divided in two sections:

- 2in2 strategy: This approach uses two PSresin in tandem and involves two measurements for the determination of ^{90}Sr and ^{89}Sr, as well as ^{90}Sr and ^{239}Pu mixtures.
- 2in1 strategy: This approach involves a mixture of PSresins and α/β discrimination for the determination of ^{90}Sr and ^{239}Pu in a single measurement.

3.1. 2in2 configuration

3.1.1. ^{89}Sr and ^{90}Sr mixture

The strategy for the rapid determination of ^{90}Sr and ^{89}Sr in an environmental monitoring scenario or after an emergency was based on the retention of both strontium radionuclides in the CE-PSresin, the retention of ^{90}Y in the α-PSresin, the measurement of both PSresin, the calculation of the ^{90}Sr activity from the α-PSresin count rate (assuming secular equilibrium with ^{90}Y), and the calculation of the ^{89}Sr activity from the CE-PSresin count rate after subtracting the count rate due to ^{90}Sr.

3.1.1.1. Calibration. CE-PSresin can retain strontium with high yields in nitric acid solutions with concentrations ranging from 3 M to 8 M, without retention of yttrium [29,30,36]. Conversely, yttrium is known to be retained in the α-PSresin under almost any acidic condition, while strontium is not retained or is slightly retained in nitric acid concentrations higher than 2 M [33].

First, the optimum working medium conditions for ^{90}Y retention and measurement on the α-PSresin were assessed (Table 1). Three different nitric acid concentrations (3 M, 6 M and 8 M) were evaluated.

Yttrium retention yield on the α-PSresin ranged from 55 % to 65 % and no differences were observed between media if uncertainty of the values is considered. These medium-low retention yield values can be attributed to a too fast flow rate or lack of compaction of the PSresin inside the cartridge, which is lately addressed. The detection efficiency for 3 M and 6 M presented values around 90 %, indicating that almost all particles are detected. However, under 8 M HNO_3 conditions, the α-PSresin acquired a slight yellow color, likely due to a reaction with the extractant; therefore, this medium was not considered in further experiments. In all cases, the retention of strontium in the α-PS resin was evaluated by loading 1 mg of Sr^{2+} and measuring the Sr^{2+} content in the waste. Results showed a retention lower than 5 %, which can be disregarded considering that strontium is retained first and almost quantitatively in the CE-PSresin.

The same media, excluding 8 M, were studied in the CE-PSresin for strontium isotopes. In both media, the retention of strontium was quantitative and no retention of yttrium was observed. The detection efficiency of ^{90}Sr and ^{89}Sr was 94 % and 98 % in 6 M nitric acid and 94 % for both isotopes in 3 M nitric acid.

Fig. 1 shows the spectra for ^{90}Sr and ^{89}Sr in the CE-PSresin and ^{90}Y in the α-PSresin in 6 M nitric acid (spectrum in 3 M medium was in the same position).

It was expected ^{90}Y to appear at higher energy channels due to its higher energy compared to the other isotopes. However, since different PSresin were used, the spectrum position may vary. For radiostrontium, ^{90}Sr appears at lower energy channels compared to ^{89}Sr, which is consistent with the higher energy of ^{89}Sr relative to ^{90}Sr.

Both working media allowed for accurate quantification of radiostrontium isotopes. Nevertheless, 6 M nitric acid was chosen as the optimal medium due to its slightly better performance and its status as the reference medium for strontium in the CE-PSresin.

3.1.1.2. Evaluation of the ^{90}Sr: ^{89}Sr ratio. Once the parameters of the column were established, both columns were connected and the different solutions (conditioning, sample and rinsing) were passed through them. The levels of ^{89}Sr in a sample can range from 3 to 24 times higher than those of ^{90}Sr [9]. However, the ratio of ^{89}Sr:^{90}Sr will gradually decrease over time due to the more rapid decay of ^{89}Sr. To account for the variability in possible ^{89}Sr:^{90}Sr ratios and to demonstrate the viability of the strategy under high disproportion ratios, the tandem

Table 1
Yttrium retention yield and ^{90}Y detection efficiency on α-PSresin regarding the nitric acid concentration.

	3 M HNO_3	6 M HNO_3	8 M HNO_3
Yttrium yield (%)	62 (5)	57 (5)	60.6 (0.3)
^{90}Y detection efficiency	88 (2)	96.9 (0.7)	79 (2)

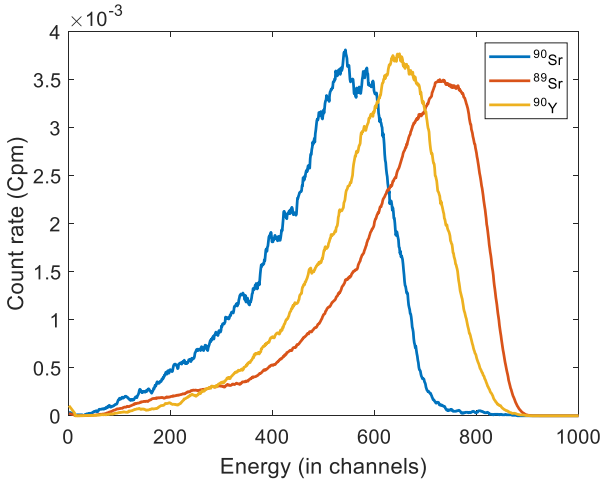

Fig. 1. Normalized count rate spectra for each radionuclide.

separation was tested on seven different ^{89}Sr:^{90}Sr ratios. Additionally, to calculate the yield, Sr and Y content in the solutions passed through the column were analyzed by ICP-OES, assuming no retention of Sr on the α-PSresin and no retention of Y on the CE-PSresin. The quantification errors for each isotope can be seen in Table 2.

Quantification errors for ^{90}Sr were low across all studied ratios, which was expected since it is quantified directly from the measurement of ^{90}Y in the α-PSresin. Quantification errors for ^{89}Sr were also low, however, when the activity of ^{90}Sr is higher than that of ^{89}Sr, the quantification errors increase. This is due to the uncertainty associated to the calculation, as it considers the activity obtained from the α-PSresin. The retention yields for both strontium and yttrium were nearly quantitative (>96 %). This represents an improvement over calibration, where the retention yield for yttrium was around 60 %. This improvement can be attributed to the flow of the solution in the tandem separation, as the solution from the CE-PSresin arrives drop by drop to the α-PSresin, increasing the yield to 98 %.

3.1.1.3. River water sample analysis. To validate the strategy, 100 mL spiked river water samples were analyzed. Four ^{90}Sr:^{89}Sr ratios were studied (1:1, 3:1, 3:1 and 1:4). Organic matter was removed by evaporating the sample to dryness, treating the residue with 8 M HNO_3 and 30 % H_2O_2, and then reconstructing the sample in 6 M nitric acid. In all cases, the quantification errors were lower than 15 % (Table 3).

The method proved to be fast, with results available in less than 5 h from sample reception, making it suitable for rapid analysis purposes. The detection limit, calculated using the Currie equation, was 0.13 $Bq{\cdot}L^{-1}$ for a 100 mL volume sample and 1 h of measurement in a Quantulus detector [37]. This allows for the quantification of ^{90}Sr and ^{89}Sr with errors lower than those typically reported.

3.1.2. ^{90}Sr and plutonium isotopes determination

Since ^{90}Sr and plutonium isotopes are both artificial, long-lived radionuclides, rapid analysis of both may be necessary in the event of a nuclear emergency or for waste characterization. Tandem determination using PSresin can be achieved by retaining ^{90}Sr in a CE-PSresin and plutonium isotopes in an AL-PSresin. Both isotopes can be retained in their respective PSresin at high HNO_3 concentrations (3–8 M), typically 3 M for plutonium (combined with 0.5 M $Al(NO_3)_3$) and 6 M for ^{90}Sr. Sr^{2+} is not retained on the resins based on aliquat·336 as the AL-PSresin [38]. However, since plutonium can also be retained on the CE-PSresin, the AL-PSresin must precede the CE-PSresin. Therefore, the working medium chosen was the one optimized for plutonium, as it also ensures strong retention of strontium. Before loading, a valence adjustment pretreatment is required to obtain Pu(IV), the valence state in which plutonium has the highest affinity for the extractant. Various valence state adjustments can be applied, but previous methods described in the literature for plutonium determination using the AL-PSresin indicate that the optimal valence adjustment involves a three-steps method with iron (II) sulphamate, ascorbic acid and sodium nitrite [31]. After loading, the two PSresins were cleaned with different solutions, necessitating separate rinsing.

Table 2
Relative errors for ^{89}Sr and ^{90}Sr ratios.

^{90}Sr:^{89}Sr	^{90}Sr (%)	^{89}Sr (%)
1:1	3.0	−0.7
1:2	8.8	−5.4
2:1	4.4	−15.8
1:5	−0.1	5.1
5:1	−0.5	10.4
1:10	3.6	−0.3
10:1	−1.9	11.8

Table 3
Relative errors for ^{89}Sr and ^{90}Sr respectively on river spiked water samples.

^{90}Sr:^{89}Sr	^{90}Sr (%)	^{89}Sr (%)
1:1	−10.7	11.1
3:1	−9.2	−8.9
1:3	6.5	−5.7
1:4	8.6	1.3

^{90}Sr and plutonium standard samples were first loaded separately into both PSresin in tandem to determine in which extent cross contamination could take place. Fig. 2 shows the spectra of each standard sample in each PSresin, whereas Table 4 shows the count rate of the background and the standard sample and the retention of the radionuclides in the PSresin where they are not supposed to be retained.

The results indicate that cross-contamination did not occur with the CE-PSresin being free of ^{239}Pu and AL-PSresin free of ^{90}Sr, as the count rate of the standard is lower than the count rate of the background, supposing a retention lower than 1 %. Retention was 99 % for plutonium in the AL-PSresin and 94 % for strontium in the CE-PSresin. Detection efficiency in triple coincidence mode was 91 (2)% for ^{239}Pu and 58 (2)% for ^{90}Sr.

A 100 mL river water spiked with ^{90}Sr (0.5 Bq) and ^{239}Pu (0.5 Bq) was analyzed in triplicate to validate the procedure. Sample treatment involved the destruction of organic matter, following the previously described method, and adjustment of plutonium valence to Pu(IV). To calculate the separation yield, stable strontium was measured by ICP-OES in the solutions passed through the column, while quantitative retention was assumed plutonium. Although, gold could be used as a tracer for plutonium, it introduces quenching in the PSresin. Given that this measurement is intended for emergency situations, assuming quantitative retention for plutonium can be considered safe. The quantification errors obtained (Table 5) were sufficiently low, demonstrating that the method can be applied successfully.

The limits of detection achieved for ^{90}Sr and ^{239}Pu were 0.33 $Bq{\cdot}L^{-1}$ and 0.18 $Bq{\cdot}L^{-1}$, respectively, considering 3 h of counting time, a sample volume of 100 mL and measurement using a Hidex 300 SL detector in triple coincidence counting mode. The total time of analysis, including counting time, was established at 12 h.

3.2. 2in1 configuration

A faster alternative for the simultaneous analysis of ^{90}Sr and plutonium isotopes was developed, involving a mixture of both PSresin in the same cartridge, with a single measurement and the use of alpha/beta discrimination to differentiate between the signal from ^{90}Sr and plutonium isotopes.

To achieve this, the composition of the AL-PSresin was modified to

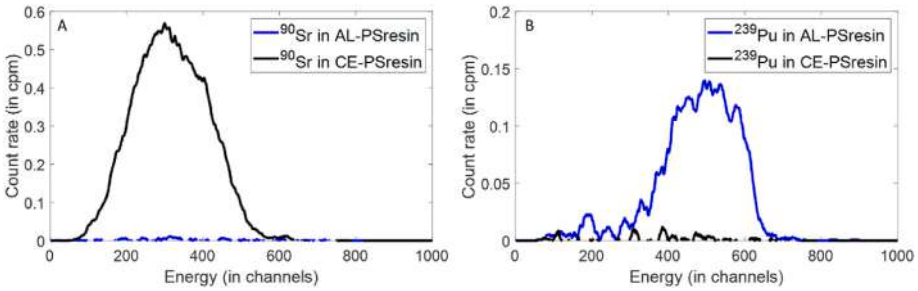

Fig. 2. (a) $^{90}Sr/^{90}Y$ and (b)^{239}Pu standard passed though CE-PSresin and AL-PSresin.

Table 4
Evaluation of cross-contamination: background and standard count rate and retention in triple coincidence mode (Pu in CE-PSresin and^{90}Sr in AL-PSresin).

	Background (cpm)	Standard (cpm)	Retention (%)
CE-PSresin (n = 5)	8.1 (0.4)	7.4 (0,3) (^{239}Pu)	<1 %[a]
AL-PSresin (n = 5)	8.0 (0.4)	8.3 (0.6) (^{90}Sr)	<0.8 %[a]

[a] Retention calculated considering the limit of detection.

Table 5
Relative errors for^{239}Pu and^{90}Sr in 2in2 tandem analysis.

	^{239}Pu(%)	^{90}Sr (%)
Sample 1	11.8	−1.4
	−2.6	−5.7
Sample 2		
	−5.0	−0.5
Sample 3		

delay the scintillation pulses generated by ^{239}Pu through the incorporation of *p*-terphenyl and biphenyl into the PSm, resulting in a new PSresin, mAL-PSresin [39,40]. P-terphenyl and biphenyl influence the timing and intensity of the scintillation signal by modifying the energy transfer processes within the scintillator molecules. P-terphenyl shifts the emission spectrum, while biphenyl modifies the ratio of singlet to triplet state excitations, increasing triple excitations. This change extends the pulse decay time, as triplet relaxation is slower than singlet relaxation. This modification provides an effective method for delaying the scintillation pulses in one of the resins (mAL-PSresin), allowing the recognition and differentiation of signals produced by the CE-PSresin and the mAL-PSresin based on pulse duration.

This modification allows for the correct quantification of both radionuclides in a mixture by including two PSresin in the same cartridge: one selective for a beta-emitting radionuclide that generates fast pulses, and another selective for an alpha-emitting radionuclide that generates slow pulses. In this new type of PSresin cartridge, called MSP-PSresin, the two PSresins are separated by a frit to prevent beta particles from interacting with the PSresin for the alpha-emitting radionuclide. In this setup, the MSP-PSresin has been applied to the determination of ^{90}Sr and ^{239}Pu, with the mAL-PSresin positioned at the top and the CE-PSresin at the bottom.

3.2.1. Calibration

The conditions used were the same as those in the 2in2 tandem separation: 3 M HNO_3 and 0.5 M $Al(NO_3)_3$ as separation medium, with valence adjustment using iron sulphamate, ascorbic acid and sodium nitrate. In this case, since separate rinsing for each PSresin was not possible, the cleaning process consisted of passing four times 2 mL of 3 M HNO_3.

Calibration involved studying both radionuclides separately in the MSP-PSresin by the preparing independent standards and measuring with a HIDEX 300 SL detector. Samples were measured after 2 h of darkness to minimize chemiluminescence effects caused by residual reactions from the valence state adjustment. The 3D spectrum obtained from the HIDEX detector allowed for the determination of the optimum PLI value, which defines the integration windows with the best α/β discrimination performance.

Fig. 3 shows the 3D spectra obtained for the standards in the doble coincidence configuration, as the 3D spectrum cannot be obtained in triple coincidence mode. Despite the prominent chemiluminescence (high signal at low energy values), it was possible to stablish an optimal PLI value of 19. At this PLI values, the misclassification rates for strontium and plutonium were 2.3 (0.6)% and 11 (2)% respectively. Table 6 presents the retention and detection efficiencies obtained for ^{90}Sr and ^{239}Pu using PLI value of 19 in the triple coincidence counting mode.

Fig. 4 shows the spectra for ^{90}Sr and ^{239}Pu in the optimum windows (PLI<19 for ^{90}Sr and PLI>19 for ^{239}Pu) in the triple configuration mode. In this configuration no luminescence was observed. However, ^{239}Pu measurements can be slightly affected by quenching effects, as the spectrum was slightly shifted to lower energy channels compared to the AL-PSresin (Fig. 2). This shift can be attributed to two factors: changes in the composition of the plastic scintillator to enhance α/β discrimination and a slight blue color due to valence treatment. This blue color was also present in the 2in2 configuration but was removed after cleaning with 9 M HCL and 0.5 M HNO_3, which is not possible in this configuration due to the elution of Sr from the column. Quenching effects, triple coincidence counting, and misclassification were the reasons beyond the 64 % of total detection efficiency for ^{239}Pu.

Since both radionuclides were satisfactorily measured when loaded separately in the MSP-PSresin, four 10 mL standard samples containing both radionuclides at a 1:1 activity ratio were analyzed. Yield calculation was performed using the same strategy as with the 2in2 separation.

Table 7 presents the quantification errors for each sample after activity calculation, applying misclassification correction (eqs. (3) and (4)).

The quantification error for all four samples was below 5 % for both radionuclides, except for ^{90}Sr in the fourth sample, which was 11 %. Values from ^{90}Sr were negative in all cases, although low enough to consider that this could be due to the uncertainty associated with the analysis. The results confirm the suitability of the 2in1 strategy for the simultaneous determination of both radionuclides.

3.2.2. River water sample analysis

Finally, two river water samples spiked with ^{90}Sr and ^{239}Pu in 1:1 ratio, each with an activity of 5 $Bq{\cdot}L^{-1}$, were analyzed. As in previous cases, organic matter was destroyed and valence was adjusted before sample loading. The quantification errors for the samples were all below 8 % (Table 8).

This strategy was demonstrated to be fast, with results for both radionuclides available in less than 8 h from sample reception. This makes it suitable for rapid environmental monitoring or emergency needs, with detection limits of 0.18 $Bq{\cdot}L^{-1}$ for ^{90}Sr and 0.04 $Bq{\cdot}L^{-1}$ for ^{239}Pu, considering a 100 mL sample volume and 3 h of measurement in a Hidex

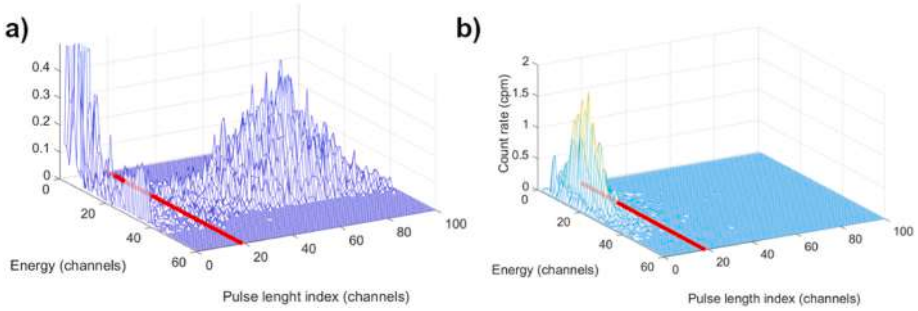

Fig. 3. 3D spectra for ^{239}Pu (a) and ^{90}Sr (b) with MPS-PSresin in Hidex 300 SL detector in double coincidence count rate configuration.

Table 6
Detection efficiency of ^{90}Sr and ^{239}Pu in the MSP-PSresin.

	^{90}Sr (PLI<19)	^{239}Pu (PLI>19)
Background (cpm)[b]	7.35	0.61
Retention (%)	70 %	64 (2)[a]
Detection efficiency (%)[b]	69 (5)	
Misclassification (%)[b]	2.3 (0.6)	11 (2)

[a] combined value of retention and detection efficiency.
[b] triple coincidence counting mode.

300 SL detector in triple coincidence counting mode.

Comparing the two strategies for the simultaneous analysis of ^{90}Sr and ^{239}Pu, the 2in1 strategy reduces the analysis time from 12 to 8 h, since only one measurement is performed. Moreover, the application of α/β discrimination in the 2in1 configuration lowers the background in the alpha window, reducing the detection limit for ^{239}Pu from 0.18 to 0.04 Bq L^{-1}. Conversely, the 2in2 configuration allows for more rinsing steps, as cartridges can be separated. This is particularly useful for removing thorium from the AL-PSresin with HCl 9 M in ^{90}Sr and ^{239}Pu mixtures. Moreover, the 2in1 configuration uses a smaller amount of resin in the cartridge, which reduces its capacity. This could affect the retention of strontium in samples with high natural strontium content (e.g., milk samples or high-volume samples).

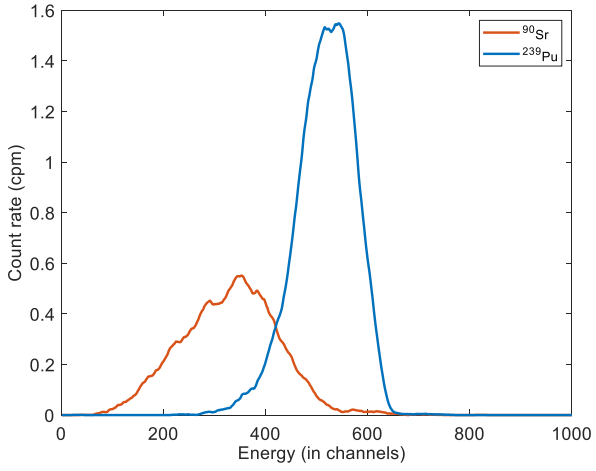

Fig. 4. Triple coincidence spectra for standards of ^{90}Sr (PLI< 19) and ^{239}Pu (PLI>19).

Table 7
Quantification errors for each sample and radionuclide.

	^{239}Pu(%)	^{90}Sr (%)
Sample 1	−3.6	−5.4
	−2.5	−1.8
Sample 2		
	1.7	−4.2
Sample 3		
	4.3	−10.8
Sample 4		

Table 8
Relative errors for ^{90}Sr and ^{239}Pu in river water samples.

	^{239}Pu(%)	^{90}Sr (%)
Sample 1	7.8	1.6
	6.6	−1.3
Sample 2		

4. Conclusions

The use of PSresin in tandem for the simultaneous determination of multiple radionuclides has been demonstrated to be feasible in two configurations: two PSresin in two cartridges (2in2) and two PSresin in one cartridge (2in1). For the 2in1 configuration, the quantification is possible as long as the signals from the two PSresin are not overlapped.

For ^{90}Sr and ^{89}Sr mixtures, the quantification of both radionuclides was achieved by measuring ^{90}Y in the α-PSresin and radiostrontium in the CE-PSresin. A 2 h measurement (1 h per PSresin cartridge) was sufficient to achieve a limit of detection of 0.013 Bq·L^{-1}, lower than the detection limits required by the legislation [41], and with quantification errors, for river water samples with high disproportion ratios, below 10 %, improving conventional methods that do not achieve quantification errors lower than 30 %. Additionally, this strategy can provide the result in 5 h since sample reception, which is much faster than conventional methods where a 1-month delayed measurement is required, regardless of whether the sample is in secular equilibrium or not. Nevertheless, the strategy proposed can only be applied for environmental monitoring or emergency situations, where secular equilibrium between ^{90}Sr and ^{90}Y has been established.

Simultaneous determination of ^{90}Sr and plutonium has been successfully achieved using both the 2in2 and 2in1 configurations. Both methods effectively halve the sample processing time, achieving similar analytical performances than conventional methods and without using liquid scintillation cocktails. This makes them particularly efficient in emergency scenarios where speed and accuracy are required.

In the 2in2 configuration, a 100 mL sample can be analyzed in 12 h (6 h per cartridge), achieving a limit of detection of 0.33 Bq·L^{-1} for ^{90}Sr and 0.18 Bq·L^{-1} for ^{239}Pu. Quantification errors are close to or below 10 % for a 1:1 ratio, making these values acceptable for emergency analysis purposes. The time of analysis and detection limits can be improved using the 2in1 strategy, as the counting time is halved and the detection limit for ^{239}Pu can be lowered to 0.04 Bq·L^{-1} thanks to α/β discrimination. With this strategy, quantification errors are close to or below 8 %, similar to those of the 2in2 strategy.

In conclusion, PSresin in tandem can provide faster results than

conventional methods, reducing the cost, time and effort required.

CRediT authorship contribution statement

I. Giménez: Writing – review & editing, Writing – original draft, Visualization, Methodology, Investigation, Formal analysis, Data curation, Conceptualization. **H. Bagán:** Writing – review & editing, Supervision, Resources, Methodology, Funding acquisition, Conceptualization. **A. Tarancón:** Writing – review & editing, Writing – original draft, Supervision, Project administration, Methodology, Funding acquisition, Formal analysis, Conceptualization.

Declaration of competing interest

The authors declare that they have no known competing financial interests or personal relationships that could have appeared to influence the work reported in this paper.

Acknowledgments

This work was carried out in a Generalitat de Catalunya Research Group (2021 SGR 01342) and has received funding from the Ministerio de Ciencia, Innovación y Universidades (MICIU) de España through project PID2020-114551RB-I00 funded by MICIU/AEI/10.13039/501100011033. I. Giménez thanks the Universitat de Barcelona for the PREDOCS-UB grant.

Appendix A. Supplementary data

Supplementary data to this article can be found online at https://doi.org/10.1016/j.aca.2024.343573.

Data availability

Data will be made available on request.

References

[1] N. Vajda, C.K. Kim, Determination of radiostrontium isotopes: a review of analytical methodology, Appl. Radiat. Isot. 68 (2010) 2306–2326, https://doi.org/10.1016/j.apradiso.2010.05.013.
[2] R. Chobola, P. Mell, L. Daróczi, A. Vincze, Rapid determination of radiostrontium isotopes in samples of NPP origin, J. Radioanal. Nucl. Chem. 267 (2006) 297–304, https://doi.org/10.1007/s10967-006-0044-6.
[3] M. Tayeb, X. Dai, S. Sdraulig, Rapid and simultaneous determination of Strontium-89 and Strontium-90 in seawater, J. Environ. Radioact. 153 (2016) 214–221, https://doi.org/10.1016/j.jenvrad.2016.01.003.
[4] IAEA, Rapid simultaneous determination of 89sr and 90sr in milk: a procedure using cerenkov and scintillation counting. IAEA Analytical Quality in Nuclear Applications No. IAEA/AQ/27, 2013. ISSN 2074–7659.
[5] H. Kim, Y.G. Kang, Y.-J. Lee, S.-D. Choi, J.-M. Lim, J.-H. Lee, Automated extraction chromatographic radionuclide separation system for analysis of 90Sr in seawater, Talanta 217 (2020) 121055, https://doi.org/10.1016/j.talanta.2020.121055.
[6] M. Uesugi, R. Watanabe, H. Sakai, A. Yokoyama, Rapid method for determination of 90Sr in seawater by liquid scintillation counting with an extractive scintillator, Talanta 178 (2018) 339–347, https://doi.org/10.1016/j.talanta.2017.09.041.
[7] A. Habibi, B. Boulet, M. Gleizes, D. Larivière, G. Cote, Rapid determination of actinides and 90Sr in river water, Anal. Chim. Acta 883 (2015) 109–116, https://doi.org/10.1016/j.aca.2015.04.025.
[8] Ž. Grahek, N.Z. Zečević, S.L. Lulić, Possibility of rapid determination of low-level 90 Sr activity by combination of extraction chromatography separation and Cherenkov counting. https://doi.org/10.1016/S0003-2670(99)00469-9, 1999.
[9] M. Tayeb, X. Dai, E.C. Corcoran, D.G. Kelly, Rapid determination of 90Sr from 90Y in seawater, J. Radioanal. Nucl. Chem. 304 (2015) 1043–1052, https://doi.org/10.1007/s10967-015-3935-6.
[10] K. Günther, S. Lange, M. Veit, A rapid method for determining 89Sr and 90Sr by Cerenkov counting, Appl. Radiat. Isot. 67 (2009) 781–785, https://doi.org/10.1016/j.apradiso.2009.01.035.
[11] J. Eikenberg, H. Beer, M. Rüthi, I. Zumsteg, A. Vetter, Precise determination of 89Sr and 90Sr/90Y in various matrices: the LSC 3-window approach. LSC. Advances in Liquid Scintillation Spectrometry, Radiocarbon, AZ, 2005, pp. 237–249.
[12] P.A. Pittet, F. Bochud, P. Froidevaux, Determination of 89 Sr and 90 Sr in fresh cow milk and raw urine using crystalline synthetic tunnel manganese oxides and layered metal sulfides, Anal. Chim. Acta 1047 (2019) 267–274, https://doi.org/10.1016/j.aca.2018.10.007.
[13] National Research Council The Radiochemistry of Plutonium, The Radiochemistry of Plutonium, The National Academies Press, Washington, DC, 1965, https://doi.org/10.17226/21553.
[14] H. Michel, G. Barci-Funel, J. Dalmasso, G. Ardisson, One step ion exchange process for the radiochemical separation of americium, plutonium and neptunium in sediments, J. Radioanal. Nucl. Chem. 240 (1999) 467–470, https://doi.org/10.1007/BF02349397.
[15] M. Toribio, J.F. García, G. Rauret, R. Pilviö, M. Bickel, Plutonium determination in mineral soils and sediments by a procedure involving microwave digestion and extraction chromatography, Anal. Chim. Acta 447 (2001) 179–189, https://doi.org/10.1016/S0003-2670(01)01294-6.
[16] H. Kim, K.H. Chung, Y. Jung, M. Jang, M. ja Kang, G.S. Choi, A rapid and efficient automated method for the sequential separation of plutonium and radiostrontium in seawater, J. Radioanal. Nucl. Chem. 304 (2015) 321–327, https://doi.org/10.1007/s10967-014-3595-y.
[17] E. Chamizo, M. García-León, S.M. Enamorado, M.C. Jiménez-Ramos, L. Wacker, Measurement of plutonium isotopes, 239Pu and 240Pu, in air-filter samples from Seville (2001–2002), Atmos. Environ. 44 (2010) 1851–1858, https://doi.org/10.1016/j.atmosenv.2010.02.030.
[18] S. Salminen, I. Outola, T. Jaakkola, S. Pulli, R. Zilliacus, J. Lehto, Method for determining plutonium in air filters in detection of nuclear activities, Radiochim. Acta 92 (2004) 467–473, https://doi.org/10.1524/ract.92.8.467.39273.
[19] J. Qiao, X. Hou, M. Miró, P. Roos, Determination of plutonium isotopes in waters and environmental solids: a review, Anal. Chim. Acta 652 (2009) 66–84, https://doi.org/10.1016/j.aca.2009.03.010.
[20] A.R. King, D. Knight, A. Fairhead, Analysis of uranium and plutonium following adsorption on actinide resin, J. Radioanal. Nucl. Chem. 304 (2015) 163–169, https://doi.org/10.1007/s10967-014-3759-9.
[21] C. Landstetter, V. Damberger, M. Zapletal, C. Katzlberger, Development of a rapid method to determine plutonium in foodstuffs, J. Radioanal. Nucl. Chem. 304 (2015) 343–347, https://doi.org/10.1007/s10967-014-3582-3.
[22] I.W. Croudace, P.E. Warwick, R.C. Greenwood, A novel approach for the rapid decomposition of Actinide^{TM} resin and its application to measurement of uranium and plutonium in natural waters, Anal. Chim. Acta 577 (2006) 111–118, https://doi.org/10.1016/j.aca.2006.06.012.
[23] N. Vajda, C.K. Kim, Determination of Pu isotopes by alpha spectrometry: a review of analytical methodology, J. Radioanal. Nucl. Chem. 283 (2010) 203–223, https://doi.org/10.1007/s10967-009-0342-x.
[24] T. Bisinger, S. Hippler, R. Michel, L. Wacker, H.-A. Synal, Determination of plutonium from different sources in environmental samples using alpha-spectrometry and AMS, Nucl. Instrum. Methods Phys. Res. B 268 (2010) 1269–1272, https://doi.org/10.1016/j.nimb.2009.10.150.
[25] S.K. Aggarwal, G. Chourasiya, R.K. Duggal, C.P. Singh, A.S. Rawat, H.C. Jain, A comparative study of different methods of preparation of sources for alpha spectrometry of plutonium, Nucl. Instrum. Methods Phys. Res. 238 (1985) 463–468, https://doi.org/10.1016/0168-9002(85)90485-1.
[26] Z. Varga, G. Surányi, N. Vajda, Z. Stefánka, Rapid sequential determination of americium and plutonium in sediment and soil samples by ICP-SFMS and alpha-spectrometry, Radiochim. Acta 95 (2007) 81–87, https://doi.org/10.1524/ract.2007.95.2.81.
[27] E. Hrnecek, P. Steier, A. Wallner, Determination of plutonium in environmental samples by AMS and alpha spectrometry, Appl. Radiat. Isot. 63 (2005) 633–638, https://doi.org/10.1016/j.apradiso.2005.05.012.
[28] I. Dolique, E. Kabai, M. Schuster, Fast method for the determination of radiostrontium and plutonium isotopes in food samples, J. Radioanal. Nucl. Chem. 322 (2019) 1423–1430, https://doi.org/10.1007/s10967-019-06850-w.
[29] H. Bagán, A. Tarancón, G. Rauret, J.F. García, Radiostrontium separation and measurement in a single step using plastic scintillators plus selective extractants. Application to aqueous sample analysis, Anal. Chim. Acta 686 (2011) 50–56, https://doi.org/10.1016/j.aca.2010.11.048.
[30] M. Sáez-Muñoz, H. Bagán, A. Tarancón, J.F. García, J. Ortiz, S. Martorell, Rapid method for radiostrontium determination in milk in emergency situations using PS resin, J. Radioanal. Nucl. Chem. 315 (2018) 543–555, https://doi.org/10.1007/s10967-017-5682-3.
[31] A. Torres, I. Giménez, H. Bagán, A. Tarancón, Analysis of isotopes of plutonium in water samples with a PSresin based on aliquat·336, Appl. Radiat. Isot. 187 (2022) 110333, https://doi.org/10.1016/j.apradiso.2022.110333.
[32] I. Giménez, H. Bagán, A. Tarancón, J.F. García, PSresin for the analysis of alpha-emitting radionuclides: comparison of diphosphonic acid-based extractants, Appl. Radiat. Isot. 178 (2021) 109969, https://doi.org/10.1016/J.APRADISO.2021.109969.
[33] I. Giménez, H. Bagán, A. Tarancón, Fast analysis of gross alpha with a new plastic scintillation resin, Anal. Chim. Acta 1248 (2023) 340905, https://doi.org/10.1016/j.aca.2023.340905.
[34] J. Barrera, A. Tarancón, H. Bagán, J.F. García, A new plastic scintillation resin for single-step separation, concentration and measurement of technetium-99, Anal. Chim. Acta 936 (2016) 259–266, https://doi.org/10.1016/j.aca.2016.07.008.
[35] L.M. Santiago, H. Bagán, A. Tarancón, J.F. Garcia, Synthesis of plastic scintillation microspheres: Evaluation of scintillators, Nucl. Instrum. Methods Phys. Res. 698 (2013) 106–116, https://doi.org/10.1016/j.nima.2012.09.028.
[36] Triskem international, PRODUCT SHEET SR Resin, vol. 33, 2015, pp. 3–6.
[37] L.A. Currie, Limits for qualitative detection and quantitative determination. Application to radiochemistry, Anal. Chem. 40 (3) (1968) 586–593, https://doi.org/10.1021/ac60259a007.

[38] E.P. Horwitz, M.L. Dietz, R. Chiarizia, H. Diamond, S.L. Maxwell, M.R. Nelson, Separation and preconcentration of actinides by extraction chromatography using a supported liquid anion exchanger: application to the characterization of high-level nuclear waste solutions, Anal. Chim. Acta 310 (1) (1995) 63–78, https://doi.org/10.1016/0003-2670(95)00144-O.

[39] L.M. Santiago, H. Bagán, A. Tarancón, J.F. Garcia, Synthesis of plastic scintillation microspheres: alpha/beta discrimination, Appl. Radiat. Isot. 93 (2014) 18–28, https://doi.org/10.1016/j.apradiso.2014.04.002.

[40] V. Todorov, S. Georgiev, M. Hamel, C. Dutsov, B. Sabot, I. Dimitrova, K. Mitev, Evaluation of radon absorption and detection properties of a plastic scintillator developed for PSD measurements, Measurement 231 (2024), https://doi.org/10.1016/j.measurement.2024.114554.

[41] Real Decreto 3/2023, de 10 de Enero, por el que se Establecen los Criterios Técnico-Sanitarios de la Calidad Del Agua de Consumo, su Control y Suministro, Govierno de España - Ministerio de la Presidencia (MPR): Madrid, Spain, 2023.

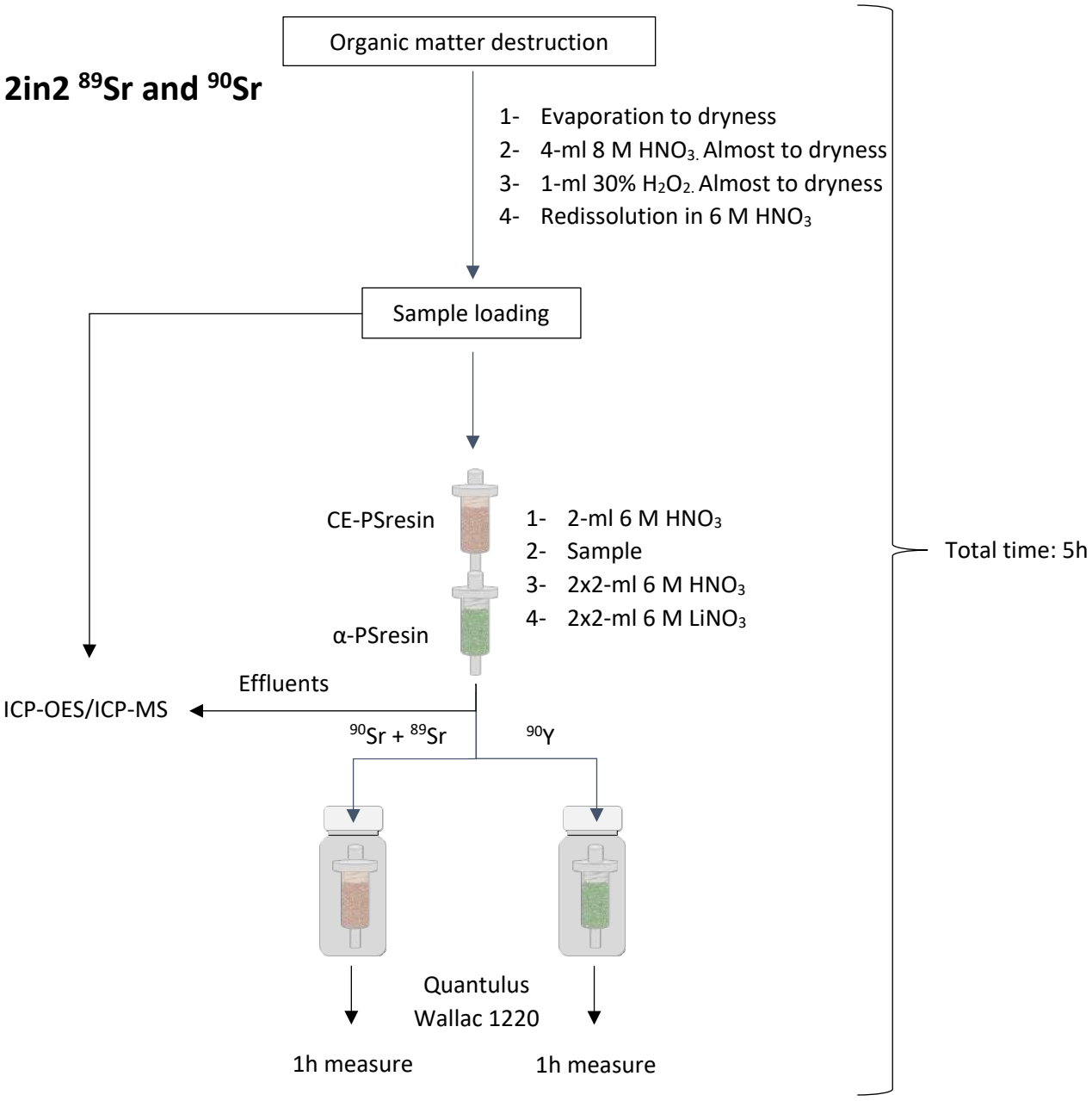

Figure. S1. Diagram for ^{89}Sr and ^{90}Sr determination with the 2in2 configuration

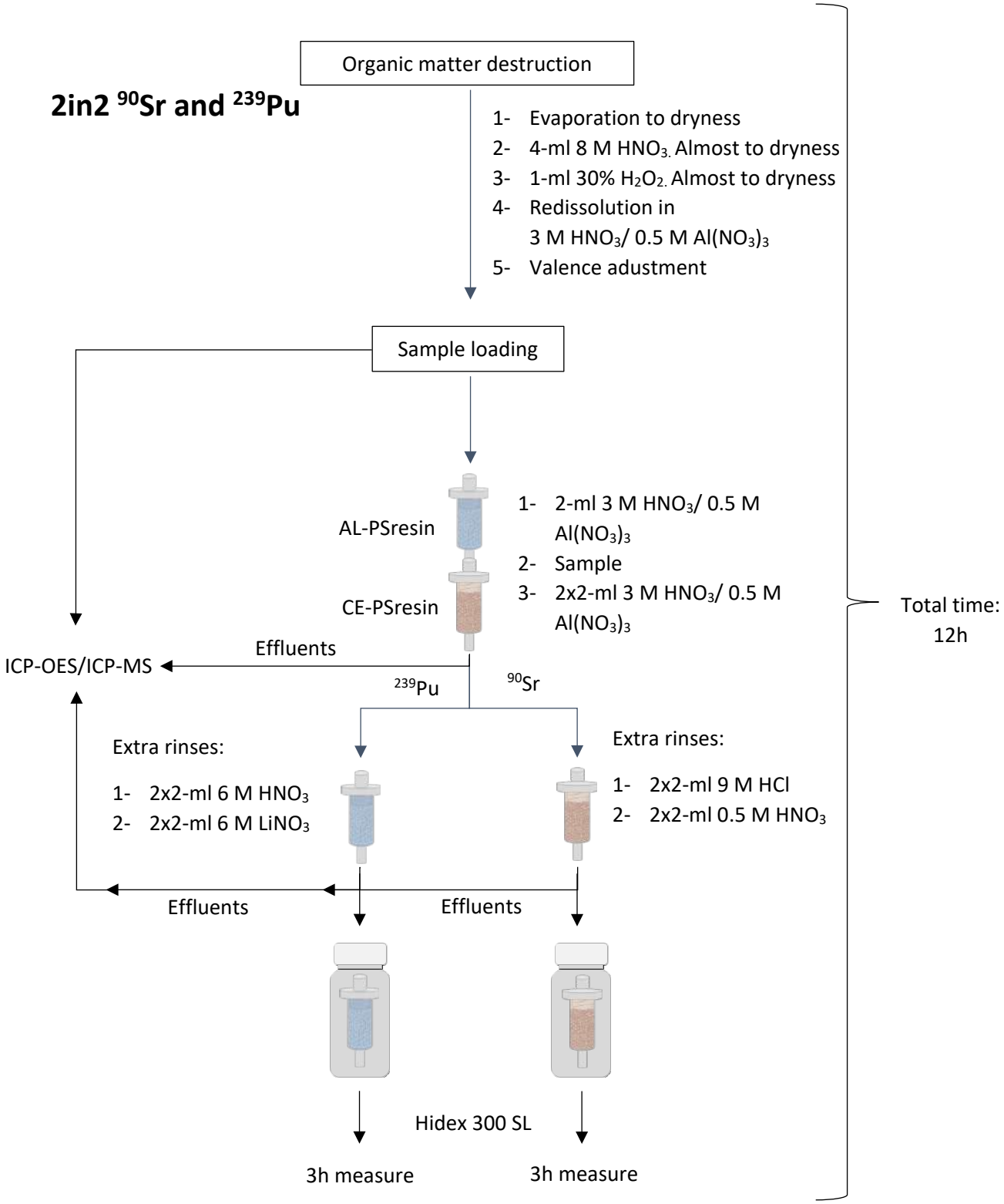

Figure. S2. Diagram for ^{90}Sr and ^{239}Pu determination with the 2in2 configuration

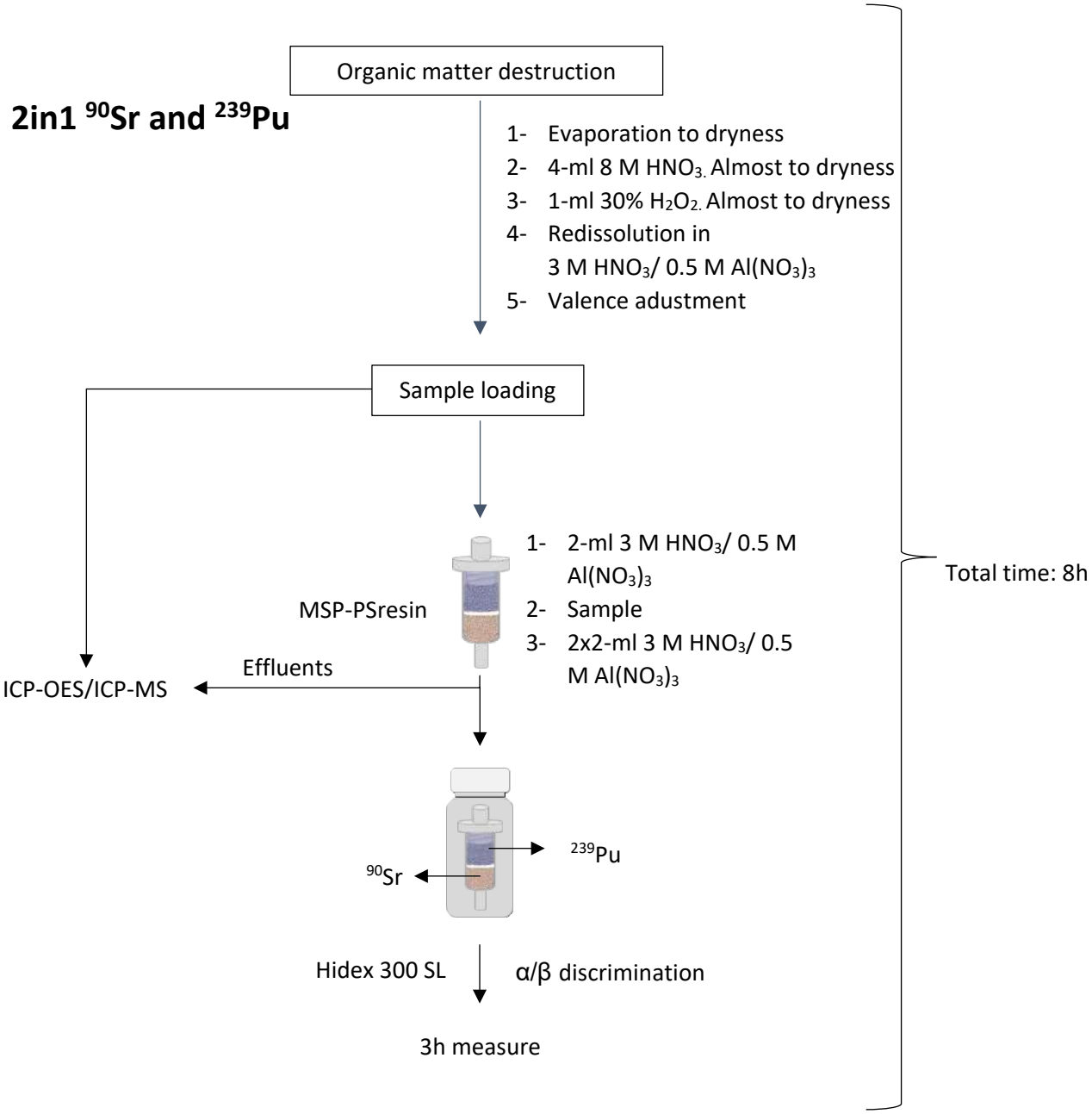

Figure. S3. Diagram for ^{90}Sr and ^{239}Pu determination with the 2in1 configuration

4.3. Discussion

4.3.1. Determination of ^{90}Sr in presence of ^{210}Pb

- Preliminary study

Due to the inability to efficiently elute lead from the CE-PSresin, a new separation strategy was developed based on a previous chemical precipitation to separate lead from strontium. This task was challenging since many precipitating agents that are effective for strontium isolation also precipitate lead. For that reason, some initial trials were conducted to evaluate several precipitating agents, including oxalate, chromate, citrate, hydrogen phosphate, and iodate. For this trials, stable isotope analogues were used and analysed via ICP-OES and ICP-MS.

Table 4.1 summarizes the recovery yields of Sr^{2+} and Pb^{2+} in solution after each precipitation method. Among the tested agents, the chromate-based method showed some potential but achieved only about 30 % strontium recovery, which was deemed inadequate. Moreover, due to the toxicity of chromium compounds, this approach was discarded. The iodate-based method at pH 1-8, however, demonstrated more promising results, with a strontium recovery rate of 72 % and only 5 % lead retention, making it the most effective among the tested methods.

Table 4.1 Recovery of strontium and lead from the sample after applying the precipitation procedure, expressed as the mean plus standard deviation in brackets. 4 replicates were done for each method.

Method	Sr %	Pb %
Oxalate	83 (2)	103 (4)
Hydrogen phosphate + citrate	59 (11)	6 (8)
Chromate	31 (15)	0.65 (0.03)
Iodate	72 (2)	5 (1)

The iodates separation turned out to be temperature-dependent, as strontium iodate solubility increases with temperature [15]. Consequently, achieving consistent separation was challenging. To optimize the iodate method, adjustments were made by increasing the solubility of strontium iodate. The separation process was modified to

include calcium as a coprecipitating agent and by boiling the sample in slightly acidic media, which increased the solubility of strontium iodate, allowing it to remain in solution while lead iodate precipitated. After the removal of the lead iodate precipitate, strontium was subsequently precipitated using hydrogen phosphate in a basic medium to isolate strontium to reduce the sample volume. The resulting strontium precipitate was then dissolved in 8 M nitric acid for its pass through the CE-PSresin. This optimized method achieved near-complete recovery of strontium with only 3 % of lead, effectively minimizing matrix interference and demonstrating good reproducibility. Once the method development was complete, the detection efficiency for ^{90}Sr in the PSresin was determined. The integration window was selected following the study of the figure of merit, which involved choosing the window with the highest difference between the ^{210}Pb and ^{90}Sr spectra. This approach generated a channel range where the influence of ^{210}Pb on ^{90}Sr was minimal. Table 4.2 presents the detection efficiency values immediately after separation and after a 21-day period in the optimal window.

Table 4.2 Detection efficiency for 90Sr at separation (t = 0) and after 21 days (t > 21 days) in the full and optimal windows. Three 100 mL replicate standard samples were analysed.

t = 0		t > 21 days	
Full (1:1024)	**Optimal (450:632)**	**Full (1:1024)**	**Optimal (517:875)**
86 (4)	51 (3)	179 (8)	126 (6)

The complete method was initially validated by analysing two different interlaboratory samples (MAPEP-16-MaW34 and MAPEP-10-MaW22). Table 4.3 shows the results obtained for both samples. For the MAPEP-16-MaW34 sample, the results obtained fell within the acceptable range for both time zero (^{90}Sr) and secular equilibrium (^{90}Sr+^{90}Y).

Table 4.3 Quantification of ^{90}Sr in MAPEP samples. Three replicates were performed.

	Activity ($Bq \cdot L^{-1}$)		
	t = 0	**t > 21 days**	**Acceptance range 2019**
MAPEP-16-MaW34	7.2 (0.7)	5.6 (0.5)	5.65–10.48
MAPEP-10-MaW22	<0.37	<0.20	Not present

- Validation through method comparation

After verifying that the method was suitable for ^{90}Sr determination, it was compared with two conventional methods: extraction chromatography and LSC (EC-LSC) and the successive precipitation and LSC (SUC-LSC).

The PSresin method was firstly compared with the EC-LSC using 100 ml samples from the Consejo de Seguridad Nuclear (CSN), with a theoretical ^{90}Sr activity of 4.1(0.2) $Bq \cdot L^{-1}$. The obtained results are summarized in Table 4.4.

Table 4.4 Results obtained in the analysis of CSN sample with medium activity containing interferents using the EC-LSC and PSresin methods. Three 100 mL replicate samples were analysed.

	Recovery (%)		Activity of ^{90}Sr ($Bq \cdot kg^{-1}$)	
	Sr	**Pb**	**t = 0**	**t > 21 days**
EC-LSC	69 (2)	/	3.9(0.2)	4.09(0.08)
PSresin	87.6(0.4)	6(2)	4.6(0.6)	4.1 (0.1)

The determination of ^{90}Sr activity using EC-LSC method consistently yielded accurate and reproducible results. In comparison, the PSresin method for immediate measurements initially yielded slightly higher ^{90}Sr activity values. However, these results were still within the acceptance range, considering the measurement variability. Notably, after 21 days, the bias in the PSresin method was corrected, resulting in values that closely approached both the theoretical activity and the values obtained through the EC-LSC method. The results demonstrated the viability of the method by using the PSresin, since none of the other radionuclides present in the sample, including ^{210}Pb,

were detected. Finally, the results and variability of the EC-LSC and PSresin methods were equivalent after 21 days.

Further comparison was made between the PSresin method and the SUC-LSC method by analysing 1 L river water samples spiked with 0.4 Bq of ^{90}Sr. Both methods yielded optimal and consistent results, as summarized in Table 4.5.

Table 4.5 Results for the spiked river water samples at environmental levels. One replicate sample was analysed by SUC-LSC and three with PSresin.

Method	Sr^{2+} recovery (%)	Bias (%)	
		t = 0	t > 21 days
SUC-LSC (n = 1)	80.3	1.0	3.5
PSresin	63.3	4.7	−1.1
PSresin	81.3	12.8	−8.3
PSresin	75.5	12.7	−1.9

Both the PSresin and SUC-LSC methods yielded optimal results. At t=0, the SUC-LSC method exhibited a lower bias, while the PSresin method's bias remained within an acceptable range for fast analysis. At secular equilibrium (t>21 days), both methods demonstrated equivalent bias, indicating that the PSresin method can achieve results comparable to the reference SUC-LSC procedure for environmental samples. Additionally, the PSresin method offers a less labour-intensive process with the capability to handle multiple samples simultaneously.

When comparing all three methods (PSresin, EC-LSC, and SUC-LSC), as shown in Table 4.6, all were effective in quantifying strontium activity. Notably, the PSresin method demonstrated having a lower background count rate, resulting in a reduced limit of detection. The analysis time using the PSresin method (5–6 hours) was significantly shorter than the SUC-LSC method (20 hours) and slightly faster than the EC-LSC method (6–7 hours). However, in terms of detection efficiency, the PSresin method has a lower detection efficiency due to the need for optimal window selection,

whereas the EC-LSC and SUC-LSC methods can utilize the full energy windows, enhancing their detection efficiency.

Table 4.6 Summary of the quality parameters of the methods studied.

	Efficiency		Background (cpm)	LoD (Bq/L)	Time of analysis (hours)
	t = 0	t > 21 days			
EC-LSC	96.5(0.4)	193 (1)	4.1	0.081∗∗	6-7
SUC-LSC				0.068∗∗	20
PSresin	51∗ (3)	126∗ (6)	0.3	0.027∗∗	5-6

∗Optimum windows detection efficiency ∗∗(1 L and 1 h counting time)

In this study, a new analytical method for ^{90}Sr determination in the presence of ^{210}Pb was developed, addressing objective number 2 of this thesis, which focuses on radiostrontium quantification methods. Thus, the developed PSresin method is a viable option for ^{90}Sr analysis, offering a faster and more environmentally friendly alternative to conventional methods by eliminating the need for LSC cocktails.

However, based on findings from Chapter 3, Article #4, there is potential for optimizing the method further. Experimenting with a working medium involving acetic acid could enable selective separation of strontium and lead without requiring prior precipitation steps.

4.3.2. Simultaneous measure of ^{89}Sr and ^{90}Sr

The developed methodology utilizes two different PSresins placed in tandem: CE-PSresin and α-PSresin, the last one developed in this thesis. This method involves retaining radiostrontium isotopes on the CE-PSresin cartridge and ^{90}Y on the α-PSresin cartridge. The calculation of the ^{90}Sr activity is done from the α-PSresin count rate (assuming secular equilibrium with ^{90}Y), and the calculation of the ^{89}Sr activity from the CE-PSresin count rate after subtracting the count rate due to ^{90}Sr. The approach assumes a secular equilibrium between ^{90}Sr and ^{90}Y, achieved 21 days post-incident. This dual-resin system is intended for environmental monitoring where the assumption of secular equilibrium is valid.

- Separation medium determination

Initially, it was essential to ensure the selective retention of yttrium on the α-PSresin while preventing strontium retention, using a separation medium where strontium is quantitatively retained in the CE-PSresin. To achieve this, different concentrations of nitric acid (ranging from 3 to 8 M) were tested. Under these conditions, yttrium was successfully retained on the α-PSresin with yields of approximately 60 %, while no strontium retention was observed at any of the tested nitric acid concentrations. Yttrium retention yield on the α-PSresin ranged from 55 % to 65 % and no differences were observed between media if uncertainty of the values is considered. These medium-low retention yield values can be attributed to a too fast flow rate or lack of compaction of the PSresin inside the cartridge, which is lately addressed. The detection efficiency for 3 M and 6 M presented values around 90 %, indicating that almost all particles were detected. However, under 8 M HNO_3 conditions, the α-PSresin acquired a slight yellow colour, likely due to a reaction with the extractant; therefore, this medium was not considered in further experiments. The same media, excluding 8 M, were studied in the CE-PSresin for strontium isotopes. In both media, the retention of strontium was quantitative and no retention of yttrium was observed. The detection efficiency of ^{90}Sr and ^{89}Sr was 94 % and 98 % in 6 M nitric acid and 94% for both isotopes in 3 M nitric acid. Therefore, given the slightly better detection efficiencies values in 6 M nitric acid medium, it was selected as preferred medium.

- Ratio evaluation

With the optimal working medium established, the tandem configuration was tested to evaluate its viability. In real samples, ^{89}Sr can be present at levels 3 to 24 times higher than ^{90}Sr [16,17]. Therefore, the tandem configuration was tested with seven different ratios, ranging from 1:1 to 1:10 and 10:1. Results are shown in Table 4.7.

Table 4.7 Quantification errors for ^{89}Sr and ^{90}Sr respectively

^{90}Sr:^{89}Sr ratio	^{89}Sr quantification error (%)	^{90}Sr quantification error (%)
1_1	-0.7	3.0
1_2	-5.4	8.8
2_1	-15.8	4.4
1_5	5.1	-0.1
5_1	10.4	-0.5
1_10	-0.3	3.6
10_1	11.8	-1.9

Quantification errors for both radionuclides were generally below 10% across most activity ratios tested. However, a trend was identified: higher ^{90}Sr activity relative to ^{89}Sr led to higher quantification errors for ^{89}Sr. However, in those situations where ^{89}Sr activity is much higher than ^{90}Sr, optimal quantification errors are achieved. In scenarios where ^{90}Sr activity greatly exceeds that of ^{89}Sr, measuring total radiostrontium (^{89}Sr+^{90}Sr) may be a more effective approach for assessing contamination levels, thus simplifying the analysis.

- Validation of spiked water samples

The strategy demonstrated promising results in spiked deionized water samples. To assess its applicability 100 mL river water, spiked with four different ratios. were studied (1:1, 3:1, 3:1 and 1:4). Organic matter was removed by evaporating the sample to dryness, treating the residue with 8 M HNO_3 and 30 % H_2O_2, and then reconstructing the sample in 6 M HNO_3. In all cases, the quantification errors were lower than 15 % (Table 4.8).

Table 4. 8 Quantification error for ^{89}Sr and ^{90}Sr respectively on river spiked water samples

^{90}Sr:^{89}Sr ratio	^{89}Sr quantification error (%)	^{90}Sr quantification error (%)
1:1	11.1	-10.7
3:1	-8.9	-9.2
1:3	-5.7	6.5
1:4	1.3	8.6

The method proved to be fast, with results available in less than 5 h from sample reception, making it suitable for rapid analysis purposes, even with the measure of two PSresin per sample. The detection limit, calculated using the Currie equation [18], was 0.13 $Bq \cdot L^{-1}$ for a 100 mL volume sample and 1 h of measurement in a Quantulus detector. This method allows for the quantification of ^{90}Sr and ^{89}Sr with errors lower than those typically reported, around 20 % or 30 %. However, this strategy is suitable only for samples where secular equilibrium between ^{90}Sr and ^{90}Y has been achieved.

4.3.3. Plutonium determination

- Plutonium separation condition in AL-PSresin

The methodology developed is based on AL-PSresin, initially designed for the determination of ^{99}Tc. This PSresin employs aliquat·336, a quaternary amine that, depending on the working medium, has affinity for different radionuclides.

There are two critical factors that affect plutonium's affinity for the aliquat·336 extractant; the working medium and the oxidation state of plutonium. Maximum retention of plutonium occurs in 9 M hydrochloric acid and within the range of 0.5 to 4 M nitric acid, with 3 M nitric acid being the most commonly used. The optimal oxidation state for maximum retention is plutonium (IV). For this reason this project started with the evaluation of the optimum working medium and valence adjustment method for the isolation of plutonium as Pu(IV) with the AL-PSresin as well as assessing the detection efficiency under the studied conditions.

Two valence adjustment strategies were evaluated:

- Hydroxylamine method: it was performed in a 9 M HCl medium where plutonium was first reduced to plutonium (III) using hydroxylamine, then oxidized to plutonium (IV) with sodium nitrate.
- Iron sulphamate method: it was performed in a 3 M HNO_3 medium and 3 M HNO_3 plus 0.5M $Al(NO_3)_3$. Plutonium was reduced to plutonium (III) using iron (II) sulphamate. Ascorbic acid was then added to reduce any iron (III) back to iron (II), which could interfere with plutonium retention. Sodium nitrite was subsequently added to achieve the desired plutonium (IV) valence state.

All methods achieved quantitative retention yields and high detection efficiencies (See Table 4.9); however, the hydroxylamine method (method A) experienced quenching phenomena due to the high HCl concentration required for the valence adjustment in this method, shifting the spectrum to lower energy channels. The iron sulphamate method did not had such quenching and was therefore chosen as the optimal strategy.

Table 4.9 Detection efficiency, plutonium retention and SQP(E) for each valence adjustment tested

Method	Medium	Valence adjustment	Detection efficiency (%)	Retention (%)	SQP(E)
A	9 M HCl	$NH_2OH/NaNO_2$	97	96	616
B	3 M HNO_3	$FeH_4N_2O_6S_2/C_6H_8O_6/NaNO_2$	91	96	680
C	3 M HNO_3 + 0.5 M $Al(NO_3)_3$	$FeH_4N_2O_6S_2/C_6H_8O_6/NaNO_2$	97	96	670

When comparing the presence or not of $Al(NO_3)_3$, the detection efficiency increased from 91 % to 97 %. $Al(NO_3)_3$ is added in this type of separation to stabilize Pu(IV) and enhance the extraction of plutonium nitrate complexes. In this case, there was no difference in the isolation of plutonium, but in the detection efficiency which slightly increased, for that reason the working medium chosen as optimum was 3 M HNO_3 plus 0.5 M $Al(NO_3)_3$ with the sulphamate valance adjustment. Additionally, the methodology included two rinse cycles after loading the sample onto the PSresin: the first with 9 M HCl to elute thorium and the second with 0.5 M nitric acid to elute neptunium.

- Interferences assessment

The chosen method was tested for potential interferences, including ^{238}U plus daughters, ^{230}Th, ^{210}Pb plus daughters, ^{241}Am, and ^{99}Tc. Table 4.10 shows the obtained results.

Table 4.10 Amount of interferent radionuclides retained in the PSresin together with the amount eluted in each method step.

Radionuclide	% Retained in AL-Psresin	%not retained in loading step + eluted with HNO_3 and $Al(NO_3)_3$	% eluted with HCl 9 M	% eluted with HNO_3 0.5 M
^{238}U and daughters	2	76.8	15.8	5.3
^{230}Th	3.6	1.2	88.9	6.4
^{210}Pb and daughters	3.6	81.2	14.9	0.4
^{241}Am	1	99.0	0.0	0.0
^{99}Tc	11.2	83.3	4.3	1.4

The retention of each interferent, once all the separation process was complete, was below 4% for all, with the exception of ^{99}Tc, for which a 11.2% was retained in the AL-PSresin. Nevertheless, ^{99}Tc spectrum position (from the 0 to 650 channels) was sufficiently different to that of Pu to allow its identification in the spectrum and correct the Pu determination. It is important to notice that the majority of the interferents were directly not retained in during the loading, with the exception of ^{230}Th, which was eluted in the 9 M HCl cleaning step as expected. Therefore, it can be concluded that the media selected can be used for column cleaning and decontamination from interferences, which could be improved further by performing cleaning steps with higher volumes. Thus, Pu can be quantified using AL-PSresin.

- Pu stable tracer

The retention of plutonium in all the trials performed was shown to be quantitative, however, using a tracer is recommended to address potential losses during methodology execution. ^{242}Pu is commonly used as a tracer in alpha spectrometry due to its absence in natural samples. However, when using scintillation techniques samples cannot incorporate radioactive tracers as their signals overlap with those of the plutonium isotopes. For this reason stable analogous were tested looking for someone which resemblance the Pu(IV) behaviour in the AL-PSresin. Elements took into

consideration were those with at least one of the following characteristics: a similar chemistry to Pu; similar oxidation states (i.e. III and IV); retention in strong anionic exchange resins [19–21]; and to be close to Pu in the periodic table. The list of studied included Eu, Mo, Sn, Ce, Sm and Au. Samples containing 1 mg of the corresponding element were treated following the same procedure used for standard samples. The proportion of stable element eluted in each step relative to the total content of each one is shown in Table 4.11.

Table 4.11 proportion of stable element eluted in each step during the developed method for Pu(IV) in AL-PSresin.

	Eu (%)	Mo (%)	Sn (%)	Ce (%)	Sm (%)	Au (%)
Effluent of the Loading (3 M HNO_3 + 0.5 M $Al(NO_3)_3$)	54	97.3	75.4	100	100	0
Effluent of the 1st cleaning (9 M HCl)	0	0.3	19.3	0	0	0
Effluent of the 2nd cleaning (0.5 M HNO_3)	46	2.4	5.3	0	0	0

None of the elements studied were retained with the exception of gold (III) which results in an experimental behaviour similar to plutonium in AL-PSresin, even though both elements do not even share the same valence state. The fact that plutonium (IV) and gold (III) differ in its chemistry was put into evidence during valence adjustment, as the addition of the reagents in some samples reduced gold precipitating part of it as metal gold. To solve this, 1 M HCl was added to the working media solution in a ratio 5:4 3 M HNO_3 + 0.5 M $Al(NO_3)_3$ to 1 M HCl ratio. The presence of Cl^- in solution stabilized gold as $[AuCl_4]^-$, allowing the application of the valence adjustment without affecting the previous parameters observed for plutonium, giving as a result a method for the quantitative isolation of Pu(IV) with high detection efficiency (>96 %) and a tracer that behaves equally as plutonium in the AL-PSresin.

- Validation with spiked water, vegetable and air-filters samples

The viability of the developed method was tested on different samples. First of all, river and sea water samples spiked with 10 $Bq \cdot L^{-1}$ were analysed by triplicate and using gold (III) as tracer. Each sample was evaporated to dryness and treated with aqua regia solution and 1 % H_2O_2 for organic matter destruction. The sample was then reconstituted in the working medium solution and the plutonium separation in the AL-PSresin was conducted. The results obtained are shown in Table 4.12.

Table 4.12 Yield and quantification deviation obtained in the analysis of spiked river water and seawater samples treated though evaporation to dryness and aqua regia redissolution

Sample	Yield (%)	Quantification error (%)
River water (blank)	99.3	
River water (1st replicate)	92.2	9
River water (2nd replicate)	99.4	6
River water (3rd replicate)	99.9	8
Seawater (blank)	72.9	
Seawater (1st replicate)	76.6	-4
Seawater (2nd replicate)	99.9	-4
Seawater (3rd replicate)	99.9	10

The recovery was high and quantification errors were below 10 % for both water matrices in all replicates. The results confirmed that gold works well as a tracer of plutonium as in sea water 1st replicate, the retention was correctly evaluated through the measurement of gold, achieving a -4 % quantification error. Therefore, it can be concluded that developed methodology facilitates rapid plutonium determination with a limit of detection of 0.073 $Bq \cdot L^{-1}$ for a 100 mL sample and 3 hours of measurement time, demonstrating a significant improvement over the conventional method for water matrices.

This method was also validated with vegetation and air filters samples, in collaboration with Universitat Politecnica de Valencia (UPV). Samples were calcinated to remove organic matter, followed by acidic digestion using a mixture of nitric acid, hydrochloric acid, and hydrogen peroxide. The sample was then evaporated to dryness and reconstituted in diluted nitric acid.

To preconcentrate plutonium in vegetation and air-filter samples, precipitation methods are recommended. In this study, iron precipitation in basic medium was utilized for this purpose. The use of gold as a tracer was deemed unsuitable for these samples, as gold does not have a similar behaviour to that of plutonium during the iron precipitation step. Consequently, for establishing the methodology for vegetation and

air filter samples the total efficiency, combining both retention and detection efficiencies, is assessed.

The total efficiency achieved was 89.9(0.4) % slightly lower than the detection efficiency observed for water samples. This reduction in efficiency is due to the more complex matrix of the vegetation and filter samples. The spectra of the replicates are illustrated in Figure 4.1.

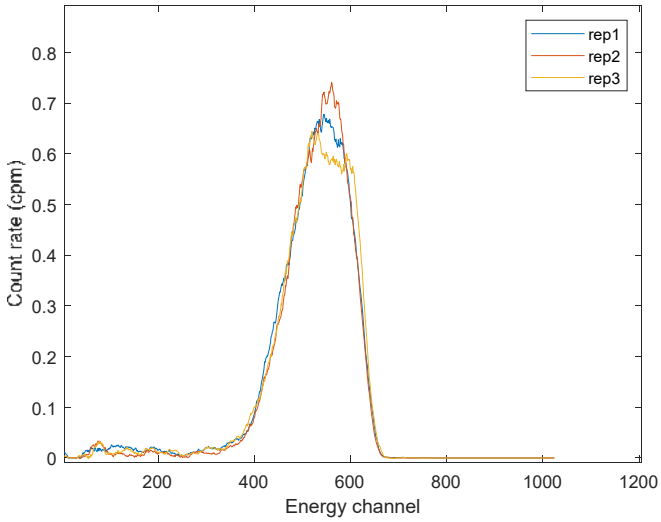

Fig 4. 1 Spectra of all replicates for grass matrix.

The method was applied to a natural grass sample spiked with 7 $Bq \cdot Kg^{-1}$ as was found that polish grass containing plutonium activities between 7-11 $Bq \cdot Kg^{-1}$ due to the Chornobyl accident [22]. Grass samples were analysed with quantification errors lower than 8 % (Table 4.13) and a LoD of 1.2 $Bq \cdot Kg^{-1}$ and 3 h counting time.

Table 4. 13 Quantification error for three samples of natural grass spiked with 7 Bq Kg^{-1}

Sample	Quantification error %
Sample_1	-1.6
Sample_2	7.6
Sample_3	3.5

The same procedure was employed on an air sample collected using a cellulose filter. Similarly, obtaining quantification errors not exceeding 7 % and a LoD of 0.01 $Bq \cdot filter^{-1}$ for 3 h counting time.

Given the results, it can be concluded that the developed method is a greener alternative to conventional methods involving less reagent and time with low LoDs and high detection efficiencies and plutonium recoveries. Additionally, the implementation of AL-PSresin avoids the use of LSC cocktails, not generating mixed wastes. The developed method has been proved to be accurate in a large range of sample matrices, including water, vegetation and air-filters samples. However, in vegetation and filter samples, gold (III) cannot be used as a tracer for the whole process, as do not behave as plutonium in the iron coprecipitation step, needing to assume a quantitative recovery in the whole procedure or just including the tracer for the AL-PSresin separation step.

4.3.4. Radiostrontium and plutonium sequential determination

This project was motivated given the common origin of radiostrontium and plutonium. In order to reduce the time involved in the measurement of both elements, a common method for it has been developed in this thesis using the AL-PSresin and the CE-PSresin in tandem configuration.

Tandem determination using PSresin can be achieved by retaining ^{90}Sr in the CE-PSresin and plutonium isotopes in the AL-PSresin. Both isotopes can be retained in their respective PSresin at high HNO_3 concentrations (3 to 8 M), typically 3 M for plutonium (combined with 0.5 M $Al(NO_3)_3$) and 6 M for ^{90}Sr. However, since plutonium can also be retained on the CE-PSresin, the AL-PSresin must precede the CE-PSresin. Therefore, the working medium chosen was the one optimized for plutonium in section 4.3.3, including the valence adjustment, as it also ensures strong retention of strontium in CE-PSresin.

- Cross-contamination evaluation

First of all, it was studied in which extent cross contamination could take place by loading a ^{90}Sr or a ^{239}Pu standard in the AL-PSresin and the CE-PSresin in tandem and under the working conditions chosen.

Fig 4.2. shows the spectrum of each standard sample in each PSresin. The results indicate that cross-contamination did not occur with the CE-PSresin being free of ^{239}Pu and AL-PSresin free of ^{90}Sr. Moreover, the retention was of 99 % for plutonium in the

AL-PSresin and 94 % for strontium in the CE-PSresin, proving that the strontium retention is not affected by the reagents used for the valence adjustment of plutonium. Detection efficiencies in triple coincidence mode in Hidex 300 SL detector were 91(2) % for ^{239}Pu and 58(2) % for ^{90}Sr.

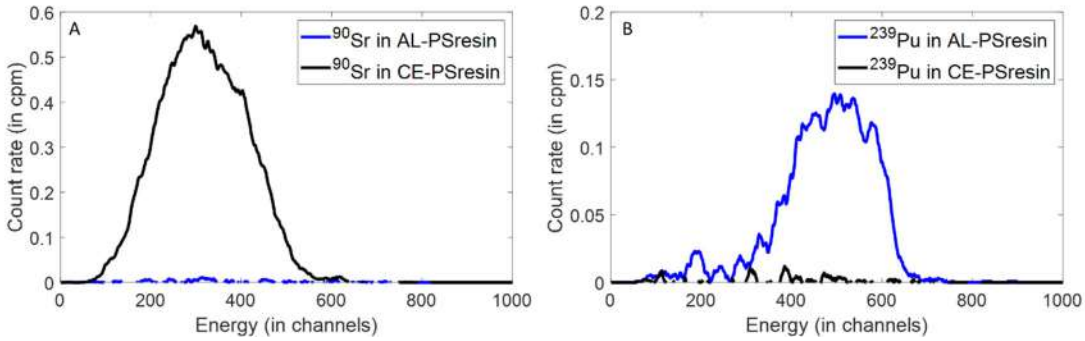

Fig 4.2 (a) ^{90}Sr/^{90}Y and (b)^{239}Pu standard passed though CE-PSresin and AL-PSresin.

- 2in2 and 2in1 configurations approach

Two different configurations were studied, based on the different emission of ^{239}Pu(α) and ^{90}Sr(β) that allow α/β discrimination (See Fig 4.3):

- 2in2 configuration: This approach uses both PSresin in tandem, and two measurements, one per PSresin cartridge, for the determination of ^{239}Pu and ^{90}Sr. For the 2in2 configuration, the AL-PSresin, containing 1 g of PSresin, is located on the top and the CE-PSresin cartridge, containing 1.4 g of PSresin, connected in tandem at the bottom.

- 2in1 configuration: This approach involves the use of both PSresins in the same cartridge and α/β discrimination for the discrimination of ^{90}Sr and ^{239}Pu in a single measurement.

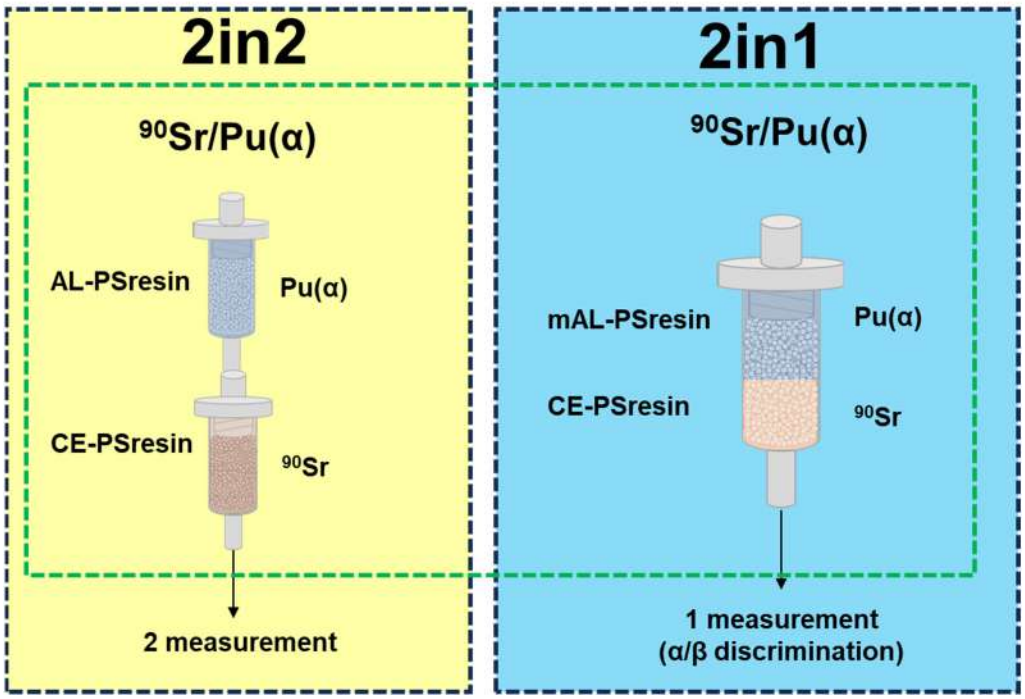

Fig 4.3 Configuration studied for the simultaneous determination of ^{90}Sr and Pu(α)

For the 2in1 configuration, as α/β discrimination is needed, the AL-PSresin was modified using PSm with biphenyl and p-terphenyl as fluorescent solutes as it enhances the α/β discrimination, leading to the mAL-PSresin. In this case 0.5 g of the CE-PSresin are located at the bottom of the cartridge and separated with a frit and 0.5 g of mAL-PSresin at the top, giving as a result a PSresin which was named MSP-PSresin.

The separation procedure for each configuration approach differs in the rinses used. For both configurations, the sample was loaded in 3 M HNO_3 plus 0.5 M $Al(NO_3)_3$ medium and two rinses of 2 ml with the same working medium were performed. In the 2in2 configuration, once the sample is loaded, both cartridges were then rinsed separately with 6 M HNO_3 (2 mL, twice) and 6 M LiNO3 (2 mL, twice) for the CE-PSresin and 9 M HCl (2 mL, twice) and 0.5 M HNO_3 (2 mL, twice) for AL-PSresin. These rinses cannot be performed in the 2in1 configuration as 9 M HCl elute strontium from the CE-PSresin.

First of all, the retention and detection efficiency in each configuration was evaluated, as well as, the optimum pulse length index (PLI), for the α/β discrimination in the 2in1 configuration.

In Table 4.14, it is shown the comparative of the values obtained for each configuration.

Table 4.14 Comparative of calibration parameter for each configuration approach

Parameter	Radionuclide	2in2	2in1
Total efficiency (whole window) (%)**	^{239}Pu*	91(2)	72(1)
	^{90}Sr	58(2)	70(5)
Retention (%)	^{239}Pu*	-	-
	^{90}Sr	94	70
PLI α/β	-	-	19
Total efficiency PLI 19 (%)**	^{239}Pu*	-	64(2)
	^{90}Sr	-	69(5)
Misclassification (%)	^{239}Pu	-	11(2)
	^{90}Sr	-	2.3(0.6)

*** Combined value of retention and detection efficiency**

**** Triple coincidence counting mode**

Comparing the detection efficiencies obtained for each radionuclide, in each configuration, for plutonium the total efficiency was higher in the 2in2 configuration, as expected, due to the presence of more PSresin in the cartridge (1 g versus 0.5 g). In the case of strontium, this effect is observed on the retention where in the 2in2 configuration the retention is 94 % and in the 2in1 70 %. However, the detection efficiency was higher in the 2in1 than in the 2in2.

For the 2in1 configuration, the 3D spectrum obtained from the HIDEX detector (Fig 4.4) allowed for the determination of the optimum PLI value, which defines the integration windows with the best α/β discrimination performance.

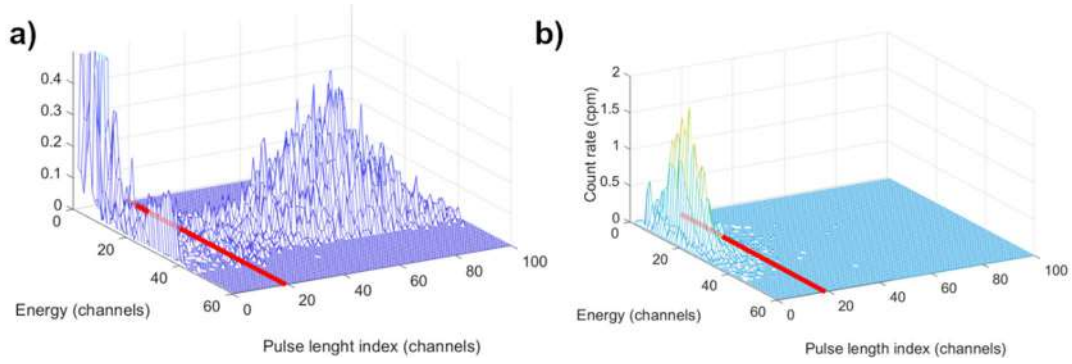

Fig 4.4 3D spectra for ^{239}Pu (a) and ^{90}Sr (b) with MPS-PSresin in Hidex 300 SL detector in double coincidence count rate configuration

The 3D spectra, shown in Fig 4.4, was obtained from the standards in the double coincidence configuration, as the 3D spectrum cannot be obtained in triple coincidence mode. Despite the prominent chemiluminescence (high signal at low energy values) in the AL-PSresin, it was possible to stablish an optimal PLI value of 19. At this PLI values, the misclassification rates for strontium and plutonium were 2.3(0.6) % and 11(2) % respectively, and detection efficiencies in the corresponding windows of 64(2) % and 69(5) % for ^{239}Pu and ^{90}Sr respectively.

- Validation of both configurations with 5 Bq·L^{-1} river water sample

The viability of both configurations was tested in the analysis of river water samples spiked with 5 Bq·L^{-1} in a ratio 1:1 of ^{90}Sr to ^{239}Pu. 100 ml volume sample was analysed in each case. Previously each sample was evaporated until dryness and treated with 8 M nitric acid and 1 % of H_2O_2 to finally be reconstituted in the working medium (HNO_3+$Al(NO_3)_3$) to performed the valence adjustment. The quantification errors obtained for each sample in each configurated is shown in Table 4.15.

Table 4. 15 quantification errors for ^{239}Pu and ^{90}Sr in each configuration for river water samples

Configuration	River water sample	^{239}Pu	^{90}Sr
2in2	Sample_1	11.8 %	-1.4 %
	Sample_2	-2.6 %	-5.7 %
	Sample_3	-5.0 %	-0.5 %
2in1	Sample_1	7.8 %	1.6 %
	Sample_2	6.6 %	-1.3 %

Both configurations allowed a good quantification of both radionuclides below a 10 % error for almost all the cases. It can be concluded that the developed methodology allows the quantification of both radionuclide in 8-12 h since sample reception, reducing the time required by conventional methods.

- Configuration comparation

Both configurations methods accurately quantified the strontium and plutonium activity, however, comparing both configurations (Table 4.16), the 2in1 configuration demonstrated to be faster than the 2in2, as only one cartridge needs to be measured. Regarding the LoDs, the 2in1 configuration also showed lower limits, for both

radionuclides. In the case of ^{90}Sr, the main contribution to background is the amount of PSresin used, which is higher in the 2in2 configuration, 1.4 g of CE-PSresin, than in the 2in1, 1 g of MSP-PSresin. For ^{239}Pu the use of an integration window for α/β discrimination notably reduces the background contribution in the alpha widow (0.61 cpm) compared to the background of the whole window (between 7.5-8 cpm).

Table 4. 16 Summary of the quality parameters of both configurations studied.

	2in2	**2in1**
Analysis time (h)	12	8
LoD (Bq·L^{-1}):		
^{90}Sr	0.33	0.18
^{239}Pu	0.18	0.04
N° cartridges	2	1
Counting time (h)	6 (3+3)	3
Background (cpm):		
^{90}Sr	8.2	7.35
^{239}Pu	7.4	0.61

In terms of quality parameters, 2in1 configuration can be considered slightly better option than the 2in2, as it is faster and had lower LoDs. However, the 2in2 configuration main advantage is the possibility of performing extra rinses to elute interferences that can be present in a real sample like thorium and neptunium contrary to the 2in1 configuration. Additionally, the 2in1 configuration as it is based on the determination through α/β discrimination only alpha plutonium emitters could be determined, while in the 2in2 configuration, it is possible to determine the beta plutonium emitter, ^{241}Pu, as the resins are measured separately. Regarding the analysis time, it could be reduced to even 5 h for the 2in1 and 8 h for the 2in2 if a coprecipitation is performed, instead of an evaporation until dryness.

Given the obtained results, it can be concluded that the methodologies discussed in this chapter introduce innovative alternatives for the determination of radiostrontium and plutonium isotopes. These approaches are not only faster but also more environmentally friendly, as they do not produce mixed waste. This achievement aligns with and fulfils objectives number 2 and 3 of the presented thesis, demonstrating that the newly developed methods can provide efficient and sustainable solutions for radionuclide analysis.

4.4. References

[1] N. Vajda, C.K. Kim, Determination of radiostrontium isotopes: A review of analytical methodology, Applied Radiation and Isotopes 68 (2010) 2306–2326. https://doi.org/10.1016/j.apradiso.2010.05.013.

[2] INTERNATIONAL ATOMIC ENERGY AGENCY, Rapid Simultaneous Determination of ^{89}Sr and ^{90}Sr in Milk: A Procedure Using Cerenkov and Scintillation Counting, IAEA Analytical Quality in Nuclear Applications Series No. 27, IAEA, Vienna (2013).

[3] M. Tayeb, X. Dai, E.C. Corcoran, D.G. Kelly, Rapid determination of 90Sr from 90Y in seawater, J Radioanal Nucl Chem 304 (2015) 1043–1052. https://doi.org/10.1007/s10967-015-3935-6.

[4] C.K. Kim, S. Tarján, E. Bokori, Z. Molnár, P. Cassette, Improved rapid determination of 89Sr and 90Sr in milk using Cerenkov and scintillation counting, Advances in Liquid Scintillation Spectrometry (2010) 125–138.

[5] K. Günther, S. Lange, M. Veit, A rapid method for determining ^{89}Sr and ^{90}Sr by Cerenkov counting, Applied Radiation and Isotopes 67 (2009) 781–785. https://doi.org/10.1016/j.apradiso.2009.01.035.

[6] J. Eikenberg, H. Beer, M. Rüthi, I. Zumsteg, A. Vetter, Precise determination of ^{89}Sr and ^{90}Sr/^{90}Y in various matrices: the LSC 3-window approach. LSC Advances in Liquid Scintillation Spectrometry, Radiocarbon, (2005) 17 237–249.

[7] P.A. Pittet, F. Bochud, P. Froidevaux, Determination of 89 Sr and 90 Sr in fresh cow milk and raw urine using crystalline synthetic tunnel manganese oxides and layered metal sulfides, Anal Chim Acta 1047 (2019) 267–274. https://doi.org/10.1016/j.aca.2018.10.007.

[8] J. Qiao, X. Hou, M. Miró, P. Roos, Determination of plutonium isotopes in waters and environmental solids: A review, Anal Chim Acta 652 (2009) 66–84. https://doi.org/10.1016/j.aca.2009.03.010.

[9] K. Norisuye, K. Okamura, Y. Sohrin, H. Hasegawa, T. Nakanishi, Large volume preconcentration and purification for determining the240Pu/239 Pu isotopic ratio and ^{238}Pu/$^{239+240}$Pu alpha-activity ratio in seawater, J Radioanal Nucl Chem 267 (2005) 183–193. https://doi.org/10.1007/s10967-006-0026-8.

[10] N. Momoshima, H. Kakiuchi, Y. Maeda, E. Hirai, T. Ono, Identification of the contamination source of plutonium in environmental samples with isotopic ratios determined by inductively coupled plasma mass spectrometry and alpha-spectrometry, J Radioanal Nucl Chem 221 (1997) 213–217. https://doi.org/10.1007/BF02035270.

[11] J. Moreno, N. Vajda, P.R. Danesi, J.J. Larosa, E. Zeiller, M. Sinojmeri, Combined procedure for the determination of ^{90}Sr, ^{241}Am and Pu radionuclides in soil samples, J Radioanal Nucl Chem 226 (1997) 279–284. https://doi.org/10.1007/BF02063661.

[12] M.P.R. Montero, A.M. Sánchez, M.T.C. Vázquez, J.L.G. Murillo, Analysis of plutonium in soil samples, App Rad and Iso 53 (2000) 259–264. https://doi.org/10.1016/s0969-8043(00)00141-x.

[13] Z. Varga, G. Surányi, N. Vajda, Z. Stefánka, Rapid sequential determination of americium and plutonium in sediment and soil samples by ICP-SFMS and alpha-spectrometry, Radiochim Acta 95 (2007) 81–87. https://doi.org/10.1524/ract.2007.95.2.81.

[14] J. Barrera, A. Tarancón, H. Bagán, J.F. García, A new plastic scintillation resin for single-step separation, concentration and measurement of technetium-99, Anal Chim Acta 936 (2016) 259–266. https://doi.org/10.1016/j.aca.2016.07.008.

[15] D.N. Sunderman, C.W. Townley, The Radiochemistry of Barium, Calcium, and Strontium, Battelle Memorial Inst. Nuclear Science Series (1960) 125. https://doi.org/10.2172/4140481.

[16] M. Tayeb, X. Dai, S. Sdraulig, Rapid and simultaneous determination of Strontium-89 and Strontium-90 in seawater, J Environ Radioact 153 (2016) 214–221. https://doi.org/10.1016/j.jenvrad.2016.01.003.

[17] N. Casacuberta, P. Masqué, J. Garcia-Orellana, R. García-Tenorio, K.O. Buesseler, ^{90}Sr and ^{89}Sr in seawater off Japan as a consequence of the Fukushima Dai-ichi nuclear accident, Biogeosciences 10 (2013) 3649–3659. https://doi.org/10.5194/bg-10-3649-2013.

[18] L.A. Currie, Limits for qualitative detection and quantitative determination. Application to radiochemistry. Analytical chemistry 40.3 (1968): 586-593. https://doi.org/10.1021/ac60259a007.

[19] S. Bajo, C. Gann, J. Eikenberg, L. Wyer, H. Beer, M. Ruthi, M. Jaggi, I. Zumsteg, P. Scherrer, Separation of Plutonium on the Anion Exchanger BIO-RAD 1-X2 and its Application to Radiochemical Analysis, Paul Scherrer Institute (PSI), Department Logistics, Division for Radiation Safety and Security, Villigen (Switzerland) (2007). ISSN: 1019-0643, 2007.

[20] J.D. Despotopulos, K.N. Kmak, N. Gharibyan, T.A. Brown, P.M. Grant, R.A. Henderson, K.J. Moody, S.J. Tumey, D.A. Shaughnessy, R. Sudowe, Production and isolation of homologs of flerovium and element 115 at the Lawrence Livermore National Laboratory Center for Accelerator Mass Spectrometry, J Radioanal Nucl Chem 308 (2016) 567–572. https://doi.org/10.1007/s10967-015-4500-z.

[21] W.D. Xing, M.S. Lee, Recovery of gold(III) from the stripping solution containing palladium(II) by ion exchange and synthesis of gold particles, Journal of Industrial and Engineering Chemistry 69 (2019) 255–262. https://doi.org/10.1016/j.jiec.2018.09.038.

[22] J.W. Mietelski, B. Was, Plutonium from chernobyl in Poland, Applied Radiation and Isotopes 46 (1995) 1203–1211. https://doi.org/10.1016/0969-8043(95)00162-7.

CHAPTER 5 - Conclusions

5.1. Conclusions

The development of new materials and greener strategies presented and discussed in this thesis has led to the following conclusions:

1. The developed α-PSresin allowed the determination of the gross total alpha parameter in 5 h since sample reception, in contrast to the 24-48 h required by the conventional methods.
2. The development of the first scintillating ion-imprinted polymer for ^{55}Fe was successfully developed, using AAC, St and DVB in its composition. However, further studies are needed to improve the scintillating capabilities and fine-tune the polymerization condition to be reproducible.
3. Comparing the different strategies presented in this thesis for the development of new selective scintillating materials. PSresin strategy is presented as the easiest one due to its higher reproducibility. However, PSresin development is limited to the availability of selective extractants. In case of lack, the synthesis of them can be performed, but increasing the time and cost of the developing PSresin. The Sc-IIP preparation is challenging and it can lack reproducibly, as very small changes during the polymerization can lead to large changes in the capacity and selectivity of the final material, but not selective extractant is required, making possible the development of a selective material for almost every element.
4. Regarding the results obtained from the molecular dynamics, the resulting simulations correlate well with the experimental D_w. Among the different working media studied acetate medium allows the correct retention of strontium with no lead interaction. This outcome could lead to a new methodology to be applied in the proper CE-PSresin for the development of a new methodology for Sr and Pb separation. The obtained results proved that MD simulations could be used for the prediction affinity of organic extractant with radionuclides, simplifying the cost and time for the development of new resins.
5. Regarding radiostrontium determination, two novel methods involving PSresin have been developed. The first one was for environmental samples with high ^{210}Pb content and was based on a previous precipitation with KIO_3 in HNO_3 while

boiling the sample. Determination of ^{90}Sr, was done at almost the same time as the conventional methods with the main advantage of non-generating mixed wastes and without interference of ^{210}Pb. The second method was developed for the simultaneous measurement of ^{89}Sr and ^{90}Sr and was based on tandem separation of ^{89}Sr/^{90}Sr and ^{90}Y in CE-PSresin and α-PSresin. This method allowed the fast determination of both radionuclides, in a single measurement, in contrast to the 1-2 months required by the conventional methods. Nevertheless, this method can be only applied under the assumption of secular equilibrium.

6. Regarding plutonium isotope determination, a new strategy has been developed taking advantage of the AL-PSresin versatility. The developed strategy allowed the plutonium determination in a large number of matrices with low quantification errors using gold as tracer. However, the tracer used is only suitable for the pass through the PSresin, but not for previous pre-treatments. This makes the procedure less robust (for vegetation and air filter samples) if compared to conventional methods as a quantitative retention has to be assumed.
7. Given the common origin of radiostrontium and plutonium isotopes, two strategies based on using the CE-PSresin and AL-PSresin in tandem were developed to reduce the analysis time to half. The tandem configuration strategy, with two cartridges, allowed the determination of both radionuclides with low quantification errors. In contrast, the single-cartridge MSP-PSresin method allowed for a faster analysis as only one cartridge is measured thanks to the use of alpha-beta discrimination parameters. However, this strategy only allows for the analysis of plutonium alpha emitters.

In conclusion, the work carried out during this thesis underscores the critical importance of radioactivity analysis and monitoring, not only in emergencies but also in routine environmental assessments. Radioactive elements, whether of natural origin or introduced through human activity, can accumulate and concentrate in specific areas due to natural processes, potentially posing significant risks to human health and environment.

While this thesis has contributed to the development of novel green methods for the rapid and effective analysis of specific radionuclides, there remains an ongoing need for innovative strategies and alternatives to ensure even faster and more comprehensive analysis across all radionuclides. This work also highlights the importance of interdisciplinary collaboration within the field of chemistry. Achieving robust and reliable outcomes requires integrating knowledge and techniques from various branches of chemistry, rather than working in isolation within a single specialization.